ISSN 1007-9327 (print)
ISSN 2219-2840 (online)

World Journal of *Gastroenterology*

World J Gastroenterol 2023 October 21; 29(39): 5435-5525

Published by Baishideng Publishing Group Inc

World Journal of Gastroenterology

Contents

Weekly Volume 29 Number 39 October 21, 2023

REVIEW

ORIGINAL ARTICLE

Basic Study

Retrospective Cohort Study

Observational Study

SYSTEMATIC REVIEWS

World Journal of Gastroenterology

Weekly Volume 29 Number 39 October 21, 2023

Contents

ABOUT COVER

Editorial Board Member of *World Journal of Gastroenterology*, Serag M Esmat, MD, Professor, Department of Internal Medicine, Faculty of Medicine, Cairo University, Cairo 11562, Egypt. Seragesmat@yahoo.com

AIMS AND SCOPE

The primary aim of *World Journal of Gastroenterology* (*WJG*, *World J Gastroenterol*) is to provide scholars and readers from various fields of gastroenterology and hepatology with a platform to publish high-quality basic and clinical research articles and communicate their research findings online. *WJG* mainly publishes articles reporting research results and findings obtained in the field of gastroenterology and hepatology and covering a wide range of topics including gastroenterology, hepatology, gastrointestinal endoscopy, gastrointestinal surgery, gastrointestinal oncology, and pediatric gastroenterology.

INDEXING/ABSTRACTING

The *WJG* is now abstracted and indexed in Science Citation Index Expanded (SCIE), MEDLINE, PubMed, PubMed Central, Scopus, Reference Citation Analysis, China Science and Technology Journal Database, and Superstar Journals Database. The 2023 edition of Journal Citation Reports® cites the 2022 impact factor (IF) for *WJG* as 4.3; Quartile category: Q2. The *WJG*'s CiteScore for 2021 is 8.3.

RESPONSIBLE EDITORS FOR THIS ISSUE

NAME OF JOURNAL
World Journal of Gastroenterology

ISSN
ISSN 1007-9327 (print) ISSN 2219-2840 (online)

LAUNCH DATE
October 1, 1995

FREQUENCY
Weekly

PUBLICATION DATE
October 21, 2023

PUBLISHING PARTNER
Shanghai Pancreatic Cancer Institute and Pancreatic Cancer Institute, Fudan University
Biliary Tract Disease Institute, Fudan University

INSTRUCTIONS TO AUTHORS
https://www.wjgnet.com/bpg/gerinfo/204

GUIDELINES FOR ETHICS DOCUMENTS
https://www.wjgnet.com/bpg/GerInfo/287

GUIDELINES FOR NON-NATIVE SPEAKERS OF ENGLISH
https://www.wjgnet.com/bpg/gerinfo/240

PUBLICATION ETHICS
https://www.wjgnet.com/bpg/GerInfo/288

PUBLICATION MISCONDUCT
https://www.wjgnet.com/bpg/gerinfo/208

POLICY OF CO-AUTHORS
https://www.wjgnet.com/bpg/GerInfo/310

ARTICLE PROCESSING CHARGE
https://www.wjgnet.com/bpg/gerinfo/242

STEPS FOR SUBMITTING MANUSCRIPTS
https://www.wjgnet.com/bpg/GerInfo/239

ONLINE SUBMISSION
https://www.f6publishing.com

PUBLISHING PARTNER's OFFICIAL WEBSITE
https://www.shca.org.cn
https://www.zs-hospital.sh.cn

World Journal of Gastroenterology

Submit a Manuscript: https://www.f6publishing.com

World J Gastroenterol 2023 October 21; 29(39): 5435-5451

DOI: 10.3748/wjg.v29.i39.5435

ISSN 1007-9327 (print) ISSN 2219-2840 (online)

REVIEW

Function and biomedical implications of exosomal microRNAs delivered by parenchymal and nonparenchymal cells in hepatocellular carcinoma

Hai-Chen Wang, Wen-Xuan Yin, Meng Jiang, Jia-Yi Han, Xing-Wang Kuai, Rui Sun, Yu-Feng Sun, Ju-Ling Ji

Specialty type: Gastroenterology and hepatology

Provenance and peer review: Invited article; Externally peer reviewed.

Peer-review model: Single blind

Peer-review report's scientific quality classification

Grade A (Excellent): A
Grade B (Very good): B, B, B, B, B
Grade C (Good): 0
Grade D (Fair): 0
Grade E (Poor): 0

P-Reviewer: Ghazy A, Egypt; Granito A, Italy; Haque N, Bangladesh; Tsai HW, Taiwan; Wang YG, China

Received: May 26, 2023
Peer-review started: May 26, 2023
First decision: July 23, 2023
Revised: August 13, 2023
Accepted: October 16, 2023
Article in press: October 16, 2023
Published online: October 21, 2023

Hai-Chen Wang, Wen-Xuan Yin, Meng Jiang, Jia-Yi Han, Xing-Wang Kuai, Rui Sun, Yu-Feng Sun, Ju-Ling Ji, Department of Pathology, Medical School of Nantong University, Nantong 226001, Jiangsu Province, China

Meng Jiang, Jia-Yi Han, Xing-Wang Kuai, Rui Sun, Yu-Feng Sun, Ju-Ling Ji, Key Laboratory of Microenvironment and Translational Cancer Research, Science and Technology Bureau of Nantong City, Nantong 226001, Jiangsu Province, China

Ju-Ling Ji, Department of Pathology, The Affiliated Hospital of Nantong University, Nantong 226001, Jiangsu Province, China

Corresponding author: Ju-Ling Ji, MD, PhD, Professor, Department of Pathology, Medical School of Nantong University, No. 19 Qixiu Road, Nantong 226001, Jiangsu Province, China. jijuling@ntu.edu.cn

Abstract

Small extracellular vesicles (exosomes) are important components of the tumor microenvironment. They are small membrane-bound vesicles derived from almost all cell types and play an important role in intercellular communication. Exosomes transmit biological molecules obtained from parent cells, such as proteins, lipids, and nucleic acids, and are involved in cancer development. MicroRNAs (miRNAs), the most abundant contents in exosomes, are selectively packaged into exosomes to carry out their biological functions. Recent studies have revealed that exosome-delivered miRNAs play crucial roles in the tumorigenesis, progression, and drug resistance of hepatocellular carcinoma (HCC). In addition, exosomes have great industrial prospects in the diagnosis, treatment, and prognosis of patients with HCC. This review summarized the composition and function of exosomal miRNAs of different cell origins in HCC and highlighted the association between exosomal miRNAs from stromal cells and immune cells in the tumor microenvironment and the progression of HCC. Finally, we described the potential applicability of exosomal miRNAs derived from mesenchymal stem cells in the treatment of HCC.

Key Words: Hepatocellular carcinoma; MicroRNA; Exosomes; Extracellular vesicles; Nonparenchymal cells

Core Tip: Hepatocellular carcinoma (HCC) is one of the most serious cancers in adults, and microRNAs (miRNAs) in small extracellular vesicles (exosomes) play a vital role in the pathological processes of HCC. Recent studies on exosomal miRNAs in HCC mainly focus on miRNA profiling but place little emphasis on where miRNAs come from and what target cells they act on. This review focused on the origin of exosomal miRNAs according to their parent cells in the tumor microenvironment and their role in HCC pathogenesis, contributing to a better understanding of exosomal miRNAs in the tumor microenvironment.

Citation: Wang HC, Yin WX, Jiang M, Han JY, Kuai XW, Sun R, Sun YF, Ji JL. Function and biomedical implications of exosomal microRNAs delivered by parenchymal and nonparenchymal cells in hepatocellular carcinoma. *World J Gastroenterol* 2023; 29(39): 5435-5451
URL: https://www.wjgnet.com/1007-9327/full/v29/i39/5435.htm
DOI: https://dx.doi.org/10.3748/wjg.v29.i39.5435

INTRODUCTION

In 2020, liver cancer was ranked the sixth most frequent malignant solid cancer globally. It was also the third-leading cause of cancer-related deaths in the world[1]. Hepatocellular carcinoma (HCC) is the primary histological type of liver cancer, comprising 80% of primary liver cancer cases[2]. It is characterized by the high degree of malignancy and poor prognosis. It is a threat to the health of humans. The symptoms of incipient-stage HCC are strong concealment, and it is challenging to diagnose HCC early. In addition, approximately 70% of patients undergo recurrence and experience metastasis within 5 years after surgical resection[3].

The tumor microenvironment (TME) is important in the development of HCC[3] and primarily comprises host cells, both resident and recruited, along with the secreted molecules and extracellular matrix (ECM) proteins[4]. Nonparenchymal cells in the liver, such as sinusoidal endothelial cells, hepatic stellate cells (HSCs), and macrophages, have a critical role in establishing the TME and mediating tumorigenesis by paracrine communication *via* cytokines and/or angiocrine factors[5]. Accumulating investigations on the TME have revealed novel perceptions of tumor growth as well as metastasis therein exosomes play a crucial function[6-8].

Small extracellular vesicles, also known as exosomes, refer to a specific type of extracellular vesicles with a size of 40-160 nm that originate from multivesicular bodies (MVBs), which act as carriers for biological information exchange to shape the cellular microenvironment[9]. To maintain consistency in nomenclature across studies published at different stages, we will use the name exosome for the rest of this review. Studies have shown that exosomes contain various cargoes including DNA, lipids, proteins, and RNA such as microRNAs (miRNAs), circular RNAs (circRNAs), long noncoding RNAs, and messenger RNAs, which are involved in intercellular communication[10,11].

More and more molecules of different classes carried by exosomes have been reported. Based on data retrieved from the ExoCarta database (http://www.exocarta.org), the identified components within exosomes consist of 9769 unique proteins, 3408 distinct messenger RNAs, 2838 different miRNAs, and 1116 lipids. Initially, exosomes were considered carriers of cellular waste, and their functions were underestimated[12]. Over the past few decades, the crucial functions of exosomes in facilitating intercellular communication in both physiological and pathological processes have been extensively studied and validated[13].

In 1996, exosomes derived from murine and human B lymphocytes were proven to execute a crucial function in transporting MHC molecules and eliciting MHC-II restricted T-cell responses[14]. Later, cancer cells and non-tumor cells in the TME were also found to be able to deliver exosomes and thereby participate in the malignant progression of tumors through molecular exchanges mediated by them[15,16]. Exosomes, hence, are recognized as important contributors to cancer initiation and progression[17-19].

MiRNAs represent an extensive collection of post-transcriptional gene expression regulators in eukaryotes. These regulatory molecules typically consist of 20-24 nucleotides and exert their function over various developmental and cellular processes[20]. Due to their essential role in gene expression, exosomal miRNAs have also been widely studied. In 2007, Valadi *et al*[21] reported that exosomes contained miRNAs, which could be delivered to other cells and exert their functions. Studies have demonstrated that exosomes are loaded with a high abundance of miRNAs, which play a crucial role in immune modulation, resistance to chemotherapy, and metastasis in diverse malignancies[22]. These miRNAs can promote tumor development in a paracrine manner in the surrounding microenvironment[23-25]. Furthering the comprehension of cancer mechanisms will require the identification of exosomal miRNAs, which are abnormally expressed in pathological states.

Numerous scientific studies have demonstrated that exosomes play a critical role in the genesis and malignant progression of tumors by transmitting signals between cells and regulating the TME[26]. This paper summarizes the studies of exosomal miRNAs released from nonparenchymal cells in the TME of HCC and discusses the association between these exosomal miRNAs and HCC. This study will help researchers in the field to better understand the role of exosomal miRNAs from stromal cells and immune cells in HCC and develop innovative strategies for HCC prevention

and treatment.

FORMATION, COMPOSITION, AND FUNCTION OF EXOSOMES

Unlike other types of vesicles, exosomes have a different formation mechanism. First, the plasma membrane germinates inwards to form early endosomes (membrane-bound vacuoles)[27,28]. By further inwards budding of early endosomes encompassing miRNAs, proteins, and other selected substances, late endosomes called MVBs are formed[29]. Following this, the MVBs undergo fusion with the cell membrane, and the intraluminal endosomal vesicles are released into the extracellular area. These vesicles subsequently form exosomes[30] or fuse with the lysosome to decompose the biological information[31].

Studies revealed that the essential system involved in the biogenesis of exosomes is the endosomal sorting complex required for transport[32]. The endosomal sorting complex required for transport- identifies the ubiquitin-labeled "cargo" protein, guides it to MVBs, and subsequently separates the MVB from the peripheral membrane in a highly conserved process similar to the process of cytokinesis and virus budding[33].

Exosomes can be produced by any cell under normal or pathological conditions and might be taken up by other cells, hereby executing their designated tasks[34,35]. Exosomes transport multiple biologically active substances, such as proteins, RNA, DNA, and cholesterol[36-38]. The sucrose gradient density range in which exosomes float is 1.13-1.19 g/mL[39]. Of note, the composition of exosomes varies depending on their cellular origin[40], and different cell-derived exosomes or even the same cell-derived exosomes contain different components in different physiological or pathological states[41]. The amount of exosomal miRNAs secreted by hepatoma cells could also vary under different stimuli[42]. Research has shown that 55 miRNAs in Heb3B cell-derived exosomes were expressed at levels that were four times higher than those in donor cells, while 30 miRNAs were expressed at lower levels, and 11 miRNAs were expressed only in exosomes[43]. These changes may be a potential mechanism for disease progression.

EXOSOMAL MIRNAS AND LIVER CANCER

In the past few years, exosomes have been shown to be crucial mediators of intercellular material and information exchange that can modulate the TME by transmitting nucleic acids and proteins between cells; hence, they are involved in tumor cell proliferation and migration, immune regulation, and drug resistance[44,45]. As an essential component of exosomes, exosomal miRNAs exert crucial functions in HCC tumorigenesis and progression.

First, we will review the function of exosomal miRNAs derived from HCC cells. MiR-122, which proved to be the most enriched miRNA in the human liver, is found to be decreased in the liver of HCC patients[46-48]. It is expressed and delivered by Huh7 cells (human HCC cell line) and can be transferred into HepG2 cells (human HCC cell line, of which the basal expression of miR-122 is low) in the form of exosomes, reducing the growth and proliferation of recipient HepG2 cells. The restoration of miR-122 inhibits HCC growth and enhances HCC sensitivity to chemotherapeutic drugs [49]. In addition, exosomes delivered by liver cancer cells can affect nonparenchymal cells in the microenvironment, promoting the malignant progression of tumors, which will be discussed in subsequent sections.

On the other hand, exosomal miRNAs secreted by tumor cells other than liver cancer cells can also promote the formation of premetastatic niches in the liver. Colon cancer cell-derived exosomes are able to deliver miR-21, miR-192, and miR-221 to hepatoma cells[50]. Exosomal miR-25-3p delivered by colon cancer cells promotes premetastatic niche formation in the liver by improving vascular permeability and angiogenesis[51]. Exosomes from colorectal cancer highly expressed miR-135a-5p, which could be transmitted to hepatic Kupffer cells to regulate the LATS2-YAP1/TEAD1-matrix metalloproteinase (MMP) 7 pathway and promote cell adhesion, forming premetastatic niches[52]. These results showed that exosomes could communicate between different types of cancers, even remodeling the microenvironment to boost liver metastasis[53].

Exosomal miRNAs might also be linked to different etiology of liver disease related to HCC. The connection between miRNAs and different liver diseases covering hepatitis B virus (HBV) infection, hepatitis C virus (HCV) infection, alcohol-associated liver disease (ALD), nonalcoholic steatohepatitis (NASH), nonalcoholic fatty liver disease, autoimmune hepatitis, and drug-induced liver injury has been discussed in-depth in previous high-quality reviews[54-56]. In the liver of ALD, NASH, and HCC patients, the level of hepatocyte-specific miR-122 exhibits a remarkable decrease. This specific miRNA directly targets distinct regions at the 5′-UTR of the HCV RNA genome, thereby facilitating the replication of HCV RNA[57]. When it comes to HBV replication, miR-122 functions oppositely. It acts as an inhibitor by downregulating the cyclin G1-p53 complex and preventing the specific interaction between p53 and HBV enhancers[58].

In simple steatosis, the liver shows an increase in the expression of miR-192, which is enriched in hepatocytes. However, this elevation is not observed in NASH[59]. On the other hand, the expression of miR-192 is decreased in HCC [60]. It is the most significantly downregulated miRNA in hepatic cancer stem cells and plays a role in the activation of cancer stem cells. Due to the anti-tumor property of miR-192, administering miR-192 to individuals with HCC can be a potential strategy for HCC therapy[60].

The expression of miR-155, a highly abundant miRNA in immune cells, including macrophages, is elevated in the liver tissues of patients with ALD, autoimmune hepatitis, and HCC. It is an oncogenic miRNA that links inflammation with tumorigenesis[61,62]. The activation of NF-κB signaling was reported to induce an upregulation in miR-155 levels in hepatocytes and liver cancer when mice were fed a choline-deficient and amino acid-defined diet[61] or in HCV infection

in patients[62]. However, few studies have focused on the etiology of HCC and miRNAs delivered by exosomes.

According to a recent investigation, extracellular vesicles derived from neutrophils have the capability to transfer miR-223 to macrophages, stimulating the resolution of liver fibrosis[63]. Neutrophil/myeloid-specific miR-223 has been extensively studied for its anti-inflammatory properties. Its function involves the suppression of IL-6 expression, effectively reducing the activation of the IL-6-p47phox-ROS pathway within neutrophils[64]. The upregulation of miR-223 is observed in the serum and/or liver of patients or mouse models experiencing ALD or NASH, both diseases characterized by significant hepatic neutrophil infiltration. Consequently, the compensatory increase in miR-223 expression is a protective mechanism against ALD[64] and NASH[65]. At the same time, the reduction of miR-223 in HCC might be a causal factor in promoting HCC progression[66]. Therefore, the administration of miR-223 is thought to be a potent treatment in murine models of acute hepatitis and NASH[67]. Future studies of the above-reported miRNAs associated with different etiologies of liver diseases underlying HCC could be extended to the area of exosomes.

THE INTERACTIONS BETWEEN TME AND TUMOR CELLS *VIA* EXOSOMAL MIRNAS IN HCC

Since Stephen Paget proposed the "seed-soil" theory of tumor metastasis in 1889 to explain the organ specificity of tumor metastasis, there has been increasing evidence that tumor metastasis requires coordination between tumor cells and the TME, which has been identified as an evolutionary and ecological process characterized by constant, dynamic, and reciprocal action upon each other. Nonparenchymal cells in the liver cancer TME, such as HSCs, cancer-associated fibroblasts (CAFs), immune cells [T lymphocytes, B lymphocytes, natural killer (NK) cells, NK T cells, and tumor-associated macrophages (TAMs)], and endothelial cells, are pivotal in mediating tumor-stromal communications, thus regulating the biological processes of HCC[68]. Noncellular components are composed of growth factors like transforming growth factor-β (TGF-β), insulin-like growth factor, fibroblast growth factor, hepatocyte growth factor, vascular endothelial growth factor, proteolytic enzymes, ECM, and inflammatory cytokines. These components create a beneficial environment for the formation and proliferation of HCCs. Exosomal miRNAs, a crucial element of the TME, play a significant role in transmitting signals between cells and contribute to the development and advancement of tumors. In the next section, the role of the exosomal miRNAs from different nonparenchymal cells in HCC formation and metastasis is thoroughly discussed. The related investigations are paving the way for novel strategies in clinical diagnosis and treatments aimed at HCC (Figure 1).

Exosome-mediated cell-cell communication between activated HSCs and HCC cells

HSCs can be observed in the space of Disse, located between liver sinusoidal endothelial cells and hepatocytes. These cells are responsible for storing lipid droplets containing vitamin A[69,70]. When there is damage to the liver, quiescent HSCs transform to activated HSCs, which resemble myofibroblasts and produce excessive fibrotic ECM[70]. The migration and accumulation of myofibroblasts are thought to be the key events that initiate liver fibrosis. Although many cell types, such as HSCs[71-73], portal fibroblasts[71,72], mesenchymal stem cell (MSC)-like cells[74], mesothelial cells[75] and bone marrow-derived cells[76], have been reported to contribute to the myofibroblast pool, recently researchers have evidence that 82%-96% of myofibroblasts in models with toxic, cholestatic, and fatty liver diseases are generated from activated HSCs[73].

The initiation and promotion of liver cancer are significantly correlated to the existence of liver fibrosis[70]. Activated HSC is a major factor mediating liver fibrosis and promotes liver cancer progression. Activated HSCs cocultured with HCC cells promoted tumor growth and invasiveness in nude mice[77]. In 2022, Zhang *et al*[78] reported that reducing activated HSC-delivered exosomal miR-148a-3p inhibited HCC initiation through the ITGA5/PI3K/Akt pathway. Another group found that HSC-HCC cell coculture reduced intracellular miR-335-5p expression in both types of cells. Additionally, *in vitro* and *in vivo* experiments showed that miR-335-5p-loaded HSC exosomes inhibited cancer growth and invasion[79]. In summary, activated HSCs can promote the development of HCC *via* various miRNAs delivered by exosomes, and targeting activated HSC-exosome miRNAs represents an innovative therapeutic strategy in HCC. At the same time, exosomes derived from HCC cells also promote the activation of HSCs. The HCC cell-derived exosome-miRNA-21, which targets the *PTEN* gene in HSCs, activates the PDK1/AKT pathway and converts HSCs to CAFs[80]. The progression of cancer was further accelerated by the activation of CAFs, which release angiogenic cytokines such as vascular endothelial growth factor, basic fibroblast growth factor, TGF-β, MMP2, and MMP9[80]. Another study suggested that a high level of serum exosomal miRNA-21 is associated with increased activation of CAFs and a higher vessel density in patients with HCC[80].

Exosome-mediated cell-cell communication between CAFs and HCC cells

CAFs are an important component of the TME[81]. However, the concepts of HSCs and CAFs in early literature sometimes need to be clarified. Researchers used to believe that in the HCC microenvironment, HSCs frequently differentiated into CAFs, which have been extensively reported to influence HCC progression[81-84]. In the latest study, Zhu *et al*[85] successfully identified five CAF subtypes within HCC tumors through single-cell RNA sequencing data obtained from both mouse and human HCC tumors. The subtypes include vascular CAFs, matrix CAFs, lipid processing-matrix CAFs (also known as $CD36^+$ CAFs), lipid-processing CAFs, and antigen-presenting CAFs. In these cells, CD36+ CAFs are derived from HSCs[85]. Another group also showed that Tcf21 was explicitly expressed in HSCs in mouse and human livers. Tcf21-positive HSCs, representing approximately 10% of all HSCs, can transdifferentiate into the majority of myofibroblasts in fibrotic liver and CAFs in HCC[86].

As crucial contributors to the alterations of the ECM that contribute to the development of HCC, CAFs have the potential to stimulate the progression of HCC through communication mediated by exosomes. A recent study found that the miR-320a level was remarkably decreased in CAF-derived exosomes compared with corresponding para-neoplastic fibroblast-derived exosomes in HCC patients. *In vitro* and *in vivo* experiments showed the anti-tumor effects of miR-320a when it was delivered to malignant cells through exosomes. The anti-tumor effect of miR-320a might be achieved by effectively targeting PBX3, thereby impeding the activation of the MAPK pathway[87]. Another study confirmed that miR-150-3p was lost in exosomes released by CAFs. CAF-delivered exosomes potently accelerate the malignant progression of HCC due to the absence of anti-tumoral miR-150-3p. Restoring the expression level of miR-150-3p by delivering miR-150-3p-loaded exosomes to HCC cells can effectively suppress their migration and invasiveness. Therefore, exosomal miR-150-3p can serve as a prognostic biomarker for HCC, and a supplement with exosomal miR-150-3p might be a potential treatment option[88].

Apart from those underexpressed anti-tumor miRNAs found in CAF-derived exosomes, the oncogenic miR-20a-5p was enriched in CAFs compared to HCC cells. MiR-20a-5p can be transferred from CAFs to HCC cells through exosomes and thereby suppress the expression of the tumor suppressor LIM domain and actin binding 1, which in turn inhibits the Wnt/β-catenin signaling pathway in HCC[89]. Thus, the distinct expression of exosomal miRNAs in CAFs plays a crucial part in the malignant progression of HCC. Therefore, potential therapeutic implications can be expected from anti-CAF medications that aim at certain exosomal miRNAs.

However, exosomal noncoding RNAs other than miRNAs also participate in the CAF-tumor cell communication. Chemoresistance in HCC can be influenced by CAF-exosomal circRNAs. Circular RNA ZFR is highly expressed in CAFs and CAF exosomes. CAF-exosomes transfer circular RNA ZFR to tumor cells, suppress the STAT3/NF-κB signaling pathway, and consequently enhance the growth of HCC cells as well as stimulate chemoresistance to cisplatin[90]. In addition, the migration, invasion, and glycolytic abilities of HCC cells were enhanced by long noncoding RNA TUG1 loaded in CAF-exosomes by targeting the miR-524-5p/SIX1 axis[91].

Exosome-mediated cell-cell communication between adipocytes and HCC cells

The involvement of adipose tissue in tumor progression has long been recognized[92]. Adipocytes play a crucial role in the hepatic microenvironment of nonalcoholic fatty liver disease, which is also a proven risk factor for HCC[44]. There is a close association between the adipocyte-HCC cell interaction and the risk of HCC development and progression[93]. Adipocyte-derived exosomes can affect the gene expression of liver cancer cells. In 2014, Koeck *et al*[94] found that exosomes from obese donors' visceral adipose tissues caused dysregulation of genes involved in the TGF-β pathway in HepG2 cells. Recently, Liu *et al*[95] found that the levels of miR-23a/b in serum exosomes and tumor tissues were significantly elevated in high-body fat ratio (BFR) HCC patients compared to their low-BFR counterparts. In tumor tissues, it is highly probable that miR-23a/b can be transported from adipocytes into cancer cells *via* exosomes, thus promoting the malignant progression of HCC[95]. Moreover, exosomal miR-23a/b affects the von Hippel-Lindau/hypoxia-inducible factor pathway, thus promoting chemoresistance[95]. Exosomal circRNAs also play a role. Adipocyte exosomal circDB can suppress miR-34a expression in HCC cells and subsequently activate the deubiquitination-related USP7/cyclin A2 signaling pathway and promote tumor growth of HCC[96]. These studies provided evidence that high BFR-related exosomal miRNA could be valuable therapeutic targets for HCC.

On the other hand, HCC cell-derived exosomes can educate adjacent adipocytes and generate a microenvironment that promotes tumor formation and progression. HepG2-exosomes induced an inflammatory phenotype in adipocytes by activating several phosphorylated kinases (p-AKT, p-Erk1/2, p-GSKb, p-stat5a, and p-p38) and the NF-kB signaling pathway[44]. Adipocytes treated by tumor-derived exosomes enhance tumor development, angiogenesis, and macrophage recruitment in a mouse xenograft model[44]. The specific exosomal miRNAs that play a role in the process remain to be revealed.

In addition, it was observed in experimental models and human studies that the exposure to the adipocyte exosome increased the expression of various profibrotic molecules in HSCs, including tissue inhibitor of metal protease 1 and 4, Smad-3, integrins αvβ-5 and αvβ-8, and MMP-9[94].

Exosome-mediated cell-cell communication between vascular endothelial cells and HCC cells

It is widely acknowledged that angiogenic factors from tumor cells activate vascular endothelial cells, promote their proliferation and migration, and contribute to aberrant tumor angiogenesis[97]. HCC is a typical hypervascular tumor, and understanding the mechanisms of angiogenesis in HCC is very important[98]. In an early study, Shih *et al*[99] discovered that the decrease of miR-214 in HCC cells contributed to the upregulation of hepatoma-derived growth factor, stimulating vascular endothelial cells to promote angiogenesis and tumor growth. Therefore, miR-214 is a potent suppressor of angiogenesis. It was also shown that exosomes derived from HCC cells are able to induce the formation of lumens of human umbilical vein endothelial cells[98].

Recently, several HCC cell-derived exosomal miRNAs were found to be vital to angiogenesis. Fang *et al*[100] reported that hepatoma cell-derived exosomal miR-103 can be internalized by endothelial cells and damage the integrity of endothelial junctions and a subsequent elevation in vascular permeability that facilitates tumor metastasis. The underlying mechanism involves the specific targeting of crucial endothelial junction proteins, such as vascular endothelial-cadherin and p120-catenin, by exosomal miR-103[100]. Exosomal miR-210, derived from HCC cells, can be delivered to endothelial cells and lead to the promotion of tumor angiogenesis. This effect is mediated by the specific targeting of SMAD4 and STAT6, key regulators involved in modulating angiogenic processes[101]. Exosomal miRNAs (miR-638, miR-663a, miR-3648, and miR-4258) from HuH-7M (which is established from luciferase-expressing human hepatoma Huh-7 and deemed as a new, highly intrahepatic metastatic cell line) are able to attenuate the integrity of endothelial junctions, thus enhancing permeability by reducing vascular endothelial cadherin and zonula occludens-1

expression[102]. These findings revealed that HCC-exosomal miRNAs could be delivered to endothelial cells to promote HCC progression.

On the other hand, the exosomes released by endothelial cells might also affect tumor cells. A recent study showed that engineered human cerebral endothelial cell-derived exosomes containing increased miR-214 (hCEC-Exo-214) could enhance the sensitivity of HCC cells to anticancer drugs, such as oxaliplatin and sorafenib[103]. However, how endothelial cell-derived exosomes and exosomal miRNAs act on HCC cells is poorly studied. It is worth paying attention to in the follow-up studies.

Exosome-mediated cell-cell communication between immune cells and HCC cells

The tumor immune microenvironment (TIME) is an important part of the TME[104]. The complicated interactions between cancer cells and host immune cells significantly influence TIME[105]. In HCC, the poor overall survival outcome arises as a result of immune surveillance disruption, which is strongly associated with the suppression of host immune reactions[105-107]. The growing evidence shows that the intricate interplay of exosome exchange-based cancer immunity shapes the tumor microenvironment, causing immune suppression and immune tolerance.

TAM presents the major leukocyte component infiltrating the HCC TIME[107]. Hepatic macrophages, also known as Kupffer cells, are the most abundant immune cells in the liver[108]. During the early stages of carcinogenesis, proinflammatory activation of Kupffer cells is important in tumor development. Once the primary tumor is established, the liver-infiltrating macrophages play a more critical role than Kupffer cells in HCC progression[109]. M2-polarized TAMs promote HCC progression by preventing T cells from recognizing and killing cancer cells, promoting tumor growth, angiogenesis, invasion, metastasis, and evasion of immune attack[110,111].

The role of TAM-derived exosomes is now attracting more and more attention. Liu *et al*[112] found a role of exosomal miR-92a-2-5p derived from M2 macrophages in promoting HCC cell invasion. This process is mediated through the regulation of the AR/PHLPP/p-AKT/β-catenin signaling pathway by miR-92a-2-5p. Increased expression of miR-27a-3p and miR-660-5p in M2 macrophage-derived exosomes facilitates HCC development by downregulating thioredoxin-interacting protein and KLF Transcription Factor 3 (KLF3)[113,114]. Exosomes derived from TAMs exhibit a reduction of miR-125a and miR-125b expression, which have been proven to promote HCC cell proliferation, sphere cell formation, and metastasis. MiR-125a/b exerts inhibitory effects on the HCC proliferation and attenuates their stem cell-like characteristics by specifically targeting CD90, a recognized stem cell marker in HCC[115].

Modulating TAM exosomal miRNAs provides a new way to suppress HCC. A tumor suppressor miRNA, miR-375, which is enriched in exosomes from IL-2 modulated TAMs, can ameliorate HCC development[116]. Moreover, propofol can stimulate TAMs to secrete exosomes overexpressing miR-142-3p. When miR-142-3p exosomes are transferred to HCC cells, they can inhibit HCC cell invasion[117]. Conversely, M1 macrophages contribute to proinflammatory and anti-tumor effects. M1 macrophage-derived exosomal miR-628-5p suppresses HCC development by restraining the m6A modification of circFUT8[118]. Peripheral blood monocyte-derived exosomal miR-142 and miR-223 can directly inhibit the proliferation of HCC[119].

The exosomes from other immune cells are also involved in HCC. In mice, NK-exosomes rich in miR-223 inhibited carbon tetrachloride-induced liver fibrosis by inhibiting TGF-β1 induced HSC activation by directly targeting ATG7. Therefore, the overexpression of ATG7 in HSCs abolished the HSC activation-suppressive effect of NK cell exosomes [120]. Hepatitis C virus E2 envelope glycoprotein can stimulate mast cells, which in turn secrete a considerable amount of miR-490 enriched exosomes. When these exosomes are transferred into HCC cells, they inhibit tumor cell metastasis through the ERK1/2 pathway[121]. In addition, miR-150-5p and miR-142-3p can be transferred from regulatory T cells (Tregs) to dendritic cells *via* exosomes, resulting in the induction of a tolerant phenotype in these cells, characterized by elevated IL-10 production and decreased IL-6 production upon lipopolysaccharide stimulation[122].

On the other hand, tumor-derived exosomal miRNAs also affect the distribution and function of immune cells. Tregs constitute the most prominent subset of suppressor cells in the TME and release immunosuppressive factors, including IL-10 and TGF-β, contributing to tumor progression. Tregs also present various chemokine receptors and surface molecules like CTLA4 and PD-1, which make them susceptible to immune checkpoint inhibitor immunotherapy. The development of immune-related adverse events may partly be attributed to Treg destabilization[123]. Tumor cell-delivered miR-214 has the potential to augment the population of CD4+CD25highFoxp3+ Treg by reducing the expression of PTEN in CD4+ T cells, which results in the suppression of the host immune response and accelerates tumor development[124]. Indeed, the expansion of Treg populations through tumor-secreted miR-214 is believed to be a shared mechanism employed by various cancer cells to establish an immune-tolerant environment. This miRNA is crucial in modulating immune responses and promoting immune tolerance within the tumor microenvironment. Consequently, the inhibition of tumor-secreted miR-214 transportation to immune cells shows potential as an innovative approach to counteract tumor-induced immune tolerance[124].

In summary, exosome-delivered miRNAs from immune cells were intensely involved in the biological processes of HCC, and HCC-derived exosomal miRNAs also affect the distribution and function of immune cells.

CLINICAL APPLICATIONS OF EXOSOME-DELIVERED MIRNAS IN HCC

Radical resection and transarterial chemoembolization remain the most efficacious therapeutic approaches for patients with early-stage liver cancer. Still, the treatment efficacy remains unsatisfactory due to the compensatory effect of vascular proliferation after hypoxia[125,126]. For patients with advanced liver cancer, targeted therapy and traditional chemotherapy can only prolong the survival of these patients to a certain extent. Innovative and alternative therapies are

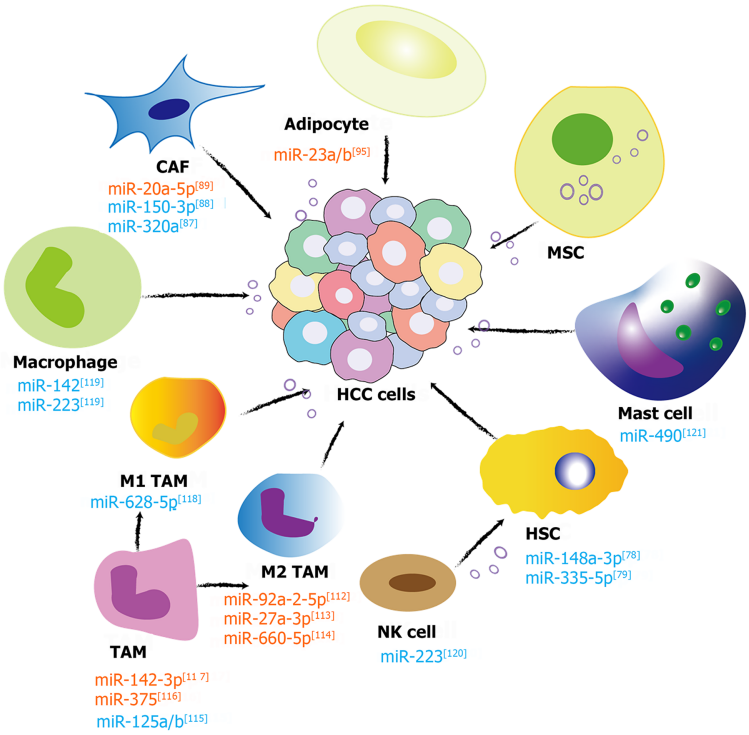

DOI: 10.3748/wjg.v29.i39.5435

Figure 1 Schematic of exosomal microRNAs in the tumor microenvironment of hepatocellular carcinoma. Orange represents the promoting effect of microRNA (miR) on hepatocellular carcinoma (HCC) proliferation, and blue represents the inhibitory effect of miR on HCC proliferation. CAF: Cancer-associated fibroblast; HSC: Hepatic stellate cell; MSC: Mesenchymal stem cell; NK: Natural killer; TAM: Tumor-associated macrophage.

continuously needed to improve the prognosis of HCC patients.

Studies have recently confirmed that specific miRNAs can be transported through exosomes, thereby controlling tumor growth and achieving therapeutic effects[127]. Since exosomes exhibit distinct characteristics as a vehicle for drug transport, encompassing diminished immunogenicity, enhanced biocompatibility, reduced toxicity, and the capacity to traverse the blood-brain barrier, exosomes have garnered considerable attention as an innate delivery vector for conveying miRNA molecules[128]. Among the various cell types recognized for their ability to produce exosomes, MSCs are a promising choice for the large-scale production of exosomes for drug delivery. It has been shown in regenerative medicine and tumor treatment studies that MSC-derived exosomes can serve as effective vehicles for drug delivery[129, 130]. Based on the above findings, engineered MSC-derived exosomes loaded with specific miRNAs present a novel therapeutic approach for HCC treatment.

Exosomal miRNAs have been utilized to enhance the chemosensitivity of tumor cells[131,132]. Recent research demonstrated that miR-122 overexpression could sensitize the response of HCC cells to chemotherapy drugs by suppressing multidrug resistance-associated genes, the anti-apoptotic gene *Bcl-w*, and the cell cycle-related gene cyclin B1 [47]. The miR-122 overexpression amniotic membrane MSCs (AMSCs) can effectively encapsulate miR-122 to secreted exosomes, which are in turn delivered to HCC cells and further increase the sensitivity of HCC cells to sorafenib[133]. The miR-199a loaded AMSC exosomes produced through miR-199a overexpression lentivirus infection and subsequent puromycin selection are able to potently transport miR-199a and enhance the sensitivity of HCC cells towards doxorubicin by specifically targeting the mTOR pathway. Furthermore, tumor tissue can be effectively targeted by AMSC exosomal miRNA-199a through intravenous injection, thereby enhancing the therapeutic effect of Dox on HCC *in vivo* [134].

Liver fibrosis is the precursor stage of cirrhosis and liver cancer. MSC-derived exosomes alleviated carbon tetrachloride-induced liver fibrosis in mice through the expression of miR-148a. MiR-148a directly targets KLF transcription factor 6 and successfully converts the M1 macrophages to M2 macrophages *in vitro* and liver fibrosis models [135]. *In vitro* studies have shown that transplanted human chorionic plate-derived MSCs reduce lung and liver fibrosis in murine models[136,137]. One study supported that chorionic plate-derived MSCs released exosomes containing miRNA-125b into hedgehog-responsive HSCs and restrained the activation of hedgehog signaling by blocking the expression of smoothened receptors, consequently reducing the severity of hepatic fibrosis[138]. As a new candidate therapeutic strategy, MSC exosomes have excellent application prospects for HCC.

In addition, human liver stem cell-derived exosomes are loaded with multiple antitumor miRNAs (miR451, miR223, miR24, miR31, miR214, and miR122), which can downregulate multi-drug resistance 1, migration inhibitory factor, ras-associated protein 14, and E2F transcription factor 1. These exosomes have been proven to be able to inhibit the growth of hepatoma cells both *in vitro* and *in vivo*[139].

Table 1 Function of exosomal microRNAs from interstitial cells in the liver

miRNA species in exosomes	Exosome secreting cells	Exosome isolation methods	Target cells	miRNA expression of exosome	Downstream targets	Functions of miRNA	Additional information	Ref.	Year
miR-148a-3p	Primary fibroblasts (the HSC cell line LX-2)	The ExoQuick-TC kit	Human HCC cell lines PLC, HCCLM3, and SMMC-7721	Reduced in the exosomes of HSCs after cocultivation with primary liver cancer-associated fibroblasts	ITGA5/PI3K/Akt axis	Inhibited HCC cell malignancy	Primary fibroblasts were isolated from primary HCC tumor and paired peritumor tissues in 17 primary HCC patient samples	[78]	2022
miR-335-5p	The HSC cell line LX-2	Ultracentrifugation	Human HCC cell lines MHCC97H, MHCC97L, HepG2, and Huh7	Reduced in the exosomes of fibroblasts as well as in HCC cells after cocultivation	CDC42? CDK2?	Inhibited neighboring cancer cell proliferation, invasion, and motility	-	[79]	2019
miR-320a	CAFs	Life Technology exosome precipitation solution	Human HCC cell lines MHCC97-H, SMMC-7721, Huh7, and the human normal liver cell line 7702	Reduced in the exosomes of CAFs derived from human HCC patients	PBX3	Inhibited HCC cell proliferation and metastasis ability	PAFs and CAFs derived from 6 pairs of matched primary hepatocarcinoma and adjacent tumor-free tissues (5 cm from the cut edge of the tumor edge)	[87]	2017
miR-150-3p	CAFs	0.22-μm PVDF filter and Total Exosome Isolation Reagent	Human HCC cell lines Huh7 and Hep3B	Decreased in CAF-derived exosomes	-	Inhibited HCC proliferation and metastasis	Stromal fibroblasts isolated from tumor tissue and adjacent (> 5 cm from the tumor edge) tissues from 6 HCC patients	[88]	2021
miR-20a-5p	CAFs	Centrifuged and filtered through a 0.22-μm PVDF membrane	Human HCC cell lines SMMC7721, Huh7, YY8103, Hep3B, Focus, HepG2, and HCCLM3 and a normal liver cell line MIHA, WRL68	Higher in exosomes from cancer tissues than in matched adjacent para-tumoral tissues	LIMA1	Contributed to HCC cell proliferation, metastasis, and EMT	CAFs were from the HCC tissues and NFs in paired adjacent normal tissues from 92 HCC patients	[89]	2022
miR-214	hCECs	Centrifuged and filtered through a 0.22-μm PVDF membrane and ultracentrifugation	Human HCC cell lines HepG2, Hep3B, the human liver epithelial cell line THLE-2	Lower levels in HCC cells than in normal human liver epithelial cells	P-gp/SF3B3	Reduced cancer cell viability and invasion compared with monotherapy with oxaliplatin or sorafenib	-	[103]	2021
miR-23a/b	Adipose cell mouse preadipocyte 3T3-L1 cells	Differential centrifugation	The human HCC cell lines BEL-7402 and BEL-7402/5-Fu murine hepatoma cell line Hepa1-6	High in exosomes from HCC patients with high BFR	VHL/HIF-1α	Promoted HCC cell growth and migration	Adipose cells were isolated from human tumor tissues from obese and nonobese patients	[95]	2019
miR-142,	Monocyte-derived	Microfiltration and	The human HCC	High when cocultured	STMN-1	Inhibited HCC	PBMCs were isolated from lymphocyte cones	[119]	2013

miR-223	macrophages; human acute monocytic leukemia THP-1, B-lymphoblastoid 721.221, and murine lymphoblast-like mastocytoma P815 cell lines	ultracentrifugation	cell lines Huh7 and HepG2	with HCC cells		proliferation	or fresh blood by density gradient centrifugation and were incubated for 2 h in plastic plates before the flask was washed intensively to remove any nonadherent cells. After 4 d of incubation in serum-free medium supplemented with 1% autologous serum, adherent cells were washed with PBS and cultured in standard DMEM-based medium for 3-6 extra days to generate monocyte-derived macrophages phenotyped to be $CD14^+$, $CD11a^+$, $CD3^-$, $CD56^-$, and $CD19^-$		
miR-490	Human MC line HMC-1 (treated with HCV-E2)	Total exosome separation reagent from Invitrogen	The human HCC cell lines HepG2 and HepG3b	High when HCV-E2-stimulated MC-derived exosomes were incubated with the two types of HCC cells for 24 h compared with the incubation with normal MC-derived exosomes	ERK1/2	Inhibited HCC proliferation		[121]	2017
miR-223	Human NK cell line NK92-MI	Differential centrifugation	The human HSC line LX-2	Higher in exosomes derived from NK cells than in parental NK-92MI cells	AGT7	Attenuated TGF-β1-induced HSC activation and inhibited liver fibrosis	LX-2 cells were treated with TGF-β1 (5 ng/mL) for 24 h to stimulate HSC activation. LX-2 cells in the exosomes derived from NK cells-treated groups were pretreated with exosomes derived from NK cells (10 μg/mL) before TGF-β1 treatment. LX-2 cells in the rapamycin-treated groups were pretreated with the autophagy activator rapamycin (2 mM) in DMSO for 12 h before TGF-β1 treatment	[120]	2020
miR-125a/b	TAMs	ExoQuick exosome precipitation solution	The human HCC cell lines Huh7, HepG2, and BEL-7404	Downregulated in exosomes from HCC-associated macrophages	CD90	Suppressed HCC cell growth and sphere formation	TAMs and nontumor macrophages were isolated from primary human HCC, adjacent nontumor liver tissues from 6 patients with HCC	[115]	2019
miR-628-5p	M1 macrophage	-	The human HCC cell lines Huh7, HCCLM3, Hep3B, and MHCC97H, immortalized human liver epithelial THLE-3 cell line	High in M1-exosomes	METTL14/circFUT4/CHMP14B	Inhibited HCC cell progression	THP-1 cells were differentiated into M0 macrophages by a 24 h incubation with 150 nM phorbol 12-myristate 13-acetate followed by a 24 h incubation in RPMI medium. M0 macrophages were polarized to M1 macrophages by incubation with 20 ng/mL IFN-γ and 10 pg/mL lipopolysaccharide	[118]	2022
miR-92a-2-5p	M2 macrophage (monocytic leukemia cell line THP-1)	Centrifuged and filtered through a 0.22-μm PVDF membrane and ultracentrifugation	Human liver cancer SK-HEP-1 and HepG2 cell lines, HA22T cell line, and murine HCC Hepa 1-6 cell line	Increased after coculture with liver cancer cells	AR/PHLPP/p-AKT/β-catenin signaling	Promoted HCC growth and invasiveness	To induce differentiation into macrophages, THP-1 cells were cultured with 100 ng/mL PMA (Sigma) for 48 h, and the macrophage was cultured with the addition of DMSO to promote M2 polarization	[112]	2020
miR-660-5p	M2 macrophage	Differential centrifu-	Human HCC cell	High	KLF3	Augmented the	THP-1 monocytes were stimulated by 100 ng	[114]	2021

	(monocytic leukemia cell line THP-1)	gation	lines HepG2 and Bel-7402			tumorigenic ability of HCC cells	of phorbol 12-myristate 13-acetate (Sigma-Aldrich, MO, United States) for 48 h, thus differentiating into M0 macrophages. Then, M0 macrophages were treated with 20 ng/mL interleukin 4 (AF-200–04-5, PeproTech, NJ, United States) for 72 h to polarize into M2 macrophages		
miR-27a-3p	M2 macrophage (monocytic leukemia cell line THP-1)	SBI ExoQuick-TC Kit	Human HCC cell lines Huh7, 97H, HepG2, LM3, and SMMC-7721	-	TXNIP	Induced the cancer stemness of HCC	Differentiation of THP-1 cells to macrophages was performed using 200 ng/mL phorbol myristic acetate, and the cells were then cultured with 20 ng/mL interleukin-4 for 72 h to induce M2-type polarization	[113]	2021
miR-142-3p	TAMs treated by propofol (the murine macrophage cell line Raw 264.7 cells)	Differential centrifu-gation	The murine HCC cell line Hepa1-6	Dose-dependent increase when treated with propofol	RAC1	Enhanced the antitumor activity of propofol	Raw 264.7 cells were cultured in complete RPMI 1640 with 10% FBS and treated with propofol (dissolved in RPMI 1640) in complete medium. TAMs were isolated from tumor-bearing mice treated with 0 mg/kg, 20 mg/kg, and 50 mg/kg propofol by i.p. injection	[117]	2014
miR-375	TAMs (IL-2 induced)	Total exosome isolation reagent	The human HCC cell lines HepG2 and QJY–7703	High	-	Ameliorated HCC development and progression	Primary human HCC specimens were collected from patients who suffered from hepatectomy. The macrophages were isolated and cultured by Percoll (GE Healthcare) density gradient centrifugation. TAMs were treated with IL-2 for 24 h before the supernatants were collected. The treatment concentration was 20 ng/mL	[116]	2022

AGT7: Autophagy-related 7; AR: Androgen receptor; BFR: Body fat ratio; CAFs: Cancer-associated fibroblasts; CDC42: Cell division cycle 42; CDK2: Cyclin dependent kinase 2; EMT: Epithelial-mesenchymal transition; ERK1/2: Extracellular regulated protein kinases 1/2; Exos: Exosomes; HCC: Hepatocellular carcinoma; hCECs: Human cerebral endothelial cells; HCV-E2: Hepatitis C virus E2 envelope glycoprotein; HIF-1α: Hypoxia-inducible factor 1α; HSCs: Hepatic stellate cells; i.p.: Intraperitoneal; ITGA5: Integrin α5; KLF3: Kruppel-like factor 3; LIMA1: LIM domain and actin binding 1; MCs: Mast cells; METTL14: Methyltransferase-like 14; miR: MicroRNA; NK: Natural killer; PAFs: Paraneoplastic fibroblasts; PBMCs: Peripheral blood mononuclear cells; PBX3: Pre-B-cell leukemia homeobox 3; P-gp: P-glycoprotein; PI3K: Phosphoinositide 3-kinase; RAC1: Rac family small GTPase 1; SF3B3: Splicing factor 3b subunit 3; STMN1: Stathmin-1; TAMs: Tumor-associated macrophages; TXNIP: thioredoxin-interacting protein; VHL: Von Hippel-Lindau.

CONCLUSION

Despite significant advances in diagnosis and therapeutics, HCC remains exceedingly fatal. In most cases, HCC develops from chronic liver inflammation, which provides a tumor-promoting microenvironment composed of immune and stromal cells. As a novel cellular communicator in TME, exosomes mediate the intricate interaction of nonparenchymal cells (including immune and stromal cells) with cancer cells. They are involved in the etiology of HCC and multiple processes related to tumor initiation, development, metastasis, and drug resistance. Exosome cargoes, especially miRNAs, are key communication factors in the complicated cross-talk, indicating that they are promising prognostic markers and therapeutic targets for HCC. In this review, we emphasized the function and mechanism of exosomal miRNAs from nonparenchymal cells for the initiation and malignant progression of HCC. Also, we introduced the influences of exosomal miRNAs delivered by tumor cells on nonparenchymal cells. The functions of the exosomal miRNAs in HCC were also summarized (Table 1). Finally, the therapeutic potential of exosomes for HCC was discussed. With the

development of nanoengineering technology, exosomes can be modified to carry specific miRNAs and target specific cells, thus enabling precision and individualized treatment of HCC.

Although significant progress has been achieved in elucidating the functions of exosomes and their miRNA cargoes in HCC, some challenges remain. Sometimes, different investigators reported different experimental observations for the same exosomal miRNAs. The inconsistency of experimental subjects and study designs might cause these discrepancies. Therefore, factors such as the environment, age and sex of the subjects, cause of HCC occurrence, and data collection from multiple centers should be considered to produce more accurate results. Moreover, different techniques can lead to the isolation of varied subtypes of extracellular vesicles, each exhibiting unique miRNA profiles, protein compositions, and biological functions[140-142]. In clinical applications, problems include low targeting efficiency and easily phagocytosed by the immune system. The exosome separation and purification method also have limitations and could be time-consuming and laborious. Therefore, further research must be done to address these problems and determine more feasible and effective clinical translational applications of exosomes. The integration of nanoengineering and molecular biology allows for the utilization of exosome-mediated miRNAs in precision nanomedicine, presenting novel approaches for the diagnosis and treatment of HCC.

ACKNOWLEDGEMENTS

The authors would like to thank the anonymous reviewers whose feedback substantially improved the quality of this article.

FOOTNOTES

Author contributions: Ji JL designed the review; Wang HC and Ji JL drafted the paper; Wang HC prepared the figure; Yin WX, Jiang M, Han JY, and Sun YF researched the background of the study; Ji JL, Kuai XW, and Sun R reviewed and revised the paper; all authors read and approved the final manuscript.

Supported by the National Natural Science Foundation of China, No. 81761128018 and No. 81572871; the Natural Science Foundation of Jiangsu Province, No. BK20151277; and the Undergraduate Training Programs for Innovation and Entrepreneurship of Jiangsu Province, No. 202110304035Z.

Conflict-of-interest statement: The authors declare having no conflicts of interest for this article.

Country/Territory of origin: China

ORCID number: Hai-Chen Wang 0000-0003-0352-630X; Wen-Xuan Yin 0000-0002-2266-7514; Meng Jiang 0000-0003-2070-0082; Jia-Yi Han 0000-0001-7983-6844; Xing-Wang Kuai 0000-0003-0527-7108; Yu-Feng Sun 0000-0003-3873-175X; Ju-Ling Ji 0000-0001-6500-8052.

S-Editor: Yan JP
L-Editor: Filipodia
P-Editor: Cai YX

REFERENCES

1 **Sung H**, Ferlay J, Siegel RL, Laversanne M, Soerjomataram I, Jemal A, Bray F. Global Cancer Statistics 2020: GLOBOCAN Estimates of Incidence and Mortality Worldwide for 36 Cancers in 185 Countries. *CA Cancer J Clin* 2021; **71**: 209-249 [PMID: 33538338 DOI: 10.3322/caac.21660]

2 **Rumgay H**, Ferlay J, de Martel C, Georges D, Ibrahim AS, Zheng R, Wei W, Lemmens VEPP, Soerjomataram I. Global, regional and national burden of primary liver cancer by subtype. *Eur J Cancer* 2022; **161**: 108-118 [PMID: 34942552 DOI: 10.1016/j.ejca.2021.11.023]

3 **Villanueva A**. Hepatocellular Carcinoma. *N Engl J Med* 2019; **380**: 1450-1462 [PMID: 30970190 DOI: 10.1056/NEJMra1713263]

4 **Anderson NM**, Simon MC. The tumor microenvironment. *Curr Biol* 2020; **30**: R921-R925 [PMID: 32810447 DOI: 10.1016/j.cub.2020.06.081]

5 **Lu C**, Rong D, Zhang B, Zheng W, Wang X, Chen Z, Tang W. Current perspectives on the immunosuppressive tumor microenvironment in hepatocellular carcinoma: challenges and opportunities. *Mol Cancer* 2019; **18**: 130 [PMID: 31464625 DOI: 10.1186/s12943-019-1047-6]

6 **Wu Q**, Zhou L, Lv D, Zhu X, Tang H. Exosome-mediated communication in the tumor microenvironment contributes to hepatocellular carcinoma development and progression. *J Hematol Oncol* 2019; **12**: 53 [PMID: 31142326 DOI: 10.1186/s13045-019-0739-0]

7 **Luo C**, Xin H, Zhou Z, Hu Z, Sun R, Yao N, Sun Q, Borjigin U, Wu X, Fan J, Huang X, Zhou S, Zhou J. Tumor-derived exosomes induce immunosuppressive macrophages to foster intrahepatic cholangiocarcinoma progression. *Hepatology* 2022; **76**: 982-999 [PMID: 35106794

DOI: 10.1002/hep.32387]

8 **Martínez-Reyes I**, Chandel NS. Cancer metabolism: looking forward. *Nat Rev Cancer* 2021; **21**: 669-680 [PMID: 34272515 DOI: 10.1038/s41568-021-00378-6]

9 **Théry C**, Witwer KW, Aikawa E, Alcaraz MJ, Anderson JD, Andriantsitohaina R, Antoniou A, Arab T, Archer F, Atkin-Smith GK, Ayre DC, Bach JM, Bachurski D, Baharvand H, Balaj L, Baldacchino S, Bauer NN, Baxter AA, Bebawy M, Beckham C, Bedina Zavec A, Benmoussa A, Berardi AC, Bergese P, Bielska E, Blenkiron C, Bobis-Wozowicz S, Boilard E, Boireau W, Bongiovanni A, Borràs FE, Bosch S, Boulanger CM, Breakefield X, Breglio AM, Brennan MÁ, Brigstock DR, Brisson A, Broekman ML, Bromberg JF, Bryl-Górecka P, Buch S, Buck AH, Burger D, Busatto S, Buschmann D, Bussolati B, Buzás EI, Byrd JB, Camussi G, Carter DR, Caruso S, Chamley LW, Chang YT, Chen C, Chen S, Cheng L, Chin AR, Clayton A, Clerici SP, Cocks A, Cocucci E, Coffey RJ, Cordeiro-da-Silva A, Couch Y, Coumans FA, Coyle B, Crescitelli R, Criado MF, D'Souza-Schorey C, Das S, Datta Chaudhuri A, de Candia P, De Santana EF, De Wever O, Del Portillo HA, Demaret T, Deville S, Devitt A, Dhondt B, Di Vizio D, Dieterich LC, Dolo V, Dominguez Rubio AP, Dominici M, Dourado MR, Driedonks TA, Duarte FV, Duncan HM, Eichenberger RM, Ekström K, El Andaloussi S, Elie-Caille C, Erdbrügger U, Falcón-Pérez JM, Fatima F, Fish JE, Flores-Bellver M, Försönits A, Frelet-Barrand A, Fricke F, Fuhrmann G, Gabrielsson S, Gámez-Valero A, Gardiner C, Gärtner K, Gaudin R, Gho YS, Giebel B, Gilbert C, Gimona M, Giusti I, Goberdhan DC, Görgens A, Gorski SM, Greening DW, Gross JC, Gualerzi A, Gupta GN, Gustafson D, Handberg A, Haraszti RA, Harrison P, Hegyesi H, Hendrix A, Hill AF, Hochberg FH, Hoffmann KF, Holder B, Holthofer H, Hosseinkhani B, Hu G, Huang Y, Huber V, Hunt S, Ibrahim AG, Ikezu T, Inal JM, Isin M, Ivanova A, Jackson HK, Jacobsen S, Jay SM, Jayachandran M, Jenster G, Jiang L, Johnson SM, Jones JC, Jong A, Jovanovic-Talisman T, Jung S, Kalluri R, Kano SI, Kaur S, Kawamura Y, Keller ET, Khamari D, Khomyakova E, Khvorova A, Kierulf P, Kim KP, Kislinger T, Klingeborn M, Klinke DJ 2nd, Kornek M, Kosanović MM, Kovács ÁF, Krämer-Albers EM, Krasemann S, Krause M, Kurochkin IV, Kusuma GD, Kuypers S, Laitinen S, Langevin SM, Languino LR, Lannigan J, Lässer C, Laurent LC, Lavieu G, Lázaro-Ibáñez E, Le Lay S, Lee MS, Lee YXF, Lemos DS, Lenassi M, Leszczynska A, Li IT, Liao K, Libregts SF, Ligeti E, Lim R, Lim SK, Linē A, Linnemannstöns K, Llorente A, Lombard CA, Lorenowicz MJ, Lörincz ÁM, Lötvall J, Lovett J, Lowry MC, Loyer X, Lu Q, Lukomska B, Lunavat TR, Maas SL, Malhi H, Marcilla A, Mariani J, Mariscal J, Martens-Uzunova ES, Martin-Jaular L, Martinez MC, Martins VR, Mathieu M, Mathivanan S, Maugeri M, McGinnis LK, McVey MJ, Meckes DG Jr, Meehan KL, Mertens I, Minciacchi VR, Möller A, Møller Jørgensen M, Morales-Kastresana A, Morhayim J, Mullier F, Muraca M, Musante L, Mussack V, Muth DC, Myburgh KH, Najrana T, Nawaz M, Nazarenko I, Nejsum P, Neri C, Neri T, Nieuwland R, Nimrichter L, Nolan JP, Nolte-'t Hoen EN, Noren Hooten N, O'Driscoll L, O'Grady T, O'Loghlen A, Ochiya T, Olivier M, Ortiz A, Ortiz LA, Osteikoetxea X, Østergaard O, Ostrowski M, Park J, Pegtel DM, Peinado H, Perut F, Pfaffl MW, Phinney DG, Pieters BC, Pink RC, Pisetsky DS, Pogge von Strandmann E, Polakovicova I, Poon IK, Powell BH, Prada I, Pulliam L, Quesenberry P, Radeghieri A, Raffai RL, Raimondo S, Rak J, Ramirez MI, Raposo G, Rayyan MS, Regev-Rudzki N, Ricklefs FL, Robbins PD, Roberts DD, Rodrigues SC, Rohde E, Rome S, Rouschop KM, Rughetti A, Russell AE, Saá P, Sahoo S, Salas-Huenuleo E, Sánchez C, Saugstad JA, Saul MJ, Schiffelers RM, Schneider R, Schøyen TH, Scott A, Shahaj E, Sharma S, Shatnyeva O, Shekari F, Shelke GV, Shetty AK, Shiba K, Siljander PR, Silva AM, Skowronek A, Snyder OL 2nd, Soares RP, Sódar BW, Soekmadji C, Sotillo J, Stahl PD, Stoorvogel W, Stott SL, Strasser EF, Swift S, Tahara H, Tewari M, Timms K, Tiwari S, Tixeira R, Tkach M, Toh WS, Tomasini R, Torrecilhas AC, Tosar JP, Toxavidis V, Urbanelli L, Vader P, van Balkom BW, van der Grein SG, Van Deun J, van Herwijnen MJ, Van Keuren-Jensen K, van Niel G, van Royen ME, van Wijnen AJ, Vasconcelos MH, Vechetti IJ Jr, Veit TD, Vella LJ, Velot É, Verweij FJ, Vestad B, Viñas JL, Visnovitz T, Vukman KV, Wahlgren J, Watson DC, Wauben MH, Weaver A, Webber JP, Weber V, Wehman AM, Weiss DJ, Welsh JA, Wendt S, Wheelock AM, Wiener Z, Witte L, Wolfram J, Xagorari A, Xander P, Xu J, Yan X, Yáñez-Mó M, Yin H, Yuana Y, Zappulli V, Zarubova J, Žėkas V, Zhang JY, Zhao Z, Zheng L, Zheutlin AR, Zickler AM, Zimmermann P, Zivkovic AM, Zocco D, Zuba-Surma EK. Minimal information for studies of extracellular vesicles 2018 (MISEV2018): a position statement of the International Society for Extracellular Vesicles and update of the MISEV2014 guidelines. *J Extracell Vesicles* 2018; **7**: 1535750 [PMID: 30637094 DOI: 10.1080/20013078.2018.1535750]

10 **Isaac R**, Reis FCG, Ying W, Olefsky JM. Exosomes as mediators of intercellular crosstalk in metabolism. *Cell Metab* 2021; **33**: 1744-1762 [PMID: 34496230 DOI: 10.1016/j.cmet.2021.08.006]

11 **Krylova SV**, Feng D. The Machinery of Exosomes: Biogenesis, Release, and Uptake. *Int J Mol Sci* 2023; **24** [PMID: 36674857 DOI: 10.3390/ijms24021337]

12 **Johnstone RM**, Adam M, Hammond JR, Orr L, Turbide C. Vesicle formation during reticulocyte maturation. Association of plasma membrane activities with released vesicles (exosomes). *J Biol Chem* 1987; **262**: 9412-9420 [PMID: 3597417]

13 **Kalluri R**, LeBleu VS. The biology, function, and biomedical applications of exosomes. *Science* 2020; **367** [PMID: 32029601 DOI: 10.1126/science.aau6977]

14 **Raposo G**, Nijman HW, Stoorvogel W, Liejendekker R, Harding CV, Melief CJ, Geuze HJ. B lymphocytes secrete antigen-presenting vesicles. *J Exp Med* 1996; **183**: 1161-1172 [PMID: 8642258 DOI: 10.1084/jem.183.3.1161]

15 **Rak J**. Microparticles in cancer. *Semin Thromb Hemost* 2010; **36**: 888-906 [PMID: 21049390 DOI: 10.1055/s-0030-1267043]

16 **Hood JL**, San RS, Wickline SA. Exosomes released by melanoma cells prepare sentinel lymph nodes for tumor metastasis. *Cancer Res* 2011; **71**: 3792-3801 [PMID: 21478294 DOI: 10.1158/0008-5472.CAN-10-4455]

17 **Zhang L**, Yu D. Exosomes in cancer development, metastasis, and immunity. *Biochim Biophys Acta Rev Cancer* 2019; **1871**: 455-468 [PMID: 31047959 DOI: 10.1016/j.bbcan.2019.04.004]

18 **Rupaimoole R**, Slack FJ. MicroRNA therapeutics: towards a new era for the management of cancer and other diseases. *Nat Rev Drug Discov* 2017; **16**: 203-222 [PMID: 28209991 DOI: 10.1038/nrd.2016.246]

19 **Kim SB**. Function and therapeutic development of exosomes for cancer therapy. *Arch Pharm Res* 2022; **45**: 295-308 [PMID: 35604532 DOI: 10.1007/s12272-022-01387-1]

20 **Krol J**, Loedige I, Filipowicz W. The widespread regulation of microRNA biogenesis, function and decay. *Nat Rev Genet* 2010; **11**: 597-610 [PMID: 20661255 DOI: 10.1038/nrg2843]

21 **Valadi H**, Ekström K, Bossios A, Sjöstrand M, Lee JJ, Lötvall JO. Exosome-mediated transfer of mRNAs and microRNAs is a novel mechanism of genetic exchange between cells. *Nat Cell Biol* 2007; **9**: 654-659 [PMID: 17486113 DOI: 10.1038/ncb1596]

22 **Qiu S**, Xie L, Lu C, Gu C, Xia Y, Lv J, Xuan Z, Fang L, Yang J, Zhang L, Li Z, Wang W, Xu H, Li B, Xu Z. Gastric cancer-derived exosomal miR-519a-3p promotes liver metastasis by inducing intrahepatic M2-like macrophage-mediated angiogenesis. *J Exp Clin Cancer Res* 2022; **41**: 296 [PMID: 36217165 DOI: 10.1186/s13046-022-02499-8]

23 **Nallasamy P**, Nimmakayala RK, Parte S, Are AC, Batra SK, Ponnusamy MP. Tumor microenvironment enriches the stemness features: the architectural event of therapy resistance and metastasis. *Mol Cancer* 2022; **21**: 225 [PMID: 36550571 DOI: 10.1186/s12943-022-01682-x]

24 **Yuan X**, Qian N, Ling S, Li Y, Sun W, Li J, Du R, Zhong G, Liu C, Yu G, Cao D, Liu Z, Wang Y, Qi Z, Yao Y, Wang F, Liu J, Hao S, Jin X,

Zhao Y, Xue J, Zhao D, Gao X, Liang S, Song J, Yu S. Breast cancer exosomes contribute to pre-metastatic niche formation and promote bone metastasis of tumor cells. *Theranostics* 2021; **11**: 1429-1445 [PMID: 33391543 DOI: 10.7150/thno.45351]

25 **Chen B**, Sang Y, Song X, Zhang D, Wang L, Zhao W, Liang Y, Zhang N, Yang Q. Exosomal miR-500a-5p derived from cancer-associated fibroblasts promotes breast cancer cell proliferation and metastasis through targeting USP28. *Theranostics* 2021; **11**: 3932-3947 [PMID: 33664871 DOI: 10.7150/thno.53412]

26 **Han QF**, Li WJ, Hu KS, Gao J, Zhai WL, Yang JH, Zhang SJ. Exosome biogenesis: machinery, regulation, and therapeutic implications in cancer. *Mol Cancer* 2022; **21**: 207 [PMID: 36320056 DOI: 10.1186/s12943-022-01671-0]

27 **Tan S**, Xia L, Yi P, Han Y, Tang L, Pan Q, Tian Y, Rao S, Oyang L, Liang J, Lin J, Su M, Shi Y, Cao D, Zhou Y, Liao Q. Exosomal miRNAs in tumor microenvironment. *J Exp Clin Cancer Res* 2020; **39**: 67 [PMID: 32299469 DOI: 10.1186/s13046-020-01570-6]

28 **Shao H**, Im H, Castro CM, Breakefield X, Weissleder R, Lee H. New Technologies for Analysis of Extracellular Vesicles. *Chem Rev* 2018; **118**: 1917-1950 [PMID: 29384376 DOI: 10.1021/acs.chemrev.7b00534]

29 **Han J**, Zhang Y, Ge P, Dakal TC, Wen H, Tang S, Luo Y, Yang Q, Hua B, Zhang G, Chen H, Xu C. Exosome-derived CIRP: An amplifier of inflammatory diseases. *Front Immunol* 2023; **14**: 1066721 [PMID: 36865547 DOI: 10.3389/fimmu.2023.1066721]

30 **Sun Z**, Shi K, Yang S, Liu J, Zhou Q, Wang G, Song J, Li Z, Zhang Z, Yuan W. Effect of exosomal miRNA on cancer biology and clinical applications. *Mol Cancer* 2018; **17**: 147 [PMID: 30309355 DOI: 10.1186/s12943-018-0897-7]

31 **Fei X**, Li Z, Yang D, Kong X, Lu X, Shen Y, Li X, Xie S, Wang J, Zhao Y, Sun Y, Zhang J, Ye Z, Cai Z. Neddylation of Coro1a determines the fate of multivesicular bodies and biogenesis of extracellular vesicles. *J Extracell Vesicles* 2021; **10**: e12153 [PMID: 34623756 DOI: 10.1002/jev2.12153]

32 **Lee YJ**, Shin KJ, Jang HJ, Ryu JS, Lee CY, Yoon JH, Seo JK, Park S, Lee S, Je AR, Huh YH, Kong SY, Kwon T, Suh PG, Chae YC. GPR143 controls ESCRT-dependent exosome biogenesis and promotes cancer metastasis. *Dev Cell* 2023; **58**: 320-334 [PMID: 36800996 DOI: 10.1016/j.devcel.2023.01.006]

33 **Shinde SR**, Mick DU, Aoki E, Rodrigues RB, Gygi SP, Nachury MV. The ancestral ESCRT protein TOM1L2 selects ubiquitinated cargoes for retrieval from cilia. *Dev Cell* 2023; **58**: 677-693.e9 [PMID: 37019113 DOI: 10.1016/j.devcel.2023.03.003]

34 **Hirsova P**, Ibrahim SH, Verma VK, Morton LA, Shah VH, LaRusso NF, Gores GJ, Malhi H. Extracellular vesicles in liver pathobiology: Small particles with big impact. *Hepatology* 2016; **64**: 2219-2233 [PMID: 27628960 DOI: 10.1002/hep.28814]

35 **Yokoi A**, Yoshioka Y, Yamamoto Y, Ishikawa M, Ikeda SI, Kato T, Kiyono T, Takeshita F, Kajiyama H, Kikkawa F, Ochiya T. Malignant extracellular vesicles carrying MMP1 mRNA facilitate peritoneal dissemination in ovarian cancer. *Nat Commun* 2017; **8**: 14470 [PMID: 28262727 DOI: 10.1038/ncomms14470]

36 **Wang Y**, Balaji V, Kaniyappan S, Krüger L, Irsen S, Tepper K, Chandupatla R, Maetzler W, Schneider A, Mandelkow E, Mandelkow EM. The release and trans-synaptic transmission of Tau *via* exosomes. *Mol Neurodegener* 2017; **12**: 5 [PMID: 28086931 DOI: 10.1186/s13024-016-0143-y]

37 **Chivet M**, Javalet C, Hemming F, Pernet-Gallay K, Laulagnier K, Fraboulet S, Sadoul R. Exosomes as a novel way of interneuronal communication. *Biochem Soc Trans* 2013; **41**: 241-244 [PMID: 23356290 DOI: 10.1042/BST20120266]

38 **Kowal J**, Arras G, Colombo M, Jouve M, Morath JP, Primdal-Bengtson B, Dingli F, Loew D, Tkach M, Théry C. Proteomic comparison defines novel markers to characterize heterogeneous populations of extracellular vesicle subtypes. *Proc Natl Acad Sci U S A* 2016; **113**: E968-E977 [PMID: 26858453 DOI: 10.1073/pnas.1521230113]

39 **Pužar Dominkuš P**, Stenovec M, Sitar S, Lasič E, Zorec R, Plemenitaš A, Žagar E, Kreft M, Lenassi M. PKH26 labeling of extracellular vesicles: Characterization and cellular internalization of contaminating PKH26 nanoparticles. *Biochim Biophys Acta Biomembr* 2018; **1860**: 1350-1361 [PMID: 29551275 DOI: 10.1016/j.bbamem.2018.03.013]

40 **Mathivanan S**, Lim JW, Tauro BJ, Ji H, Moritz RL, Simpson RJ. Proteomics analysis of A33 immunoaffinity-purified exosomes released from the human colon tumor cell line LIM1215 reveals a tissue-specific protein signature. *Mol Cell Proteomics* 2010; **9**: 197-208 [PMID: 19837982 DOI: 10.1074/mcp.M900152-MCP200]

41 **Ruan Z**, Liang Y, Chen Z, Yin J, Li C, Pan P, Zhang Q, Wu J, Luo Z. Enterovirus 71 non-structural protein 3A hijacks vacuolar protein sorting 25 to boost exosome biogenesis to facilitate viral replication. *Front Microbiol* 2022; **13**: 1024899 [PMID: 36274707 DOI: 10.3389/fmicb.2022.1024899]

42 **Lin H**, Zhang R, Wu W, Lei L. miR-4454 Promotes Hepatic Carcinoma Progression by Targeting Vps4A and Rab27A. *Oxid Med Cell Longev* 2021; **2021**: 9230435 [PMID: 34777698 DOI: 10.1155/2021/9230435]

43 **Kogure T**, Lin WL, Yan IK, Braconi C, Patel T. Intercellular nanovesicle-mediated microRNA transfer: a mechanism of environmental modulation of hepatocellular cancer cell growth. *Hepatology* 2011; **54**: 1237-1248 [PMID: 21721029 DOI: 10.1002/hep.24504]

44 **Wang S**, Xu M, Li X, Su X, Xiao X, Keating A, Zhao RC. Exosomes released by hepatocarcinoma cells endow adipocytes with tumor-promoting properties. *J Hematol Oncol* 2018; **11**: 82 [PMID: 29898759 DOI: 10.1186/s13045-018-0625-1]

45 **Zhang H**, Deng T, Liu R, Ning T, Yang H, Liu D, Zhang Q, Lin D, Ge S, Bai M, Wang X, Zhang L, Li H, Yang Y, Ji Z, Wang H, Ying G, Ba Y. CAF secreted miR-522 suppresses ferroptosis and promotes acquired chemo-resistance in gastric cancer. *Mol Cancer* 2020; **19**: 43 [PMID: 32106859 DOI: 10.1186/s12943-020-01168-8]

46 **Bandiera S**, Pfeffer S, Baumert TF, Zeisel MB. miR-122--a key factor and therapeutic target in liver disease. *J Hepatol* 2015; **62**: 448-457 [PMID: 25308172 DOI: 10.1016/j.jhep.2014.10.004]

47 **Xu Y**, Xia F, Ma L, Shan J, Shen J, Yang Z, Liu J, Cui Y, Bian X, Bie P, Qian C. MicroRNA-122 sensitizes HCC cancer cells to adriamycin and vincristine through modulating expression of MDR and inducing cell cycle arrest. *Cancer Lett* 2011; **310**: 160-169 [PMID: 21802841 DOI: 10.1016/j.canlet.2011.06.027]

48 **Girard M**, Jacquemin E, Munnich A, Lyonnet S, Henrion-Caude A. miR-122, a paradigm for the role of microRNAs in the liver. *J Hepatol* 2008; **48**: 648-656 [PMID: 18291553 DOI: 10.1016/j.jhep.2008.01.019]

49 **Basu S**, Bhattacharyya SN. Insulin-like growth factor-1 prevents miR-122 production in neighbouring cells to curtail its intercellular transfer to ensure proliferation of human hepatoma cells. *Nucleic Acids Res* 2014; **42**: 7170-7185 [PMID: 24813441 DOI: 10.1093/nar/gku346]

50 **Chiba M**, Kimura M, Asari S. Exosomes secreted from human colorectal cancer cell lines contain mRNAs, microRNAs and natural antisense RNAs, that can transfer into the human hepatoma HepG2 and lung cancer A549 cell lines. *Oncol Rep* 2012; **28**: 1551-1558 [PMID: 22895844 DOI: 10.3892/or.2012.1967]

51 **Zeng Z**, Li Y, Pan Y, Lan X, Song F, Sun J, Zhou K, Liu X, Ren X, Wang F, Hu J, Zhu X, Yang W, Liao W, Li G, Ding Y, Liang L. Cancer-derived exosomal miR-25-3p promotes pre-metastatic niche formation by inducing vascular permeability and angiogenesis. *Nat Commun* 2018; **9**: 5395 [PMID: 30568162 DOI: 10.1038/s41467-018-07810-w]

52 **Sun H**, Meng Q, Shi C, Yang H, Li X, Wu S, Familiari G, Relucenti M, Aschner M, Wang X, Chen R. Hypoxia-Inducible Exosomes Facilitate Liver-Tropic Premetastatic Niche in Colorectal Cancer. *Hepatology* 2021; **74**: 2633-2651 [PMID: 34110633 DOI: 10.1002/hep.32009]

53 **Xie Z**, Gao Y, Ho C, Li L, Jin C, Wang X, Zou C, Mao Y, Li Q, Fu D, Zhang YF. Exosome-delivered CD44v6/C1QBP complex drives pancreatic cancer liver metastasis by promoting fibrotic liver microenvironment. *Gut* 2022; **71**: 568-579 [PMID: 33827783 DOI: 10.1136/gutjnl-2020-323014]

54 **Xie KL**, Zhang YG, Liu J, Zeng Y, Wu H. MicroRNAs associated with HBV infection and HBV-related HCC. *Theranostics* 2014; **4**: 1176-1192 [PMID: 25285167 DOI: 10.7150/thno.8715]

55 **Wang X**, He Y, Mackowiak B, Gao B. MicroRNAs as regulators, biomarkers and therapeutic targets in liver diseases. *Gut* 2021; **70**: 784-795 [PMID: 33127832 DOI: 10.1136/gutjnl-2020-322526]

56 **Hochreuter MY**, Dall M, Treebak JT, Barrès R. MicroRNAs in non-alcoholic fatty liver disease: Progress and perspectives. *Mol Metab* 2022; **65**: 101581 [PMID: 36028120 DOI: 10.1016/j.molmet.2022.101581]

57 **Sarnow P**, Sagan SM. Unraveling the Mysterious Interactions Between Hepatitis C Virus RNA and Liver-Specific MicroRNA-122. *Annu Rev Virol* 2016; **3**: 309-332 [PMID: 27578438 DOI: 10.1146/annurev-virology-110615-042409]

58 **Wang S**, Qiu L, Yan X, Jin W, Wang Y, Chen L, Wu E, Ye X, Gao GF, Wang F, Chen Y, Duan Z, Meng S. Loss of microRNA 122 expression in patients with hepatitis B enhances hepatitis B virus replication through cyclin G(1) -modulated P53 activity. *Hepatology* 2012; **55**: 730-741 [PMID: 22105316 DOI: 10.1002/hep.24809]

59 **Pirola CJ**, Fernández Gianotti T, Castaño GO, Mallardi P, San Martino J, Mora Gonzalez Lopez Ledesma M, Flichman D, Mirshahi F, Sanyal AJ, Sookoian S. Circulating microRNA signature in non-alcoholic fatty liver disease: from serum non-coding RNAs to liver histology and disease pathogenesis. *Gut* 2015; **64**: 800-812 [PMID: 24973316 DOI: 10.1136/gutjnl-2014-306996]

60 **Gu Y**, Wei X, Sun Y, Gao H, Zheng X, Wong LL, Jin L, Liu N, Hernandez B, Peplowska K, Zhao X, Zhan QM, Feng XH, Tang ZY, Ji J. miR-192-5p Silencing by Genetic Aberrations Is a Key Event in Hepatocellular Carcinomas with Cancer Stem Cell Features. *Cancer Res* 2019; **79**: 941-953 [PMID: 30530815 DOI: 10.1158/0008-5472.CAN-18-1675]

61 **Wang B**, Majumder S, Nuovo G, Kutay H, Volinia S, Patel T, Schmittgen TD, Croce C, Ghoshal K, Jacob ST. Role of microRNA-155 at early stages of hepatocarcinogenesis induced by choline-deficient and amino acid-defined diet in C57BL/6 mice. *Hepatology* 2009; **50**: 1152-1161 [PMID: 19711427 DOI: 10.1002/hep.23100]

62 **Zhang Y**, Wei W, Cheng N, Wang K, Li B, Jiang X, Sun S. Hepatitis C virus-induced up-regulation of microRNA-155 promotes hepatocarcinogenesis by activating Wnt signaling. *Hepatology* 2012; **56**: 1631-1640 [PMID: 22610915 DOI: 10.1002/hep.25849]

63 **Calvente CJ**, Tameda M, Johnson CD, Del Pilar H, Lin YC, Adronikou N, De Mollerat Du Jeu X, Llorente C, Boyer J, Feldstein AE. Neutrophils contribute to spontaneous resolution of liver inflammation and fibrosis *via* microRNA-223. *J Clin Invest* 2019; **129**: 4091-4109 [PMID: 31295147 DOI: 10.1172/JCI122258]

64 **Li M**, He Y, Zhou Z, Ramirez T, Gao Y, Ross RA, Cao H, Cai Y, Xu M, Feng D, Zhang P, Liangpunsakul S, Gao B. MicroRNA-223 ameliorates alcoholic liver injury by inhibiting the IL-6-p47(phox)-oxidative stress pathway in neutrophils. *Gut* 2017; **66**: 705-715 [PMID: 27679493 DOI: 10.1136/gutjnl-2016-311861]

65 **He Y**, Hwang S, Cai Y, Kim SJ, Xu M, Yang D, Guillot A, Feng D, Seo W, Hou X, Gao B. MicroRNA-223 Ameliorates Nonalcoholic Steatohepatitis and Cancer by Targeting Multiple Inflammatory and Oncogenic Genes in Hepatocytes. *Hepatology* 2019; **70**: 1150-1167 [PMID: 30964207 DOI: 10.1002/hep.30645]

66 **Wong QW**, Lung RW, Law PT, Lai PB, Chan KY, To KF, Wong N. MicroRNA-223 is commonly repressed in hepatocellular carcinoma and potentiates expression of Stathmin1. *Gastroenterology* 2008; **135**: 257-269 [PMID: 18555017 DOI: 10.1053/j.gastro.2008.04.003]

67 **Jimenez Calvente C**, Del Pilar H, Tameda M, Johnson CD, Feldstein AE. MicroRNA 223 3p Negatively Regulates the NLRP3 Inflammasome in Acute and Chronic Liver Injury. *Mol Ther* 2020; **28**: 653-663 [PMID: 31585800 DOI: 10.1016/j.ymthe.2019.09.013]

68 **Ogunwobi OO**, Harricharran T, Huaman J, Galuza A, Odumuwagun O, Tan Y, Ma GX, Nguyen MT. Mechanisms of hepatocellular carcinoma progression. *World J Gastroenterol* 2019; **25**: 2279-2293 [PMID: 31148900 DOI: 10.3748/wjg.v25.i19.2279]

69 **Jenne CN**, Kubes P. Immune surveillance by the liver. *Nat Immunol* 2013; **14**: 996-1006 [PMID: 24048121 DOI: 10.1038/ni.2691]

70 **Tsuchida T**, Friedman SL. Mechanisms of hepatic stellate cell activation. *Nat Rev Gastroenterol Hepatol* 2017; **14**: 397-411 [PMID: 28487545 DOI: 10.1038/nrgastro.2017.38]

71 **Lua I**, Li Y, Zagory JA, Wang KS, French SW, Sévigny J, Asahina K. Characterization of hepatic stellate cells, portal fibroblasts, and mesothelial cells in normal and fibrotic livers. *J Hepatol* 2016; **64**: 1137-1146 [PMID: 26806818 DOI: 10.1016/j.jhep.2016.01.010]

72 **Iwaisako K**, Jiang C, Zhang M, Cong M, Moore-Morris TJ, Park TJ, Liu X, Xu J, Wang P, Paik YH, Meng F, Asagiri M, Murray LA, Hofmann AF, Iida T, Glass CK, Brenner DA, Kisseleva T. Origin of myofibroblasts in the fibrotic liver in mice. *Proc Natl Acad Sci U S A* 2014; **111**: E3297-E3305 [PMID: 25074909 DOI: 10.1073/pnas.1400062111]

73 **Mederacke I**, Hsu CC, Troeger JS, Huebener P, Mu X, Dapito DH, Pradere JP, Schwabe RF. Fate tracing reveals hepatic stellate cells as dominant contributors to liver fibrosis independent of its aetiology. *Nat Commun* 2013; **4**: 2823 [PMID: 24264436 DOI: 10.1038/ncomms3823]

74 **Kramann R**, Schneider RK, DiRocco DP, Machado F, Fleig S, Bondzie PA, Henderson JM, Ebert BL, Humphreys BD. Perivascular Gli1+ progenitors are key contributors to injury-induced organ fibrosis. *Cell Stem Cell* 2015; **16**: 51-66 [PMID: 25465115 DOI: 10.1016/j.stem.2014.11.004]

75 **Li Y**, Wang J, Asahina K. Mesothelial cells give rise to hepatic stellate cells and myofibroblasts *via* mesothelial-mesenchymal transition in liver injury. *Proc Natl Acad Sci U S A* 2013; **110**: 2324-2329 [PMID: 23345421 DOI: 10.1073/pnas.1214136110]

76 **Kisseleva T**, Uchinami H, Feirt N, Quintana-Bustamante O, Segovia JC, Schwabe RF, Brenner DA. Bone marrow-derived fibrocytes participate in pathogenesis of liver fibrosis. *J Hepatol* 2006; **45**: 429-438 [PMID: 16846660 DOI: 10.1016/j.jhep.2006.04.014]

77 **Amann T**, Bataille F, Spruss T, Mühlbauer M, Gäbele E, Schölmerich J, Kiefer P, Bosserhoff AK, Hellerbrand C. Activated hepatic stellate cells promote tumorigenicity of hepatocellular carcinoma. *Cancer Sci* 2009; **100**: 646-653 [PMID: 19175606 DOI: 10.1111/j.1349-7006.2009.01087.x]

78 **Zhang X**, Chen F, Huang P, Wang X, Zhou K, Zhou C, Yu L, Peng Y, Fan J, Zhou J, Lu Z, Hu J, Wang Z. Exosome-depleted MiR-148a-3p derived from Hepatic Stellate Cells Promotes Tumor Progression *via* ITGA5/PI3K/Akt Axis in Hepatocellular Carcinoma. *Int J Biol Sci* 2022; **18**: 2249-2260 [PMID: 35414782 DOI: 10.7150/ijbs.66184]

79 **Wang F**, Li L, Piontek K, Sakaguchi M, Selaru FM. Exosome miR-335 as a novel therapeutic strategy in hepatocellular carcinoma. *Hepatology* 2018; **67**: 940-954 [PMID: 29023935 DOI: 10.1002/hep.29586]

80 **Zhou Y**, Ren H, Dai B, Li J, Shang L, Huang J, Shi X. Hepatocellular carcinoma-derived exosomal miRNA-21 contributes to tumor progression by converting hepatocyte stellate cells to cancer-associated fibroblasts. *J Exp Clin Cancer Res* 2018; **37**: 324 [PMID: 30591064 DOI: 10.1186/s13046-018-0965-2]

81 **Song M**, He J, Pan QZ, Yang J, Zhao J, Zhang YJ, Huang Y, Tang Y, Wang Q, Gu J, Li Y, Chen S, Zeng J, Zhou ZQ, Yang C, Han Y, Chen H, Xiang T, Weng DS, Xia JC. Cancer-Associated Fibroblast-Mediated Cellular Crosstalk Supports Hepatocellular Carcinoma Progression. *Hepatology* 2021; **73**: 1717-1735 [PMID: 33682185 DOI: 10.1002/hep.31792]

82 **Song T**, Dou C, Jia Y, Tu K, Zheng X. TIMP-1 activated carcinoma-associated fibroblasts inhibit tumor apoptosis by activating SDF1/CXCR4 signaling in hepatocellular carcinoma. *Oncotarget* 2015; **6**: 12061-12079 [PMID: 25909286 DOI: 10.18632/oncotarget.3616]

83 **Fang T**, Lv H, Lv G, Li T, Wang C, Han Q, Yu L, Su B, Guo L, Huang S, Cao D, Tang L, Tang S, Wu M, Yang W, Wang H. Tumor-derived exosomal miR-1247-3p induces cancer-associated fibroblast activation to foster lung metastasis of liver cancer. *Nat Commun* 2018; **9**: 191 [PMID: 29335551 DOI: 10.1038/s41467-017-02583-0]

84 **Zheng X**, Xu M, Yao B, Wang C, Jia Y, Liu Q. IL-6/STAT3 axis initiated CAFs *via* up-regulating TIMP-1 which was attenuated by acetylation of STAT3 induced by PCAF in HCC microenvironment. *Cell Signal* 2016; **28**: 1314-1324 [PMID: 27297362 DOI: 10.1016/j.cellsig.2016.06.009]

85 **Zhu GQ**, Tang Z, Huang R, Qu WF, Fang Y, Yang R, Tao CY, Gao J, Wu XL, Sun HX, Zhou YF, Song SS, Ding ZB, Dai Z, Zhou J, Ye D, Wu DJ, Liu WR, Fan J, Shi YH. CD36(+) cancer-associated fibroblasts provide immunosuppressive microenvironment for hepatocellular carcinoma *via* secretion of macrophage migration inhibitory factor. *Cell Discov* 2023; **9**: 25 [PMID: 36878933 DOI: 10.1038/s41421-023-00529-z]

86 **Wang SS**, Tang XT, Lin M, Yuan J, Peng YJ, Yin X, Shang G, Ge G, Ren Z, Zhou BO. Perivenous Stellate Cells Are the Main Source of Myofibroblasts and Cancer-Associated Fibroblasts Formed After Chronic Liver Injuries. *Hepatology* 2021; **74**: 1578-1594 [PMID: 33817801 DOI: 10.1002/hep.31848]

87 **Zhang Z**, Li X, Sun W, Yue S, Yang J, Li J, Ma B, Wang J, Yang X, Pu M, Ruan B, Zhao G, Huang Q, Wang L, Tao K, Dou K. Loss of exosomal miR-320a from cancer-associated fibroblasts contributes to HCC proliferation and metastasis. *Cancer Lett* 2017; **397**: 33-42 [PMID: 28288874 DOI: 10.1016/j.canlet.2017.03.004]

88 **Yugawa K**, Yoshizumi T, Mano Y, Itoh S, Harada N, Ikegami T, Kohashi K, Oda Y, Mori M. Cancer-associated fibroblasts promote hepatocellular carcinoma progression through downregulation of exosomal miR-150-3p. *Eur J Surg Oncol* 2021; **47**: 384-393 [PMID: 32883551 DOI: 10.1016/j.ejso.2020.08.002]

89 **Qi Y**, Wang H, Zhang Q, Liu Z, Wang T, Wu Z, Wu W. CAF-Released Exosomal miR-20a-5p Facilitates HCC Progression *via* the LIMA1-Mediated β-Catenin Pathway. *Cells* 2022; **11** [PMID: 36497115 DOI: 10.3390/cells11233857]

90 **Zhou Y**, Tang W, Zhuo H, Zhu D, Rong D, Sun J, Song J. Cancer-associated fibroblast exosomes promote chemoresistance to cisplatin in hepatocellular carcinoma through circZFR targeting signal transducers and activators of transcription (STAT3)/ nuclear factor -kappa B (NF-κB) pathway. *Bioengineered* 2022; **13**: 4786-4797 [PMID: 35139763 DOI: 10.1080/21655979.2022.2032972]

91 **Lu L**, Huang J, Mo J, Da X, Li Q, Fan M, Lu H. Exosomal lncRNA TUG1 from cancer-associated fibroblasts promotes liver cancer cell migration, invasion, and glycolysis by regulating the miR-524-5p/SIX1 axis. *Cell Mol Biol Lett* 2022; **27**: 17 [PMID: 35193488 DOI: 10.1186/s11658-022-00309-9]

92 **Chang KS**, Ng PN, Lee MM, Chan SJ. Sexual maturation of chinese boys in Hong Kong. *Pediatrics* 1966; **37**: 804-811 [PMID: 5932630]

93 **Fujiwara N**, Nakagawa H, Kudo Y, Tateishi R, Taguri M, Watadani T, Nakagomi R, Kondo M, Nakatsuka T, Minami T, Sato M, Uchino K, Enooku K, Kondo Y, Asaoka Y, Tanaka Y, Ohtomo K, Shiina S, Koike K. Sarcopenia, intramuscular fat deposition, and visceral adiposity independently predict the outcomes of hepatocellular carcinoma. *J Hepatol* 2015; **63**: 131-140 [PMID: 25724366 DOI: 10.1016/j.jhep.2015.02.031]

94 **Koeck ES**, Iordanskaia T, Sevilla S, Ferrante SC, Hubal MJ, Freishtat RJ, Nadler EP. Adipocyte exosomes induce transforming growth factor beta pathway dysregulation in hepatocytes: a novel paradigm for obesity-related liver disease. *J Surg Res* 2014; **192**: 268-275 [PMID: 25086727 DOI: 10.1016/j.jss.2014.06.050]

95 **Liu Y**, Tan J, Ou S, Chen J, Chen L. Adipose-derived exosomes deliver miR-23a/b to regulate tumor growth in hepatocellular cancer by targeting the VHL/HIF axis. *J Physiol Biochem* 2019; **75**: 391-401 [PMID: 31321740 DOI: 10.1007/s13105-019-00692-6]

96 **Zhang H**, Deng T, Ge S, Liu Y, Bai M, Zhu K, Fan Q, Li J, Ning T, Tian F, Li H, Sun W, Ying G, Ba Y. Exosome circRNA secreted from adipocytes promotes the growth of hepatocellular carcinoma by targeting deubiquitination-related USP7. *Oncogene* 2019; **38**: 2844-2859 [PMID: 30546088 DOI: 10.1038/s41388-018-0619-z]

97 **Viallard C**, Larrivée B. Tumor angiogenesis and vascular normalization: alternative therapeutic targets. *Angiogenesis* 2017; **20**: 409-426 [PMID: 28660302 DOI: 10.1007/s10456-017-9562-9]

98 **Yukawa H**, Suzuki K, Aoki K, Arimoto T, Yasui T, Kaji N, Ishikawa T, Ochiya T, Baba Y. Imaging of angiogenesis of human umbilical vein endothelial cells by uptake of exosomes secreted from hepatocellular carcinoma cells. *Sci Rep* 2018; **8**: 6765 [PMID: 29713019 DOI: 10.1038/s41598-018-24563-0]

99 **Shih TC**, Tien YJ, Wen CJ, Yeh TS, Yu MC, Huang CH, Lee YS, Yen TC, Hsieh SY. MicroRNA-214 downregulation contributes to tumor angiogenesis by inducing secretion of the hepatoma-derived growth factor in human hepatoma. *J Hepatol* 2012; **57**: 584-591 [PMID: 22613005 DOI: 10.1016/j.jhep.2012.04.031]

100 **Fang JH**, Zhang ZJ, Shang LR, Luo YW, Lin YF, Yuan Y, Zhuang SM. Hepatoma cell-secreted exosomal microRNA-103 increases vascular permeability and promotes metastasis by targeting junction proteins. *Hepatology* 2018; **68**: 1459-1475 [PMID: 29637568 DOI: 10.1002/hep.29920]

101 **Lin XJ**, Fang JH, Yang XJ, Zhang C, Yuan Y, Zheng L, Zhuang SM. Hepatocellular Carcinoma Cell-Secreted Exosomal MicroRNA-210 Promotes Angiogenesis In Vitro and In Vivo. *Mol Ther Nucleic Acids* 2018; **11**: 243-252 [PMID: 29858059 DOI: 10.1016/j.omtn.2018.02.014]

102 **Yokota Y**, Noda T, Okumura Y, Kobayashi S, Iwagami Y, Yamada D, Tomimaru Y, Akita H, Gotoh K, Takeda Y, Tanemura M, Murakami T, Umeshita K, Doki Y, Eguchi H. Serum exosomal miR-638 is a prognostic marker of HCC *via* downregulation of VE-cadherin and ZO-1 of endothelial cells. *Cancer Sci* 2021; **112**: 1275-1288 [PMID: 33426736 DOI: 10.1111/cas.14807]

103 **Semaan L**, Zeng Q, Lu Y, Zhang Y, Zreik MM, Chamseddine MB, Chopp M, Zhang ZG, Moonka D. MicroRNA-214 enriched exosomes from human cerebral endothelial cells (hCEC) sensitize hepatocellular carcinoma to anti-cancer drugs. *Oncotarget* 2021; **12**: 185-198 [PMID: 33613846 DOI: 10.18632/oncotarget.27879]

104 **Binnewies M**, Roberts EW, Kersten K, Chan V, Fearon DF, Merad M, Coussens LM, Gabrilovich DI, Ostrand-Rosenberg S, Hedrick CC, Vonderheide RH, Pittet MJ, Jain RK, Zou W, Howcroft TK, Woodhouse EC, Weinberg RA, Krummel MF. Understanding the tumor immune

microenvironment (TIME) for effective therapy. *Nat Med* 2018; **24**: 541-550 [PMID: 29686425 DOI: 10.1038/s41591-018-0014-x]

105 **Ma L**, Hernandez MO, Zhao Y, Mehta M, Tran B, Kelly M, Rae Z, Hernandez JM, Davis JL, Martin SP, Kleiner DE, Hewitt SM, Ylaya K, Wood BJ, Greten TF, Wang XW. Tumor Cell Biodiversity Drives Microenvironmental Reprogramming in Liver Cancer. *Cancer Cell* 2019; **36**: 418-430.e6 [PMID: 31588021 DOI: 10.1016/j.ccell.2019.08.007]

106 **Zhang Q**, He Y, Luo N, Patel SJ, Han Y, Gao R, Modak M, Carotta S, Haslinger C, Kind D, Peet GW, Zhong G, Lu S, Zhu W, Mao Y, Xiao M, Bergmann M, Hu X, Kerkar SP, Vogt AB, Pflanz S, Liu K, Peng J, Ren X, Zhang Z. Landscape and Dynamics of Single Immune Cells in Hepatocellular Carcinoma. *Cell* 2019; **179**: 829-845.e20 [PMID: 31675496 DOI: 10.1016/j.cell.2019.10.003]

107 **Lu Y**, Yang A, Quan C, Pan Y, Zhang H, Li Y, Gao C, Lu H, Wang X, Cao P, Chen H, Lu S, Zhou G. A single-cell atlas of the multicellular ecosystem of primary and metastatic hepatocellular carcinoma. *Nat Commun* 2022; **13**: 4594 [PMID: 35933472 DOI: 10.1038/s41467-022-32283-3]

108 **Ju C**, Tacke F. Hepatic macrophages in homeostasis and liver diseases: from pathogenesis to novel therapeutic strategies. *Cell Mol Immunol* 2016; **13**: 316-327 [PMID: 26908374 DOI: 10.1038/cmi.2015.104]

109 **Wu J**, Li J, Salcedo R, Mivechi NF, Trinchieri G, Horuzsko A. The proinflammatory myeloid cell receptor TREM-1 controls Kupffer cell activation and development of hepatocellular carcinoma. *Cancer Res* 2012; **72**: 3977-3986 [PMID: 22719066 DOI: 10.1158/0008-5472.CAN-12-0938]

110 **Chanmee T**, Ontong P, Konno K, Itano N. Tumor-associated macrophages as major players in the tumor microenvironment. *Cancers (Basel)* 2014; **6**: 1670-1690 [PMID: 25125485 DOI: 10.3390/cancers6031670]

111 **Mantovani A**, Marchesi F, Malesci A, Laghi L, Allavena P. Tumour-associated macrophages as treatment targets in oncology. *Nat Rev Clin Oncol* 2017; **14**: 399-416 [PMID: 28117416 DOI: 10.1038/nrclinonc.2016.217]

112 **Liu G**, Ouyang X, Sun Y, Xiao Y, You B, Gao Y, Yeh S, Li Y, Chang C. The miR-92a-2-5p in exosomes from macrophages increases liver cancer cells invasion *via* altering the AR/PHLPP/p-AKT/β-catenin signaling. *Cell Death Differ* 2020; **27**: 3258-3272 [PMID: 32587378 DOI: 10.1038/s41418-020-0575-3]

113 **Li W**, Xin X, Li X, Geng J, Sun Y. Exosomes secreted by M2 macrophages promote cancer stemness of hepatocellular carcinoma via the miR-27a-3p/TXNIP pathways. *Int Immunopharmacol* 2021; **101**: 107585 [PMID: 34601333 DOI: 10.1016/j.intimp.2021.107585]

114 **Tian B**, Zhou L, Wang J, Yang P. miR-660-5p-loaded M2 macrophages-derived exosomes augment hepatocellular carcinoma development through regulating KLF3. *Int Immunopharmacol* 2021; **101**: 108157 [PMID: 34673296 DOI: 10.1016/j.intimp.2021.108157]

115 **Wang Y**, Wang B, Xiao S, Li Y, Chen Q. miR-125a/b inhibits tumor-associated macrophages mediated in cancer stem cells of hepatocellular carcinoma by targeting CD90. *J Cell Biochem* 2019; **120**: 3046-3055 [PMID: 30536969 DOI: 10.1002/jcb.27436]

116 **Chen H**, Tang C, Tan C, Wu F, Li Z, Ji W, Lu L, Xu C, Shen Z, Huang Y. IL-2 Modulates TAMs Derived Exosomal MiRNAs to Ameliorate Hepatocellular Carcinoma Development and Progression. *J Oncol* 2022; **2022**: 3445350 [PMID: 36284632 DOI: 10.1155/2022/3445350]

117 **Zhang J**, Shan WF, Jin TT, Wu GQ, Xiong XX, Jin HY, Zhu SM. Propofol exerts anti-hepatocellular carcinoma by microvesicle-mediated transfer of miR-142-3p from macrophage to cancer cells. *J Transl Med* 2014; **12**: 279 [PMID: 25292173 DOI: 10.1186/s12967-014-0279-x]

118 **Wang L**, Yi X, Xiao X, Zheng Q, Ma L, Li B. Exosomal miR-628-5p from M1 polarized macrophages hinders m6A modification of circFUT8 to suppress hepatocellular carcinoma progression. *Cell Mol Biol Lett* 2022; **27**: 106 [PMID: 36474147 DOI: 10.1186/s11658-022-00406-9]

119 **Aucher A**, Rudnicka D, Davis DM. MicroRNAs transfer from human macrophages to hepato-carcinoma cells and inhibit proliferation. *J Immunol* 2013; **191**: 6250-6260 [PMID: 24227773 DOI: 10.4049/jimmunol.1301728]

120 **Wang L**, Wang Y, Quan J. Exosomal miR-223 derived from natural killer cells inhibits hepatic stellate cell activation by suppressing autophagy. *Mol Med* 2020; **26**: 81 [PMID: 32873229 DOI: 10.1186/s10020-020-00207-w]

121 **Xiong L**, Zhen S, Yu Q, Gong Z. HCV-E2 inhibits hepatocellular carcinoma metastasis by stimulating mast cells to secrete exosomal shuttle microRNAs. *Oncol Lett* 2017; **14**: 2141-2146 [PMID: 28781655 DOI: 10.3892/ol.2017.6433]

122 **Tung SL**; Boardman DA, Sen M, Letizia M, Peng Q, Cianci N, Dioni L, Carlin LM, Lechler R, Bollati V, Lombardi G, Smyth LA. Regulatory T cell-derived extracellular vesicles modify dendritic cell function. *Sci Rep* 2018; **8**: 6065 [PMID: 29666503 DOI: 10.1038/s41598-018-24531-8]

123 **Granito A**, Muratori L, Lalanne C, Quarneti C, Ferri S, Guidi M, Lenzi M, Muratori P. Hepatocellular carcinoma in viral and autoimmune liver diseases: Role of CD4+ CD25+ Foxp3+ regulatory T cells in the immune microenvironment. *World J Gastroenterol* 2021; **27**: 2994-3009 [PMID: 34168403 DOI: 10.3748/wjg.v27.i22.2994]

124 **Yin Y**, Cai X, Chen X, Liang H, Zhang Y, Li J, Wang Z, Zhang W, Yokoyama S, Wang C, Li L, Hou D, Dong L, Xu T, Hiroi T, Yang F, Ji H, Zhang J, Zen K, Zhang CY. Tumor-secreted miR-214 induces regulatory T cells: a major link between immune evasion and tumor growth. *Cell Res* 2014; **24**: 1164-1180 [PMID: 25223704 DOI: 10.1038/cr.2014.121]

125 **Kudo M**, Ueshima K, Ikeda M, Torimura T, Tanabe N, Aikata H, Izumi N, Yamasaki T, Nojiri S, Hino K, Tsumura H, Kuzuya T, Isoda N, Yasui K, Aino H, Ido A, Kawabe N, Nakao K, Wada Y, Yokosuka O, Yoshimura K, Okusaka T, Furuse J, Kokudo N, Okita K, Johnson PJ, Arai Y; TACTICS study group. Randomised, multicentre prospective trial of transarterial chemoembolisation (TACE) plus sorafenib as compared with TACE alone in patients with hepatocellular carcinoma: TACTICS trial. *Gut* 2020; **69**: 1492-1501 [PMID: 31801872 DOI: 10.1136/gutjnl-2019-318934]

126 **Chan SL**, Yeo W, Mo F, Chan AWH, Koh J, Li L, Hui EP, Chong CCN, Lai PBS, Mok TSK, Yu SCH. A phase 2 study of the efficacy and biomarker on the combination of transarterial chemoembolization and axitinib in the treatment of inoperable hepatocellular carcinoma. *Cancer* 2017; **123**: 3977-3985 [PMID: 28640364 DOI: 10.1002/cncr.30825]

127 **Inoue J**, Inazawa J. Cancer-associated miRNAs and their therapeutic potential. *J Hum Genet* 2021; **66**: 937-945 [PMID: 34088973 DOI: 10.1038/s10038-021-00938-6]

128 **Liao W**, Du Y, Zhang C, Pan F, Yao Y, Zhang T, Peng Q. Exosomes: The next generation of endogenous nanomaterials for advanced drug delivery and therapy. *Acta Biomater* 2019; **86**: 1-14 [PMID: 30597259 DOI: 10.1016/j.actbio.2018.12.045]

129 **Shi Y**, Du L, Lin L, Wang Y. Tumour-associated mesenchymal stem/stromal cells: emerging therapeutic targets. *Nat Rev Drug Discov* 2017; **16**: 35-52 [PMID: 27811929 DOI: 10.1038/nrd.2016.193]

130 **Zhang Z**, Mi T, Jin L, Li M, Zhanghuang C, Wang J, Tan X, Lu H, Shen L, Long C, Wei G, He D. Comprehensive proteomic analysis of exosome mimetic vesicles and exosomes derived from human umbilical cord mesenchymal stem cells. *Stem Cell Res Ther* 2022; **13**: 312 [PMID: 35841000 DOI: 10.1186/s13287-022-03008-6]

131 **Jayaraj R**, Raymond G, Krishnan S, Tzou KS, Baxi S, Ram MR, Govind SK, Chandramoorthy HC, Abu-Khzam FN, Shaw P. Clinical Theragnostic Potential of Diverse miRNA Expressions in Prostate Cancer: A Systematic Review and Meta-Analysis. *Cancers (Basel)* 2020; **12** [PMID: 32397507 DOI: 10.3390/cancers12051199]

132 **Zuo Y**, Zheng W, Liu J, Tang Q, Wang SS, Yang XS. MiR-34a-5p/PD-L1 axis regulates cisplatin chemoresistance of ovarian cancer cells. *Neoplasma* 2020; **67**: 93-101 [PMID: 31777260 DOI: 10.4149/neo_2019_190202N106]

133 **Lou G**, Song X, Yang F, Wu S, Wang J, Chen Z, Liu Y. Exosomes derived from miR-122-modified adipose tissue-derived MSCs increase chemosensitivity of hepatocellular carcinoma. *J Hematol Oncol* 2015; **8**: 122 [PMID: 26514126 DOI: 10.1186/s13045-015-0220-7]

134 **Lou G**, Chen L, Xia C, Wang W, Qi J, Li A, Zhao L, Chen Z, Zheng M, Liu Y. MiR-199a-modified exosomes from adipose tissue-derived mesenchymal stem cells improve hepatocellular carcinoma chemosensitivity through mTOR pathway. *J Exp Clin Cancer Res* 2020; **39**: 4 [PMID: 31898515 DOI: 10.1186/s13046-019-1512-5]

135 **Tian S**, Zhou X, Zhang M, Cui L, Li B, Liu Y, Su R, Sun K, Hu Y, Yang F, Xuan G, Ma S, Zheng X, Guo C, Shang Y, Wang J, Han Y. Mesenchymal stem cell-derived exosomes protect against liver fibrosis *via* delivering miR-148a to target KLF6/STAT3 pathway in macrophages. *Stem Cell Res Ther* 2022; **13**: 330 [PMID: 35858897 DOI: 10.1186/s13287-022-03010-y]

136 **Lee MJ**, Jung J, Na KH, Moon JS, Lee HJ, Kim JH, Kim GI, Kwon SW, Hwang SG, Kim GJ. Anti-fibrotic effect of chorionic plate-derived mesenchymal stem cells isolated from human placenta in a rat model of CCl(4)-injured liver: potential application to the treatment of hepatic diseases. *J Cell Biochem* 2010; **111**: 1453-1463 [PMID: 20830742 DOI: 10.1002/jcb.22873]

137 **Cargnoni A**, Gibelli L, Tosini A, Signoroni PB, Nassuato C, Arienti D, Lombardi G, Albertini A, Wengler GS, Parolini O. Transplantation of allogeneic and xenogeneic placenta-derived cells reduces bleomycin-induced lung fibrosis. *Cell Transplant* 2009; **18**: 405-422 [PMID: 19622228 DOI: 10.3727/096368909788809857]

138 **Hyun J**, Wang S, Kim J, Kim GJ, Jung Y. MicroRNA125b-mediated Hedgehog signaling influences liver regeneration by chorionic plate-derived mesenchymal stem cells. *Sci Rep* 2015; **5**: 14135 [PMID: 26370741 DOI: 10.1038/srep14135]

139 **Fonsato V**, Collino F, Herrera MB, Cavallari C, Deregibus MC, Cisterna B, Bruno S, Romagnoli R, Salizzoni M, Tetta C, Camussi G. Human liver stem cell-derived microvesicles inhibit hepatoma growth in SCID mice by delivering antitumor microRNAs. *Stem Cells* 2012; **30**: 1985-1998 [PMID: 22736596 DOI: 10.1002/stem.1161]

140 **Nordin JZ**, Lee Y, Vader P, Mäger I, Johansson HJ, Heusermann W, Wiklander OP, Hällbrink M, Seow Y, Bultema JJ, Gilthorpe J, Davies T, Fairchild PJ, Gabrielsson S, Meisner-Kober NC, Lehtiö J, Smith CI, Wood MJ, El Andaloussi S. Ultrafiltration with size-exclusion liquid chromatography for high yield isolation of extracellular vesicles preserving intact biophysical and functional properties. *Nanomedicine* 2015; **11**: 879-883 [PMID: 25659648 DOI: 10.1016/j.nano.2015.01.003]

141 **Van Deun J**, Mestdagh P, Sormunen R, Cocquyt V, Vermaelen K, Vandesompele J, Bracke M, De Wever O, Hendrix A. The impact of disparate isolation methods for extracellular vesicles on downstream RNA profiling. *J Extracell Vesicles* 2014; **3** [PMID: 25317274 DOI: 10.3402/jev.v3.24858]

142 **Nawaz M**, Camussi G, Valadi H, Nazarenko I, Ekström K, Wang X, Principe S, Shah N, Ashraf NM, Fatima F, Neder L, Kislinger T. The emerging role of extracellular vesicles as biomarkers for urogenital cancers. *Nat Rev Urol* 2014; **11**: 688-701 [PMID: 25403245 DOI: 10.1038/nrurol.2014.301]

World Journal of Gastroenterology

Submit a Manuscript: https://www.f6publishing.com

World J Gastroenterol 2023 October 21; 29(39): 5452-5470

DOI: 10.3748/wjg.v29.i39.5452

ISSN 1007-9327 (print) ISSN 2219-2840 (online)

ORIGINAL ARTICLE

Basic Study

Prostaglandin $F_{2\alpha}$ synthase promotes oxaliplatin resistance in colorectal cancer through prostaglandin $F_{2\alpha}$-dependent and $F_{2\alpha}$-independent mechanism

Yi-Jun Wang, Xiao-Li Xie, Hong-Qun Liu, Hui Tian, Xiao-Yu Jiang, Jiu-Na Zhang, Sheng-Xiong Chen, Ting Liu, Shu-Ling Wang, Xue Zhou, Xiao-Xu Jin, Shi-Mao Liu, Hui-Qing Jiang

Specialty type: Gastroenterology and hepatology

Provenance and peer review: Unsolicited article; Externally peer reviewed.

Peer-review model: Single blind

Peer-review report's scientific quality classification

Grade A (Excellent): 0
Grade B (Very good): B, B
Grade C (Good): 0
Grade D (Fair): 0
Grade E (Poor): E

P-Reviewer: Liao Z, Singapore; Liu H, United States; Sahin TT, Turkey

Received: July 3, 2023
Peer-review started: July 3, 2023
First decision: August 25, 2023
Revised: September 14, 2023
Accepted: September 26, 2023
Article in press: September 26, 2023
Published online: October 21, 2023

Yi-Jun Wang, Xiao-Li Xie, Hui Tian, Xiao-Yu Jiang, Xue Zhou, Xiao-Xu Jin, Hui-Qing Jiang, Department of Gastroenterology, The Second Hospital of Hebei Medical University, Shijiazhuang 050000, Hebei Province, China

Hong-Qun Liu, Liver Unit, University of Calgary, Calgary T1W0K6, Canada

Jiu-Na Zhang, Department of Gastroenterology, The Affiliated Hospital of Hebei Engineering University, Handan 056000, Hebei Province, China

Sheng-Xiong Chen, Department of Hepatobiliary Surgery, The Second Hospital of Hebei Medical University, Shijiazhuang 050000, Hebei Province, China

Ting Liu, Shu-Ling Wang, Department of Gastroenterology, The First Hospital of Hebei Medical University, Shijiazhuang 050000, Hebei Province, China

Shi-Mao Liu, Department of Gastroenterology, Hebei Youfu Hospital, Shijiazhuang 050000, Hebei Province, China

Corresponding author: Hui-Qing Jiang, Doctor, Chief Physician, Director, Department of Gastroenterology, The Second Hospital of Hebei Medical University, No. 215 Heping West Road, Shijiazhuang 050000, Hebei Province, China. jianghuiqing1959@sina.com

Abstract

BACKGROUND

Oxaliplatin (Oxa) is the first-line chemotherapy drug for colorectal cancer (CRC), and Oxa resistance is crucial for treatment failure. Prostaglandin $F_{2\alpha}$ synthase (PG-$F_{2\alpha}$) (PGFS), an enzyme that catalyzes the production of $PGF_{2\alpha}$, is involved in the proliferation and growth of a variety of tumors. However, the role of PGFS in Oxa resistance in CRC remains unclear.

AIM

To explore the role and related mechanisms of PGFS in mediating Oxa resistance in CRC.

METHODS

The PGFS expression level was examined in 37 pairs of CRC tissues and paracancerous tissues at both the mRNA and protein levels. Overexpression or knockdown of PGFS was performed in CRC cell lines with acquired Oxa resistance (HCT116-OxR and HCT8-OxR) and their parental cell lines (HCT116 and HCT8) to assess its influence on cell proliferation, chemoresistance, apoptosis, and DNA damage. For determination of the underlying mechanisms, CRC cells were examined for platinum-DNA adducts and reactive oxygen species (ROS) levels in the presence of a PGFS inhibitor or its products.

RESULTS

Both the protein and mRNA levels of PGFS were increased in the 37 examined CRC tissues compared to the adjacent normal tissues. Oxa induced PGFS expression in the parental HCT116 and HCT8 cells in a dose-dependent manner. Furthermore, overexpression of PGFS in parental CRC cells significantly attenuated Oxa-induced proliferative suppression, apoptosis, and DNA damage. In contrast, knockdown of PGFS in Oxa-resistant HCT116 and HCT8 cells (HCT116-OxR and HCT8-OxR) accentuated the effect of Oxa treatment *in vitro* and *in vivo*. The addition of the PGFS inhibitor indomethacin enhanced the cytotoxicity caused by Oxa. Treatment with the PGFS-catalyzed product $PGF_{2\alpha}$ reversed the effect of PGFS knockdown on Oxa sensitivity. Interestingly, PGFS inhibited the formation of platinum-DNA adducts in a $PGF_{2\alpha}$-independent manner. $PGF_{2\alpha}$ exerts its protective effect against DNA damage by reducing ROS levels.

CONCLUSION

PGFS promotes resistance to Oxa in CRC *via* both $PGF_{2\alpha}$-dependent and $PGF_{2\alpha}$-independent mechanisms.

Key Words: Prostaglandin $F_{2\alpha}$synthase; Colorectal cancer; Oxaliplatin; Drug resistance; DNA damage

Core Tip: Prostaglandin $F_{2\alpha}$ synthase ($PGF_{2\alpha}$) (PGFS) is an enzymatic catalyst responsible for the biosynthesis of $PGF_{2\alpha}$. Our study revealed that PGFS exerts an inhibitory effect on the generation of reactive oxygen species by means of its downstream product $PGF_{2\alpha}$, and consequently facilitates resistance to oxaliplatin in colorectal cancer. Simultaneously, PGFS suppresses the formation of platinum-DNA adducts in a manner that is not reliant on $PGF_{2\alpha}$, which is rarely reported.

Citation: Wang YJ, Xie XL, Liu HQ, Tian H, Jiang XY, Zhang JN, Chen SX, Liu T, Wang SL, Zhou X, Jin XX, Liu SM, Jiang HQ. Prostaglandin $F_{2\alpha}$ synthase promotes oxaliplatin resistance in colorectal cancer through prostaglandin $F_{2\alpha}$-dependent and $F_{2\alpha}$-independent mechanism. *World J Gastroenterol* 2023; 29(39): 5452-5470
URL: https://www.wjgnet.com/1007-9327/full/v29/i39/5452.htm
DOI: https://dx.doi.org/10.3748/wjg.v29.i39.5452

INTRODUCTION

Colorectal cancer (CRC) is one of the most frequently diagnosed cancers and a leading cause of cancer death worldwide [1]. In China, CRC is the third most common cancer, and the incidence rate also exceeds that of liver cancer, ranking third in cancer[2]. The current clinical treatment regimen for CRC involves surgical resection followed by chemotherapy, radiotherapy and combination therapy. For prevention of tumor recurrence, surgery alone or combined with adjuvant chemotherapy remains the cornerstone of the treatment of nonmetastatic CRC[3]. Adjuvant oxaliplatin (Oxa)-based fluorouracil, leucovorin, and Oxa (FOLFOX) or capecitabine plus Oxa chemotherapy is the standard for patients with stage II or III colon cancer following surgery, as recommended by several treatment guidelines[4,5].

Oxa, as an alternative to cisplatin, is a third-generation platinum agent. Several multicenter clinical trials have been conducted on the therapies with Oxa shown in preclinical and single-center trials to have beneficial anticancer effects. Oxa can significantly reduce the risk of recurrence and mortality of CRC and prolong disease-free survival and overall survival[6,7]. However, resistance to chemotherapy remains a major clinical issue in the treatment of CRC[8]. However, only half of CRC patients respond to FOLFOX, and this half of chemotherapy-resistant patients also develop resistance during chemotherapy, a type of resistance known as secondary resistance. That is, cancer drug resistance includes two types: Intrinsic (also called innate or primary resistance) and acquired (also called avoidant, adaptive, or secondary resistance).

Cisplatin resistance likely occurs for complex reasons, including increased drug efflux, drug breakdown, increased repair of damaged DNA, and increased activation of prosurvival pathways or inhibition of pathways that promote cell death[9]. Several studies have also shown that for Oxa resistance, the reduction in damage formation rather than the increase in damage repair is the main factor in the acquired resistance to Oxa[10]. Compared with cisplatin, Oxa has a large platinum atom ring, which can bind more DNA molecules to form platinum-DNA complexes and cause DNA damage to cells. Then, the DNA repair mechanism is activated. Once the repair is successful, Oxa will be excreted from the body, resulting in drug resistance. If DNA damage repair fails, the cell will undergo apoptosis[11]. Several studies

have shown that although Oxa has greater cell lethality than cisplatin, side effects such as ototoxicity and nephrotoxicity are weaker than those of cisplatin, and this drug can treat cisplatin-resistant tumors, but Oxa more easily results in resistance than cisplatin[12,13]. Therefore, studying the resistance to Oxa has important clinical value.

Prostaglandins (PGs) are a group of biologically active lipid mediators derived from the cyclooxygenase (COX) pathway of the arachidonic acid cascade[14]. PGs are involved in growth and development, inflammation, and cancer progression by binding to their respective receptors[15]. Prostaglandin $F_{2\alpha}$ ($PGF_{2\alpha}$) is one of the main PGs produced by the COX pathway. $PGF_{2\alpha}$ is synthesized by $PGF_{2\alpha}$ synthase (PGFS), which is a member of the aldo-keto reductase (AKR) family and a key enzyme in steroid metabolism[16]. PGFS converts prostaglandin D2 (PGD2) into 11β-$PGF_{2\alpha}$[17,18]. Recently, the cancer-promoting effects of PGFS in prostate cancer, gastric cancer, lung cancer, and other tumors have been confirmed[19,20].

Oxidative stress is related to the occurrence and development of tumors, with reactive oxygen species (ROS) playing an important role in inducing oxidative stress. Excessive ROS production is caused by the imbalance between defense and metabolic mechanisms. Low concentrations of ROS induce cell proliferation and regulate the activation of several signaling pathways[21]; however, high concentrations of ROS induce changes in gene expression and promote the accumulation of mutations and DNA damage[22]. ROS can promote the generation of PGD2 and $PGF_{2\alpha}$[3,23], but the relationship between $PGF_{2\alpha}$ and ROS and CRC treatment remains unclear.

In CRC, PGFS overexpression was reported to reduce the DNA damage caused by oxidative stress and thereby induce cisplatin resistance[24]. However, studies on the drug resistance of Oxa are scarce. Moreover, the role and mechanism of PGFS in CRC drug resistance and the relationship between $PGF_{2\alpha}$ and DNA damage require further study. In this study, Oxa-resistant CRC cell lines with PGFS overexpression and knockdown were evaluated, revealing its mediating effect on Oxa resistance. Thus, this study provides novel ideas for the diagnosis and treatment of CRC.

MATERIALS AND METHODS

Patients and samples

Fresh CRC tissues and adjacent nontumor tissue samples were acquired from 37 patients with CRC who underwent surgical resection at the Second Hospital of Hebei Medical University, Shijiazhuang, China. This study was approved by the Ethics Committee of the Second Hospital of Hebei Medical University (approval No. 2021-R441). Each tissue was divided into three parts: one part was directly snap-frozen in liquid nitrogen and stored at -80 ℃ for western blotting, a second part was immediately frozen with TRIzol and stored at -80 °C for RNA extraction, and the third part was immersed in 4% paraformaldehyde and stored at 4 ℃ for further paraffin embedding.

Resistance signature analysis

The different gene expression levels were compared between the nonresponse and response groups. The data on the expression of PGFS in CRC patients with or without response to an Oxa-containing regimen are available in the cancer treatment response gene signature database (http://ctrdb.ncpsb.org.cn/)[25]. Data were generated from the merged dataset of CTR_Microarray_35 and CTR_Microarray_90. We found that 29 out of 45 patients were nonresponsive, and the remaining 16 were responsive. The expression levels of PGFS in the two groups of patients were calculated using the website tool.

Histology and immunohistochemical analysis

Sections were stained for hematoxylin and eosin and immunofluorescence staining. Immunohistochemistry (IHC) was performed as previously described[26]. Briefly, the slides were routinely deparaffinized, rehydrated, subjected to antigen retrieval, and incubated in 3% hydrogen peroxide to block endogenous peroxidase. Subsequently, the slides were blocked and incubated with primary antibodies against PGFS (diluted 1:1000, Proteintech, Wuhan, China) and proliferating cell nuclear antigen (PCNA) (diluted 1:500, Proteintech, Wuhan China) at 4 ℃ overnight, followed by incubation with polymer-horseradish peroxidase-conjugated anti-rabbit secondary antibody the next day. Then, the section was stained with 3,3′-diaminobenzidine and counterstained with hematoxylin, dehydrated and coverslipped.

Cell culture

The human CRC HCT116 cell line was obtained from the Shanghai Institute of Biochemistry and Cell Biology, Chinese Academy of Sciences (Shanghai, China). Oxa-resistant cell lines (HCT116-OxR and HCT8-OxR) and HCT8 cells were purchased from Oulu Biotechnology (Shanghai, China). HCT116 and HCT8 cells were cultured in roswell park memorial institute (RPMI) 1640 medium (Gibco BRL, Rockville, MD, United States), which was supplemented with 10% fetal bovine serum (Gibco BRL), 100 U/mL penicillin, and 100 μg/mL streptomycin at 37 ℃ in a humidified incubator with 5% CO_2. HCT116-OxR and HCT8-OxR cells were cultured in Oxa-containing RPMI 1640 medium. HCT116, HCT116-OxR, HCT8, and HCT8-OxR cells were certified by Viva Cell Biosciences Ltd. (Shanghai, China). The reagents used in this study were Oxa (Selleck, Shanghai, China), indomethacin (MCE, Shanghai, China), and PGF2α (Merck, Jiangsu Province, China).

Western blot analysis

Proteins were extracted from CRC and adjacent tissues and cells using radio immunoprecipitation assay lysis buffer with proteinase inhibitors. Protein concentrations were measured using bicinchoninic acid (Sigma-Aldrich St. Louis, MO,

United States). The primary antibodies used included anti-PGFS antibody (diluted 1:500, Abways, Shanghai, China), anti-β-actin antibody (diluted 1:1000, Abways), anti-cleaved-caspase 3 antibody (diluted 1:200, Abways), anti-cleaved poly ADP-ribose polymerase (PARP) antibody (diluted 1:500, Abways), anti-PCNA (diluted 1:500, Abways), and anti-[γ-H2A histone family member X (γ-H2AX), diluted 1:500, Abways]. Briefly, protein purification was confirmed using electrophoresis on a sodium dodecyl sulfate-polyacrylamide gel, which was then transferred onto a polyvinylidene difluoride membrane. Membranes were incubated in 5% milk for 1 h before incubation with primary antibodies at 4 ℃ overnight. The following day, the membrane was washed three times with TBS with Tween-20. Secondary antibodies were incubated for 1 h at room temperature. The bands were visualized using an Odyssey infrared imaging system (LI-COR Biosciences), and protein quantification was performed using ImageJ software (National Institutes of Health, Bethesda, MD, United States).

Virus and small interfering RNA (siRNA) transfection

For generation of stable reporter lines, HCT116 and HCT8 cells were infected with lentiviral particles expressing PGFS, and the empty vector was used as a control. Lentiviruses for PGFS knockdown were infected into the Oxa-resistant cell lines HCT116-OxR and HCT8-OxR following the manufacturer's instructions. Subsequently, transfected cells were selected for 14-d incubations in 5 ng/mL puromycin. The construction of PGFS knockdown and overexpression lentiviruses was completed by GeneChem Co., Ltd. (Shanghai, China).

RNA extraction and real-time polymerase chain reaction (RT-PCR)

Total RNA was extracted from tissues using TRIzol reagent (Tiangen). Complementary DNA (cDNA) was synthesized from total RNA through reverse transcription using the PrimeScript RT reagent kit from TaKaRa Biomedical Technology Co., Ltd. (Beijing, China). cDNA was used for RT-PCR using the above PrimeScript RT reagent kit on a StepOnePlus™ RT-PCR system (Applied Biosystems, MS). Glyceraldehyde 3-phosphate dehydrogenase (GAPDH) was used as an internal control. Specific primer sequences were designed as follows: PGFS-forward: *5′-GTC ATC CGT ATT TCA ACC GGAG-3′*; PGFS-reverse: *5′-CCA CCC ATC GTT TGT CTC GTT-3′*; GAPDH-forward: *5′-AGG GGG GAG CCA AAA GGG TCA-3′*; GAPDH-reverse: *5′-TGG GTG GCA GTG ATG GCA TGG A-3′*.

Cell viability assay

Cell viability was determined using a cell counting kit-8 (CCK-8) kit (Dojindo Laboratories, Kumamoto, Japan) following the manufacturer's instructions. Briefly, CCK-8 solution (10 μL) was added to each well and incubated for 2 h at 37 ℃. Absorbance was measured at 450 nm using a plate reader (BioTek, Winooski, VT, United States). CCK-8 assays were used to examine the half-inhibitory concentration (IC_{50}). The inhibition concentration (%) was calculated as [(anegative - blank) - (Aexp - blank)]/(anegative-blank) × 100%. The IC_{50} was calculated from the survival curves using GraphPad Prism 7 (Version X; La Jolla, CA, United States). Each assay was performed in triplicate.

Colony formation assays

Cells stably transfected with lentiviruses were reseeded (3×10^3 cells per well) in 6-well plates and cultured for two weeks. The colonies were subsequently stained with 0.05% crystal violet for visualization. After routine culture for 2 wk, colony numbers were counted under a microscope.

Apoptosis assays

For analysis of early/late apoptotic or necrotic cell death, cells were measured with the Annexin V-FITC apoptosis detection kit (Beyotime, Shanghai, China) using flow cytometric analysis. We also detected total apoptosis by a terminal deoxynucleotidyl transferase dUTP nick end labeling (TUNEL) assay (Beyotime, Shanghai, China).

Immunofluorescence assay

Stably transfected cells were seeded onto cover glasses in 24-well plates. After 24 h of intervention, cells were fixed in 4% paraformaldehyde for 30 min, permeabilized with 0.1% Triton X-100, diluted in phosphate-buffered saline (PBS) for 10 min, and blocked with 5% normal goat serum for 30 min at room temperature. The cells were incubated with rabbit anti-PGFS or rabbit anti-γ-H2AX overnight at 4 ℃. After washing with PBS, the cells were incubated with the secondary antibody (594 goat anti-rabbit immunoglobulin G) for 1 h at room temperature. After washing, the slides were counterstained with 4′6′-diamidino-2-phenylindole dihydrochloride (Sigma-Aldrich) for 5 min. Images were acquired using a laser scanning confocal microscope (Olympus, Tokyo, Japan).

Assays for intracellular ROS levels

Intracellular ROS levels were evaluated using a ROS assay kit (KGAF019, KeyGEN Biotech, Nanjing, China) following the manufacturer's instructions. Briefly, cells were stained with dihydroethidium (DHE) for 30 min and analyzed for intracellular ROS levels under a fluorescence microscope (Olympus, Tokyo, Japan). The mean fluorescence intensity, as an index of the amount of ROS, was measured using ImageJ software.

Platinum-DNA adduct determination

The DNA concentration was determined using a nanodrop spectrophotometer (Thermo Fisher Scientific), and the DNA-bound platinum content was quantified using inductively coupled plasma-mass spectrometry.

Alkaline comet assay

DNA damage was detected using a comet assay. CRC cells were administered different drug concentrations and had different exposure times. The comet assay was performed according to the alkaline comet assay protocol (KeyGEN Biotech, Nanjing, China). Nuclear DNA and migrating DNA (comet tail) labeled with propidium iodide appeared red and were observed at 515-560 nm using a fluorescence microscope (Olympus, Tokyo, Japan). Comet tail length and tail moment (percentage of DNA in the tail to the total DNA) were analyzed using ImageJ software.

Animal study

Nude mice were implanted subcutaneously with HCT8-OXR cells. When the average volume of the tumors reached approximately 100 mm^3. The nude mice in the LV-shNC + Oxa and LV-shPGFS + Oxa groups were treated with Oxa by gavage at a dosage of 10 mg/kg/d for 14 d, and the volume of tumors was measured. We sacrificed the nude mice when the treatment was completed, and the tissues were fixed with 4% paraformaldehyde or immediately placed at -80 ℃. The animal protocol was designed to minimize pain and discomfort to animals. The nude mice were acclimatized to laboratory conditions for 1 wk prior to our experiment. Intragastric gavage administration was conducted by using straight gavage needles (22 gauge). All the animals in our study received humane care, and the ethics committee of the Second Hospital of Hebei Medical University approved our study (approval letter No. 2022-AE010).

Statistical analyses

Data are presented as the mean ± SD. The association between PGFS expression and clinicopathological features was evaluated using a nonparametric test. The statistical analyses included analysis of variance (ANOVA) with the Student-Newman-Keuls post hoc test and a standard two-tailed Student's *t* test. Student's *t* test was used for comparisons between two groups, while comparisons between three or more groups were conducted using one or two-way ANOVA with the Brown-Forsythe test for equality of group variances. Statistical analysis was performed using SPSS software version 25.0 (Chicago, IL, United States). $P < 0.05$ was considered statistically significant.

RESULTS

PGFS expression is elevated in CRC tissues

We first tested the expression of PGFS in 37 pairs of CRC tissues and matched paracarcinoma tissues. PGFS was significantly upregulated at both the protein and RNA levels in cancerous tissues compared with adjacent nontumor tissues (Figure 1A and B). IHC analysis showed that the strong positive PGFS signals were mainly detected in the nuclei of the cancerous epithelial cells. In contrast, the normal tissue samples showed low expression of PGFS homogenously distributed in the nuclei and cytoplasm (Figure 1C). Then, we investigated the relationship between PGFS and clinicopathological features. High PGFS expression was associated with advanced T stage (Tables 1 and 2). Moreover, PGFS expression was higher in the Oxa-nonresponsive group than in the Oxa-responsive group (Figure 1D).

PGFS is upregulated in Oxa-resistant CRC cells

To assess the role of PGFS in Oxa resistance in CRC cells, we used two Oxa-resistant CRC cell lines derived from HCT116 and HCT8 (hereafter named HCT116-OxR and HCT8-OxR). The resistance of the two Oxa-resistant cell lines was determined by measuring the resistance index (RI), which was calculated as the IC_{50} ratio of drug-resistant cells to their parent cells. Both HCT116-OxR and HCT8-OxR cells showed moderate Oxa resistance, with RIs of 10.1 and 5.86, respectively (IC_{50}-HCT116-OxR *vs.* IC_{50}-HCT116: 64.2 μM *vs.* 6.315 μM; IC_{50}-HCT8-OxR *vs.* IC_{50}-HCT8: 6.241 μM *vs.* 1.064 μM; Supplementary Figure 1A). Colony formation assays revealed increased colony formation efficiency in the two Oxa-resistant cell lines (Supplementary Figure 1B). PGFS expression was significantly increased in HCT116-OxR and HCT8-OxR cells compared with their parent cells (HCT116 and HCT8) (Supplementary Figure 1C). The elevated PGFS expression in the resistant cells was confirmed using immunofluorescence staining and was largely localized in the cytoplasm and nuclei (Supplementary Figure 1D). Furthermore, Oxa induced PGFS expression in a dose-dependent manner, peaking at 24 h, in both parent and Oxa-resistant cells (Supplementary Figure 1E-H). Therefore, upregulated PGFS is associated with acquired Oxa resistance in CRC cells.

PGFS attenuates Oxa-induced proliferation inhibition, apoptosis, and DNA damage in CRC cells

To further confirm the role of PGFS in Oxa resistance, we performed lentivirus-mediated overexpression of PGFS in HCT116 and HCT8 cells, which showed low levels of PGFS. Overexpression of PGFS was verified by western blotting (Supplementary Figure 2A). Stable overexpression of PGFS induced a significant right shift of the IC_{50} value for Oxa, which indicated a reduction in sensitivity to Oxa (Figure 2A). To validate this result, we designed three siRNAs to target PGFS and evaluated their knockdown efficiency in Oxa-resistant cells with high PGFS expression. The short hairpin RNA (shRNA) sequence that caused an obvious reduction in PGFS expression was cloned and inserted into a lentiviral vector for the stable knockdown of PGFS (Supplementary Figure 2B and C). Lentiviral shRNA-mediated knockdown of PGFS decreased the IC_{50} value for Oxa in HCT116-OxR and HCT8-OxR cells (Figure 2B). We then examined the effect of PGFS on the expression of PCNA (a marker of cell proliferation). Treatment with Oxa resulted in a decrease in PCNA expression, which was diminished by overexpression of PGFS in HCT116 and HCT8 cells (Figure 2C). In contrast, knockdown of PGFS further exacerbated the Oxa-induced reduction in PCNA expression in HCT116-OxR and HCT8-OxR cells (Figure 2D). Additionally, overexpression of PGFS restored the colony-forming capacity of CRC cells treated with

Table 1 Correlation between prostaglandin $F_{2\alpha}$ synthase expression level and clinicopathological characteristics in 37 colorectal cancer patients, *n* (%)

Variables	No. of patients	Relatives PGFS expressions (mean ± SD)	*P* value
All cases	37 (100)		
Gender			0.376
Male	22 (59)	1.84 ± 1.67	
Female	15 (41)	1.68 ± 1.02	
Age (yr)			0.495
≥ 60	19 (51)	1.40 ± 0.8	
< 60	18 (49)	2.12 ± 1.8	
Tumor location			0.066
Colon	15 (41)	1.71 ± 1.2	
Rectum	22 (59)	1.84 ± 1.65	
Differentiations			0.437
Well and Moderately	26 (70)	1.65 ± 1.29	
Poorly	11 (30)	1.81 ± 1.08	
T stage			0.023[a]
T1 or T2	25 (68)	1.26 ± 0.52	
T3 or T4	12 (32)	2.47 ± 0.87	
Lymph node metastasis			0.063
No	25 (68)	1.17 ± 0.56	
Yes	12 (32)	2.09 ± 1.69	
AJCC stage			0.069
I or II	29 (78)	1.44 ± 0.89	
III or IV	8 (22)	3.09 ± 2.69	

[a]*P* < 0.05 concluded that T stage was correlated with prostaglandin F2α synthase expression level. PGFS: Prostaglandin $F_{2\alpha}$ synthase; AJCC: American Joint Committee on Cancer.

Table 2 Spearman analysis of the correlation between prostaglandin $F_{2\alpha}$ synthase expression level with clinicopathological, *n* (%)

Variables	No. of patients	PGFS expression level Spearman correlation	*P* value
T stage		0.666	0[a]
T1 or T2	25 (68)		
T3 or T4	12 (32)		
AJCC stage		0.113	0.504
I or II	29 (78)		
III or IV	8 (22)		

[a]*P* < 0.05 indicates that there is a significant relationship between T stage and prostaglandin F2α synthase (PGFS) expression level in tissues. The Spearman correlation of PGFS expression level, also known as the sample correlation coefficient, was 0.666, that is, the significance relationship was moderately correlated and passed the significance test. PGFS: Prostaglandin $F_{2\alpha}$ synthase; AJCC: American Joint Committee on Cancer.

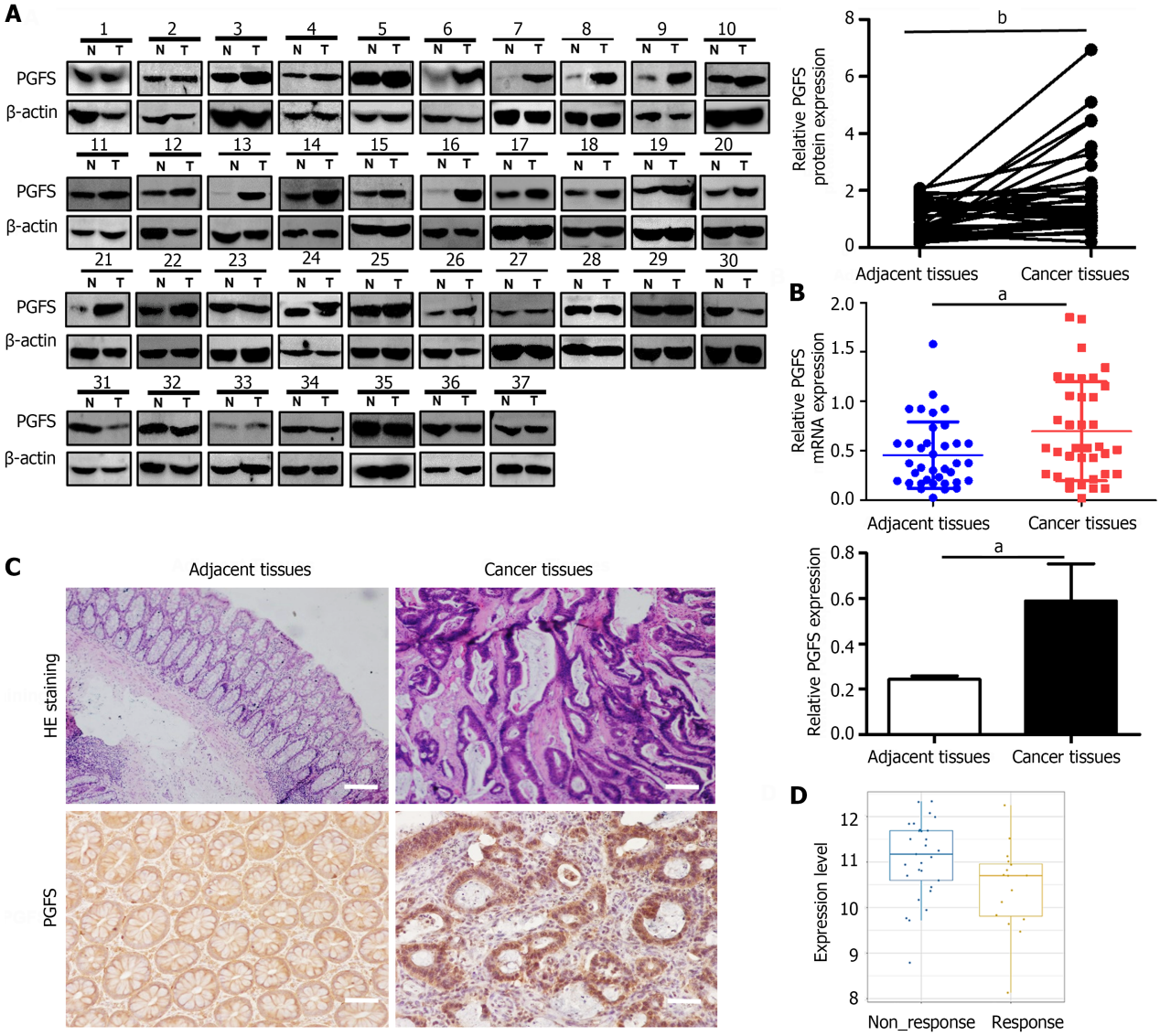

DOI: 10.3748/wjg.v29.i39.5452 **Copyright** ©The Author(s) 2023.

Figure 1 Prostaglandin $F_{2\alpha}$ synthase is upregulation in patients with colorectal cancer. A: Prostaglandin $F_{2\alpha}$ synthase (PGFS) protein expression was verified using western blot in 37 pairs of colorectal cancer (CRC) and adjacent normal tissues; B: Real-time polymerase chain reaction analysis of PGFS mRNA expression in 37 pairs of CRC and adjacent normal tissues; C: Hematoxylin and eosin staining and immunohistochemistry for PGFS expression (scale bar, 50 μm); D: PGFS expression in non-response and response patients analyzed by the Cancer Treatment Response gene signature DataBase (http://ctrdb.ncpsb.org.cn/). $^{a}P < 0.05$, $^{b}P < 0.01$. T: Tumor; N: Adjacent normal tissues; PGFS: Prostaglandin $F_{2\alpha}$ synthase; HE: Hematoxylin and eosin.

Oxa. However, knockdown of PGFS caused a further decrease in clonogenic capacity (Figure 2E and F). In summary, PGFS attenuates Oxa-induced proliferation suppression.

We then tested the effect of PGFS on apoptosis induced by Oxa. Western blotting showed that treatment with Oxa elevated the levels of cleaved PARP and cleaved caspase 3 in HCT116 and HCT8 cells. However, overexpression of PGFS inhibited the Oxa-induced increase in the two proteins (Figure 3A). Conversely, silencing PGFS in HCT116-OxR and HCT8-OxR cells led to a further increase in the two apoptosis markers caused by Oxa (Figure 3B). Furthermore, we examined apoptosis by TUNEL staining. We observed that PGFS overexpression reduced the increase in TUNEL-positive cells induced by Oxa treatment. In contrast, the number of apoptotic cells was further increased by infection with lentivirus expressing sh-PGFS (Figure 3C and D). In addition, we performed flow cytometry as further evidence of apoptosis. The percentage of apoptotic cells was decreased in the PGFS-overexpressing CRC cells but increased in the Oxa-resistant cells with PGFS knockdown (Figure 3E and F). These observations suggested that PGFS protects CRC cells against Oxa-induced apoptosis.

Oxa induces DNA damage by directly binding to DNA. We investigated the role of PGFS in DNA damage caused by Oxa by detecting the expression of γ-H2AX (a marker for DNA damage). The γ-H2AX level was increased by treatment with Oxa, which was diminished by PGFS overexpression in the parental CRC cells, while it was elevated by knockdown of PGFS in the Oxa-resistant CRC cells (Figure 4A and B). We then examined DNA double-strand breaks (DSBs) by γ-H2AX immunofluorescence staining. Overexpression of PGFS in HCT116 and HCT8 cells led to a reduction in the number of γ-H2AX-positive DNA damage foci induced by Oxa treatment. Conversely, the number of γ-H2AX foci was

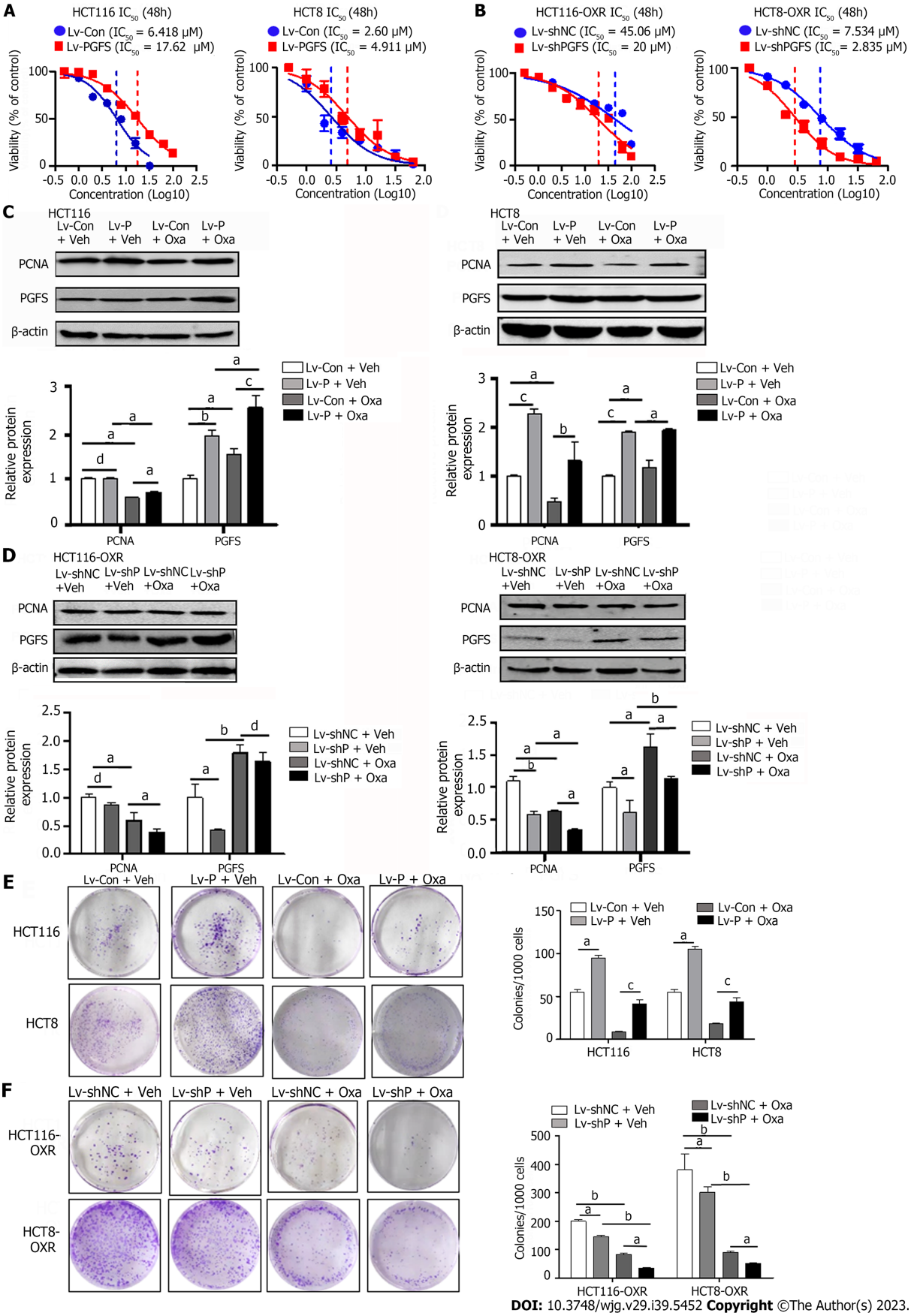

DOI: 10.3748/wjg.v29.i39.5452

Figure 2 Prostaglandin $F_{2\alpha}$ synthase resists the inhibitory effect of oxaliplatin on colorectal cancer cell proliferation. A: The effects of prostaglandin $F_{2\alpha}$ synthase (PGFS) overexpression on cell viability in HCT116 and HCT8 cells; B: The effects of PGFS knockdown on cell viability in HCT116-OxR and HCT8-OxR cells; C and D: Western blot analysis showed proliferating cell nuclear antigen levels in parental and oxaliplatin-resistant (OR) colorectal cancer (CRC) cells; E and F: Plate colony formation assay in parental and OR CRC cells. $^{a}P < 0.05$, $^{b}P < 0.01$, $^{c}P < 0.001$, ^{d}No significance. PCNA: Proliferating cell nuclear

antigen; PGFS: Prostaglandin $F_{2\alpha}$ synthase; Oxa: Oxaliplatin; IC_{50}: Half-inhibitory concentration.

increased in the drug-resistant CRC cells upon PGFS knockdown (Figure 4C). In addition, we used a comet assay to determine DNA damage. Tail length and DNA content percentage (tail DNA%) were significantly increased after incubation with Oxa in HCT116 and HCT8 cells, and these changes were attenuated by overexpression of PGFS. Moreover, PGFS knockdown resulted in enhanced DNA damage induced by Oxa (Figure 4D and E). These results showed that PGFS is resistant to Oxa-induced DNA damage. Collectively, these findings indicated that PGFS promotes Oxa resistance in CRC cell lines.

PGFS knockdown enhances the efficiency of Oxa in vivo

HCT8-OxR cells with stable PGFS knockdown were inoculated subcutaneously into nude mice. Treatment with Oxa caused a decrease in tumor volume and weight, which were further decreased by knockdown of PGFS (Figure 5A-C). Immunohistochemical staining was used to evaluate PCNA expression in the xenograft tumors. Knockdown of PGFS further exacerbated the Oxa-induced reduction in PCNA expression (Figure 5D). These data indicated that PGFS knockdown enhances the sensitivity of CRC to Oxa.

PGFS exerts an Oxa-resistant effect through its $PGF_{2\alpha}$ synthase activity

PGFS catalyzed synthesis of $PGF_{2\alpha}$. To clarify whether the Oxa-resistant effect of PGFS is dependent on its enzymatic action, we blocked PGFS activity by its inhibitor indomethacin. PCNA expression was upregulated by PGFS overexpression in CRC cells treated with Oxa, and this effect was inhibited after indomethacin administration. Moreover, overexpression of PGFS attenuated the upregulation of cleaved PARP and cleaved caspase-3 caused by Oxa treatment, while indomethacin treatment reversed the effect of PGFS overexpression on the expression of apoptotic proteins (Supplementary Figure 3A). Flow cytometric analysis showed that Oxa-induced apoptosis was suppressed by infecting CRC cells with a lentivirus expressing PGFS. Treatment with indomethacin abolished the ability of PGFS to resist Oxa-induced apoptosis (Supplementary Figure 3B). Western blot analysis revealed that overexpression of PGFS inhibited the upregulation of γ-H2AX caused by Oxa, which was diminished by indomethacin incubation (Supplementary Figure 3C). A comet assay further revealed that overexpression of PGFS in CRC cells inhibited the increase in comet DNA tail length and percentage of DNA in the tail induced by Oxa, while the inhibitory function of PGFS was attenuated by indomethacin (Supplementary Figure 3D). These findings suggested that the effect of PGFS on increasing CRC resistance to Oxa depends on its $PGF_{2\alpha}$ synthase activity.

PGFS promotes resistance to Oxa through its product $PGF_{2\alpha}$

PGFS catalyzes the reduction of PGD2 to $PGF_{2\alpha}$. To confirm the role of PGF2α in PGFS-mediated Oxa resistance, we performed rescue experiments by introducing $PGF_{2\alpha}$ to HCT116-OxR and HCT8-OxR cells with PGFS knockdown. Western blot analysis revealed that PCNA expression was further decreased by the depletion of PGFS in HCT116 and HCT8 cells treated with Oxa, which was alleviated by the addition of $PGF_{2\alpha}$. Knockdown of PGFS further increased Oxa-induced elevation of cleaved PARP and cleaved caspase 3, which was partially rescued by $PGF_{2\alpha}$ supplementation (Figure 6A). TUNEL staining results showed that the percentage of apoptotic cells was increased after the knockdown of PGFS in Oxa-treated cells, while the addition of $PGF_{2\alpha}$ decreased apoptosis (Figure 6B). Moreover, knockdown of PGFS further increased the upregulation of γ-H2AX expression caused by Oxa, while supplementation with $PGF_{2\alpha}$ attenuated the effect of PGFS depletion (Figure 6C). Similarly, comet assays showed that the percentage of comet tail DNA and tail length were elevated by Oxa stimulation and were further increased in HCT116-OxR and HCT8-OxR cells with PGFS knockdown, which was alleviated by the addition of $PGF_{2\alpha}$ (Figure 6D). These data indicate that $PGF_{2\alpha}$, the product catalyzed by PGFS, plays an important role in PGFS-mediated Oxa resistance.

PGFS promotes Oxa resistance through both $PGF_{2\alpha}$-dependent and $PGF_{2\alpha}$-independent mechanisms

Oxa exerts its cytotoxic effect by forming platinum-DNA adducts or by generating a large amount of ROS, thereby causing DNA damage. To explore the role of PGFS in the formation of platinum-DNA adducts, we measured the amount of platinum on DNA after treatment with Oxa by inductively coupled plasma mass spectrometry. Overexpression of PGFS did not affect the platinum concentrations in HCT116 and HCT8 cells (Figure 7A). In contrast, knockdown of PGFS induced an increase in the platinum concentrations in HCT116-OxR and HCT8-OxR cells (Figure 7B). However, the addition of $PGF_{2\alpha}$ did not affect the formation of platinum-DNA adducts in HCT8-OxR cells with knockdown of PGFS (Figure 7C). These findings suggested that PGFS may suppress the formation of platinum-DNA adducts in a $PGF_{2\alpha}$-independent manner.

As Oxa exerts its antitumor effect through the induction of ROS, we explored the role of PGFS in the generation of ROS by DHE staining. Compared with that of the parent CRC cells, ROS production was reduced in drug-resistant cells (Figure 7D). In addition, overexpression of PGFS led to a decrease in Oxa-induced ROS (Figure 7E). Conversely, the increased ROS induced by Oxa was further elevated by knockdown of PGFS (Figure 7F), which was alleviated by supplementation with $PGF_{2\alpha}$ (Figure 7G). These data indicated that PGFS inhibits the generation of ROS in a $PGF_{2\alpha}$-dependent manner.

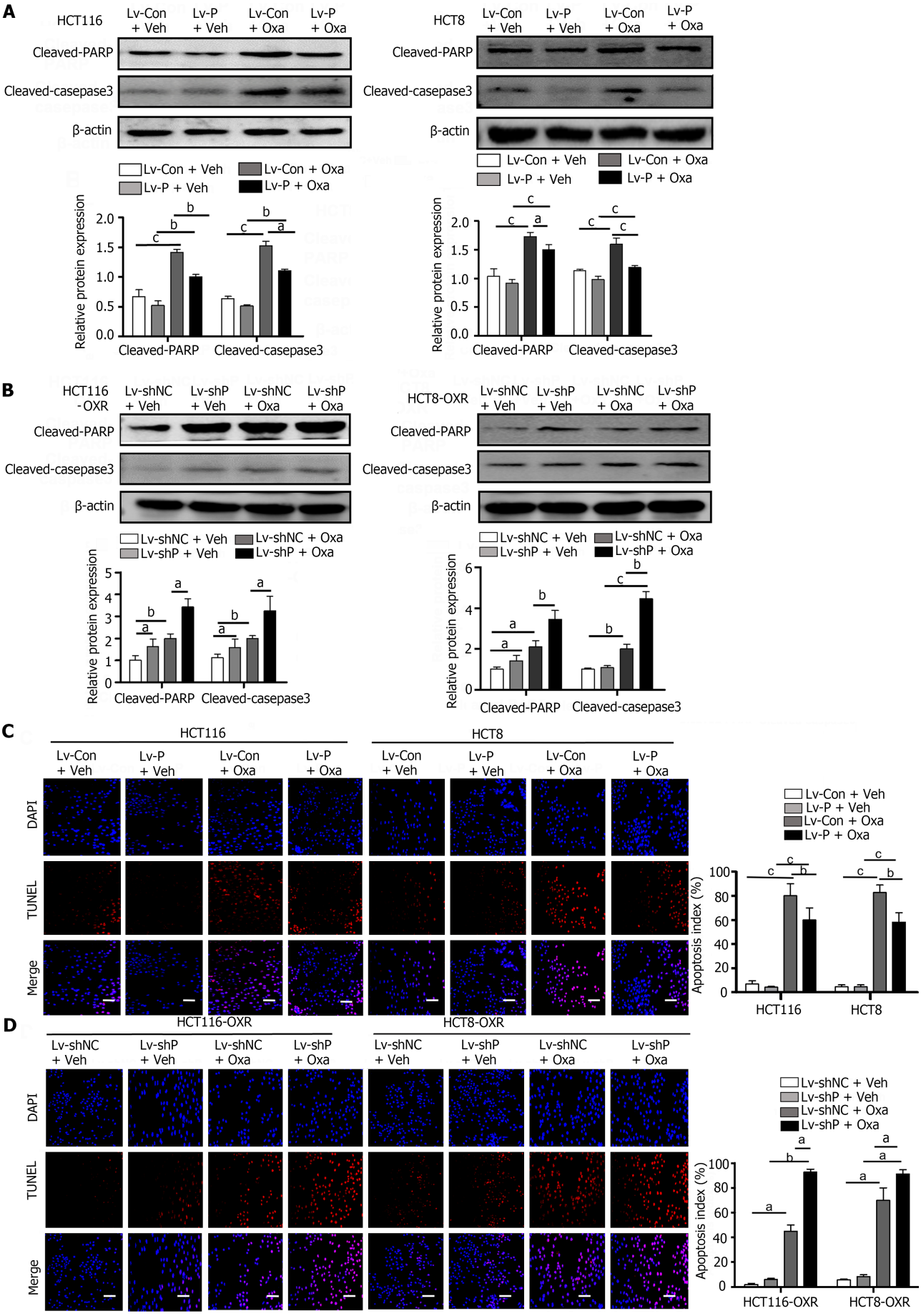
A
HCT116
Lv-Con + Veh
Lv-P + Veh
Lv-Con + Oxa
Lv-P + Oxa
Cleaved-PARP
Cleaved-casepase3
β-actin
Relative protein expression
HCT8
B
HCT116 -OXR
Lv-shNC + Veh
Lv-shP + Veh
Lv-shNC + Oxa
Lv-shP + Oxa
HCT8-OXR
C
DAPI
TUNEL
Merge
Apoptosis index (%)
D

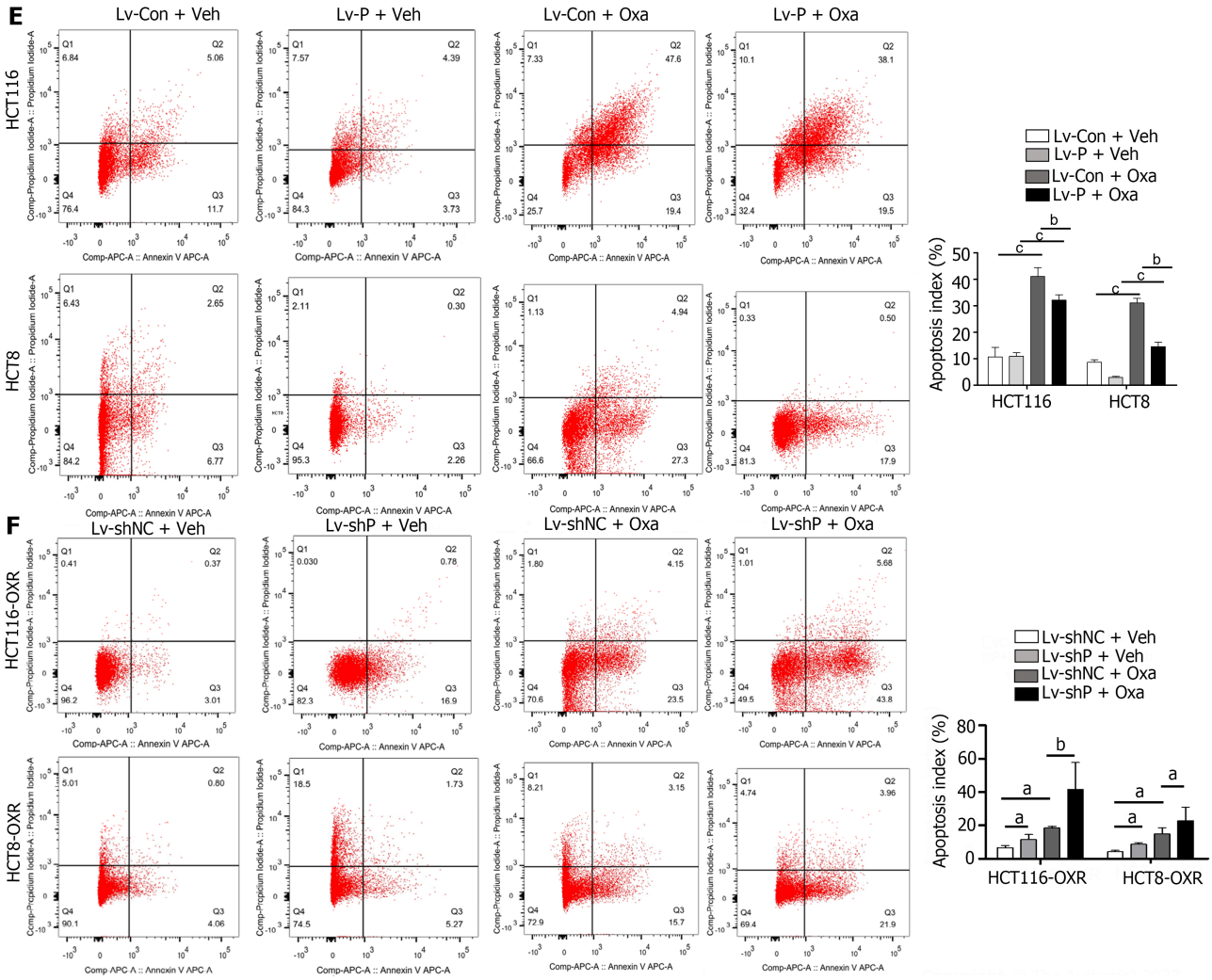

DOI: 10.3748/wjg.v29.i39.5452

Figure 3 Prostaglandin $F_{2\alpha}$ synthase suppresses apoptosis induced by oxaliplatin in colorectal cancer cell lines. A and B: Western blot analysis showed cleaved poly ADP-ribose polymerase and cleaved caspase-3 were assessed in colorectal cancer (CRC) cells or in oxaliplatin-resistant (OR) CRC cells; C and D: Apoptosis of parental and OR CRC cells evaluation by terminal deoxynucleotidyl transferase dUTP nick end labeling assay, scale bar 100 μm; E and F: Apoptosis was measured by the Annexin V-PI staining in parental and OR CRC cells. $^{a}P < 0.05$, $^{b}P < 0.01$, $^{c}P < 0.001$. Oxa: Oxaliplatin; PARP: Poly ADP-ribose polymerase.

DISCUSSION

PGFS belongs to the AKR superfamily of NADP (H)-dependent enzymes, which play central roles in the proinflammation [20,27], proliferation[15,28] and drug resistance of tumors[29-31]. Previous studies have shown that Oxa suppresses cell proliferation and induces apoptosis in CRC cells[32]. The involvement of PGFS in resistance to cisplatin has been reported previously[24]. However, the role of PGFS in Oxa resistance in CRC and its molecular mechanism remain unclear.

Our study revealed that PGFS expression was significantly higher in human CRC tissues than in adjacent normal tissues, and PGFS may be correlated with tumor stage[28] and lymph node metastasis[33]. Therefore, how PGFS regulates CRC progression and metastasis warrants further investigation.

Induction of cell death is one of the challenges for chemotherapy. Any factors that enhance the effect of Oxa on cell proliferation and apoptosis may improve the therapeutic effect of Oxa on tumors[34,35]. PGFS-$PGF_{2\alpha}$ may be a target in tumor chemotherapy. Zhou *et al*[33] recently found that PGFS activates nuclear factor kappaB and promotes hepatocellular carcinoma proliferation and metastasis. Other studies found that $PGF_{2\alpha}$ enhances mitogen-activated protein kinase signaling and inhibits peroxisome proliferator-activated receptor-gamma, a cancer inhibitor; therefore, $PGF_{2\alpha}$ promotes cancer cell proliferation and inhibits differentiation[36-38]. The present study found that PGFS was induced by Oxa in a dose-dependent manner. These findings indicated that PGFS was related to Oxa resistance in CRC. In our *in vitro* study, we constructed PGFS-overexpressing and PGFS knockdown cells in both parental and Oxa-resistant CRC cell lines. We proved that the effect of Oxa on apoptosis and proliferation was suppressed by PGFS overexpression and enhanced by PGFS knockdown. These results indicated that PGFS was involved in Oxa resistance in CRC.

The main mechanism of DNA damage caused by Oxa is the direct combination of platinum with DNA, ultimately destroying tumors[39]. Oxa is a platinum-based chemotherapy that induces a complex spectrum of DNA damage, including DSBs, single-strand breaks, and DNA crosslinks[40], and oxidized bases elicit DNA damage[41]. Indomethacin, a PGFS-specific inhibitor, has additive/synergistic effects on Oxa-induced proliferative inhibition, apoptosis, and DNA

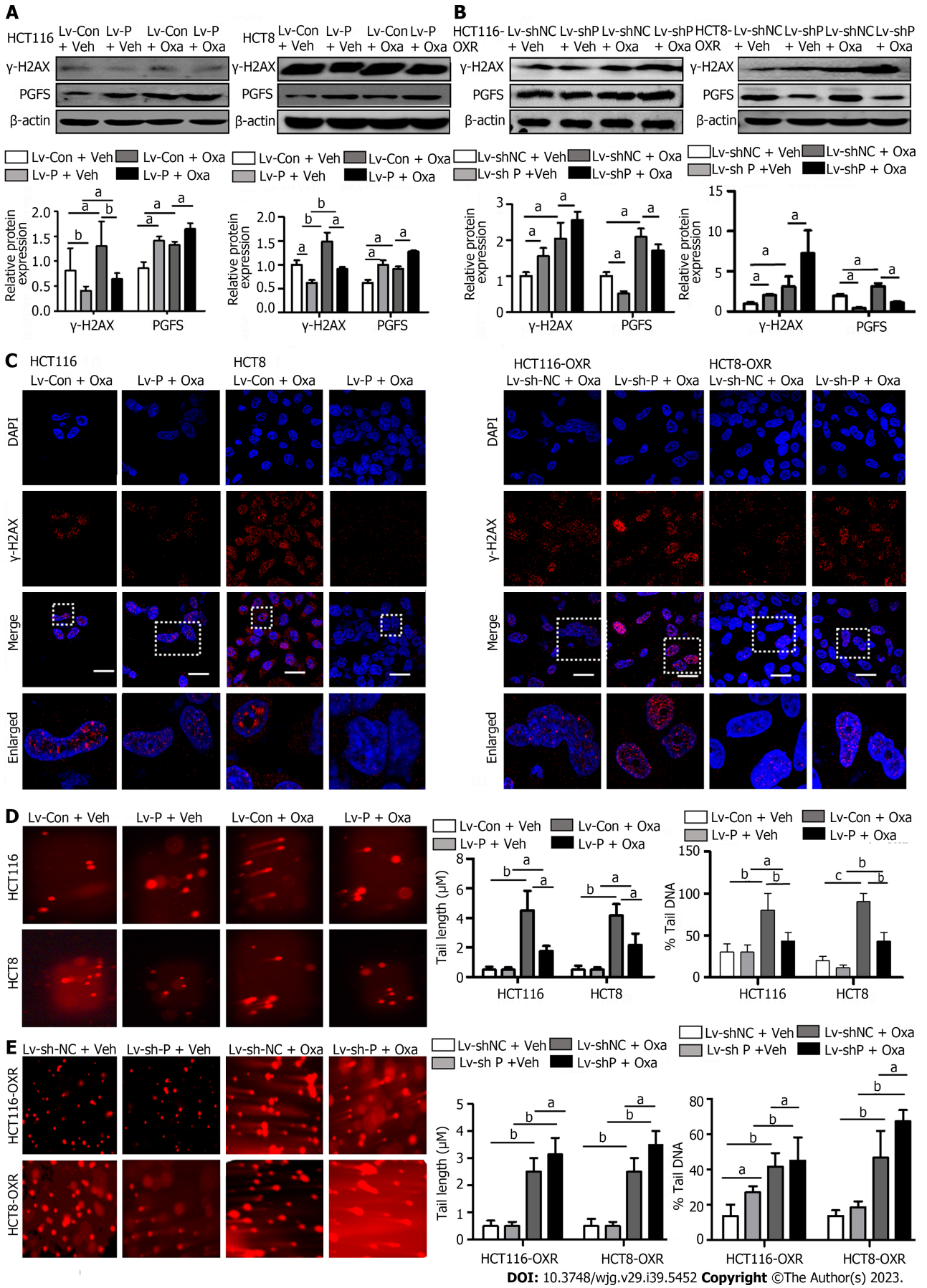

DOI: 10.3748/wjg.v29.i39.5452 **Copyright** ©The Author(s) 2023.

Figure 4 The protective effect of prostaglandin $F_{2\alpha}$ synthase on DNA damage induced by oxaliplatin in colorectal cancer cells. A and B: DNA damage marker protein γ-H2A histone family member X (γ-H2AX) was determined using western blot in HCT116 and HCT8 cells and HCT116-OxR and HCT8-OxR

cells; C: γ-H2AX fluorescent spots were detected using immunofluorescence staining; D and E: Detection of DNA damage using single-cell gel electrophoresis (comet assay) in parent and drug-resistant cells (scale bar, 50 μm). [a]*P* < 0.05, [b]*P* < 0.01, [c]*P* < 0.001. PGFS: Prostaglandin $F_{2\alpha}$ synthase; Oxa: Oxaliplatin; γ-H2AX: γ-H2A histone family member X.

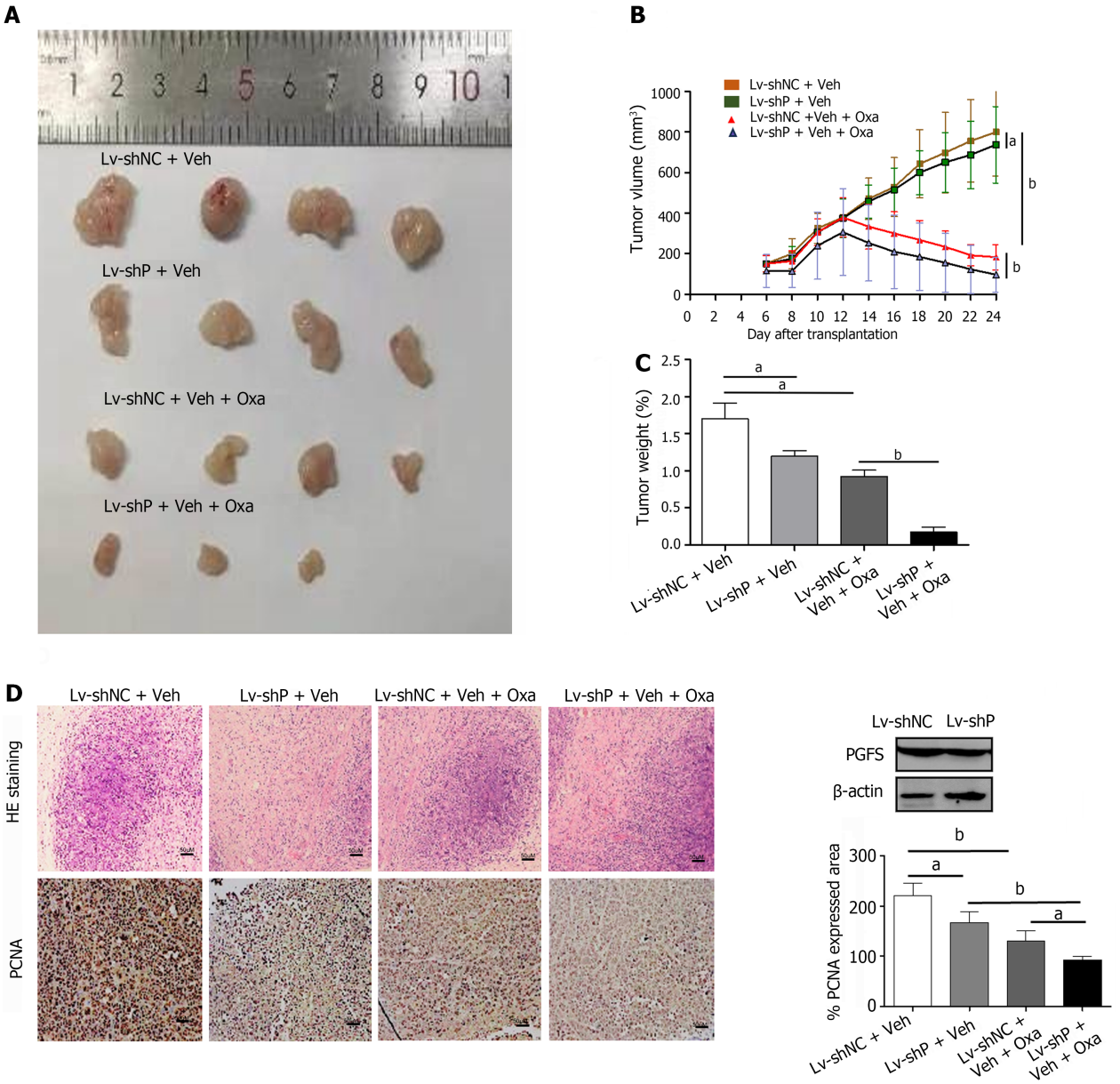

DOI: 10.3748/wjg.v29.i39.5452

Figure 5 Prostaglandin $F_{2\alpha}$ synthase knockdown improves oxaliplatin efficiency *in vivo*. A: Morphologies of collected tumors in subcutaneous HCT8-OxR xenografts in nude mice; B: Curves of tumor growth in each group; C: Tumor weights were measured after collection; D: Hematoxylin-eosin (upper panel; magnification, × 200) and immunohistochemical staining for proliferating cell nuclear antigen (bottom panel; magnification, × 200) using xenograft tumor samples from each group. [a]*P* < 0.05, [b]*P* < 0.01. PCNA: Proliferating cell nuclear antigen; PGFS: Prostaglandin $F_{2\alpha}$ synthase; HE: Hematoxylin and eosin; Oxa: Oxaliplatin.

damage, whereas the administration of $PGF_{2\alpha}$ partially alleviated the above effects[42]. In summary, our data implied that the effect of PGFS on resistance in CRC is $PGF_{2\alpha}$ dependent. The knockdown of PGFS sensitizes CRC to Oxa treatment.

Several studies have demonstrated that Oxa-resistant cells can modulate the cellular resistance capacity to oxidative stress by regulating key detoxification enzymes[43,44]. The present study found that PGFS inhibited the effect of Oxa on DNA damage and thereby promoted Oxa resistance in CRC.

In the present study, PGFS was significantly increased in CRC tissues, PGFS overexpression inhibited the cytotoxic effect of Oxa on CRC cells, and downregulation of PGFS improved the efficacy of Oxa in the treatment of CRC. PGFS promotes CRC resistance to Oxa in a $PGF_{2\alpha}$-dependent manner; therefore, the PGFS-$PGF_{2\alpha}$ pathway may be a potential target for the treatment of CRC patients with Oxa resistance.

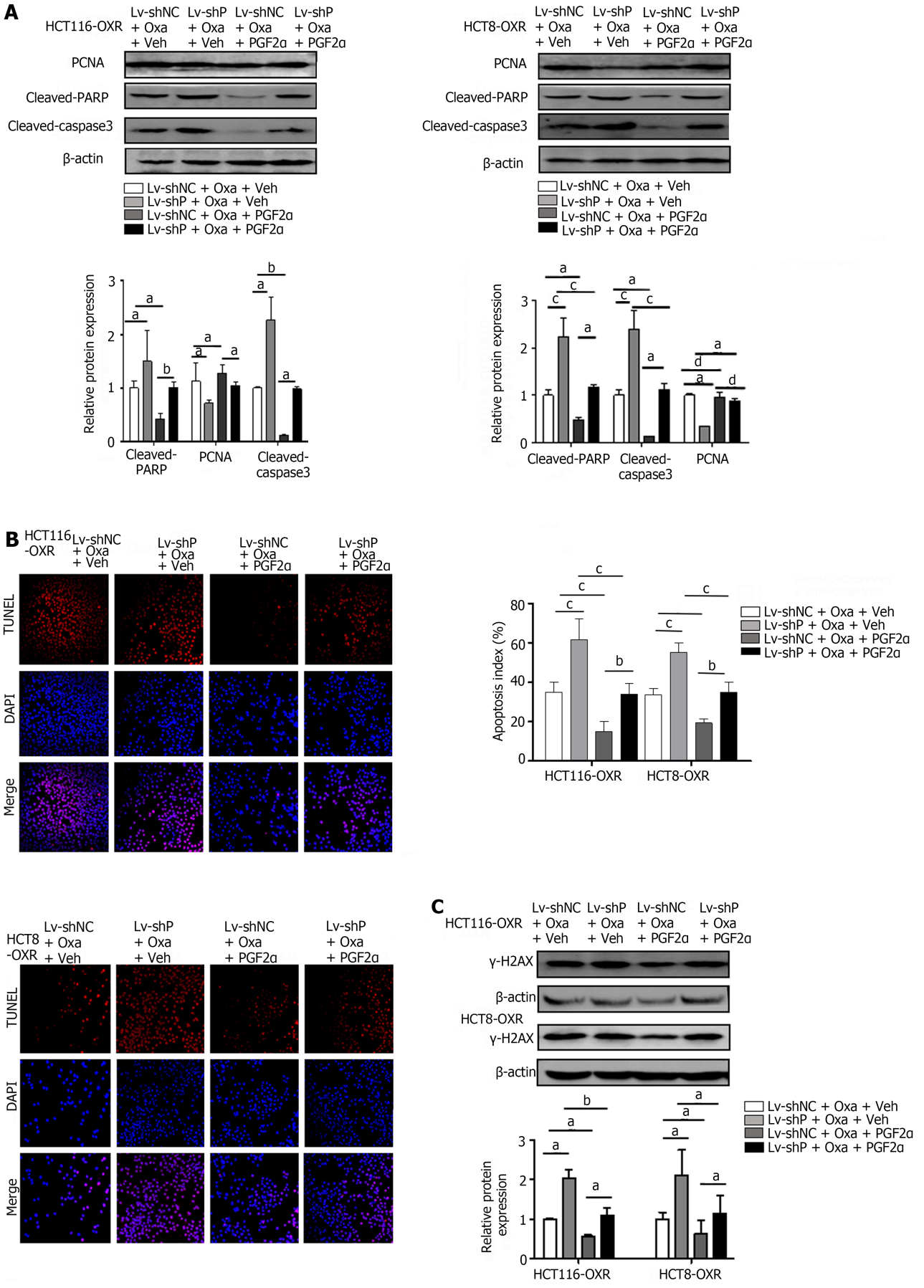
A
HCT116-OXR
Lv-shNC + Oxa + Veh
Lv-shP + Oxa + Veh
Lv-shNC + Oxa + PGF2α
Lv-shP + Oxa + PGF2α
PCNA
Cleaved-PARP
Cleaved-caspase3
β-actin
Lv-shNC + Oxa + Veh
Lv-shP + Oxa + Veh
Lv-shNC + Oxa + PGF2α
Lv-shP + Oxa + PGF2α
Relative protein expression
Cleaved-PARP
PCNA
Cleaved-caspase3
HCT8-OXR
Lv-shNC + Oxa + Veh
Lv-shP + Oxa + Veh
Lv-shNC + Oxa + PGF2α
Lv-shP + Oxa + PGF2α
PCNA
Cleaved-PARP
Cleaved-caspase3
β-actin
Lv-shNC + Oxa + Veh
Lv-shP + Oxa + Veh
Lv-shNC + Oxa + PGF2α
Lv-shP + Oxa + PGF2α
Relative protein expression
Cleaved-PARP
Cleaved-caspase3
PCNA
B
HCT116-OXR
Lv-shNC + Oxa + Veh
Lv-shP + Oxa + Veh
Lv-shNC + Oxa + PGF2α
Lv-shP + Oxa + PGF2α
TUNEL
DAPI
Merge
Apoptosis index (%)
Lv-shNC + Oxa + Veh
Lv-shP + Oxa + Veh
Lv-shNC + Oxa + PGF2α
Lv-shP + Oxa + PGF2α
HCT116-OXR
HCT8-OXR
HCT8-OXR
Lv-shNC + Oxa + Veh
Lv-shP + Oxa + Veh
Lv-shNC + Oxa + PGF2α
Lv-shP + Oxa + PGF2α
TUNEL
DAPI
Merge
C
HCT116-OXR
Lv-shNC + Oxa + Veh
Lv-shP + Oxa + Veh
Lv-shNC + Oxa + PGF2α
Lv-shP + Oxa + PGF2α
γ-H2AX
β-actin
HCT8-OXR
γ-H2AX
β-actin
Lv-shNC + Oxa + Veh
Lv-shP + Oxa + Veh
Lv-shNC + Oxa + PGF2α
Lv-shP + Oxa + PGF2α
Relative protein expression
HCT116-OXR
HCT8-OXR

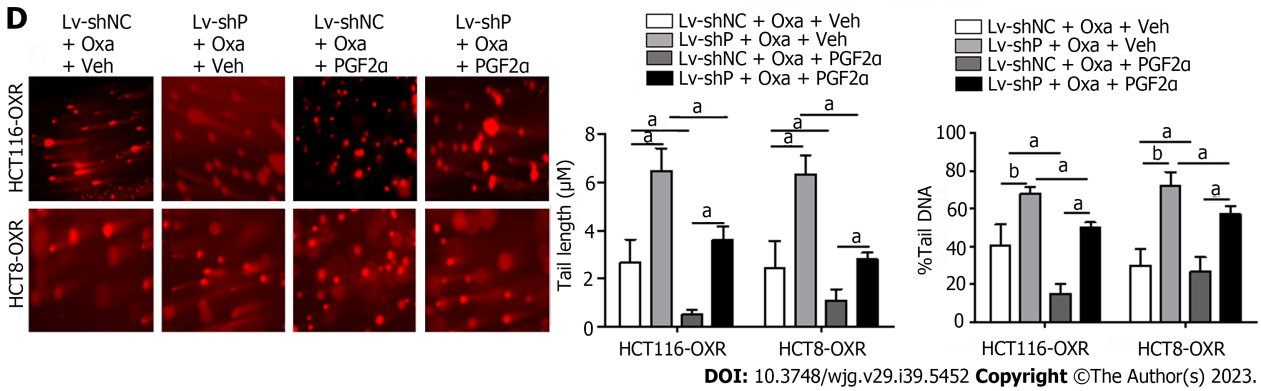

DOI: 10.3748/wjg.v29.i39.5452

Figure 6 The inhibitory effect of prostaglandin $F_{2\alpha}$ on oxaliplatin-induced cytotoxicity. A: Western blots showed the effect of prostaglandin F2α synthase ($PGF_{2\alpha}$) (PGFS) on the expressions of proliferating cell nuclear antigen, cleaved-poly ADP-ribose polymerase, and γ-H2A histone family member X (γ-H2AX) in PGFS knockdown, oxaliplatin-resistant (OR) cells; B: The effect of PGF2α on apoptosis in PGFS knockdown, OR cells evaluated by immunofluorescence. scale bar 100 uM; C: The effect of PGF2α on the cleavage of γ-H2AX protein expressions in PGFS knockdown, OR cells; D: The effect of PGF2α on DNA damage in PGFs knockdown, OR cells evaluated by single-cell gel electrophoresis. scale bar 50 μm). $^{a}P < 0.05$, $^{b}P < 0.01$, $^{c}P < 0.001$, ^{d}No significance. PCNA: Proliferating cell nuclear antigen; PARP: Poly ADP-ribose polymerase; γ-H2AX: γ-H2A histone family member X; TUNEL: Terminal deoxynucleotidyl transferase dUTP nick end labeling.

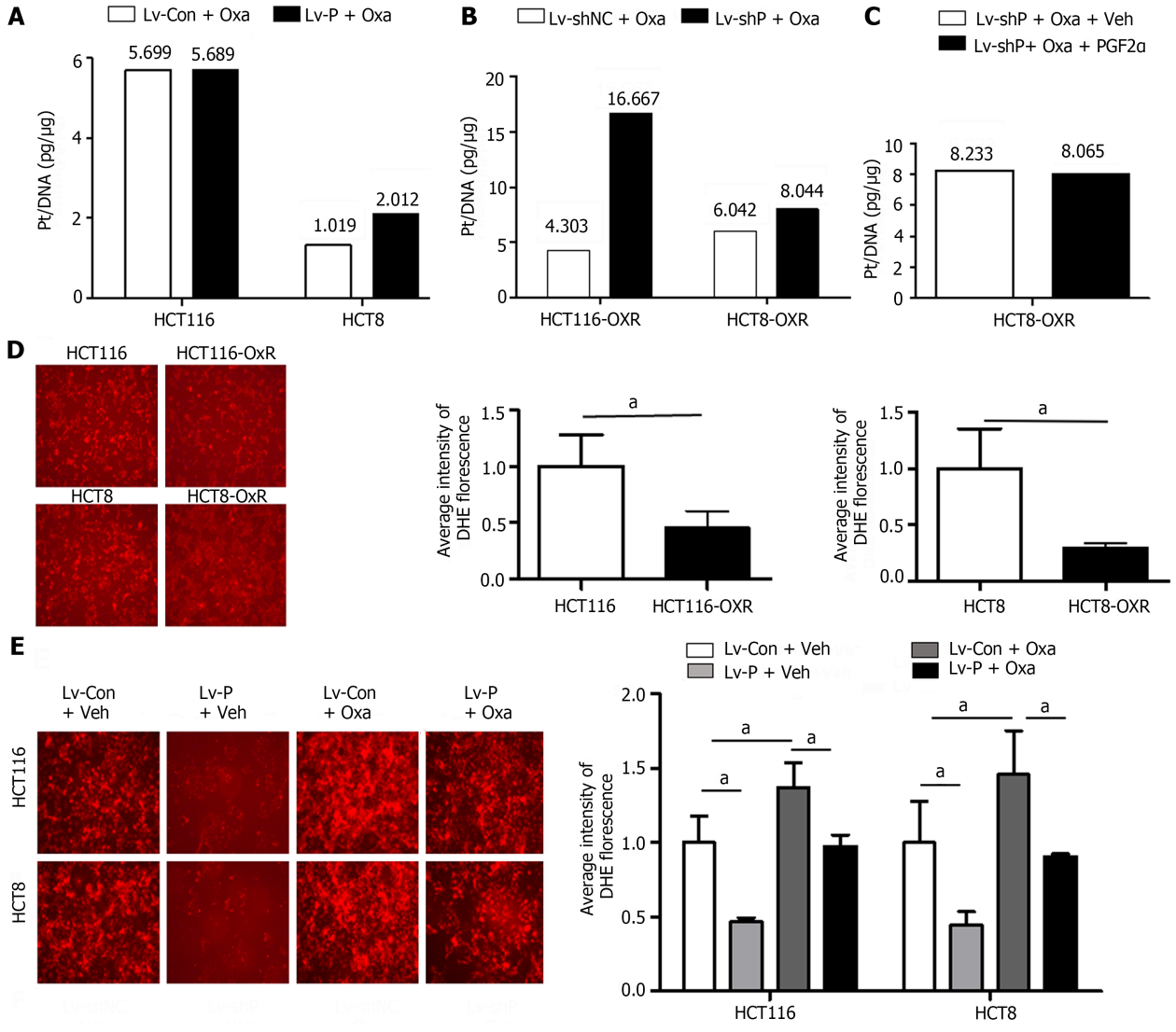

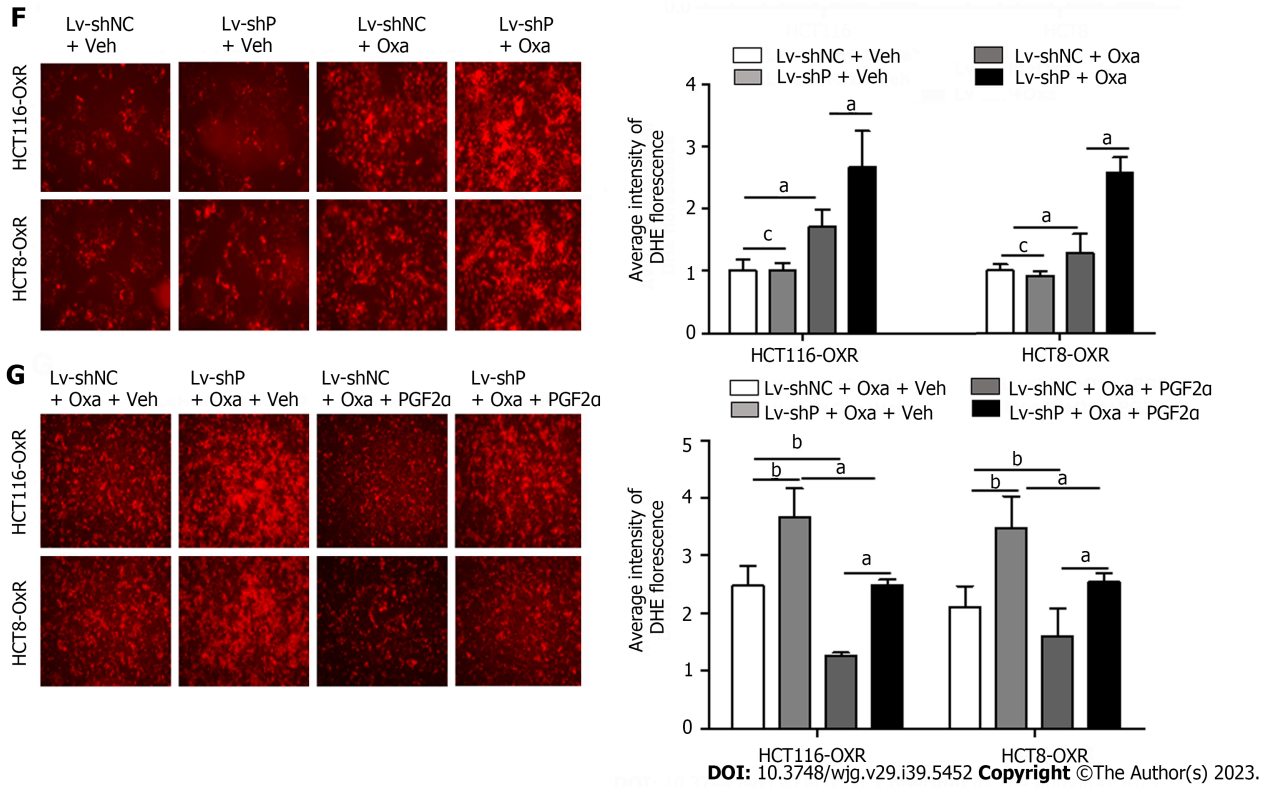

DOI: 10.3748/wjg.v29.i39.5452

Figure 7 Prostaglandin $F_{2\alpha}$ synthase may suppresses the formation of platinum-DNA adducts. A: The effect of Prostaglandin $F_{2\alpha}$ synthase (PGF2α) (PGFS) overexpression on the formation of platinum-DNA adducts was determined using inductively coupled plasma mass spectrometry in colorectal cancer (CRC) cells; B: The effect of PGFS knockdown on the formation of platinum-DNA adducts in oxaliplatin-resistant (OR) CRC cells; C: The effect of PGF2α on the formation of platinum-DNA adducts in OR CRC cells; D: The reactive oxygen species (ROS) content were significantly decreased in OR CRC cells; E: PGFS overexpression significantly decreased ROS content in CRC cells; F: PGFS knockdown significantly decreased ROS content in OR CRC cells; G: PGFS knockdown significantly decreased ROS content in OR CRC cells (scale bar, 50 μm). $^{a}P < 0.05$, $^{b}P < 0.01$; ^{c}No significance. $PGF_{2\alpha}$: Prostaglandin $F_{2\alpha}$; Oxa: Oxaliplatin.

CONCLUSION

PGFS knockdown effectively inhibited the resistance of CRC to Oxa. Mechanistically, PGFS knockdown increased DNA and platinum binding. Moreover, the downstream product PGF2α of PGFS was reduced. The production of ROS was increased. In summary, the above function causes reduced cell death. Hence, we surmise that downregulation of PGFS could improve the efficacy of Oxa in the treatment of CRC.

ARTICLE HIGHLIGHTS

Research background

Chemoresistance is a major obstacle in colorectal cancer (CRC) therapy. Therefore, characterizing mechanisms of chemoresistance is beneficial to improve the treatment efficacy and survival rate of CRC patients. In this study, we identify the role and potential mechanism of prostaglandin $F2_{\alpha}$ synthase ($PGF_{2\alpha}$) (PGFS) in drug resistance to CRC, providing a novel therapeutic target against cancer drug resistance in the treatment of CRC.

Research motivation

The new theory of this study is that PGFS resistance to oxaliplatin (Oxa) has two effects, one is to reduce the production of reactive oxygen species (ROS) through the generation of $PGF_{2\alpha}$ products, and the other is the direct protective effect of PGFS on CRC nucleus. The new method in this study is the application of comet experiment to detect DNA damage, and the other is the application of inductively coupled plasma mass spectrometry (ICP-MS) to directly detect the platinum content of DNA in the nucleus, so as to directly detect the effect of PGFS on the binding of platinum and DNA.

Research objectives

This study was designed to exploit the function and mechanism of PGFS in chemoresistance in CRC. Our study reveals the different ways in which PGFS promotes chemoresistance in CRC, and provides a potential target for predicting and reversing chemoresistance of CRC.

Research methods

The expression level of PGFS is assessed in 37 pairs of CRC tissues and para-cancer tissues by as detected by quantitative polymerase chain reaction and western blot. We examined the influence of PGFS overexpression or knockdown in acquired Oxa-resistant CRC cell lines (HCT116-OxR and HCT8-OxR) and their parental cell lines (HCT116 and HCT8). In order to analyze how PGFS affects colon cancer cell proliferation, A cholecystokinin octapeptide assay was utilized to determine the half-inhibitory concentration value of the cells, a plate clone formation assay was used to determine the clonogenesis ability, and an analysis of proliferating cell nuclear antigen expression was performed to determine the growth rate. Transferase dUTP nick end labeling and Annexin V/propidium iodide stainings, as well as the apoptotic markers cleaved-poly ADP-ribose polymerase and cleaved-caspase 3, were used to detect apoptosis. Western blot and cellular immunofluorescence were used to detect the expression and morphology of the DNA damage marker γ-H2AX. The DNA damage was detected by single-cell gel electrophoresis. Indomethacin, an inhibitor of prostaglandin synthase of PGFS, was used to elucidate the underlying mechanisms. Rescue experiments were conducted by introducing $PGF_{2\alpha}$, the product of PGFS, subsequent to the knockdown of PGFS. The platinum-DNA adducts were quantified using ICP-MS, and intracellular ROS levels were measured using a kit for measuring reactive oxygen species.

Research results

We found that PGFS reduced the production of ROS through its downstream product $PGF_{2\alpha}$, and thereby promotes Oxa resistance in CRC, meanwhile, it inhibited the formation of platinum-DNA adducts in a $PGF_{2\alpha}$-independent manner. The suppressive role of PGFS in the formation of platinum-DNA adducts has never been reported before. However, some questions need to be further clarified, for example, by what mechanism does PGFS suppress the formation of platinum-DNA adducts?

Research conclusions

This study aims to explore the relationship between PGFS and the occurrence and development of CRC, and the relationship between PGFS and Oxa resistance in CRC as well as the related mechanisms. In the future, it is hoped to predict whether patients with CRC are resistant to Oxa by detecting PGFS genes.

Research perspectives

Further work will be needed to clarify the function of PGFS in the nucleus and its mechanisms of action. Moreover, the inhibition mechanism of PGFS in the formation of platinum-DNA adducts needs to be further elucidated.

FOOTNOTES

Author contributions: Wang YJ, Xie XL, and Jiang HQ conceived, and designed the study; Wang YJ, Xie XL, Zhang JN, Zhou X, Chen SX, and Liu T performed most experiments, analyzed the data, wrote the manuscript and edited the paper; Xie XL and Jiang HQ helped to supervise the study; Tian H, Jiang XY, Wang SL, Zhang JN, Jin XX, and Liu SM helped to perform the experiments and analyzed the data; Xie XL, Liu HQ, and Jiang HQ helped to edit the paper; All authors have read and approved the final manuscript.

Supported by the S and T Program of Hebei, No. 22377704D; Medical Science Research Project of Hebei Province, No. 20190510; Postgraduate's Innovation Fund Project of Hebei Province, No. CXZZBS2021077.

Institutional review board statement: This study was reviewed and approved by the Ethics Committee of the Second Hospital of Hebei Medical University (No. 2021-R441).

Institutional animal care and use committee statement: All animal experiments conformed to the internationally accepted principles for the care and use of laboratory animals (The Animal Experiments Inspectorate, Second Hospital of Hebei Medical University; protocol no. 2022-AE010, The Institutional Animal Care and Use Committee at the Second Hospital of Hebei Medical University, Hebei Province, China).

Informed consent statement: All study participants or their legal guardian provided informed written consent about personal and medical data collection prior to study enrolment.

Conflict-of-interest statement: The authors declare that there are no conflicts of interest in our study.

Data sharing statement: No additional data are available.

ARRIVE guidelines statement: The authors have read the ARRIVE guidelines, and the manuscript was prepared and revised according to the ARRIVE guidelines.

Country/Territory of origin: China

ORCID number: Yi-Jun Wang 0000-0002-3918-1051; Xiao-Li Xie 0000-0001-5910-0231; Hong-Qun Liu 0000-0002-6805-5177; Hui Tian 0000-0003-3125-3820; Xiao-Yu Jiang 0000-0003-3592-9197; Jiu-Na Zhang 0000-0003-3813-9369; Sheng-Xiong Chen 0000-0002-1566-3064; Ting Liu 0000-0002-0874-9775; Shu-Ling Wang 0000-0002-9798-1604; Xue Zhou 0000-0002-5683-1861; Xiao-Xu Jin 0000-0002-2307-9888; Shi-Mao Liu 0000-0003-2535-2638; Hui-Qing Jiang 0000-0001-8706-0943.

S-Editor: Qu XL
L-Editor: A
P-Editor: Cai YX

REFERENCES

1 **Sung H**, Ferlay J, Siegel RL, Laversanne M, Soerjomataram I, Jemal A, Bray F. Global Cancer Statistics 2020: GLOBOCAN Estimates of Incidence and Mortality Worldwide for 36 Cancers in 185 Countries. *CA Cancer J Clin* 2021; **71**: 209-249 [PMID: 33538338 DOI: 10.3322/caac.21660]

2 **Yang Y**, Wang HY, Chen YK, Chen JJ, Song C, Gu J. Current status of surgical treatment of rectal cancer in China. *Chin Med J (Engl)* 2020; **133**: 2703-2711 [PMID: 32889914 DOI: 10.1097/CM9.0000000000001076]

3 **Taieb J**, Shi Q, Pederson L, Alberts S, Wolmark N, Van Cutsem E, de Gramont A, Kerr R, Grothey A, Lonardi S, Yoshino T, Yothers G, Sinicrope FA, Zaanan A, André T. Prognosis of microsatellite instability and/or mismatch repair deficiency stage III colon cancer patients after disease recurrence following adjuvant treatment: results of an ACCENT pooled analysis of seven studies. *Ann Oncol* 2019; **30**: 1466-1471 [PMID: 31268130 DOI: 10.1093/annonc/mdz208]

4 **Glynne-Jones R**, Wyrwicz L, Tiret E, Brown G, Rödel C, Cervantes A, Arnold D; ESMO Guidelines Committee. Rectal cancer: ESMO Clinical Practice Guidelines for diagnosis, treatment and follow-up. *Ann Oncol* 2018; **29**: iv263 [PMID: 29741565 DOI: 10.1093/annonc/mdy161]

5 **Benson AB**, Venook AP, Al-Hawary MM, Arain MA, Chen YJ, Ciombor KK, Cohen S, Cooper HS, Deming D, Garrido-Laguna I, Grem JL, Gunn A, Hoffe S, Hubbard J, Hunt S, Kirilcuk N, Krishnamurthi S, Messersmith WA, Meyerhardt J, Miller ED, Mulcahy MF, Nurkin S, Overman MJ, Parikh A, Patel H, Pedersen K, Saltz L, Schneider C, Shibata D, Skibber JM, Sofocleous CT, Stoffel EM, Stotsky-Himelfarb E, Willett CG, Johnson-Chilla A, Gurski LA. NCCN Guidelines Insights: Rectal Cancer, Version 6.2020. *J Natl Compr Canc Netw* 2020; **18**: 806-815 [PMID: 32634771 DOI: 10.6004/jnccn.2020.0032]

6 **Tougeron D**, Mouillet G, Trouilloud I, Lecomte T, Coriat R, Aparicio T, Des Guetz G, Lécaille C, Artru P, Sickersen G, Cauchin E, Sefrioui D, Boussaha T, Ferru A, Matysiak-Budnik T, Silvain C, Karayan-Tapon L, Pagès JC, Vernerey D, Bonnetain F, Michel P, Taïeb J, Zaanan A. Efficacy of Adjuvant Chemotherapy in Colon Cancer With Microsatellite Instability: A Large Multicenter AGEO Study. *J Natl Cancer Inst* 2016; **108** [PMID: 26839356 DOI: 10.1093/jnci/djv438]

7 **de Gramont A**, Schmoll HJ, Cervantes A, Tournigand C. The evolving role of oxaliplatin in the management of colorectal cancer. *Colorectal Dis* 2003; **5** Suppl 3: 10-19 [PMID: 23573556 DOI: 10.1046/j.1463-1318.5.s3.3.x]

8 **Rödel C**, Graeven U, Fietkau R, Hohenberger W, Hothorn T, Arnold D, Hofheinz RD, Ghadimi M, Wolff HA, Lang-Welzenbach M, Raab HR, Wittekind C, Ströbel P, Staib L, Wilhelm M, Grabenbauer GG, Hoffmanns H, Lindemann F, Schlenska-Lange A, Folprecht G, Sauer R, Liersch T; German Rectal Cancer Study Group. Oxaliplatin added to fluorouracil-based preoperative chemoradiotherapy and postoperative chemotherapy of locally advanced rectal cancer (the German CAO/ARO/AIO-04 study): final results of the multicentre, open-label, randomised, phase 3 trial. *Lancet Oncol* 2015; **16**: 979-989 [PMID: 26189067 DOI: 10.1016/S1470-2045(15)00159-X]

9 **Galluzzi L**, Senovilla L, Vitale I, Michels J, Martins I, Kepp O, Castedo M, Kroemer G. Molecular mechanisms of cisplatin resistance. *Oncogene* 2012; **31**: 1869-1883 [PMID: 21892204 DOI: 10.1038/onc.2011.384]

10 **Vaughn CM**, Selby CP, Yang Y, Hsu DS, Sancar A. Genome-wide single-nucleotide resolution of oxaliplatin-DNA adduct repair in drug-sensitive and -resistant colorectal cancer cell lines. *J Biol Chem* 2020; **295**: 7584-7594 [PMID: 32299912 DOI: 10.1074/jbc.RA120.013347]

11 **Assaf KI**, Nau WM. Cucurbiturils: from synthesis to high-affinity binding and catalysis. *Chem Soc Rev* 2015; **44**: 394-418 [PMID: 25317670 DOI: 10.1039/c4cs00273c]

12 **Stordal BK**, Davey MW, Davey RA. Oxaliplatin induces drug resistance more rapidly than cisplatin in H69 small cell lung cancer cells. *Cancer Chemother Pharmacol* 2006; **58**: 256-265 [PMID: 16283310 DOI: 10.1007/s00280-005-0148-7]

13 **Ekblad L**, Kjellström J, Johnsson A. Reduced drug accumulation is more important in acquired resistance against oxaliplatin than against cisplatin in isogenic colon cancer cells. *Anticancer Drugs* 2010; **21**: 523-531 [PMID: 20168208 DOI: 10.1097/CAD.0b013e328337b867]

14 **Chu C**, Wei H, Zhu W, Shen Y, Xu Q. Decreased Prostaglandin D2 Levels in Major Depressive Disorder Are Associated with Depression-Like Behaviors. *Int J Neuropsychopharmacol* 2017; **20**: 731-739 [PMID: 28582515 DOI: 10.1093/ijnp/pyx044]

15 **Wang MT**, Honn KV, Nie D. Cyclooxygenases, prostanoids, and tumor progression. *Cancer Metastasis Rev* 2007; **26**: 525-534 [PMID: 17763971 DOI: 10.1007/s10555-007-9096-5]

16 **Wang S**, Yang Q, Fung KM, Lin HK. AKR1C2 and AKR1C3 mediated prostaglandin D2 metabolism augments the PI3K/Akt proliferative signaling pathway in human prostate cancer cells. *Mol Cell Endocrinol* 2008; **289**: 60-66 [PMID: 18508192 DOI: 10.1016/j.mce.2008.04.004]

17 **Sinreih M**, Anko M, Kene NH, Kocbek V, Rižner TL. Expression of AKR1B1, AKR1C3 and other genes of prostaglandin F2α biosynthesis and action in ovarian endometriosis tissue and in model cell lines. *Chem Biol Interact* 2015; **234**: 320-331 [PMID: 25446850 DOI: 10.1016/j.cbi.2014.11.009]

18 **Watanabe K**. Recent reports about enzymes related to the synthesis of prostaglandin (PG) F(2) (PGF(2α) and 9α, 11β-PGF(2)). *J Biochem* 2011; **150**: 593-596 [PMID: 21926128 DOI: 10.1093/jb/mvr116]

19 **Fung KM**, Samara EN, Wong C, Metwalli A, Krlin R, Bane B, Liu CZ, Yang JT, Pitha JV, Culkin DJ, Kropp BP, Penning TM, Lin HK. Increased expression of type 2 3alpha-hydroxysteroid dehydrogenase/type 5 17beta-hydroxysteroid dehydrogenase (AKR1C3) and its relationship with androgen receptor in prostate carcinoma. *Endocr Relat Cancer* 2006; **13**: 169-180 [PMID: 16601286 DOI: 10.1677/erc.1.01048]

20 **Wang HW**, Lin CP, Chiu JH, Chow KC, Kuo KT, Lin CS, Wang LS. Reversal of inflammation-associated dihydrodiol dehydrogenases (AKR1C1 and AKR1C2) overexpression and drug resistance in nonsmall cell lung cancer cells by wogonin and chrysin. *Int J Cancer* 2007;

120: 2019-2027 [PMID: 17266043 DOI: 10.1002/ijc.22402]
21 **Baraibar MA**, Liu L, Ahmed EK, Friguet B. Protein oxidative damage at the crossroads of cellular senescence, aging, and age-related diseases. *Oxid Med Cell Longev* 2012; **2012**: 919832 [PMID: 23125894 DOI: 10.1155/2012/919832]
22 **Srinivas US**, Tan BWQ, Vellayappan BA, Jeyasekharan AD. ROS and the DNA damage response in cancer. *Redox Biol* 2019; **25**: 101084 [PMID: 30612957 DOI: 10.1016/j.redox.2018.101084]
23 **Sugino N**, Karube-Harada A, Kashida S, Takiguchi S, Kato H. Reactive oxygen species stimulate prostaglandin F2 alpha production in human endometrial stromal cells in vitro. *Hum Reprod* 2001; **16**: 1797-1801 [PMID: 11527878 DOI: 10.1093/humrep/16.9.1797]
24 **Matsunaga T**, Hojo A, Yamane Y, Endo S, El-Kabbani O, Hara A. Pathophysiological roles of aldo-keto reductases (AKR1C1 and AKR1C3) in development of cisplatin resistance in human colon cancers. *Chem Biol Interact* 2013; **202**: 234-242 [PMID: 23165153 DOI: 10.1016/j.cbi.2012.09.024]
25 **Liu Z**, Liu J, Liu X, Wang X, Xie Q, Zhang X, Kong X, He M, Yang Y, Deng X, Yang L, Qi Y, Li J, Liu Y, Yuan L, Diao L, He F, Li D. CTR-DB, an omnibus for patient-derived gene expression signatures correlated with cancer drug response. *Nucleic Acids Res* 2022; **50**: D1184-D1199 [PMID: 34570230 DOI: 10.1093/nar/gkab860]
26 **Tan Z**, Gao L, Wang Y, Yin H, Xi Y, Wu X, Shao Y, Qiu W, Du P, Shen W, Fu L, Jia R, Zhao C, Zhang Y, Zhao Z, Sun Z, Chen H, Hu X, Xu J. PRSS contributes to cetuximab resistance in colorectal cancer. *Sci Adv* 2020; **6**: eaax5576 [PMID: 31911942 DOI: 10.1126/sciadv.aax5576]
27 **Schiffer L**, Bossey A, Kempegowda P, Taylor AE, Akerman I, Scheel-Toellner D, Storbeck KH, Arlt W. Peripheral blood mononuclear cells preferentially activate 11-oxygenated androgens. *Eur J Endocrinol* 2021; **184**: 353-363 [PMID: 33444228 DOI: 10.1530/EJE-20-1077]
28 **Nakarai C**, Osawa K, Akiyama M, Matsubara N, Ikeuchi H, Yamano T, Hirota S, Tomita N, Usami M, Kido Y. Expression of AKR1C3 and CNN3 as markers for detection of lymph node metastases in colorectal cancer. *Clin Exp Med* 2015; **15**: 333-341 [PMID: 24934327 DOI: 10.1007/s10238-014-0298-1]
29 **Zhao J**, Xiang Y, Xiao C, Guo P, Wang D, Liu Y, Shen Y. AKR1C3 overexpression mediates methotrexate resistance in choriocarcinoma cells. *Int J Med Sci* 2014; **11**: 1089-1097 [PMID: 25170291 DOI: 10.7150/ijms.9239]
30 **Minotti G**, Menna P, Salvatorelli E, Cairo G, Gianni L. Anthracyclines: molecular advances and pharmacologic developments in antitumor activity and cardiotoxicity. *Pharmacol Rev* 2004; **56**: 185-229 [PMID: 15169927 DOI: 10.1124/pr.56.2.6]
31 **Heibein AD**, Guo B, Sprowl JA, Maclean DA, Parissenti AM. Role of aldo-keto reductases and other doxorubicin pharmacokinetic genes in doxorubicin resistance, DNA binding, and subcellular localization. *BMC Cancer* 2012; **12**: 381 [PMID: 22938713 DOI: 10.1186/1471-2407-12-381]
32 **Rixe O**, Ortuzar W, Alvarez M, Parker R, Reed E, Paull K, Fojo T. Oxaliplatin, tetraplatin, cisplatin, and carboplatin: spectrum of activity in drug-resistant cell lines and in the cell lines of the National Cancer Institute's Anticancer Drug Screen panel. *Biochem Pharmacol* 1996; **52**: 1855-1865 [PMID: 8951344 DOI: 10.1016/s0006-2952(97)81490-6]
33 **Zhou Q**, Tian W, Jiang Z, Huang T, Ge C, Liu T, Zhao F, Chen T, Cui Y, Li H, Yao M, Li J, Tian H. A Positive Feedback Loop of AKR1C3-Mediated Activation of NF-κB and STAT3 Facilitates Proliferation and Metastasis in Hepatocellular Carcinoma. *Cancer Res* 2021; **81**: 1361-1374 [PMID: 33361392 DOI: 10.1158/0008-5472.CAN-20-2480]
34 **Ruan Y**, Wang L, Lu Y. HDAC6 inhibitor, ACY1215 suppress the proliferation and induce apoptosis of gallbladder cancer cells and increased the chemotherapy effect of gemcitabine and oxaliplatin. *Drug Dev Res* 2021; **82**: 598-604 [PMID: 33428788 DOI: 10.1002/ddr.21780]
35 **Hsu HH**, Chen MC, Baskaran R, Lin YM, Day CH, Lin YJ, Tu CC, Vijaya Padma V, Kuo WW, Huang CY. Oxaliplatin resistance in colorectal cancer cells is mediated *via* activation of ABCG2 to alleviate ER stress induced apoptosis. *J Cell Physiol* 2018; **233**: 5458-5467 [PMID: 29247488 DOI: 10.1002/jcp.26406]
36 **Sales KJ**, List T, Boddy SC, Williams AR, Anderson RA, Naor Z, Jabbour HN. A novel angiogenic role for prostaglandin F2alpha-FP receptor interaction in human endometrial adenocarcinomas. *Cancer Res* 2005; **65**: 7707-7716 [PMID: 16140938 DOI: 10.1158/0008-5472.CAN-05-0101]
37 **Suzuki-Yamamoto T**, Nishizawa M, Fukui M, Okuda-Ashitaka E, Nakajima T, Ito S, Watanabe K. cDNA cloning, expression and characterization of human prostaglandin F synthase. *FEBS Lett* 1999; **462**: 335-340 [PMID: 10622721 DOI: 10.1016/s0014-5793(99)01551-3]
38 **Qualtrough D**, Kaidi A, Chell S, Jabbour HN, Williams AC, Paraskeva C. Prostaglandin F(2alpha) stimulates motility and invasion in colorectal tumor cells. *Int J Cancer* 2007; **121**: 734-740 [PMID: 17437271 DOI: 10.1002/ijc.22755]
39 **Zhang Y**, Xie C, Li A, Liu X, Xing Y, Shen J, Huo Z, Zhou S, Xie Y, Cao W, Ma Y, Xu R, Cai S, Tang X, Ma D. PKI-587 enhances chemosensitivity of oxaliplatin in hepatocellular carcinoma through suppressing DNA damage repair pathway (NHEJ and HR) and PI3K/AKT/mTOR pathway. *Am J Transl Res* 2019; **11**: 5134-5149 [PMID: 31497229]
40 **Liu J**, Fu XQ, Zhou W, Yu HG, Yu JP, Luo HS. LY294002 potentiates the anti-cancer effect of oxaliplatin for gastric cancer *via* death receptor pathway. *World J Gastroenterol* 2011; **17**: 181-190 [PMID: 21245990 DOI: 10.3748/wjg.v17.i2.181]
41 **Deb S**, Xu H, Tuynman J, George J, Yan Y, Li J, Ward RL, Mortensen N, Hawkins NJ, McKay MJ, Ramsay RG, Fox SB. RAD21 cohesin overexpression is a prognostic and predictive marker exacerbating poor prognosis in KRAS mutant colorectal carcinomas. *Br J Cancer* 2014; **110**: 1606-1613 [PMID: 24548858 DOI: 10.1038/bjc.2014.31]
42 **Liedtke AJ**, Adeniji AO, Chen M, Byrns MC, Jin Y, Christianson DW, Marnett LJ, Penning TM. Development of potent and selective indomethacin analogues for the inhibition of AKR1C3 (Type 5 17β-hydroxysteroid dehydrogenase/prostaglandin F synthase) in castrate-resistant prostate cancer. *J Med Chem* 2013; **56**: 2429-2446 [PMID: 23432095 DOI: 10.1021/jm3017656]
43 **Marzano C**, Gandin V, Folda A, Scutari G, Bindoli A, Rigobello MP. Inhibition of thioredoxin reductase by auranofin induces apoptosis in cisplatin-resistant human ovarian cancer cells. *Free Radic Biol Med* 2007; **42**: 872-881 [PMID: 17320769 DOI: 10.1016/j.freeradbiomed.2006.12.021]
44 **Rudin CM**, Yang Z, Schumaker LM, VanderWeele DJ, Newkirk K, Egorin MJ, Zuhowski EG, Cullen KJ. Inhibition of glutathione synthesis reverses Bcl-2-mediated cisplatin resistance. *Cancer Res* 2003; **63**: 312-318 [PMID: 12543781]

World Journal of Gastroenterology

Submit a Manuscript: https://www.f6publishing.com

World J Gastroenterol 2023 October 21; 29(39): 5471-5482

DOI: 10.3748/wjg.v29.i39.5471

ISSN 1007-9327 (print) ISSN 2219-2840 (online)

ORIGINAL ARTICLE

Basic Study

Enhanced glucose homeostasis *via Clostridium symbiosum*-mediated glucagon-like peptide 1 inhibition of hepatic gluconeogenesis in mid-intestinal bypass surgery

Xin Luo, Fang Tao, Cai Tan, Chi-Ying Xu, Zhi-Hua Zheng, Qiang Pang, Xiang-An He, Jia-Qing Cao, Jin-Yuan Duan

Specialty type: Gastroenterology and hepatology

Provenance and peer review: Unsolicited article; Externally peer reviewed.

Peer-review model: Single blind

Peer-review report's scientific quality classification

Grade A (Excellent): 0
Grade B (Very good): B
Grade C (Good): C
Grade D (Fair): 0
Grade E (Poor): 0

P-Reviewer: Mata-Torres G, Mexico; Thongon N, Thailand

Received: July 14, 2023
Peer-review started: July 14, 2023
First decision: September 6, 2023
Revised: September 11, 2023
Accepted: October 11, 2023
Article in press: October 11, 2023
Published online: October 21, 2023

Xin Luo, Fang Tao, Chi-Ying Xu, Jin-Yuan Duan, Department of General Surgery, The First Affiliated Hospital of Nanchang University, Nanchang 330000, Jiangxi Province, China

Cai Tan, Department of Women's Health, Jiangxi Maternal and Child Health Hospital, Nanchang 330000, Jiangxi Province, China

Zhi-Hua Zheng, Qiang Pang, Xiang-An He, Jia-Qing Cao, Department of General Surgery, The Second Affiliated Hospital of Nanchang University, Nanchang 330000, Jiangxi Province, China

Corresponding author: Jin-Yuan Duan, PhD, Associate Chief Physician, Department of General Surgery, The First Affiliated Hospital of Nanchang University, No. 1519 Dongyue Avenue, Nanchang 330000, Jiangxi Province, China. duanjy2022@outlook.com

Abstract

BACKGROUND

The small intestine is known to play a crucial role in the development and remission of diabetes mellitus (DM). However, the exact mechanism by which mid-small intestinal bypass improves glucose metabolism in diabetic rats is not fully understood.

AIM

To elucidate the mechanisms by which mid-small intestinal bypass improves glucose metabolism.

METHODS

Streptozotocin (STZ) was used to induce DM in Sprague-Dawley (SD) rats at a dose of 60 mg/kg. The rats were then randomly divided into two groups: The mid-small intestine bypass (MSIB) group and the sham group (underwent switch laparotomy). Following a 6-wk recovery period post-surgery, the rats underwent various assessments, including metabolic parameter testing, analysis of liver glycogen levels, measurement of key gluconeogenic enzyme activity, characterization of the gut microbiota composition, evaluation of hormone levels, determination of bile acid concentrations, and assessment of the expression of the intestinal receptors Takeda G protein-coupled receptor 5 and farnesoid X receptor.

RESULTS
The MSIB group of rats demonstrated improved glucose metabolism and lipid metabolism, along with increased hepatic glycogen content. Furthermore, there was a decrease in the expression of the key gluconeogenic enzymes phosphoenolpyruvate carboxykinase 1 and glucose-6-phosphatase. Importantly, the MSIB group exhibited a substantial increase in the abundances of intestinal *Lactobacillus*, *Clostridium symbiosum*, *Ruminococcus gnavus*, and *Bilophila*. Moreover, higher levels of secondary bile acids, such as intestinal lithocholic acid, were observed in this group. Remarkably, the changes in the gut microbiota showed a significant correlation with the expression of key gluconeogenic enzymes and glucagon-like peptide 1 (GLP-1) at 6 wk postoperatively, highlighting their potential role in glucose regulation. These findings highlight the beneficial effects of mid-small intestine bypass on glucose metabolism and the associated modulation of the gut microbiota.

CONCLUSION
The findings of this study demonstrate that the introduction of postoperative intestinal *Clostridium symbiosum* in the mid-small intestine contributes to the enhancement of glucose metabolism in nonobese diabetic rats. This improvement is attributed to the increased inhibition of hepatic gluconeogenesis mediated by GLP-1, resulting in a favorable modulation of glucose homeostasis.

Key Words: Gut micobiome; Glucagon-like peptide-1; Glucose metablism; Bile acid; Bariatric surgery; Gluconeogenesis

Core Tip: Intestinal function plays a pivotal role in the onset, progression, and alleviation of diabetes. However, research on surgical procedures and functions involving the mid-small intestine is limited. The precise mechanisms by which the mid-small intestine improves glucose metabolism in diabetic rats remain largely unclear. This study explores the effects of mid-small intestine bypass surgery on diabetic rats. Post-surgery, there was an increase in the abundance of *Clostridium symbiosum* in the rat gut, which contributed to improved glucose metabolism through the inhibition of hepatic gluconeogenesis mediated by glucagon-like peptide 1. These findings provide a theoretical basis for non-surgical interventions in the treatment of metabolic disorders associated with diabetes.

Citation: Luo X, Tao F, Tan C, Xu CY, Zheng ZH, Pang Q, He XA, Cao JQ, Duan JY. Enhanced glucose homeostasis *via Clostridium symbiosum*-mediated glucagon-like peptide 1 inhibition of hepatic gluconeogenesis in mid-intestinal bypass surgery. *World J Gastroenterol* 2023; 29(39): 5471-5482
URL: https://www.wjgnet.com/1007-9327/full/v29/i39/5471.htm
DOI: https://dx.doi.org/10.3748/wjg.v29.i39.5471

INTRODUCTION

Diabetes and obesity have become global health concerns, and their strong association has been widely recognized[1,2]. Bariatric surgery has gained considerable attention as a therapeutic approach for obesity and diabetes improvement[3]. The small intestine, a pivotal organ in dietary metabolism, plays a crucial role in the development of diabetes[4]. Each segment of the small intestine exhibits distinct functions[5], including the "ileal brake" mechanism at the distal ileum[6,7]. Additionally, the gut microbiota composition varies among different segments of the small intestine. While gastric bypass, a commonly employed bariatric surgery, involves bypassing a portion of the upper small intestine[8], less research has focused on the procedure and function of the middle small intestine. To investigate the role of the middle small intestine in glucose metabolism, we utilized a STZ-induced nonobese diabetic SD rat model[9] and conducted middle small intestinal bypass surgery to assess the changes in metabolic function and related factors postoperatively. This study aimed to elucidate the metabolic function and underlying mechanisms of the mid-segment small intestine, with the ultimate goal of providing a theoretical foundation for nonsurgical interventions targeting glucose metabolism disorders.

MATERIALS AND METHODS

Experimental animals

In this study, 8-wk-old male SD rats were used to investigate the metabolic improvement effect of mid-small intestine bypass (MSIB). The rats were obtained from Shanghai Slaughter Laboratory Animal Co., Ltd. and were fed a normal diet. After a one-week acclimatization period, a diabetic rat model was established by intraperitoneal administration of STZ at a dose of 60 mg/kg, divided into two doses administered on the same day. Following successful model establishment, the

rats were randomly assigned to undergo either MSIB or sham surgery (sham). The rats were maintained under identical environmental conditions for 6 wk until euthanasia. Glucose tolerance [oral glucose tolerance test (OGTT)] and insulin sensitivity [insulin tolerance test (ITT)] were assessed at 2 and 6 wk postoperatively. Venous blood, liver tissue, ileal tissue, and fecal samples were collected for analysis at 6 wk postoperatively.

The rats were individually housed in well-ventilated cages with ad libitum access to water and food. Weekly measurements of body weight and food intake were recorded. All animal experiments adhered to the relevant ethical guidelines for animal research and were approved by the Animal Ethics Committee of Nanchang University. Standard animal care and laboratory protocols were followed in accordance with the ARRIVE guidelines.

Animal operations

The rats were fasted for approximately 14 h and underwent surgery after anesthesia (isoflurane, 2% for maintenance and 4% for induction). The abdomen was prepared, and a 4-cm median incision was made to access the abdominal cavity.

In the MSIB group, the point close to the ileocecal flap was used as the reference point. Approximately 60% of the small bowel was bypassed, starting 20 cm proximal to this point and extending 20 cm distal to the flexural ligament. Intestinal continuity was restored through a lateral anastomosis between the distal and proximal small bowel segments. The lumen of the bypassed segment was occluded by silk ligation at the site of the lateral anastomosis. For the sham group, the bowel was gently manipulated upon entering the abdominal cavity. The abdominal cavity was closed with 3-0 silk sutures. The duration of the surgery was approximately 45 min. Subsequently, the rats were subcutaneously injected with 10 mL of sterile saline for fluid resuscitation and placed individually in cages to recover from anesthesia.

Biochemical tests and enzyme-linked immunosorbent assay

Blood was collected from the rat tail vein, and the blood glucose level was measured using an electronic glucometer (Accu-Chek Performa, Roche Diagnostics, Switzerland). The blood was then centrifuged at 3000 rpm for 15 min at 4 °C, and the resulting sera were immediately transferred to new tubes and stored at -80 °C until assay analysis was performed. Serum concentrations of triglycerides (TG), total cholesterol, high-density lipoprotein (HDL), low-density lipoprotein, non-HDL, and free fatty acids were determined using a fully automated biochemical analyzer. The analysis and testing procedures were conducted by the Biochemistry Laboratory at the Second Affiliated Hospital of Nanchang University. Insulin concentrations in serum were measured using an enzyme-linked immunosorbent assay (ELISA) kit (Millipore, Billerica, MA, United States). Additionally, serum concentrations of glucagon-like peptide-1 (GLP-1), peptide tyrosine tyrosine, leptin, ghrelin, and fibroblast growth factor 21 (FGF21) were determined using ELISA kits (Uscn Life Sciences, Wuhan, China).

OGTT and ITT

The OGTT and ITT were conducted at 2 and 6 wk postoperatively, respectively. The rats were fasted for 14 h prior to the tests. The OGTT was performed at 8 am by measuring the initial blood glucose level from the tail vein. Subsequently, a gavage of 20% glucose solution (1 g/kg) was administered to the rats with STZ-induced diabetes mellitus (STZ-DM). Blood glucose measurements were taken at 0, 15, 30, 60, 90, and 120 min after glucose administration, and the area under the curve (AUC) of the glucose tolerance test was calculated. Furthermore, six hours after fasting, the rats underwent ITT. After measuring the initial blood glucose level, 0.5 IU/kg human insulin (Wanbang Biopharmaceuticals, Jiangsu, China) was injected intraperitoneally, and blood glucose levels were measured at 0, 15, 30, 60, 90, and 180 min. Insulin sensitivity was assessed by calculating the ratio of blood glucose to basal blood glucose at each time point, and the AUC of the ITT was calculated.

Metabolomics

After 6 wk of surgery, each rat was placed in an individual collection box, and fecal samples were collected within 48 h. The collected samples were immediately frozen in a -80 °C freezer. Bile acid extraction was performed using methanol. For each sample, methanol (5 mL/g) was added, and the mixture was shaken and incubated at room temperature for a specified period. Subsequently, the mixture was centrifuged at 1200 rpm for 2 min at room temperature, and the supernatant was carefully transferred into a new centrifuge tube. High-performance liquid chromatography (HPLC) was employed for bile acid determination. The filtered supernatant was injected into the HPLC apparatus and passed through the separation column. Gradient elution was performed using an appropriate mobile phase, and the absorbance of bile acids was detected by an ultraviolet detector. The concentration of bile acids in rat feces was determined by referencing a known concentration of bile acids in the standard curve.

Quantitative real-time polymerase chain reaction

RNA extraction from the collected liver and ileal samples was performed using the TRIzol Plus RNA Purification Kit (Thermo Fisher) following the manufacturer's instructions. The extracted RNA samples were assessed for quantity and quality using a nanophotometer (NanoDrop-2000, Thermo Fisher Scientific, Massachusetts, United States). Reverse transcription reactions were carried out using the Reverse Transcription Kit (XYZ Company, Country) to convert RNA into cDNA, utilizing SuperScript™ III First-Strand Synthesis SuperMix (Thermo Fisher). The reverse transcription reaction mixture consisted of RNA template, reverse transcriptase, random primers, and reverse transcription buffer. The reaction conditions involved incubation at 37 °C for 30 min, followed by heat inactivation at 95 °C for 5 min. To amplify the target genes, preamplification reactions were performed using the Preamplification Kit (XYZ Company, Country). The preamplification reaction mixture included cDNA template, target gene-specific primer mixture, and preamplification buffer. The reaction conditions consisted of initial denaturation at 95 °C for 2 min, followed by 14 cycles of

denaturation (95 °C, 15 s), annealing (60 °C, 1 min), and extension (72 °C, 30 s), with a final extension at 72 °C for 5 min. Real-time fluorescent quantitative polymerase chain reaction (PCR) analysis was performed using an ABI Prism 7700 sequence detector system (Applied Biosystems, Foster City, CA, United States). The PCR mixture consisted of the preamplified product, primer mix, fluorescent probe, and PCR Master Mix. The concentrations of primers and probes were adjusted based on optimization experiments. The reaction conditions included initial denaturation at 95 °C for 2 min, followed by 40 cycles of denaturation (95 °C, 15 s) and annealing (60 °C, 1 min).

16S rRNA sequencing

Microbial DNA was extracted from frozen fecal samples using the MagPure Fecal DNA KF Kit B (Magen, China). The extraction process was performed following the manufacturer's instructions, and the concentration and purity of the DNA were measured using a nanophotometer with the Qubit dsDNA BR Analysis Kit (Invitrogen, United States). The V3-V4 region of the 16S rRNA gene was selected as the target for amplification. The PCR amplification reaction consisted of 10 ng of template DNA, 2.5 μM of each primer, and KAPA HiFi HotStart ReadyMix PCR Master Mix (Kapa Biosystems, United States). The PCR amplification conditions were as follows: Predenaturation at 95 °C for 3 min, followed by 30 cycles of denaturation at 95 °C for 30 s, annealing at 55 °C for 30 s, extension at 72 °C for 30 s, and a final extension step at 72 °C for 5 min.

The PCR products were verified by gel electrophoresis and then purified using Ampure XP beads (Beckman Coulter, United States). The purified products underwent secondary PCR amplification using Illumina aptamers and sample-specific index sequences. The secondary PCR products were again validated by gel electrophoresis and purified using Ampure XP beads.

Sequencing was performed on the PacBio Sequel platform (UW Genetics, Shenzhen, China), and the obtained sequences were assigned to operational taxonomic units (OTUs) based on 97% sequence similarity. Clean tags were clustered into OTUs using USEARCH software (v7.0.1090), and species classification of the OTUs was completed. The representative sequences of the OTUs were compared to the Greengene_2013_5_99 database using RDP classifier (v2.2) software for species annotation, with a confidence threshold set to 0.5[10]. Diversity indices of the gut flora were calculated, and the beta diversity index of the gut microbiota was visualized using principal coordinate analysis, with the Shannon index representing the alpha diversity index. The differences in OTU abundance between groups were compared, and significantly different flora were identified using the linear discriminant analysis effect sizes (LEfSe) method, available on the Galaxy (harvard.edu) website.

Quantification and statistical analysis

Graphical data are presented as the mean ± SEM. All analyses were performed using R software version 4.1.3 and GraphPad Prism version 8.4 (GraphPad Software, San Diego, CA, United States), with a significance level set at 0.05. The AUC was calculated using trapezoidal integration. Differences between the two groups were analyzed using a *t* test. Changes in body weight, food intake, fasting blood glucose, OGTT, and ITT over time were analyzed using a two-way analysis of variance (ANOVA). Student's *t* test was used for pairwise comparisons between the groups. Statistical significance was defined as follows: $^{a}P < 0.05$, $^{b}P < 0.01$, and $^{c}P < 0.001$.

RESULTS

Significant metabolic improvements were observed after MSIB (Figures 1 and 2). At 2 wk after surgery, the body weight of rats in the MSIB group decreased compared to that of rats in the sham group (Figure 1A). Additionally, mean blood glucose levels were significantly lower in the MSIB group than in the sham group after surgery (Figure 1C). The OGTT results showed a significant decrease in both the OGTT values and the area under the OGTT curve (OGTT-AUC) in the MSIB group compared to the sham group (Figure 1D-F). Moreover, the MSIB group exhibited a significant reduction in food intake compared to the sham group (Figure 1B). However, there was no significant improvement in insulin sensitivity (ITT) in the MSIB group compared to the sham group, except for the 45-min mark in the ITT test two weeks after surgery and the 60-min mark in the ITT test six weeks after surgery (Figures 1G, H and J). In conclusion, these findings suggest that MSIB has a significant positive effect on glucose metabolism in diabetic rats.

After MSIB, there was an observed increase in hepatic glycogen stores, a reduction in gluconeogenic key enzymes, and a decrease in the expression of transcription factors (Figure 3C). These changes were significantly correlated with glucose metabolism. Examination of liver tissue sections at 6 wk postoperatively revealed a higher hepatic glycogen content in the MSIB group than in the sham group (Figures 3A and B). Furthermore, the MSIB group showed reduced expression of phosphoenolpyruvate carboxykinase 1 (PCK1) and glucose-6-phosphatase (G6PC), which are key enzymes involved in hepatic gluconeogenesis. Additionally, there was a decrease in the expression of Forkhead box O1 (FOXO1) and peroxisome proliferator-activated receptor gamma coactivator 1 alpha (PGC-1α), which are transcription factors that regulate gluconeogenesis (Figure 3C).

The gut microbiome of rats in the MSIB group exhibited notable alterations compared to that of the sham group following surgery, resulting in discernible differences in beta diversity between the two groups (Figure 4A). Specifically, there was a significant increase in the abundances of several *Lactobacillus spp.* at the species level, including *Lactobacillus hamsteri*, *Lactobacillus helveticus*, *Lactobacillus pontis*, and *Lactobacillus vaginalis*. Additionally, there was a significant increase in the abundances of *Clostridium symbiosum*, *Bilophila* and *Ruminococcus gnavus* in the gut microbiome of rats in the MSIB group (Figures 4B and C). Notably, these upregulated microbial species were correlated with changes in key enzymes involved in gluconeogenesis and bile acid metabolism.

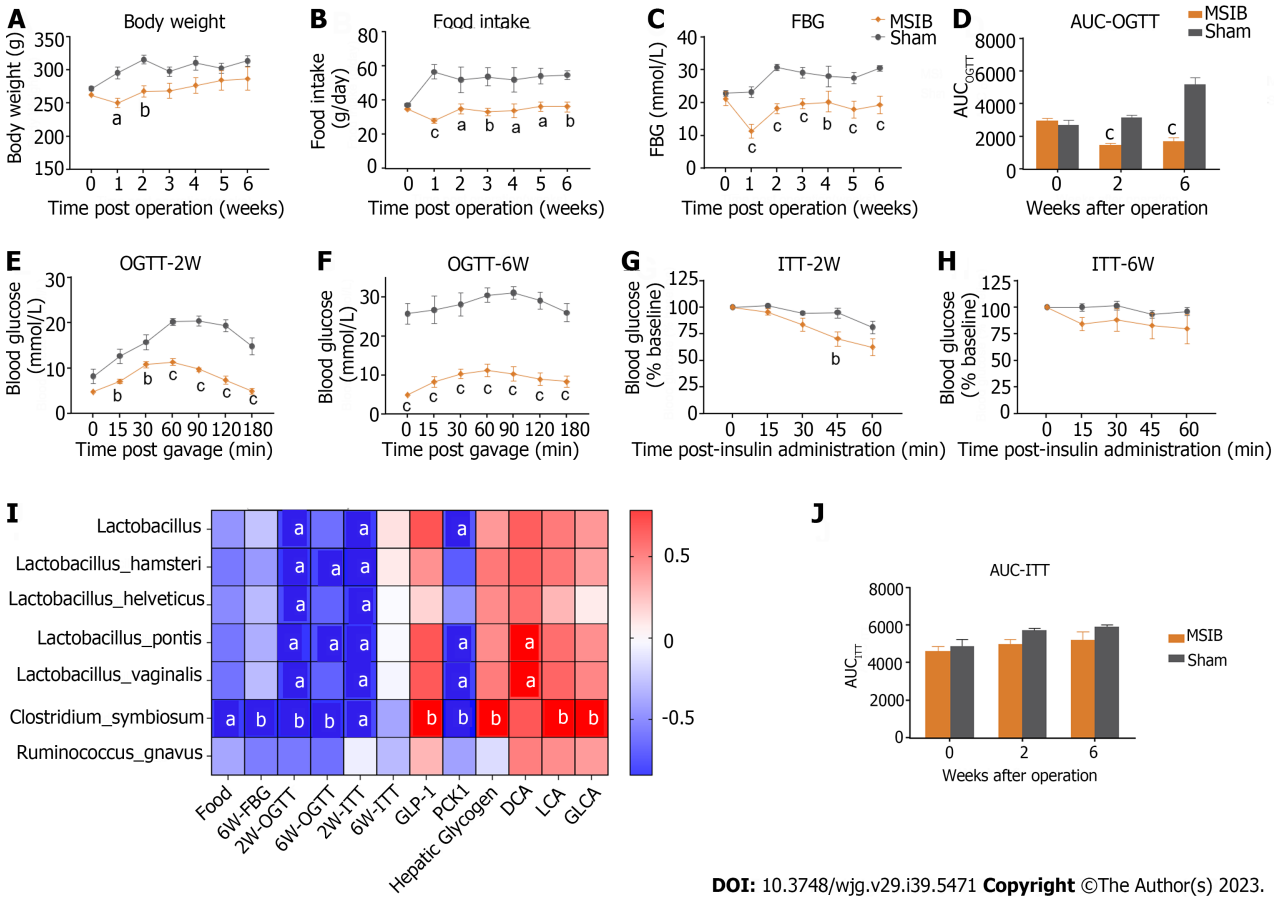

DOI: 10.3748/wjg.v29.i39.5471

Figure 1 Glucose metabolism improved after mid-small intestine bypass and was significantly correlated with postoperative increased abundance of gut microbiota. A: Postoperative body weight changes in rats; B: Postoperative food intake in rats; C: Postoperative mean random blood glucose changes in rats; D-F: Glucose tolerance test and area under the curve in rats; G-J: Insulin sensitivity test and area under the curve in rats (G, H, and J); analysis of the correlation between postoperative abundance of rising gut microbiota and glucose metabolism and bile acids (I). Data are expressed as mean ± SEM and statistical significance was determined by two-tailed Student's test or two-way ANOVA, $^{a}P < 0.05$, $^{b}P < 0.01$, $^{c}P < 0.001$. FBG: Fasting blood glucose; AUC: Area under the curve; OGTT: Oral glucose tolerance test; MSIB: Mid-small intestine bypass; ITT: Insulin tolerance test; PCK1: Phosphoenolpyruvate carboxykinase 1; DCA: Deoxycholic acid; LCA: Lithocholic acid; GLCA: Glycolithocholic acid.

After surgery, the MSIB group exhibited increased expression of farnesoid X receptor (FXR) and Takeda G protein-coupled receptor 5 (TGR5) (Figure 5E), as well as elevated levels of fecal bile acids and secondary bile acids (Figure 5B). Metabolomics analysis revealed a significant increase in fecal bile acids in the MSIB group compared to the sham group (Figure 5). Specifically, there was an increase in secondary bile acids, including chenodeoxycholic acid, deoxycholic acid (DCA), glyco-deoxycholic acid, lithocholic acid (LCA), glycolithocholic acid (GLCA), and ursodeoxycholic acid. Correlation analysis further demonstrated a significant positive correlation between the levels of the intestinal secondary bile acids LCA and GLCA and the abundance of *Clostridium_symbiosum* in the intestines (Figure 5C). Moreover, LCA showed a significant positive correlation with intestinal GLP-1 expression and a significant negative correlation with the key hepatic gluconeogenic enzyme PCK1 (Figures 5C and F).

DISCUSSION

The decrease in serum glucose levels after MSIB is associated with the inhibition of hepatic gluconeogenesis. At 6 wk post-MSIB, diabetic rats in the MSIB group exhibited a significant decrease in blood glucose levels compared to those in the sham group, as well as a significant difference in the OGTT-AUC. These findings confirmed that a 60% small intestinal resection could still improve glucose metabolism, although the effect on reducing body weight was not significant. To explore the underlying mechanism of improved glucose metabolism after MSIB, we assessed the liver tissue glycogen content of rats at 6 wk post-surgery. The results revealed a significantly higher hepatic glycogen content in the MSIB group than in the sham group, indicating that the improved glucose metabolism after MSIB is associated with enhanced serum glucose conversion. Previous studies have reported increased hepatic glucose uptake and decreased endogenous glucose production following metabolic surgery, which aligns with our findings of elevated hepatic glycogen levels[11]. Moreover, bariatric surgery has been shown to inhibit hepatic glucose production[12], further supporting our observation. Analysis of liver tissue also demonstrated significantly reduced expression of the key gluconeogenic enzymes PCK1 and G6PC in the MSIB group compared to the sham group, along with decreased

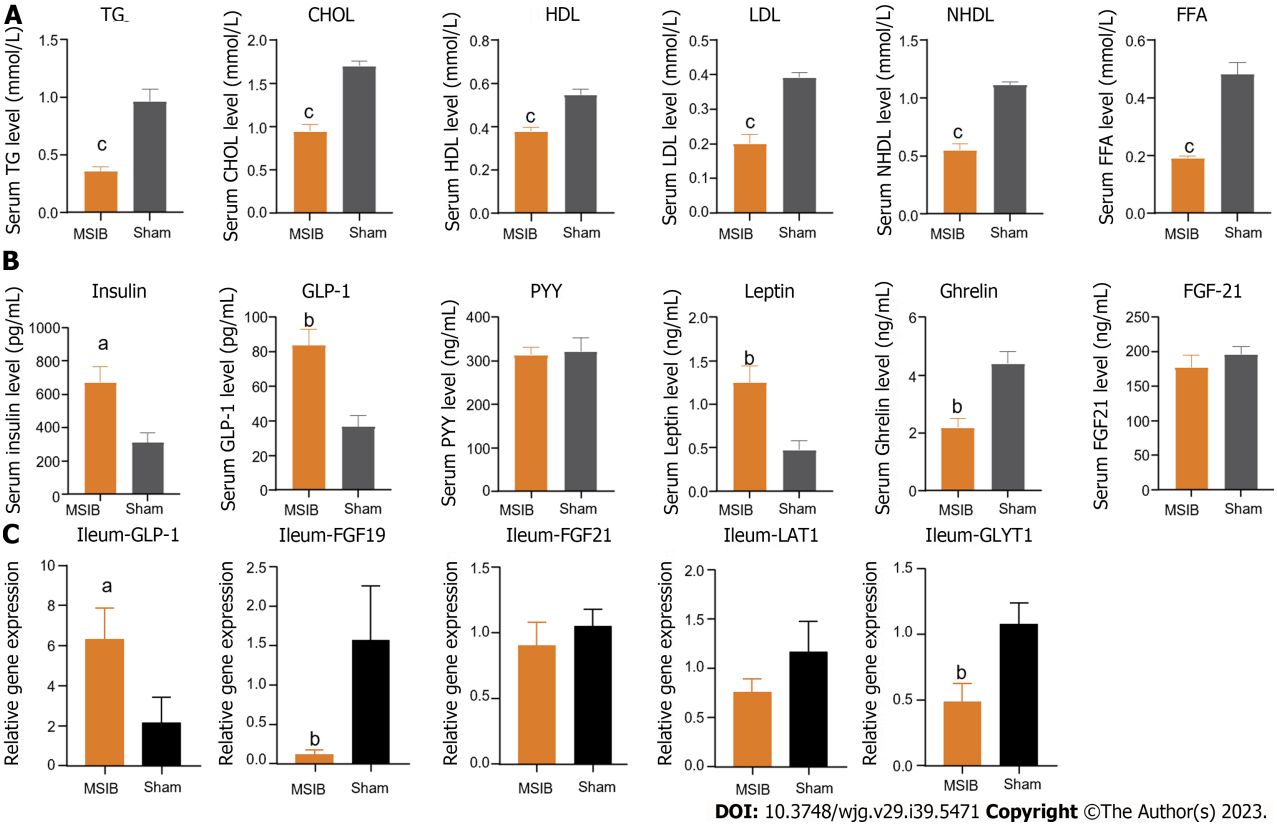

DOI: 10.3748/wjg.v29.i39.5471 **Copyright** ©The Author(s) 2023.

Figure 2 The serum lipid metabolism was improved, serum glucagon-like peptide 1 level was increased and intestinal glucagon-like peptide 1 transcript was increased in rats after mid-small intestine bypass. A: Changes in serum triglycerides, total cholesterol, high-density lipoprotein, low-density lipoprotein, non-high-density lipoprotein, and free fatty acids levels in rats after surgery; B: Changes in serum gastrointestinal hormones in rats after surgery; C: Changes in intestinal glucagon-like peptide 1, fibroblast growth factor 19, fibroblast growth factor 21, LAT1, glycine transporter 1 transcript in rats after surgery. Data are expressed as mean ± SEM and statistical significance was determined by two-tailed Student's test or two-way ANOVA, $^{a}P < 0.05$, $^{b}P < 0.01$, $^{c}P < 0.001$. TG: Triglycerides; CHOL: Cholesterol; HDL: High-density lipoprotein; LDL: Low-density lipoprotein; NHDL: Non-high-density lipoprotein; FFA: Free fatty acid; GLP-1: Glucagon-like peptide 1; PYY: Peptide tyrosine tyrosine; FGF21: Fibroblast growth factor 21; GLYT1: Glycine transporter 1.

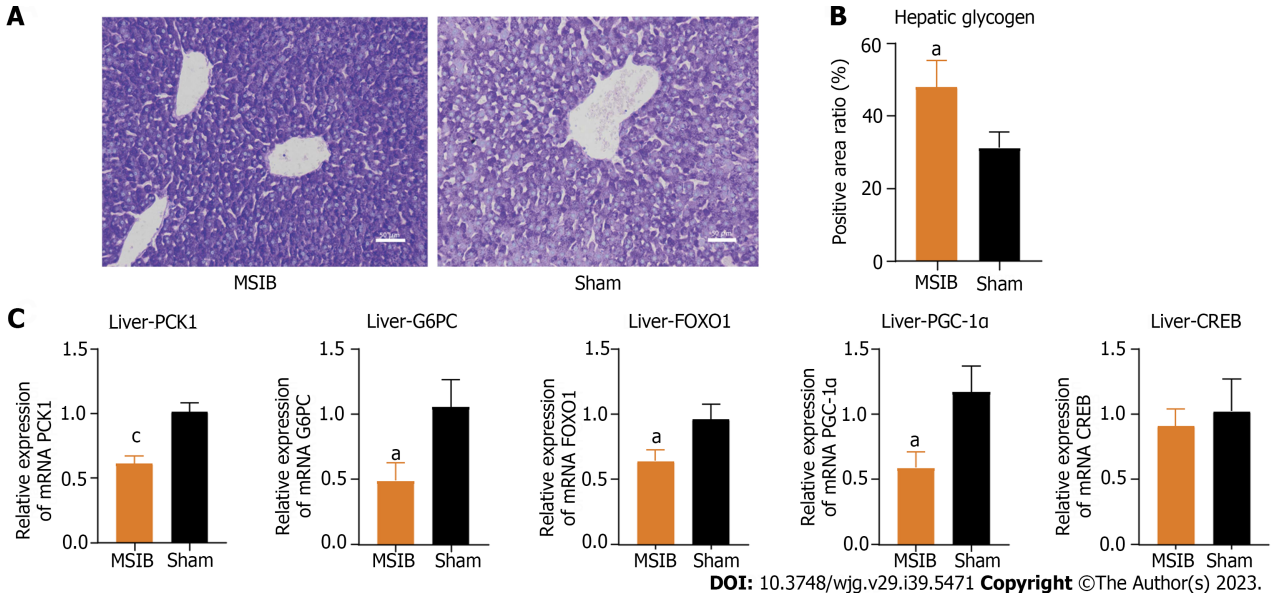

DOI: 10.3748/wjg.v29.i39.5471 **Copyright** ©The Author(s) 2023.

Figure 3 Increased glycogen reserves and decreased expression of gluconeogenesis-related enzymes and transcription factors in rat liver after mid-small intestine bypass. A and B: Glycogen staining and comparison of liver tissue sections; C: Expression of key gluconeogenesis enzymes and regulatory-related transcription factors. Data are expressed as mean ± SEM and statistical significance was determined by two-tailed Student's test or two-way ANOVA, $^{a}P < 0.05$, $^{c}P < 0.001$. MSIB: Mid-small intestine bypass; PCK1: Phosphoenolpyruvate carboxykinase 1; G6PC: Glucose-6-phosphatase; FOXO1: Forkhead box O1; PGC1α: Peroxisome proliferator-activated receptor gamma coactivator 1 alpha; CREB: cAMP response element-binding protein.

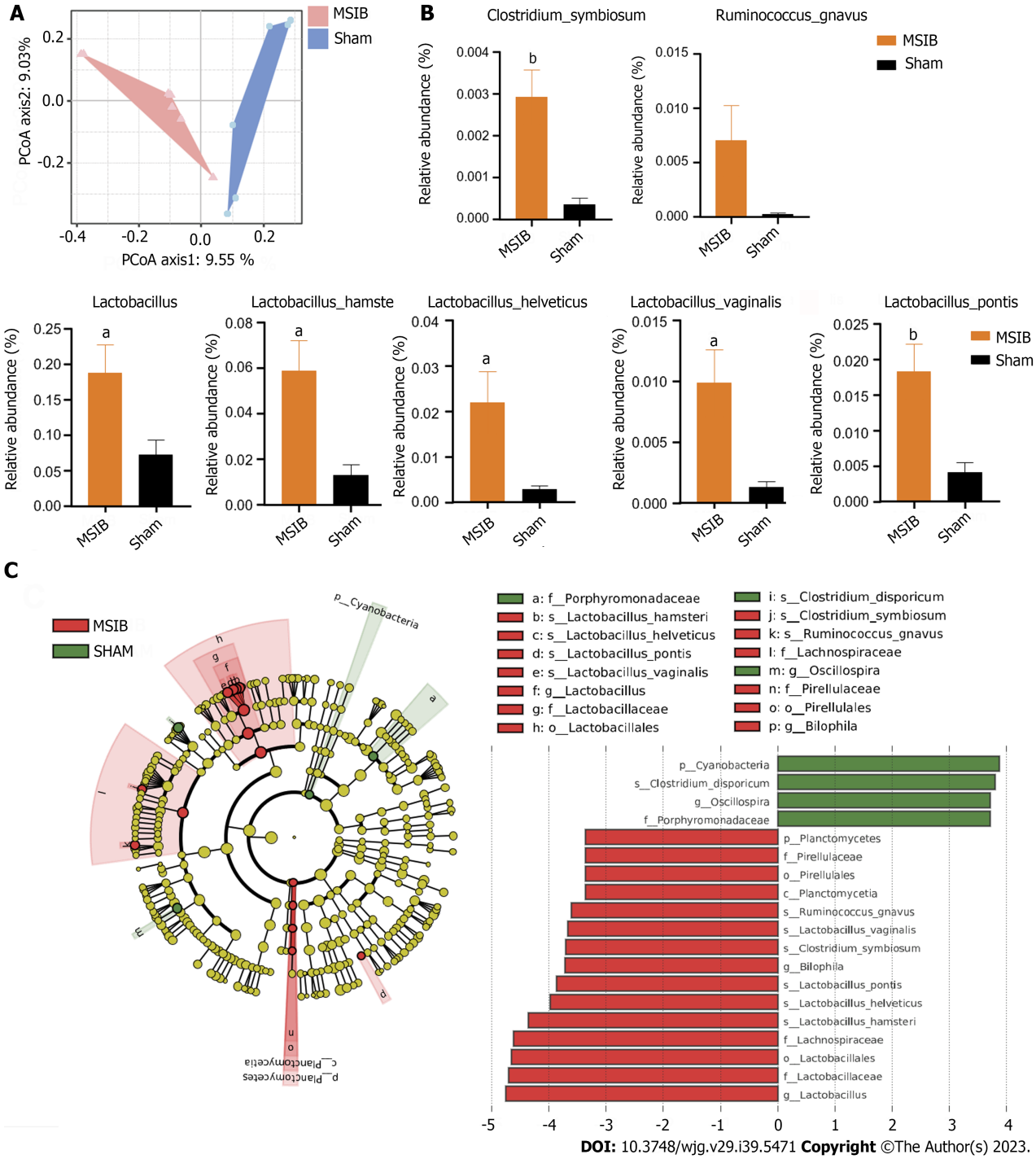

DOI: 10.3748/wjg.v29.i39.5471

Figure 4 Changes in gut microbiota after mid-small intestine bypass. A: Principal coordinate analysis of gut microbiota based on OUT data from mid-small intestine bypass (MSIB) and sham groups; B: Bacteria with increased intestinal abundance in rats after MSIB; C: Phylogenetic tree for comparison of linear discriminant analysis (LDA) effect sizes of gut microbiota in MSIB and sham groups, bacteria with significantly enriched LDA scores taxa are marked with the colours shown. Data are expressed as mean ± SEM and statistical significance was determined by two-tailed Student's test or two-way ANOVA, $^{a}P < 0.05$, $^{b}P < 0.01$. MSIB: Mid-small intestine bypass; LDA: Linear discriminant analysis; PCoA: Principal coordinate analysis.

expression of the transcription factors FOXO1 and PGC-1α, which regulate gluconeogenesis. Correlation analysis revealed a significant positive correlation between PCK1, G6PC, and glucose levels. Based on these findings, we conclude that the decrease in serum glucose levels after MSIB is attributed to the inhibition of gluconeogenesis.

The gut microbiome of rats underwent significant changes after MSIB, as revealed by LEfSe analysis. Specifically, there was a significant increase in the abundance of *Lactobacillus spp*., including specific species such as *Lactobacillus hamsteri*, *Lactobacillus helveticus*, *Lactobacillus pontis*, *Lactobacillus vaginalis*, and *Ruminococcus gnavus*. Additionally, the abundances of *Bilophila* and *Clostridium symbiosum*, which are known to metabolize bile acids, also increased significantly. Our experiments demonstrated an increase in the fecal levels of various secondary bile acids in the MSIB group compared to the sham group. Correlation analysis revealed a significant positive correlation between the levels of LCA and GLCA and the abundance of intestinal *Clostridium symbiosum*, suggesting the involvement of the intestinal flora in metabolic

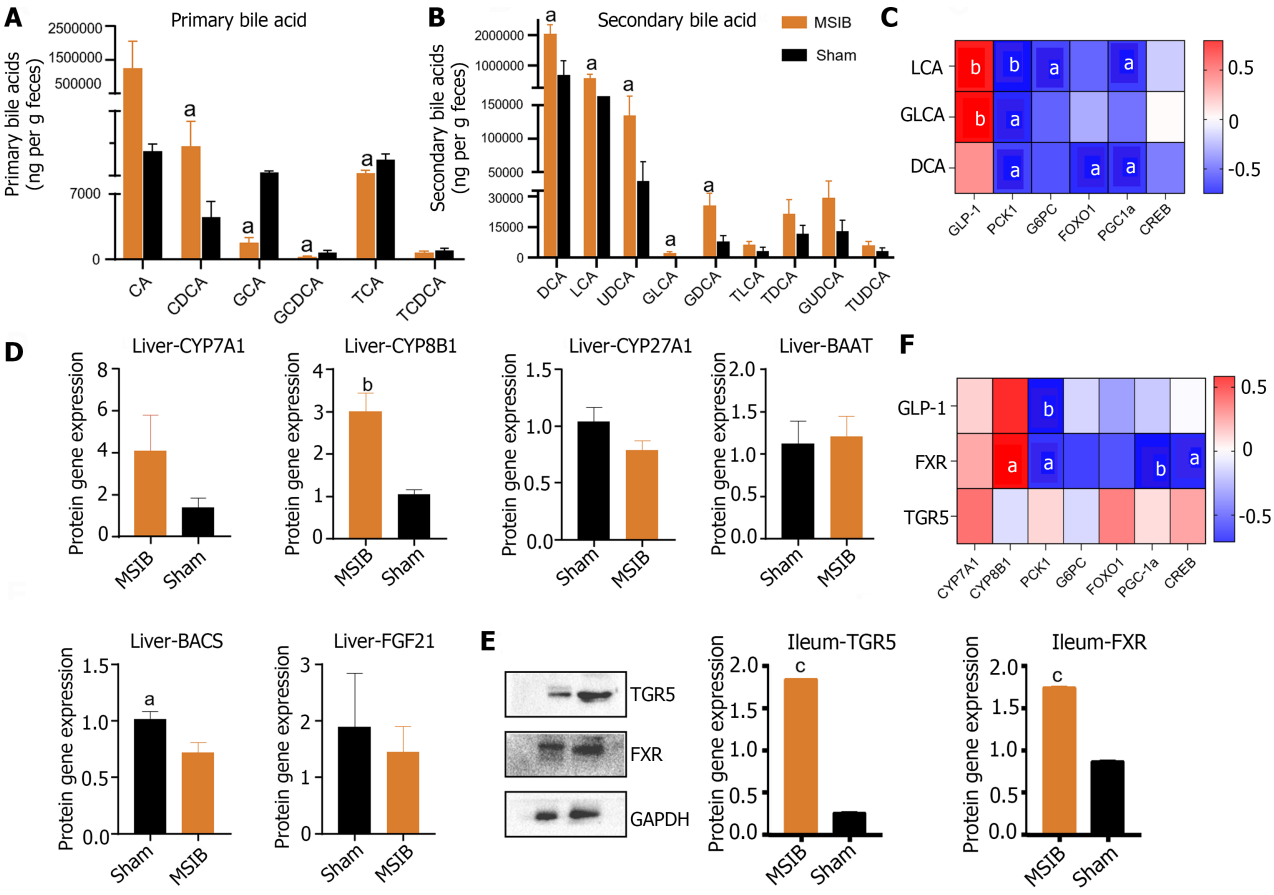

DOI: 10.3748/wjg.v29.i39.5471

Figure 5 Changes in intestinal bile acid profile in rats after mid-small intestine bypass, correlating significantly with intestinal hormones and key enzymes of gluconeogenesis. A: Changes in primary bile acid profile in rats; B: Changes in secondary bile acid profile in rats; C: Correlation analysis of bile acid with glucagon-like peptide 1 and factors regulating gluconeogenesis; D: Expression of bile acid synthase and transcription factor, fibroblast growth factor 21. E: Takeda G protein-coupled receptor 5 and farnesoid X receptor WB results. F: Correlation analysis. Data are expressed as mean ± SEM and statistical significance was determined by two-tailed Student's test or two-way ANOVA, $^{a}P < 0.05$, $^{b}P < 0.01$, $^{c}P < 0.001$. PCK1: Phosphoenolpyruvate carboxykinase 1; DCA: Deoxycholic acid; LCA: Lithocholic acid; GLCA: Glycolithocholic acid; GLP-1: Glucagon-like peptide 1; TGR5: Takeda G protein-coupled receptor 5; FXR: Farnesoid X receptor; G6PC: Glucose-6-phosphatase; CA: Cholic acid; CDCA: Chenodeoxycholic acid; GCA: Glycocholic acid; GCDCA: Glycochenodeoxycholic acid; TCA: Taurocholic acid; TCDCA: Taurochenodeoxycholic acid; UDCA: Ursodeoxycholic acid; GDCA: Glyco-deoxycholic acid; TLCA: Taurolithocholic acid; TDCA: Taurodeoxycholic acid; GUDCA: Glycoursodeoxycholic acid; TUDCA: Tauroursodeoxycholic acid; FOXO1: Forkhead box O1; PGC1α: Peroxisome proliferator-activated receptor gamma coactivator 1 alpha; CREB: cAMP response element-binding protein; MSIB: Mid-small intestine bypass; CYP: Cytochrome P450; BAAT: Bile acid-CoA amino acid N-acyltransferase; BACS: Bile acid-CoA synthetase; FGF21: Fibroblast growth aactor 21; TGR5: Takeda G protein-coupled receptor 5; FXR: Farnesol X receptor.

regulation through the catabolic production of secondary bile acids.

Remarkably, the expression levels of cytochrome P450 family 8 subfamily B member 1, an enzyme involved in bile acid synthesis, were significantly increased in the experimental group, suggesting that the elevated bile acid levels after MSIB may be attributed to augmented classical bile acid pathway synthesis. Bile acids play a crucial role in metabolic regulation as important signaling molecules. Previous studies by Steenackers *et al*[8] demonstrated that LCA can bind to hepatic vitamin D receptors, thereby promoting GLP-1 secretion from intestinal L cells (Figure 6). In our experiments, we also observed an increase in intestinal LCA levels and GLP-1 transcription in rats following MSIB surgery.

Moreover, bile acids can modulate metabolic homeostasis by activating the nuclear receptor FXR and the membrane receptor TGR5[13-15]. TGR5 receptor activation is generally believed to confer metabolic benefits, while the precise role of FXR in metabolic regulation remains to be fully elucidated. Pathak *et al*[16] demonstrated that the dual agonist INT-767 induces GLP-1 secretion from cells, which aligns with our observations. We found increased transcript levels of TGR5 and FXR in the MSIB group of rats after surgery, along with elevated GLP-1 transcript levels. GLP-1, as a gastrointestinal hormone, reduces blood glucose levels and improves insulin resistance. Importantly, we observed a positive correlation between insulin sensitivity and GLP-1 in the experimental group of rats. Based on these findings, we propose that secondary bile acids promote GLP-1 secretion through the activation of TGR5 and FXR, thus benefiting glucose metabolism in rats after MSIB. Additionally, the gut microbiota plays a crucial role as an important mediator of this process.

There was a significant negative correlation between GLP-1 levels and the transcript levels of the key enzymes PCK1 and G6PC after MSIB. We observed increased glycogen stores in liver tissue and a significant decrease in the expression

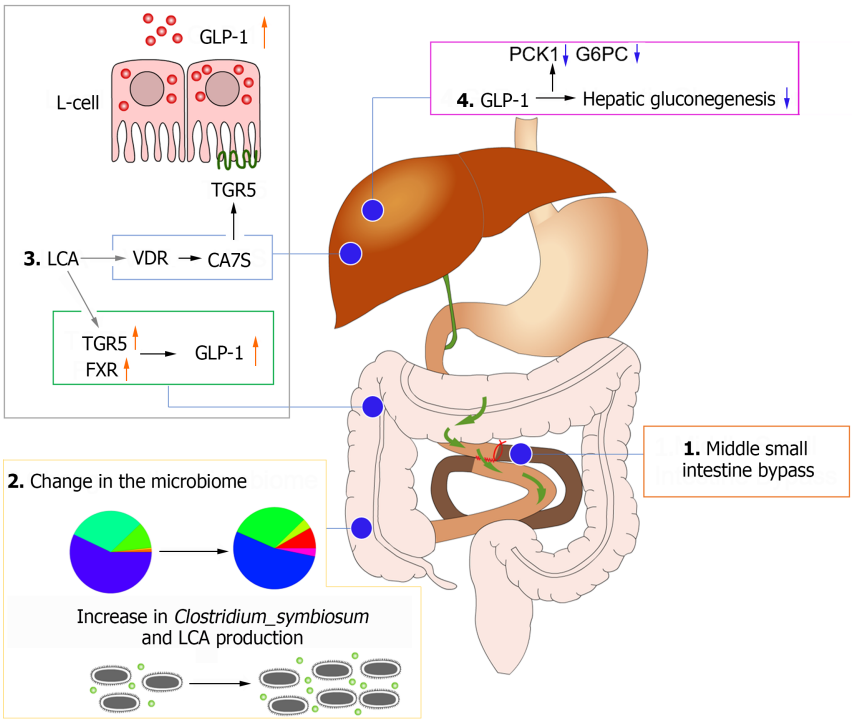

DOI: 10.3748/wjg.v29.i39.5471

Figure 6 Diagram of the mechanism of improved glucose metabolism after mid-small intestine bypass. GLP-1: Glucagon-like peptide 1; TGR5: Takeda G protein-coupled receptor 5; FXR: Farnesoid X receptor; LCA: Lithocholic acid; PCK1: Phosphoenolpyruvate carboxykinase 1; G6PC: Glucose-6-phosphatase.

of the gluconeogenic enzymes PCK1 and G6PC in the MSIB group compared to the sham group after surgery. Additionally, the transcription factors FOXO1 and CREB, which regulate gluconeogenesis, were also found to be inhibited. These findings suggest that the inhibition of gluconeogenesis played a significant role in the reduction in blood glucose levels in rats after MSIB.

Furthermore, correlation analysis revealed a significant negative correlation between PCK1 expression and GLP-1 levels, indicating that GLP-1 may be involved in the inhibition of gluconeogenesis. However, further experimental evidence is required to confirm this relationship. Previous studies by Lee *et al*[17] demonstrated that GLP-1 gene therapy reduces hepatic gluconeogenesis. Other scholars have suggested that GLP-1 may inhibit hepatic gluconeogenesis through FGF21[18] and regulate hepatic glucose production through neural circuits[19]. Additionally, intraperitoneal injection of GLP-1 has been shown to inhibit gluconeogenesis and related enzyme activity in obese mice[20]. These studies support the notion that GLP-1 can influence hepatic gluconeogenesis to improve blood glucose levels, which aligns with our observation of the decreased expression of key gluconeogenic enzymes. Therefore, we conclude that the increased levels of GLP-1 were responsible for the inhibition of postoperative gluconeogenesis in the MSIB group of rats.

In summary, our findings suggest that hepatic gluconeogenesis is inhibited by the decrease in serum glucose levels in rats after MSIB. Increased GLP-1 secretion, attributed to the elevated abundance of intestinal *Clostridium symbiosum*, serves as a potential pathway mediating these effects.

The study has some limitations, including a small sample size and a relatively short observation period. To further investigate the relationship between the intestinal *Clostridium symbiosum* abundance, bile acids, and GLP-1, future studies should consider conducting microbiota transplantation experiments and cell-based assays. Additionally, the cellular pathways connecting GLP-1 and gluconeogenesis still require further investigation.

CONCLUSION

Postoperative intestinal bypass of the midsection small intestine in nonobese diabetic rats improves glucose metabolism by increasing GLP-1 levels and inhibiting hepatic gluconeogenesis through the increased abundance of intestinal *Clostridium symbiosum*.

ARTICLE HIGHLIGHTS

Research background

The exact mechanism by which mid-small intestinal bypass (MSIB) improves glucose metabolism in diabetic rats is not fully understood.

Research motivation

To explore the role of the mid-small intestine in the onset and progression of diabetes.

Research objectives

The aim of this study was to elucidate the mechanisms by which MSIB improves glucose metabolism.

Research methods

Streptozotocin was used to induce diabetes mellitus in Sprague-Dawley rats at a dose of 60 mg/kg. The rats were then randomly divided into two groups: The MSIB group and the sham group (underwent switch laparotomy). Following a 6-wk recovery period post-surgery, the rats underwent various assessments, including metabolic parameter testing, analysis of liver glycogen levels, measurement of key gluconeogenic enzyme activity, characterization of the gut microbiota composition, evaluation of hormone levels, determination of bile acid concentrations, and assessment of the expression of the intestinal receptors Takeda G protein-coupled receptor 5 and farnesoid X receptor.

Research results

The MSIB group of rats exhibited improved glucose and lipid metabolism, increased hepatic glycogen content, and decreased expression of key gluconeogenic enzymes (phosphoenolpyruvate carboxykinase 1 and glucose-6-phosphatase). Notably, this group showed a substantial rise in specific intestinal bacteria, including *Lactobacillus*, *Clostridium symbiosum*, *Ruminococcus gnavus*, and *Bilophila*. Additionally, elevated levels of secondary bile acids, such as lithocholic acid, were observed. Importantly, changes in the gut microbiota were significantly correlated with the expression of gluconeogenic enzymes and glucagon-like peptide 1 (GLP-1) at 6 wk post-surgery, suggesting their potential involvement in regulating glucose. These findings underscore the beneficial impact of mid-small intestine bypass on glucose metabolism and its modulation of the gut microbiota.

Research conclusions

This study shows that postoperative introduction of intestinal *Clostridium symbiosum* in the mid-small intestine improves glucose metabolism in non-obese diabetic rats. This enhancement is linked to increased inhibition of hepatic gluconeogenesis mediated by GLP-1, leading to a positive impact on glucose regulation.

Research perspectives

This study explores partial mechanisms of the interaction between gut microbiota and host metabolism, providing a theoretical foundation for non-surgical interventions in diabetes-related metabolic disorders.

FOOTNOTES

Author contributions: Luo X, Tan C, Cao JQ, and Duan JY contributed to the conception of the study; Luo X, Tan C, Zheng ZH, and Pang Q performed the experiment; Luo X, Tan C, and Duan JY contributed significantly to analysis and manuscript preparation; Luo X, Tao F, Xu CY, Zheng ZH, Pang Q, He XA, Cao JQ, and Duan JY helped perform the analysis with constructive discussions; Luo X, Tan C, and Duan JY performed the data analyses and wrote the manuscript.

Supported by National Natural Science Foundation of China, No. 82060161, 81960154, and 81760156; Jiangxi Provincial Youth Science Foundation, No. 2018ACB21040; Natural Science Foundation of Jiangxi Province, No. 20212BAB206020; and Foundation of Health commission of Jiangxi Province, No. SKJP220225830.

Institutional animal care and use committee statement: The study was reviewed and approved by the the Animal Ethics Committee of Nanchang University.

Conflict-of-interest statement: All the authors report no relevant conflicts of interest for this article.

Data sharing statement: Technical appendix, statistical code, and dataset available from the corresponding author at duanjy2022@outlook.com.

ARRIVE guidelines statement: The authors have read the ARRIVE Guidelines, and the manuscript was prepared and revised according to the ARRIVE Guidelines.

Country/Territory of origin: China

ORCID number: Xin Luo 0009-0002-9361-8178; Fang Tao 0009-0003-0464-9595; Cai Tan 0009-0009-4338-1505; Chi-Ying Xu 0009-0006-2150-762X; Zhi-Hua Zheng 0009-0007-7695-6921; Qiang Pang 0009-0007-0511-3580; Xiang-An He 0009-0007-9231-7652; Jia-Qing Cao 0000-0002-7270-2779; Jin-Yuan Duan 0000-0002-7772-7844.

S-Editor: Wang JJ
L-Editor: A
P-Editor: Cai YX

REFERENCES

1 **NCD Risk Factor Collaboration (NCD-RisC)**. Worldwide trends in body-mass index, underweight, overweight, and obesity from 1975 to 2016: a pooled analysis of 2416 population-based measurement studies in 128·9 million children, adolescents, and adults. *Lancet* 2017; **390**: 2627-2642 [PMID: 29029897 DOI: 10.1016/S0140-6736(17)32129-3]

2 **Molina-Montes E**, Coscia C, Gómez-Rubio P, Fernández A, Boenink R, Rava M, Márquez M, Molero X, Löhr M, Sharp L, Michalski CW, Farré A, Perea J, O'Rorke M, Greenhalf W, Iglesias M, Tardón A, Gress TM, Barberá VM, Crnogorac-Jurcevic T, Muñoz-Bellvís L, Dominguez-Muñoz JE, Renz H, Balcells J, Costello E, Ilzarbe L, Kleeff J, Kong B, Mora J, O'Driscoll D, Poves I, Scarpa A, Yu J, Hidalgo M, Lawlor RT, Ye W, Carrato A, Real FX, Malats N; PanGenEU Study Investigators. Deciphering the complex interplay between pancreatic cancer, diabetes mellitus subtypes and obesity/BMI through causal inference and mediation analyses. *Gut* 2021; **70**: 319-329 [PMID: 32409590 DOI: 10.1136/gutjnl-2019-319990]

3 **Fink J**, Seifert G, Blüher M, Fichtner-Feigl S, Marjanovic G. Obesity Surgery. *Dtsch Arztebl Int* 2022; **119**: 70-80 [PMID: 34819222 DOI: 10.3238/arztebl.m2021.0359]

4 **Cummings BP**, Strader AD, Stanhope KL, Graham JL, Lee J, Raybould HE, Baskin DG, Havel PJ. Ileal interposition surgery improves glucose and lipid metabolism and delays diabetes onset in the UCD-T2DM rat. *Gastroenterology* 2010; **138**: 2437-2446, 2446.e1 [PMID: 20226188 DOI: 10.1053/j.gastro.2010.03.005]

5 **Zhang X**, Young RL, Bound M, Hu S, Jones KL, Horowitz M, Rayner CK, Wu T. Comparative Effects of Proximal and Distal Small Intestinal Glucose Exposure on Glycemia, Incretin Hormone Secretion, and the Incretin Effect in Health and Type 2 Diabetes. *Diabetes Care* 2019; **42**: 520-528 [PMID: 30765429 DOI: 10.2337/dc18-2156]

6 **Soper NJ**, Chapman NJ, Kelly KA, Brown ML, Phillips SF, Go VL. The 'ileal brake' after ileal pouch-anal anastomosis. *Gastroenterology* 1990; **98**: 111-116 [PMID: 2293569 DOI: 10.1016/0016-5085(90)91298-k]

7 **Jarvie BC**, Knight ZA. Breaking down a gut-to-brain circuit that prevents malabsorption. *Cell* 2022; **185**: 2393-2395 [PMID: 35803241 DOI: 10.1016/j.cell.2022.06.012]

8 **Steenackers N**, Vanuytsel T, Augustijns P, Tack J, Mertens A, Lannoo M, Van der Schueren B, Matthys C. Adaptations in gastrointestinal physiology after sleeve gastrectomy and Roux-en-Y gastric bypass. *Lancet Gastroenterol Hepatol* 2021; **6**: 225-237 [PMID: 33581761 DOI: 10.1016/S2468-1253(20)30302-2]

9 **Reed MJ**, Meszaros K, Entes LJ, Claypool MD, Pinkett JG, Gadbois TM, Reaven GM. A new rat model of type 2 diabetes: the fat-fed, streptozotocin-treated rat. *Metabolism* 2000; **49**: 1390-1394 [PMID: 11092499 DOI: 10.1053/meta.2000.17721]

10 **Bokulich NA**, Subramanian S, Faith JJ, Gevers D, Gordon JI, Knight R, Mills DA, Caporaso JG. Quality-filtering vastly improves diversity estimates from Illumina amplicon sequencing. *Nat Methods* 2013; **10**: 57-59 [PMID: 23202435 DOI: 10.1038/nmeth.2276]

11 **Immonen H**, Hannukainen JC, Iozzo P, Soinio M, Salminen P, Saunavaara V, Borra R, Parkkola R, Mari A, Lehtimäki T, Pham T, Laine J, Kärjä V, Pihlajamäki J, Nelimarkka L, Nuutila P. Effect of bariatric surgery on liver glucose metabolism in morbidly obese diabetic and non-diabetic patients. *J Hepatol* 2014; **60**: 377-383 [PMID: 24060855 DOI: 10.1016/j.jhep.2013.09.012]

12 **Ben-Haroush Schyr R**, Al-Kurd A, Moalem B, Permyakova A, Israeli H, Bardugo A, Arad Y, Hefetz L, Bergel M, Haran A, Azar S, Magenheim I, Tam J, Grinbaum R, Ben-Zvi D. Sleeve Gastrectomy Suppresses Hepatic Glucose Production and Increases Hepatic Insulin Clearance Independent of Weight Loss. *Diabetes* 2021; **70**: 2289-2298 [PMID: 34341005 DOI: 10.2337/db21-0251]

13 **Sayin SI**, Wahlström A, Felin J, Jäntti S, Marschall HU, Bamberg K, Angelin B, Hyötyläinen T, Orešič M, Bäckhed F. Gut microbiota regulates bile acid metabolism by reducing the levels of tauro-beta-muricholic acid, a naturally occurring FXR antagonist. *Cell Metab* 2013; **17**: 225-235 [PMID: 23395169 DOI: 10.1016/j.cmet.2013.01.003]

14 **Duboc H**, Taché Y, Hofmann AF. The bile acid TGR5 membrane receptor: from basic research to clinical application. *Dig Liver Dis* 2014; **46**: 302-312 [PMID: 24411485 DOI: 10.1016/j.dld.2013.10.021]

15 **Yan Y**, Niu Z, Sun C, Li P, Shen S, Liu S, Wu Y, Yun C, Jiao T, Jia S, Li Y, Fang ZZ, Zhao L, Wang J, Xie C, Jiang C, Feng X, Hu C, Jiang J, Ying H. Hepatic thyroid hormone signalling modulates glucose homeostasis through the regulation of GLP-1 production *via* bile acid-mediated FXR antagonism. *Nat Commun* 2022; **13**: 6408 [PMID: 36302774 DOI: 10.1038/s41467-022-34258-w]

16 **Pathak P**, Liu H, Boehme S, Xie C, Krausz KW, Gonzalez F, Chiang JYL. Farnesoid X receptor induces Takeda G-protein receptor 5 cross-talk to regulate bile acid synthesis and hepatic metabolism. *J Biol Chem* 2017; **292**: 11055-11069 [PMID: 28478385 DOI: 10.1074/jbc.M117.784322]

17 **Lee YS**, Shin S, Shigihara T, Hahm E, Liu MJ, Han J, Yoon JW, Jun HS. Glucagon-like peptide-1 gene therapy in obese diabetic mice results in long-term cure of diabetes by improving insulin sensitivity and reducing hepatic gluconeogenesis. *Diabetes* 2007; **56**: 1671-1679 [PMID: 17369525 DOI: 10.2337/db06-1182]

18 **Liu J**, Yang K, Yang J, Xiao W, Le Y, Yu F, Gu L, Lang S, Tian Q, Jin T, Wei R, Hong T. Liver-derived fibroblast growth factor 21 mediates effects of glucagon-like peptide-1 in attenuating hepatic glucose output. *EBioMedicine* 2019; **41**: 73-84 [PMID: 30827929 DOI: 10.1016/j.ebiom.2019.02.037]

19 **Yang M**, Wang J, Wu S, Yuan L, Zhao X, Liu C, Xie J, Jia Y, Lai Y, Zhao AZ, Boden G, Li L, Yang G. Duodenal GLP-1 signaling regulates hepatic glucose production through a PKC-δ-dependent neurocircuitry. *Cell Death Dis* 2017; **8**: e2609 [PMID: 28182013 DOI: 10.1038/cddis.2017.28]

20 **Ip W**, Shao W, Chiang YT, Jin T. GLP-1-derived nonapeptide GLP-1(28-36)amide represses hepatic gluconeogenic gene expression and improves pyruvate tolerance in high-fat diet-fed mice. *Am J Physiol Endocrinol Metab* 2013; **305**: E1348-E1358 [PMID: 24085036 DOI: 10.1152/ajpendo.00376.2013]

World Journal of Gastroenterology

Submit a Manuscript: https://www.f6publishing.com

World J Gastroenterol 2023 October 21; 29(39): 5483-5493

DOI: 10.3748/wjg.v29.i39.5483

ISSN 1007-9327 (print) ISSN 2219-2840 (online)

ORIGINAL ARTICLE

Retrospective Cohort Study

Development and validation of a nomogram for preoperative prediction of tumor deposits in colorectal cancer

Hui-Da Zheng, Yun-Huang Hu, Kai Ye, Jian-Hua Xu

Specialty type: Gastroenterology and hepatology

Provenance and peer review: Unsolicited article; Externally peer reviewed.

Peer-review model: Single blind

Peer-review report's scientific quality classification

Grade A (Excellent): A
Grade B (Very good): B
Grade C (Good): 0
Grade D (Fair): 0
Grade E (Poor): 0

P-Reviewer: Camacho S, Mexico; Ekine-Afolabi B, United Kingdom

Received: July 11, 2023
Peer-review started: July 11, 2023
First decision: September 18, 2023
Revised: September 21, 2023
Accepted: September 28, 2023
Article in press: September 28, 2023
Published online: October 21, 2023

Hui-Da Zheng, Yun-Huang Hu, Kai Ye, Jian-Hua Xu, Department of Gastrointestinal Surgery, The Second Affiliated Hospital of Fujian Medical University, Quanzhou 362000, Fujian Province, China

Corresponding author: Jian-Hua Xu, MD, Chief Physician, Dean, Research Dean, Surgeon, Surgical Oncologist, Department of Gastrointestinal Surgery, The Second Affiliated Hospital of Fujian Medical University, No. 950 Donghai Street, Fengze District, Quanzhou 362000, Fujian Province, China. xjh630913@126.com

Abstract

BACKGROUND

Based on the clinical data of colorectal cancer (CRC) patients who underwent surgery at our institution, a model for predicting the formation of tumor deposits (TDs) in this patient population was established.

AIM

To establish an effective model for predicting TD formation, thus enabling clinicians to identify CRC patients at high risk for TDs and implement personalized treatment strategies.

METHODS

CRC patients (n = 645) who met the inclusion criteria were randomly divided into training (n = 452) and validation (n = 193) cohorts using a 7:3 ratio in this retrospective analysis. Least absolute shrinkage and selection operator regression was employed to screen potential risk factors, and multivariable logistic regression analysis was used to identify independent risk factors. Subsequently, a predictive model for TD formation in CRC patients was constructed based on the independent risk factors. The discrimination ability of the model, its consistency with actual results, and its clinical applicability were evaluated using receiver-operating characteristic curves, area under the curve (AUC), calibration curves, and decision curve analysis (DCA).

RESULTS

Thirty-four (7.5%) patients with TDs were identified in the training cohort based on postoperative pathological specimens. Multivariate logistic regression analysis identified female sex, preoperative intestinal obstruction, left-sided CRC, and lymph node metastasis as independent risk factors for TD formation. The AUCs of the nomogram models constructed using these variables were 0.839 and 0.853 in

the training and validation cohorts, respectively. The calibration curve demonstrated good consistency, and the training cohort DCA yielded a threshold probability of 7%-78%.

CONCLUSION
This study developed and validated a nomogram with good predictive performance for identifying TDs in CRC patients. Our predictive model can assist surgeons in making optimal treatment decisions.

Key Words: Colorectal cancer; Tumor deposits; Nomogram

Core Tip: This article retrospectively analyzed the risk factors for tumor deposits (TDs) in colorectal cancer (CRC) and established a nomogram that included female sex, preoperative intestinal obstruction, left-sided CRC, and lymph node metastasis. This model enabled clinicians to identify high-risk populations for TDs in CRC patients and implement personalized treatment strategies.

Citation: Zheng HD, Hu YH, Ye K, Xu JH. Development and validation of a nomogram for preoperative prediction of tumor deposits in colorectal cancer. *World J Gastroenterol* 2023; 29(39): 5483-5493
URL: https://www.wjgnet.com/1007-9327/full/v29/i39/5483.htm
DOI: https://dx.doi.org/10.3748/wjg.v29.i39.5483

INTRODUCTION

Colorectal cancer (CRC) is the third most common cancer worldwide, with over 1 million new cases each year, making it the second leading cause of cancer death[1]. The current management of CRC is based on the tumor, lymph node, and metastasis (TNM) staging system. Initially developed to predict cancer prognosis, this system has evolved and now serves as the basis for determining treatment strategies and enrolling patients in clinical studies[2]. The TNM system has evolved continuously throughout scientific advancements, and its latest edition, the 8th edition of the TNM classification, was published in 2017[3]. However, the current TNM staging system exhibits limited ability to evaluate prognosis and clinical outcomes for patients with stage III CRC[4]. To improve the accuracy of staging systems in CRC, it is important to consider several key prognostic markers, including lymphatic invasion, neural invasion, and tumor deposits (TDs)[5]. TDs are defined as isolated tumor lesions found in the fat around the colon or rectum or adjacent mesentery (colon mesentery fat) far from the edge of tumor infiltration without evidence of residual lymphatic tissue[6]. Previous studies have shown that TDs are associated with early metastasis and poor prognosis[6,7]. No consensus has been reached on whether TDs should be considered positive lymph nodes in the TNM staging of CRC, leading to modifications and changes in the TNM staging system over time. Since 1997, TDs have been considered in the TNM classification[8]. In the 7th and 8th versions of the TNM staging systems, the presence of TDs without any positive lymph nodes is classified as "N1c"[9]. Some studies suggest that TDs may indicate a worse prognosis than lymph node metastasis, highlighting the importance of recognizing the role of TDs in prognostic assessment within the TNM staging system[6,10,11].

Limited research has investigated preoperative risk factors associated with TDs, particularly in the development of reliable predictive models. As a result, accurately assessing the presence of TDs before surgery remains challenging. This study aimed to address that gap by constructing a nomogram that can accurately and effectively predict the likelihood of TDs in patients with CRC. The nomogram aimed to identify individuals at high risk of recurrence, providing valuable insights for personalized treatment strategies and ultimately enhancing prognosis.

MATERIALS AND METHODS

Patients

This retrospective study was conducted at a single center and received approval from the Ethics Committee of the Second Affiliated Hospital of Fujian Medical University (2023-266). The study included a total of 645 patients diagnosed with CRC who underwent surgery between July 2019 and October 2022. The inclusion criteria were as follows: (1) Pathological confirmation of CRC; (2) undergoing surgical treatment; and (3) CRC being the primary malignant tumor. The exclusion criteria were as follows: (1) Presence of distant metastasis; (2) history of treatment with preoperative neoadjuvant radiotherapy and chemotherapy; and (3) incomplete clinical data.

The definition of TDs

TDs are characterized by the presence of tumor cells within the adipose tissue surrounding the colon or rectum, situated at a distance from the leading edge of tumor invasion. Importantly, there is no indication of residual lymph node tissue

within the lymphatic drainage region of the tumor[12]. As shown in Figure 1, we found nodular formations consisting of tumor cell extensions in the surrounding structures of the colon and rectum, which do not appear to meet the criteria for classification as lymph nodes.

Variables

In the present study, certain variables were reclassified based on specific criteria. Age was divided into two groups: ≤ 64 years old and > 64 years old. Sex was categorized as male and female. Body mass index records were classified as ≤ 25 and > 25. Tumor size was grouped as ≤ 3 cm and > 3 cm. The tumor site was divided into the right side (cecum, ascending colon, hepatic flexure, and transverse colon) and the left side (splenic flexure, descending colon, sigmoid colon, and rectum). Tumor circumference was categorized as ≤ 1/2 bowel circumference and > 1/2 bowel circumference. T staging was classified as T1-2 and T3-4. N staging was grouped as N0 and N1-2. The degree of differentiation was divided into "highly differentiated/moderately differentiated" and "poorly differentiated/undifferentiated" stages. The cutoff values for certain variables were determined using receiver-operating characteristic (ROC) curves and the Youden index[13]. For instance, the preoperative carcinoembryonic antigen (CEA) level variables were divided into ≤ 5 ng/mL and > 5 ng/mL based on the cutoff value. Similarly, the carbohydrate antigen 19-9 (CA199) level variables were categorized as ≤ 18 U/mL and > 18 U/mL. The tumor size variables were grouped as ≤ 3 cm and > 3 cm. The preoperative neutrophil-to-lymphocyte ratio was divided into ≤ 3 and > 3. Other variables, such as preoperative intestinal obstruction, hypertension, diabetes, smoking history, and previous surgery history, were classified as "yes" or "no" based on their presence or absence in the patients' medical records.

Statistical analysis

Before conducting the statistical analysis, we randomly divided the 645 patients into two cohorts: A training cohort and a validation cohort, using a 7:3 ratio. The statistical analysis was performed using IBM SPSS software (version 27.0). For normally distributed measurement data, *t* tests were employed, while the Mann-Whitney U test was used for nonnormally distributed measurement data. Chi-square tests were conducted to analyze count data. Least absolute shrinkage and selection operator (LASSO) regression, incorporating Lambda's penalty coefficient, was employed to reduce the regression coefficient of variables to zero. Variables with zero regression coefficients were excluded, while those without zero regression coefficients were recognized as being associated with TDs. Multivariate logistic analysis was performed on the selected variables to determine the most relevant variable, which formed the basis for developing a nomogram. The validation cohort was utilized to assess the predictive ability of the developed nomogram, including discrimination and calibration. Calibration curves were generated to illustrate any potential disparities between the training cohort and the validation cohort, encompassing both the original and recalibrated nomograms. The discriminative ability of the model was evaluated through ROC curve analysis, with the area under the curve (AUC) serving as a measure. The predictive ability of the final model was evaluated by comparing the observed incidence of TDs. Additionally, decision curve analysis (DCA) was performed to assess the clinical application value of the model, calculating the net benefit under various risk threshold probabilities. R version 4.2.1 software was used for statistical analysis of the predictive models, with a P value < 0.05 considered indicative of statistical significance.

RESULTS

Clinicopathologic characteristics

A total of 645 CRC patients who met the eligibility criteria were included in this study and randomly divided into a training cohort (452 individuals) and a validation cohort (193 individuals). Among the patients, 372 were male and 273 were female, indicating a higher proportion of males (57.7%). Preoperative intestinal obstruction was present in 73 cases, while 572 cases showed no symptoms of bowel obstruction. Tumors were located on the left side in 487 patients and on the right side in 158 patients. Additionally, 239 patients had tumors occupying ≤ 1/2 of the intestinal canal circumference; 137 patients had a maximum tumor diameter of ≤ 3 cm, while 508 patients had a diameter > 3 cm. Pathological staging revealed T1-2 in 109 cases and T3-4 in 536 cases. Lymph node metastasis (pN1-2) was observed in 294 patients, while 351 patients had no lymph node metastasis (pN0). Moreover, 41 patients had poor differentiation, and 604 patients had moderate and good differentiation. All patients were divided into two groups based on the presence of TDs: The TD group (n = 51) and the non-TD group (n = 594).

Upon analyzing the clinical baseline characteristics of the included patients, significant differences were observed in sex, preoperative intestinal obstruction, tumor size, serum CEA level, serum CA199 level, pathological T stage, pathological N stage, and differentiation degree (P < 0.05). However, no significant differences were observed in other factors. The basic demographics and clinicopathological characteristics can be found in Table 1.

Predictor selection and identification

In the training cohort, we employed the LASSO regression algorithm to perform feature selection. This approach helps minimize the impact of multicollinearity and offers strong predictability and stability. We selected features based on the partial likelihood binomial deviance reaching its minimum value, and eight variables with nonzero coefficients were retained in the LASSO regression (Figure 2). These variables were considered significantly associated with TDs. The identified variables included sex, preoperative intestinal obstruction, diabetes, tumor location, tumor size, serum CEA level, pathological N stage, and degree of differentiation.

Table 1 Characteristics of patients, *n* (%)

Variables	No TD	TD	Total	*P* value
Age (yr)				0.906
≤ 64	321 (54.0)	28 (54.9)	349 (54.1)	
> 64	273 (46.0)	23 (45.1)	296 (45.9)	
Sex				0.029
Male	350 (58.9)	22 (43.1)	372 (57.7)	
Female	244 (41.1)	29 (56.9)	273 (42.3)	
Preoperative obstruction				< 0.001
No	535 (90.1)	37 (72.5)	572 (88.7)	
Yes	59 (9.9)	14 (27.5)	73 (11.3)	
Hypertension				0.106
No	440 (74.1)	43 (84.3)	483 (74.9)	
Yes	154 (25.9)	8 (15.7)	162 (25.1)	
Diabetes				0.459
No	522 (87.9)	43 (84.3)	565 (87.6)	
Yes	72 (12.1)	8 (15.7)	80 (12.4)	
BMI (kg/m^2)				0.970
≤ 25	502 (84.5)	43 (84.3)	545 (84.5)	
>25	92 (15.5)	8 (15.7)	100 (15.5)	
Smoking history				0.581
No	533 (89.7)	47 (92.2)	580 (89.9)	
Yes	61 (10.3)	4 (7.8)	65 (10.1)	
Abdominal surgery				1.000
No	542 (91.2)	47 (92.2)	589 (91.3)	
Yes	52 (8.8)	4 (7.8)	56 (8.7)	
Tumor position				0.236
Right	149 (25.1)	9 (17.6)	158 (24.5)	
Left	445 (74.9)	42 (82.4)	487 (75.5)	
Occupied intestinal circumference				0.139
≤ 1/2	225 (37.9)	14 (27.5)	239 (37.1)	
> 1/2	369 (62.1)	37 (72.5)	406 (62.9)	
Tumor size (cm)				0.015
≤ 3	133 (22.4)	4 (7.8)	137 (21.2)	
> 3	461 (77.6)	47 (92.2)	508 (78.8)	
NLR				0.925
≤ 3	423 (71.2)	36 (70.6)	459 (71.2)	
> 3	171 (28.8)	15 (29.4)	186 (28.8)	
CA-199 (U/mL)				0.037
≤ 18	400 (67.3)	27 (52.9)	427 (66.2)	
> 18	194 (32.7)	24 (47.1)	218 (33.8)	
CEA (ng/mL)				0.01
≤ 5	355 (59.8)	21 (41.2)	376 (58.3)	

> 5	239 (40.2)	30 (58.8)	269 (41.7)	
T stage				0.003
T0-T2	108 (18.2)	1 (2.0)	109 (16.9)	
T3-T4	486 (81.8)	50 (98.0)	536 (83.1)	
N stage				< 0.001
N0	349 (58.8)	2 (3.9)	351 (54.4)	
N1-N2	245 (41.2)	49 (96.1)	294 (45.6)	
Differentiation				0.011
Poor	33 (5.6)	8 (15.7)	41 (6.4)	
Well/moderate	561 (94.4)	43 (84.3)	604 (93.6)	

TD: Tumor deposit; BMI: Body mass index; NLR: Neutrophil-to-lymphocyte ratio; CEA: Carcinoembryonic antigen; CA-199: Carbohydrate antigen 199.

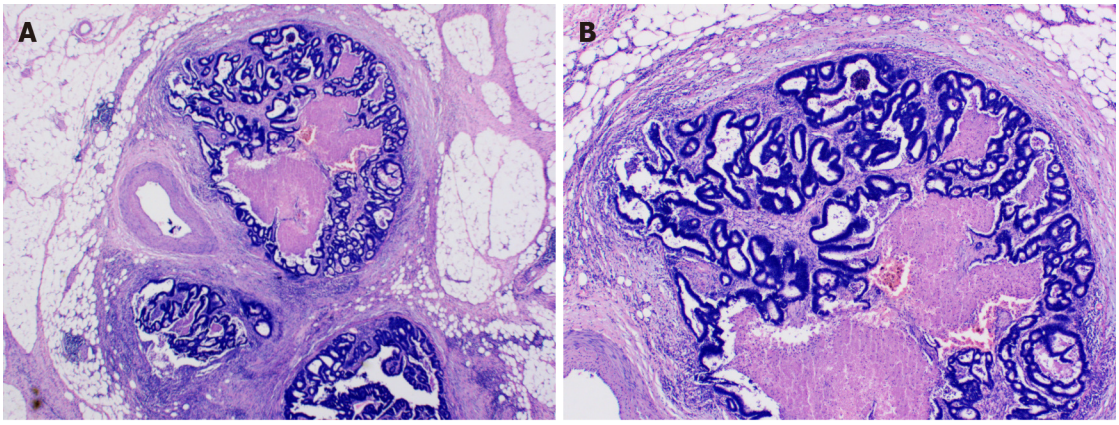

DOI: 10.3748/wjg.v29.i39.5483 **Copyright** ©The Author(s) 2023.

Figure 1 Hematoxylin-eosin staining of tumor deposits. A: Magnification (× 20); B: Magnification (× 40).

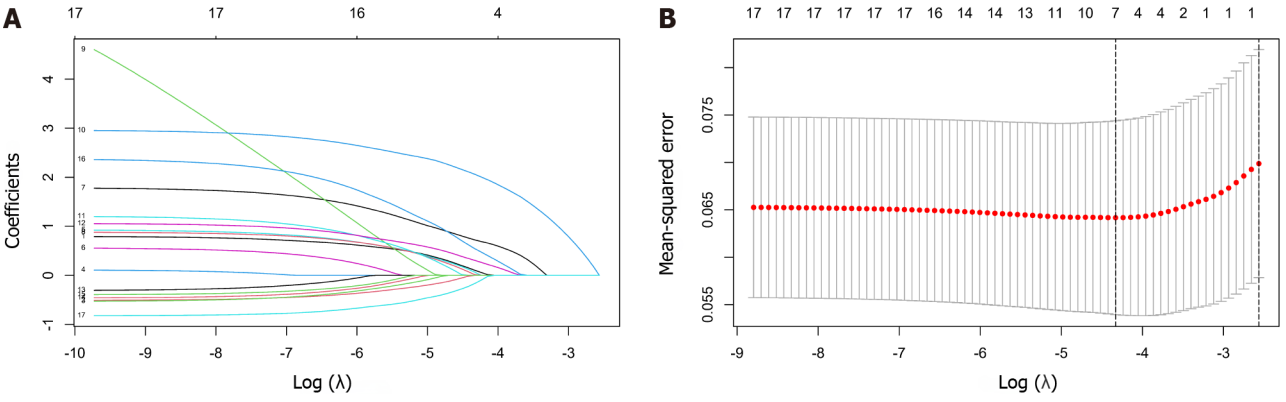

DOI: 10.3748/wjg.v29.i39.5483 **Copyright** ©The Author(s) 2023.

Figure 2 The Lasso regression method is used to screen for predictable variables. A: The coefficient distribution of 17 baseline features; B: In Lasso regression, 10-fold cross-validation was used to select predictive variables using the minimum criterion (dashed line on the left).

To further investigate their predictive significance, we conducted a multivariate logistic regression analysis using these eight variables. The results demonstrated that sex (female) [odds ratio (OR) = 2.404; 95% confidence interval (CI) = 1.249-4.626; P = 0.009], preoperative intestinal obstruction (OR = 3.119; 95%CI = 1.427-6.818; P = 0.004), tumor location (left side) (OR = 2.511; 95%CI = 1.088-5.795; P = 0.031), and pathological N stage (OR = 29.658; 95%CI = 7.051-124.744; P < 0.001) were all significant predictors of TDs. The detailed results of the multivariate logistic regression analysis can be found in Table 2.

Table 2 The multivariate logistic regression results

Variables	Odds ratio	95%CI	*P* value
Sex			
Male	1		
Female	2.404	1.249-4.626	0.009
Preoperative obstruction			
No	1		
Yes	3.119	1.427-6.818	0.004
Diabetes			
No	1		
Yes	1.485	0.602-3.663	0.391
Tumor position			
Right	1		
Left	2.511	1.088-5.795	0.031
Tumor size (cm)			
≤ 3	1		
> 3	2.631	0.867-7.977	0.088
CEA			
≤ 5	1		
> 5	1.889	0.983-3.632	0.056
N stage			
N0	1		
N1-N2	29.658	7.051-124.744	< 0.001
Differentiation			
Poor	1		
Well/moderate	0.476	0.179-1.260	0.135

CEA: Carcinoembryonic antigen; CI: Confidence interval.

Construction and evaluation of the nomogram

A nomogram was developed based on the four independent risk factors identified through multivariable logistic regression analysis (Figure 3). Each risk factor was assigned a specific score to calculate the total risk score for predicting TDs in CRC patients. The risk score for lymph node metastasis had the highest weightage (100 points), followed by preoperative symptoms of bowel obstruction (40 points). By summing the scores of the four risk factors, the total risk score can be obtained, indicating the likelihood of TDs in the patient.

To assess the predictive accuracy of the nomogram, ROC curves were generated, yielding an AUC of 0.839 for the training cohort and 0.853 for the validation cohort (Figure 4). These values indicated that the nomogram had good predictive ability. The calibration curves (Figure 5) demonstrated excellent agreement between the predicted TDs and the actual observations in both the training and validation cohorts.

Furthermore, the DCA curve was plotted for the training cohort (Figure 6). The curve showed that within a threshold probability range of 7% to 78%, using this predictive model to identify the presence of TDs in CRC patients can lead to net clinical benefits.

DISCUSSION

CRC, as one of the most common malignant tumors worldwide, has attracted significant attention in clinical and scientific research in recent years[1]. Notably, the prognosis of CRC patients has become a key area of concern for clinical practitioners. With research progress achieved on prognostic factors, emerging evidence suggests that tumor pathological characteristics play a crucial role in the prognosis of CRC patients[14]. Among these characteristics, TNM staging is

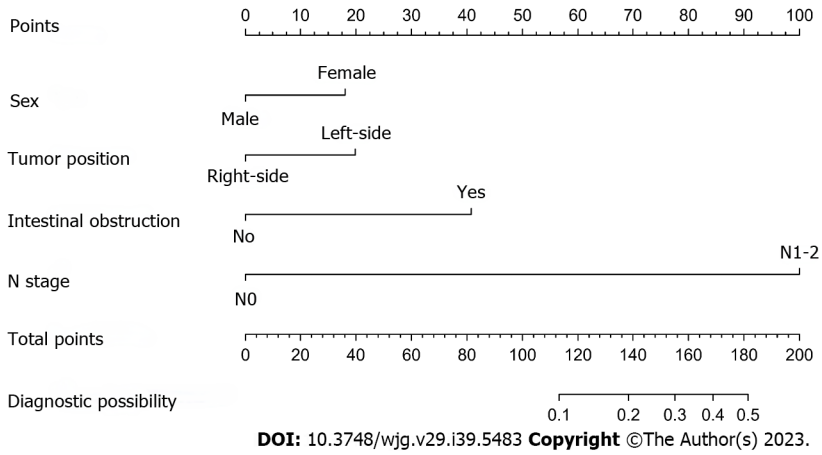

DOI: 10.3748/wjg.v29.i39.5483 **Copyright** ©The Author(s) 2023.

Figure 3 A nomogram was used to predict the risk of tumor deposits in colorectal cancer patients. The predictors included sex, tumor position, preoperative intestinal obstruction, and lymph node metastasis.

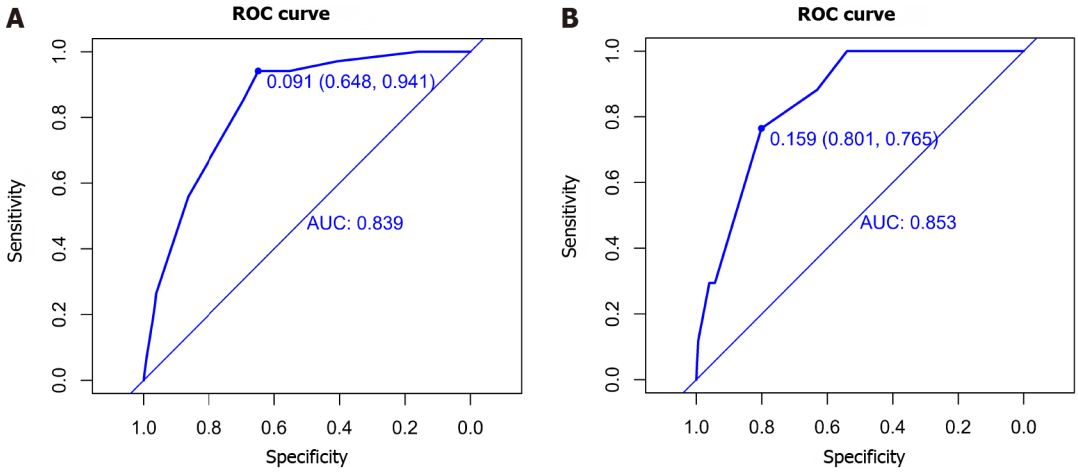

DOI: 10.3748/wjg.v29.i39.5483 **Copyright** ©The Author(s) 2023.

Figure 4 The receiver-operating characteristic curves of the nomogram for predicting tumor deposits. A: Receiver operating characteristic (ROC) curve for the nomogram based on the training cohort. The area under the curve (AUC) is 0.839; B: ROC curve for the nomogram based on the validation cohort. The AUC is 0.853. ROC: Receiver operating characteristic; AUC: Area under the curve.

widely recognized as the most crucial prognostic indicator[15]. The significance of TDs has grown in subsequent revisions of the TNM classification, with their inclusion in TNM-8 and classification as "N1c" when accompanied by lymph node negativity[9,16]. Importantly, in the 8th edition of TNM, tumor nodules with venous, lymphatic vessel, or perineural infiltration are considered distinct entities[7]. An increasing body of literature suggests that TDs carry a worse prognosis than N1 or N2 involvement[7,11,16,17]. Therefore, accurately predicting the presence of TDs in CRC patients before surgery holds immense value in guiding personalized staging, preoperative treatment decisions, and prognosis assessment. Currently, limited research exists on the risk factors associated with TDs in CRC patients. Most studies have focused on comparing TDs with the prognosis of lymph node metastasis, and only a few have established effective clinical prediction models. Our study included comprehensive baseline and pathological information and incorporated patient symptoms such as intestinal obstruction. This approach enhanced the sensitivity and specificity of the model, enabling clinicians to identify high-risk populations for TDs in CRC patients and implement personalized treatment strategies.

Nomograms are valuable tools for predicting outcomes in clinical practice. They provide a visual representation of the impact of various predictors on the outcome, offering a practical and intuitive explanation of their influence[18]. In our study, we developed a nomogram to predict the risk of TDs in CRC patients. The nomogram was constructed based on important clinical characteristics identified through LASSO regression and multivariate logistic regression. The calibration curve demonstrated high agreement between the predicted and observed TD incidence, indicating reliable prediction performance. Moreover, the AUC values exceeded 0.8 for both the training and validation cohorts, indicating good prediction model accuracy and discrimination.

Previous studies have reported that the incidence rate of TDs in CRC patients is approximately 10%[19], which is slightly higher than that in the present study. The exploration of clinical risk factors for TDs in CRC patients remains limited. However, there have been some notable studies in this field. Hong *et al*[20] investigated predictive factors for TDs

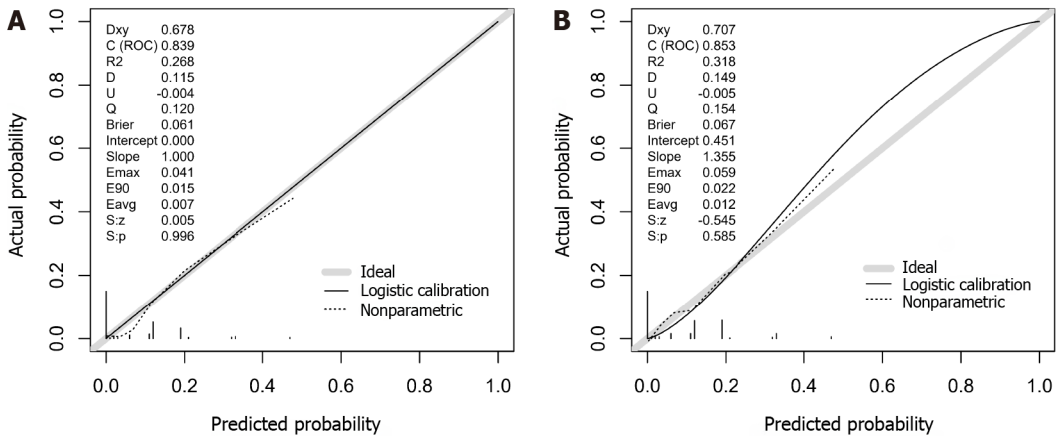

DOI: 10.3748/wjg.v29.i39.5483 **Copyright** ©The Author(s) 2023.

Figure 5 Calibration curve for the nomogram in the cohort. A: Calibration curve of the training cohort; B: Calibration curve of the validation cohort. ROC: Receiver operating characteristic.

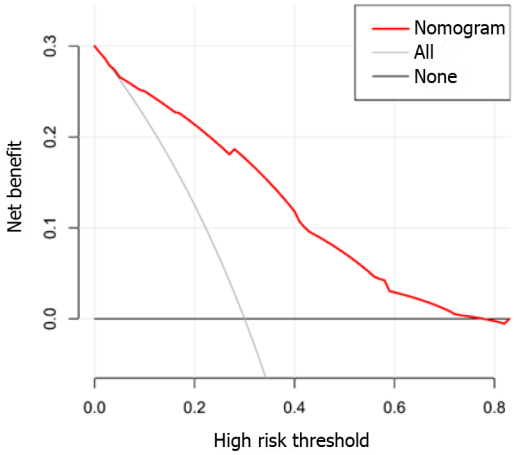

DOI: 10.3748/wjg.v29.i39.5483 **Copyright** ©The Author(s) 2023.

Figure 6 Decision curve analysis of the nomogram. The Y-axis represents net income, and the red line represents the risk nomogram. When the threshold probability is > 7% and < 78%, this predictive model can achieve net clinical benefits.

in rectal cancer using a radiomics signature and developed a predictive model based on imaging features. They identified tumor location and two imaging features (D*, α) as accurate predictors of TDs. Chen *et al*[19] extracted data from the Surveillance, Epidemiology, and End Results database and found that poor tumor differentiation, positive CEA, higher T staging, tumor location, and increased lymph node metastasis were risk factors for TDs in CRC patients. In our study, we conducted intergroup comparisons and identified age, preoperative intestinal obstruction, tumor size, serum CEA, serum CA199, pathological T stage, pathological N stage, and degree of differentiation as factors associated with TDs, which aligns with the aforementioned research. However, after applying LASSO regression and multivariable logistic regression, we determined that tumor location (left side), preoperative intestinal obstruction, female sex, and N stage were independent predictive variables. Notably, the association between sex and TDs has not been extensively explored, and our finding of a higher risk of TDs in female patients has not yet been documented. This may suggest that female patients are more susceptible to lymph node metastasis[21], but further investigation is required to clarify this relationship. We also found a significant correlation between tumor location and TDs, with the left side being prone to TDs, especially in rectal cancer cases. This discrepancy in TD location can be attributed to variations in lymphatic vessel involvement and lymph node metastasis between left-sided and right-sided colon cancers[19,22]. CRC patients often experience intestinal obstruction at advanced stages, sometimes requiring emergency surgery or the placement of an intestinal stent[23]. Previous studies have indicated that preoperative intestinal obstruction in CRC patients is associated with elevated CEA levels, poorly differentiated tumors, advanced T stage, left-sided primary tumor location, and nerve invasion, which may explain the significant association between preoperative intestinal obstruction and TDs[24-26]. Furthermore, a higher number of lymph node metastases increases the likelihood of TDs, potentially due to the involvement of peripheral nerves, lymphatic vessels, and blood vessels[19]. The fifth edition of TNM staging distinguished between TDs and lymph node metastasis based on size, classifying all nodules with a diameter larger than 3 mm as lymph node metastasis, thus highlighting the strong relationship between TDs and lymph nodes[27].

The current TNM staging only considers TDs in the absence of lymph node metastasis, which may not fully reflect the important role of TDs in prognosis and may lead to incorrect treatment strategies[3,9]. Liang *et al*[11] conducted a large retrospective study with a large sample size and found that TDs were an independent prognostic factor for gastric cancer patients after radical resection, suggesting that TDs should be included in the N staging system. In Liu *et al*'s study[28], after combining TDs and lymph node metastasis, it was observed that the prognosis of N1 patients with TD positivity was similar to that of N2 patients, while the prognosis of N2 patients with TD positivity was much worse than that of N2 patients without TDs. The researchers believe that in the presence of lymph node metastasis, TDs should also be considered in the TNM system. However, when evaluating the role of TDs, ignoring the number of TDs does not seem to be a correct decision[14]. A previous multicenter study demonstrated a significant correlation between the number of TDs and prognosis, with patients with ≥ 4 TDs experiencing a significantly worse prognosis than those with < 4 TDs under the same conditions[7]. In summary, it is necessary to fully evaluate the prognosis of CRC patients, regardless of the presence or absence of lymph node metastasis, by considering TDs and their quantity.

In conclusion, our study integrated preoperative predictive factors into a model and achieved favorable results supported by a sufficient sample size and robust testing efficacy. However, there are some limitations to consider. First, this study has a retrospective design, which may introduce inherent biases. Second, the absence of imaging data for the preoperative predictors is a limitation, and future prospective cohort studies incorporating radiomics signatures may help support our findings.

CONCLUSION

In summary, our study identified female sex, preoperative intestinal obstruction, left-sided CRC, and lymph node metastasis as predictors of TDs in CRC. Assessing these factors before surgery is crucial for accurately determining the presence of TDs. Consideration of the impact of these predictors on clinical decision-making and patient prognosis, especially for high-risk individuals, is essential for making informed decisions and obtaining optimal outcomes.

ARTICLE HIGHLIGHTS

Research background

Colorectal cancer (CRC) poses a serious threat to human life and health. Previous studies have shown that tumor deposits (TDs) are significantly associated with early metastasis and poor prognosis. However, research on related risk factors is limited, and accurate prediction of TDs remains challenging. We developed a model based on preoperative clinical and pathological features to accurately predict the likelihood of TDs in CRC patients.

Research motivation

At present, the diagnosis of TDs in CRC requires postoperative pathology, which is passive for clinicians. If TDs can be accurately identified before patients receive treatment, it is of great importance for evaluating clinical staging, selecting reasonable treatment plans, and judging the prognosis of CRC patients.

Research objectives

To develop and validate a nomogram with good predictive ability for the preoperative prediction of TDs in patients with CRC.

Research methods

We retrospectively collected the data of 645 eligible patients with CRC. SPSS 27.0 and R (version 4.2.1) were used for statistical analysis, and a prediction model for TDs in CRC patients was established.

Research results

A total of 51 patients with CRC had TDs in this study. The areas under the curve of the training cohort and the validation cohort were 0.839 and 0.853, respectively. The model showed good accuracy and discrimination ability and has broad clinical practicability. The results of this study suggest the value of preoperative indicators in predicting TDs in CRC patients and can assist in guiding clinical decision making.

Research conclusions

This nomogram based on preoperative indicators can effectively predict the preoperative TD status of CRC.

Research perspectives

In the future, we will try to apply radiomics combined with clinical indicators to construct a model to predict the status of TDs in CRC patients.

FOOTNOTES

Author contributions: Zheng HD designed/planned the study and wrote the paper; Zheng HD, Hu YH and Ye K acquired and analyzed data and performed computational modeling; Xu JH participated in discussion of related data; All authors read and approved the final manuscript.

Supported by Fujian Province Science and Technology Innovation Joint Fund Project, No. 2021Y9029.

Institutional review board statement: The study was reviewed and approved for publication by our Institutional Reviewer.

Informed consent statement: As the study used anonymous and pre-existing data, the requirement for the informed consent from patients was waived.

Conflict-of-interest statement: All the Authors have no conflict of interest related to the manuscript.

Data sharing statement: The datasets used and/or analyzed during the current study are available from the corresponding author on reasonable request.

STROBE statement: The authors have read the STROBE Statement-checklist of items, and the manuscript was prepared and revised according to the STROBE Statement-checklist of items.

Country/Territory of origin: China

ORCID number: Hui-Da Zheng 0000-0002-4986-8770; Jian-Hua Xu 0000-0001-5147-292X.

S-Editor: Qu XL
L-Editor: A
P-Editor: Yuan YY

REFERENCES

1 **Sung H**, Ferlay J, Siegel RL, Laversanne M, Soerjomataram I, Jemal A, Bray F. Global Cancer Statistics 2020: GLOBOCAN Estimates of Incidence and Mortality Worldwide for 36 Cancers in 185 Countries. *CA Cancer J Clin* 2021; **71**: 209-249 [PMID: 33538338 DOI: 10.3322/caac.21660]

2 **Quirke P**, Williams GT, Ectors N, Ensari A, Piard F, Nagtegaal I. The future of the TNM staging system in colorectal cancer: time for a debate? *Lancet Oncol* 2007; **8**: 651-657 [PMID: 17613427 DOI: 10.1016/S1470-2045(07)70205-X]

3 **Delattre JF**, Selcen Oguz Erdogan A, Cohen R, Shi Q, Emile JF, Taieb J, Tabernero J, André T, Meyerhardt JA, Nagtegaal ID, Svrcek M. A comprehensive overview of tumour deposits in colorectal cancer: Towards a next TNM classification. *Cancer Treat Rev* 2022; **103**: 102325 [PMID: 34954486 DOI: 10.1016/j.ctrv.2021.102325]

4 **Moon JY**, Lee MR, Ha GW. Prognostic value of tumor deposits for long-term oncologic outcomes in patients with stage III colorectal cancer: a systematic review and meta-analysis. *Int J Colorectal Dis* 2022; **37**: 141-151 [PMID: 34595585 DOI: 10.1007/s00384-021-04036-z]

5 **Wu W**, Zeng S, Zhang X, Liu P, Qiu T, Li S, Gong P. The value of tumor deposits in evaluating colorectal cancer survival and metastasis: a population-based retrospective cohort study. *World J Surg Oncol* 2022; **20**: 41 [PMID: 35189906 DOI: 10.1186/s12957-022-02501-9]

6 **Bouquot M**, Creavin B, Goasguen N, Chafai N, Tiret E, André T, Flejou JF, Parc Y, Lefevre JH, Svrcek M. Prognostic value and characteristics of N1c colorectal cancer. *Colorectal Dis* 2018; **20**: O248-O255 [PMID: 29894583 DOI: 10.1111/codi.14289]

7 **Cohen R**, Shi Q, Meyers J, Jin Z, Svrcek M, Fuchs C, Couture F, Kuebler P, Ciombor KK, Bendell J, De Jesus-Acosta A, Kumar P, Lewis D, Tan B, Bertagnolli MM, Philip P, Blanke C, O'Reilly EM, Shields A, Meyerhardt JA. Combining tumor deposits with the number of lymph node metastases to improve the prognostic accuracy in stage III colon cancer: a post hoc analysis of the CALGB/SWOG 80702 phase III study (Alliance)(☆). *Ann Oncol* 2021; **32**: 1267-1275 [PMID: 34293461 DOI: 10.1016/j.annonc.2021.07.009]

8 **von Winterfeld M**, Hoffmeister M, Ingold-Heppner B, Jansen L, Tao S, Herpel E, Schirmacher P, Dietel M, Chang-Claude J, Autschbach F, Brenner H, Bläker H. Frequency of therapy-relevant staging shifts in colorectal cancer through the introduction of pN1c in the 7th TNM edition. *Eur J Cancer* 2014; **50**: 2958-2965 [PMID: 25281526 DOI: 10.1016/j.ejca.2014.09.002]

9 **Lord A**, Brown G, Abulafi M, Bateman A, Frankel W, Goldin R, Gopal P, Kirsch R, Loughrey MB, Märkl B, Moran B, Puppa G, Rasheed S, Shimada Y, Snaebjornsson P, Svrcek M, Washington K, West N, Wong N, Nagtegaal I. Histopathological diagnosis of tumour deposits in colorectal cancer: a Delphi consensus study. *Histopathology* 2021; **79**: 168-175 [PMID: 33511676 DOI: 10.1111/his.14344]

10 **Wu WX**, Zhang DK, Chen SX, Hou ZY, Sun BL, Yao L, Jie JZ. Prognostic impact of tumor deposits on overall survival in colorectal cancer: Based on Surveillance, Epidemiology, and End Results database. *World J Gastrointest Oncol* 2022; **14**: 1699-1710 [PMID: 36187391 DOI: 10.4251/wjgo.v14.i9.1699]

11 **Liang Y**, Wu L, Liu L, Ding X, Wang X, Liu H, Meng J, Xu R, He D, Liang H. Impact of extranodal tumor deposits on prognosis and N stage in gastric cancer. *Surgery* 2019; **166**: 305-313 [PMID: 31221435 DOI: 10.1016/j.surg.2019.04.027]

12 **Jhuang YH**, Chou YC, Lin YC, Hu JM, Pu TW, Chen CY. Risk factors predict microscopic extranodal tumor deposits in advanced stage III

colon cancer patients. *World J Gastroenterol* 2023; **29**: 1735-1744 [PMID: 37077516 DOI: 10.3748/wjg.v29.i11.1735]

13 **Böhning D**, Holling H, Patilea V. A limitation of the diagnostic-odds ratio in determining an optimal cut-off value for a continuous diagnostic test. *Stat Methods Med Res* 2011; **20**: 541-550 [PMID: 20639268 DOI: 10.1177/0962280210374532]

14 **Arrichiello G**, Pirozzi M, Facchini BA, Facchini S, Paragliola F, Nacca V, Nicastro A, Canciello MA, Orlando A, Caterino M, Ciardiello D, Della Corte CM, Fasano M, Napolitano S, Troiani T, Ciardiello F, Martini G, Martinelli E. Beyond N staging in colorectal cancer: Current approaches and future perspectives. *Front Oncol* 2022; **12**: 937114 [PMID: 35928863 DOI: 10.3389/fonc.2022.937114]

15 **Chen K**, Collins G, Wang H, Toh JWT. Pathological Features and Prognostication in Colorectal Cancer. *Curr Oncol* 2021; **28**: 5356-5383 [PMID: 34940086 DOI: 10.3390/curroncol28060447]

16 **Li X**, An B, Zhao Q, Qi J, Wang W, Zhang D, Li Z, Qin C. Impact of tumor deposits on the prognosis and chemotherapy efficacy in stage III colorectal cancer patients with different lymph node status: A retrospective cohort study in China. *Int J Surg* 2018; **56**: 188-194 [PMID: 29936197 DOI: 10.1016/j.ijsu.2018.06.029]

17 **Pu H**, Pang X, Fu J, Zheng R, Chen Y, Zhang D, Fang X. Significance of tumor deposits combined with lymph node metastasis in stage III colorectal cancer patients: a retrospective multi-center cohort study from China. *Int J Colorectal Dis* 2022; **37**: 1411-1420 [PMID: 35595975 DOI: 10.1007/s00384-022-04149-z]

18 **Park SY**. Nomogram: An analogue tool to deliver digital knowledge. *J Thorac Cardiovasc Surg* 2018; **155**: 1793 [PMID: 29370910 DOI: 10.1016/j.jtcvs.2017.12.107]

19 **Chen J**, Zhang Z, Ni J, Sun J, Ren W, Shen Y, Shi L, Xue M. Predictive and Prognostic Assessment Models for Tumor Deposit in Colorectal Cancer Patients With No Distant Metastasis. *Front Oncol* 2022; **12**: 809277 [PMID: 35251979 DOI: 10.3389/fonc.2022.809277]

20 **Hong Y**, Song G, Jia Y, Wu R, He R, Li A. Predicting tumor deposits in patients with rectal cancer: Using the models of multiple mathematical parameters derived from diffusion-weighted imaging. *Eur J Radiol* 2022; **157**: 110573 [PMID: 36347167 DOI: 10.1016/j.ejrad.2022.110573]

21 **Naito A**, Iwamoto K, Ohtsuka M, Imasato M, Nakahara Y, Mikamori M, Furukawa K, Moon J, Asaoka T, Kishi K, Akamatsu H. Risk Factors for Lymph Node Metastasis in Pathological T1b Colorectal Cancer. *In Vivo* 2021; **35**: 987-991 [PMID: 33622893 DOI: 10.21873/invivo.12341]

22 **Xiong X**, Wang C, Cao J, Gao Z, Ye Y. Lymph node metastasis in T1-2 colorectal cancer: a population-based study. *Int J Colorectal Dis* 2023; **38**: 94 [PMID: 37055602 DOI: 10.1007/s00384-023-04386-w]

23 **Zahid A**, Young CJ. How to decide on stent insertion or surgery in colorectal obstruction? *World J Gastrointest Surg* 2016; **8**: 84-89 [PMID: 26843916 DOI: 10.4240/wjgs.v8.i1.84]

24 **Katoh H**, Yamashita K, Wang G, Sato T, Nakamura T, Watanabe M. Prognostic significance of preoperative bowel obstruction in stage III colorectal cancer. *Ann Surg Oncol* 2011; **18**: 2432-2441 [PMID: 21369738 DOI: 10.1245/s10434-011-1625-3]

25 **Nozawa H**, Morikawa T, Kawai K, Hata K, Tanaka T, Nishikawa T, Sasaki K, Shuno Y, Kaneko M, Hiyoshi M, Emoto S, Murono K, Sonoda H, Fukayama M, Ishihara S. Obstruction is associated with perineural invasion in T3/T4 colon cancer. *Colorectal Dis* 2019; **21**: 917-924 [PMID: 31017742 DOI: 10.1111/codi.14655]

26 **Lv X**, Yu H, Gao P, Song Y, Sun J, Chen X, Wang Y, Wang Z. A nomogram for predicting bowel obstruction in preoperative colorectal cancer patients with clinical characteristics. *World J Surg Oncol* 2019; **17**: 21 [PMID: 30658652 DOI: 10.1186/s12957-019-1562-3]

27 **Ueno H**, Nagtegaal ID, Quirke P, Sugihara K, Ajioka Y. Tumor deposits in colorectal cancer: Refining their definition in the TNM system. *Ann Gastroenterol Surg* 2023; **7**: 225-235 [PMID: 36998291 DOI: 10.1002/ags3.12652]

28 **Liu F**, Zhao J, Li C, Wu Y, Song W, Guo T, Chen S, Cai S, Huang D, Xu Y. The unique prognostic characteristics of tumor deposits in colorectal cancer patients. *Ann Transl Med* 2019; **7**: 769 [PMID: 32042785 DOI: 10.21037/atm.2019.11.69]

World Journal of Gastroenterology

Submit a Manuscript: https://www.f6publishing.com

World J Gastroenterol 2023 October 21; 29(39): 5494-5502

DOI: 10.3748/wjg.v29.i39.5494

ISSN 1007-9327 (print) ISSN 2219-2840 (online)

ORIGINAL ARTICLE

Observational Study

Risk assessment of venous thromboembolism in inflammatory bowel disease by inherited risk in a population-based incident cohort

Andrew S Rifkin, Zhuqing Shi, Jun Wei, Siqun Lilly Zheng, Brian T Helfand, Jonathan S Cordova, Vincent F Biank, Alfonso J Tafur, Omar Khan, Jianfeng Xu

Specialty type: Gastroenterology and hepatology

Provenance and peer review: Unsolicited article; Externally peer reviewed.

Peer-review model: Single blind

Peer-review report's scientific quality classification

Grade A (Excellent): A
Grade B (Very good): 0
Grade C (Good): C
Grade D (Fair): 0
Grade E (Poor): 0

P-Reviewer: Huang JG, Singapore; Yasuda H, Japan

Received: June 5, 2023
Peer-review started: June 5, 2023
First decision: August 8, 2023
Revised: August 18, 2023
Accepted: September 28, 2023
Article in press: September 28, 2023
Published online: October 21, 2023

Andrew S Rifkin, Zhuqing Shi, Jun Wei, Siqun Lilly Zheng, Brian T Helfand, Jianfeng Xu, Program for Personalized Cancer Care, NorthShore University HealthSystem, Evanston, IL 60201, United States

Brian T Helfand, Jianfeng Xu, Department of Surgery, NorthShore University HealthSystem, Evanston, IL 60201, United States

Brian T Helfand, Jianfeng Xu, Pritzker School of Medicine, University of Chicago, Chicago, IL 60637, United States

Jonathan S Cordova, Vincent F Biank, Department of Pediatrics, NorthShore University HealthSystem, Evanston, IL 60201, United States

Alfonso J Tafur, Cardiovascular Institute, NorthShore University HealthSystem, Evanston, IL 60201, United States

Omar Khan, Department of Medicine, NorthShore University HealthSystem, Evanston, IL 60201, United States

Corresponding author: Jianfeng Xu, MD, DrPH, Professor, Program for Personalized Cancer Care, NorthShore University HealthSystem, 1001 University Place, Evanston, IL 60201, United States. jxu@northshore.org

Abstract

BACKGROUND

Inflammatory bowel disease (IBD), including Crohn's disease (CD) and ulcerative colitis (UC), is a chronic inflammatory disease of the digestive tract with increasing prevalence globally. Although venous thromboembolism (VTE) is a major complication in IBD patients, it is often underappreciated with limited tools for risk stratification.

AIM

To estimate the proportion of VTE among IBD patients and assess genetic risk factors (monogenic and polygenic) for VTE.

METHODS
Incident VTE was followed for 8465 IBD patients in the UK Biobank (UKB). The associations of VTE with *F5* factor V leiden (FVL) mutation, *F2* G20210A prothrombin gene mutation (PGM), and polygenic score (PGS003332) were tested using Cox hazards regression analysis, adjusting for age at IBD diagnosis, gender, and genetic background (top 10 principal components). The performance of genetic risk factors for discriminating VTE diagnosis was estimated using the area under the receiver operating characteristic curve (AUC).

RESULTS
The overall proportion of incident VTE was 4.70% in IBD patients and was similar for CD (4.46%), UC (4.49%), and unclassified (6.42%), and comparable to that of cancer patients (4.66%) who are well-known at increased risk for VTE. Mutation carriers of *F5*/*F2* had a significantly increased risk for VTE compared to non-mutation carriers, hazard ratio (HR) was 1.94, 95% confidence interval (CI): 1.42-2.65. In contrast, patients with the top PGS decile had a considerably higher risk for VTE compared to those with intermediate scores (middle 8 deciles), HR was 2.06 (95%CI: 1.57-2.71). The AUC for differentiating VTE diagnosis was 0.64 (95%CI: 0.61-0.67), 0.68 (95%CI: 0.66-0.71), and 0.69 (95%CI: 0.66-0.71), respectively, for *F5*/*F2* mutation carriers, PGS, and combined.

CONCLUSION
Similar to cancer patients, VTE complications are common in IBD patients. PGS provides more informative risk information than *F5*/*F2* mutations (FVL and PGM) for personalized thromboprophylaxis.

Key Words: Inflammatory bowel disease; Venous thromboembolism; Polygenic score; Factor V leiden; Prothrombin gene mutation

Core Tip: Based on 8475 inflammatory bowel disease (IBD) patients from a population-based biobank, we showed they have an elevated risk for venous thromboembolism (VTE), with the overall proportion of incident VTE at 4.70%, similar to 4.66% observed in cancer patients. Polygenic score (PGS) is a significant predictor for VTE events, stronger than the well-known *F5* factor V leiden mutation and *F2* G20210A prothrombin gene mutation. The overall proportion of incident VTE is 8.53% in patients at the top 10 PGS percentile. These findings highlight the importance of VTE complications in IBD patients and provide genetic tools for personalized thromboprophylaxis.

Citation: Rifkin AS, Shi Z, Wei J, Zheng SL, Helfand BT, Cordova JS, Biank VF, Tafur AJ, Khan O, Xu J. Risk assessment of venous thromboembolism in inflammatory bowel disease by inherited risk in a population-based incident cohort. *World J Gastroenterol* 2023; 29(39): 5494-5502
URL: https://www.wjgnet.com/1007-9327/full/v29/i39/5494.htm
DOI: https://dx.doi.org/10.3748/wjg.v29.i39.5494

INTRODUCTION

Inflammatory bowel disease (IBD), including Crohn's disease (CD) and ulcerative colitis (UC), is a disease characterized by chronic inflammation of the digestive tract. Its prevalence was estimated at 1.3% (3 million adults) in the United States in 2015 and is expected to increase globally[1,2]. IBD is associated with several adverse complications, including venous thromboembolism (VTE). IBD patients have a 2 to 3-fold higher risk of developing a VTE as compared to the general population[3]. Although the pathophysiology underlying this observation remains largely unknown, it may involve changes in the coagulation system, increased platelet count and reactivity, and altered fibrinolysis[4]. The importance of elevated VTE risk in IBD patients is emphasized in a recent international consensus on the prevention of venous and arterial thrombotic events in patients with IBD, which encourages screening for VTE risk factors. Statement 2 of the consensus states that "Patients with IBD should be screened for VTE risk factors" (consensus reached 100%)[4].

Several inherited factors are associated with risk for VTE, including relatively common gain of function mutations in genes for coagulation factors: Factor V leiden (FVL) mutation in the *F5* gene and the G20210A prothrombin gene mutation (PGM) in the *F2* gene[5]. Recent advances in genome-wide association studies (GWAS) have also revealed multiple common single nucleotide polymorphisms (SNPs) that are associated with increased VTE risk[6]. Polygenic scores (PGS) based on these SNPs have been shown to be effective to stratify VTE risk in the general population. While the consensus recognizes several genetic factors such as *F5* and *F2* for VTE risk among IBD patients, it does not mention PGS[4].

The objectives of this study are to utilize a large population-based cohort to: (1) Estimate the proportion of VTE among IBD patients and compare it to that in cancer patients who are well-known to have an increased risk for VTE; (2) test the association of inherited risk factors (*F5*/*F2* mutations and PGS) and VTE among IBD patients; and (3) assess the

performance of PGS for predicting VTE among IBD patients, alone or in combination with *F5*/*F2* mutations. Results from this study may provide needed evidence for PGS to be included in the updated international consensus for VTE prevention among IBD patients.

MATERIALS AND METHODS

Subjects in this study were patients who had a diagnosis of IBD in the UK Biobank (UKB), a population-based study of 500000 volunteers from the United Kingdom[7]. IBD diagnoses were obtained based on International Classification of Diseases-10 (ICD-10) codes (K50 for CD and K51 for UC) of primary care, death register, inpatient diagnosis, and self-report. Incident VTE after IBD diagnosis were identified based on the inclusion criteria described by Klarin *et al*[8] Briefly, subjects were defined as a VTE case based on at least one of the following criteria: (1) VTE (deep vein thrombosis and pulmonary embolism) ascertained at baseline by self-report; (2) Hospitalization for ICD-10 Code I80.1, I80.2, I82.2, I26.0, or I26.9; and (3) Hospitalization for Office of Population and Censuses and Survey-4 Procedures Codes L79.1 or L90.2. Only incident VTE, *i.e.*, those that occurred after a diagnosis of IBD were included in the analysis. As a comparison, VTE events after a cancer diagnosis were also estimated among cancer patients (ICD-10: C00-C96) in the UKB[9].

Genotypes for the *F5* FVL mutation (c.1601G>A, rs6025) and the *F2* PGM (c.*97G>A, rs1799963) as well as genome-wide SNPs were obtained from the UKB Axiom SNP genotype array (genotyped or imputed). A published pan-ancestry PGS for VTE (PGS003332) was selected from the PGS catalog for the study because it was developed from the largest GWAS of VTE with 81190 cases and 1419671 controls sampled from six cohorts[6,10]. Based on the scoring file of the PGS, raw PGS was first calculated by taking the product of the count of risk alleles and the risk allele weight at each locus in the PGS (1092045 SNPs) and then summing across available risk loci. Ancestry-adjusted PGS was calculated based on the first four principal components using a previously described method[11]. To remove the contribution of SNPs from the *F5* and *F2* genes to the score, a modified PGS ($PGS_{nonF5/F2}$) was also calculated by removing 1515 SNPs in these two genes (chr1: 168519049-170519049 for *F5* and chr11: 45761055-47761055 for *F2*).

The proportion of incident VTE was calculated as (number of patients with incident VTE)/(number of patients with IBD). The difference in VTE proportion among groups of patients was tested using a χ^2 test. Time to VTE diagnosis from the time of IBD diagnosis was estimated using Kaplan-Meier survival analysis and its difference among various groups of IBD patients was tested using and log-rank test. Association of genetic risk factors (PGS and *F5*/*F2* mutations) and other known risk factors with VTE among IBD patients were tested using the Cox proportional hazards regression analysis, adjusting for gender, body mass index at study recruitment, and genetic background (top 10 principal components). In addition, the performance of genetic risk factors for discriminating VTE was estimated using the area under the receiver operating characteristic curve (AUC). All statistical analyses were performed using R-package.

RESULTS

As of the last UKB accession date (October 7, 2022), 8465 (1.68%) IBD patients were identified from 501095 subjects in the UKB, including 2267 (0.45%), 5233 (1.05%), and 965 (0.19%) patients with CD only, UC only, and IBD unclassified (IBD-U) (diagnosed with both CD and UC), respectively (Table 1). The median age at diagnosis was 49.60, 51.34, and 44.09 years for CD only, UC only, and IBD-U, respectively. Among these IBD patients, 398 developed VTE events after IBD diagnosis, with the overall proportion of incident VTE of 4.70%. The proportion of VTE was statistically different among patients with CD only (4.46%), UC only (4.49%), and IBD-U colitis (6.42%), χ^2 = 7.22, degree of freedom = 2, P = 0.03. It is noted that the overall proportion of incident VTE in these IBD patients was similar to that of 107520 cancer patients (4.66%) in the UKB who are well-known to have an increased risk for VTE. However, a different pattern of VTE events during the follow-up was noticed; VTE events occurred continuously throughout the follow-up period for IBD patients where a disproportionally higher number of VTE events occurred in the first several years in cancer patients (Figure 1).

Among the 8210 IBD patients with genetic data, 509 (6.20%) were carriers of *F5*/*F2* mutations, including 351 (4.28%) carriers of *F5* FVL and 163 (1.99%) carriers of *F2* PGM (Table 2). The overall proportion of incident VTE among mutation carriers was 9.04%, higher than that of non-mutation carriers (4.31%) (Table 2 and Figure 2A). In comparison, PGS was more informative in differentiating VTE events and the proportion of incident VTE increased with increasing decile of $PGS_{nonF5/F2}$, P_{trend} = 1.60E-18 (Figure 2B). For example, the proportion of incident VTE was 1.58% for IBD patients at the bottom of $PGS_{nonF5/F2}$ decile, which was considerably lower than that of non-mutation carriers of *F5*/*F2*. On the other hand, the proportion of incident VTE was 8.53% for IBD patients at the top of $PGS_{nonF5/F2}$ decile, which was higher than that of mutation carriers of *F5*/*F2*. As expected, original PGS (including SNPs in the *F5*/*F2* regions) performed well in stratifying VTE risk and is slightly better than that of $PGS_{nonF5/F2}$ (Figure 2C). For example, the proportion of incident VTE was 1.10% and 10.17% for IBD patients at the bottom and top decile, respectively.

Compared to non-mutation carriers of *F5*/*F2*, mutation carriers were at a marginally increased risk for VTE, with a hazard ratio (HR) of 1.94, 95% confidence interval (CI): 1.42-2.65 (Table 2). For $PGS_{nonF5/F2}$, patients at the top decile had a considerably higher risk for VTE compared to IBD patients with intermediate scores (middle 8 deciles), HR was 1.98 (95%CI: 1.52-2.57). Furthermore, $PGS_{nonF5/F2}$ can also identify patients at lower risk for VTE, HR was 0.36 (95%CI: 0.21-0.63) for patients at the bottom decile. In a multivariable analysis where both *F5*/*F2* mutation carrier status and $PGS_{nonF5/F2}$ (continuous variable) were included, both were significantly associated with VTE risk, P < 0.001.

Table 1 Characteristics of inflammatory bowel disease patients and incident venous thromboembolism in the UK Biobank

	Subjects, *n* (%)	Age dx, median (IQR), yr	Incident VTE, *n* (%)
IBD, all	8465 (1.68)	50.08 (35.24-61.76)	398 (4.7)
Crohn's disease	2267 (0.45)	49.68 (32.48-62.37)	101 (4.46)
Ulcerative colitis	5233 (1.05)	51.38 (36.87-62.50)	235 (4.49)
Indeterminate colitis	965 (0.19)	44.26 (31.56-54.92)	62 (6.42)

IBD: Inflammatory bowel disease; VTE: Venous thromboembolism.

Table 2 Association of venous thromboembolism risk with *F5/F2* mutations and polygenic score in the UK Biobank

	IBD patients, *n* (%)	Incident VTE, *n* (%)	HR (95%CI)[1]	*P* value
FVL/F2 carrier status				
Non-carriers	7701/8210 (93.8)	332/7701 (4.31)	Ref.	
FVL carriers	351/8210 (4.28)	37/351 (10.54)	2.27 (1.61-3.21)	2.84E-06
F2 carriers	163/8210 (1.99)	10/163 (6.13)	1.29 (0.69-2.43)	0.43
Any *FVL/F2* carriers	509/8210 (6.2)	46/509 (9.04)	1.94 (1.42-2.65)	3.27E-05
$PGS_{non\text{-}F5/F2}$ decile				
Bottom	821/8210 (10)	13/821 (1.58)	0.36 (0.21-0.63)	3.12E-04
Intermediate	6568/8210 (80)	295/6568 (4.49)	Ref.	
Top	821/8210 (10)	70/821 (8.53)	1.98 (1.52-2.57)	3.26E-07

[1]HR adjusted for gender, body mass index, and genetic background. The time in survival analysis was from inflammatory bowel disease to event.
IBD: Inflammatory bowel disease; VTE: Venous thromboembolism; 95%CI: 95% confidence interval; HR: Hazard ratio.

$PGS_{nonF5/F2}$ also had a significantly better discriminative performance for VTE diagnosis than *F5/F2* mutations, with the AUC estimated at 0.68 (95%CI: 0.65-0.71) and 0.64 (95%CI: 0.61-0.67), respectively, $P = 0.05$ (Table 3). Combining these two risk factors increased the AUC to 0.69 (95%CI: 0.66-0.71), which was also significantly higher than that of *F5/F2* mutations, $P = 0.01$. Interestingly, the original PGS for VTE, which includes SNPs in the *F5/F2* gene regions, had a similar AUC (0.69, 95%CI: 0.67-0.72) to that of combined $PGS_{nonF5/F2}$ and *F5/F2* mutations.

DISCUSSION

By following incident VTE events among 8465 IBD patients from a population-based biobank, three major findings that have potentially translational implications were obtained from our study. First, VTE was a common complication among IBD patients, with a proportion similar to diseases commonly considered at elevated risk for VTE such as cancer. This elevated VTE risk among IBD patients was also reported in previously published studies[12,13]. In a cohort of 2811 IBD patients recruited from 14 referral centers in Austria, a VTE prevalence of 5.6% was reported, similar to that in our study [12]. In another large cohort study of hospitalized and ambulatory IBD patients ($n = 13756$), as well as matched controls ($n = 71672$) from the General Practice Research Database in the United Kingdom, a higher VTE rate compared to the general population was also reported[13]. For hospitalized patients with IBD, HR for VTE was 3.2, 95%CI: 1.7-6.3. Similarly, for ambulatory patients with IBD, the HR was 8.4, 95%CI: 5.5-12.8. In addition, several studies have also indicated that there is a high risk of recurrent VTE following hospital discharge[13,14]. Interestingly, this increased VTE risk seems to be unique to IBD, setting it apart from other autoimmune diseases like rheumatoid arthritis or celiac disease where this association is not commonly observed[15]. Despite the consistent research observation of an association between IBD and VTE, VTE complication in IBD patients is commonly overlooked in clinical practice. Adherence to VTE prophylaxis among IBD patients is low and inconsistent, with only 68% of hospitalized UC patients prescribed prophylaxis[16]. Even when prescribed, one-third of the doses were not actually administered. Factors contributing to low adherence could include patient noncompliance, physician unawareness, fragmented care, and bleeding risk concerns.

Second, results from our study suggest the VTE risk conferred by *F5/F2* mutations (FVL and PGM) in IBD patients was modest and considerably lower than previously reported. For *F5* FVL, two meta-analyses published in 2011 reported a combined OR of 4.0 and 5.3, respectively, for VTE in IBD patients[17,18]. These ORs, however, were likely over-estimated due to a combination of several factors, including small sample sizes, study designs (the vast majority was case-control

Table 3 Discriminative performance of venous thromboembolism by inherited risk factors

	AUC (95%CI)[1]
F5/F2 mutations	0.64 (0.61-0.67)
$PGS_{non\text{-}F5/F2}$	0.68 (0.65-0.71)
F5/F2 mutations + $PGS_{non\text{-}F5/F2}$	0.69 (0.66-0.71)
PGS	0.69 (0.67-0.72)

[1]Model also included age, gender, body mass index and genetic background.

AUC: Area under the receiver operating characteristic curve; PGS: Polygenic score; 95%CI: 95% confidence interval.

studies), genetic heterogeneity (ancestry and genetic background were not accounted for), and publication bias (positive finding were more likely to be published). For example, in the meta-analysis performed by Zhong *et al*[17], the total sample size of IBD patients from 10 individual studies published before 2008 was 938, including 124 (13%) with VTE. In particular, 9 of the 10 studies had fewer than 80 IBD patients. The only relatively large study (477 IBD patients, including 14 (2.9%) with VTE) failed to observe a significant association between FVL and VTE, OR = 1.28, 95%CI: 0.16-10.17[19]. For *F2* PGM, its association with VTE in IBD patients was inconclusive from two small studies published prior to 2007, with fewer than 100 IBD patients in each study[20,21]. In comparison, the association results and OR estimates from our study were more reliable because the study was based on a large cohort of 8300 IBD patients whose VTE diagnosis was uniformly followed. Furthermore, our association test was performed adjusted for genetic background, therefore, reduced the confounder of genetic heterogeneity. However, additional large cohorts of IBD patients with follow-up information for VTE are still needed to validate our findings.

Third, compared to *F5/F2* mutations, we showed new PGS was more informative for stratifying VTE risk and performs better in discriminating VTE diagnosis after IBD. The better performance of PGS is consistent with the strong genetic basis for VTE where about 60% of the variance in VTE incidence is attributable to genetic effects[22]. Our finding is also consistent with a previous polygenic risk score study in 792 IBD patients where the score was based on 265 established VTE risk-associated SNPs[23]. However, the PGS used in the current study differs from the published study in that it includes many more SNPs (more than a million) and captures both established risk-associated SNPs implicated in GWAS and many more SNPs in the genome that did not reach the GWAS significance level individually (due to either modest-effect or low allele frequency)[6,23,24]. Consequently, the performance of PGS for stratifying VTE risk is improved. Additionally, our PGS not only identified patients at high-risk for VTE, but also identified patients at considerably low risk for VTE. This information is important for considering the need, dosage and duration for anticoagulant treatment to balance its potential benefits and harms. Importantly, it is worth noting that the PGS evaluated in this study was developed and validated in large external study populations with over a million subjects[6]. Our study simply assessed its performance in IBD patients, therefore, is not susceptible to issues related to model development such as overfitting and multiple testing. Furthermore, the risk estimate for PGS is not susceptible to potential observer bias because neither physicians nor patients are aware of their PGS for VTE.

Considering the similar AUC performance for the combined $PGS_{nonF5/F2}$ and *F5/F2* mutations and the original PGS, either approach may be used for VTE risk assessment in IBD patients in the clinic. While the first approach has the advantage of integrating well-known *F5/F2* mutations with new PGS, the latter approach is simpler to use (single scoring file) and easier to interpret (risk estimate derived from a large number of subjects is more reliable with a narrow CI). Furthermore, as a pan-ancestry PGS, PGS is applicable to patients of various ancestry populations. The added value of PGS over *F5/F2* mutations is more relevant in non-European ancestries because of their relatively low *F5/F2* mutation carrier rates (carrier rate of *F5/F2* mutations was 6.31% and 4.16% in European and non-European IBD patients, respectively). However, considering this PGS was developed and validated primarily in subjects of European ancestry, its performance in other ancestries is less certain. As shown in Supplementary Table 1 for the performance of PGS in 409 non-European IBD patients, compared to patients with intermediate scores, those at the top decile had HR of 1.48 (95%CI: 0.17-13.11) for VTE. Additional data for non-European IBD patients are urgently needed.

Our findings have potential clinical utilities. Genetic risk assessment using $PGS_{nonF5/F2}$ and *F5/F2* mutations may be integrated into clinical presentations to develop personalized strategies for thromboprophylaxis. For example, IBD patients with high genetic risk may consider higher dosage and longer duration of anticoagulation therapy. On the other hand, patients with low PGS and without *F5/F2* mutations may consider lower dosages and shorter duration to minimize risk for bleeding events.

Several limitations of our study are noted. Considering possible under-diagnosis of VTE (especially deep vein thrombosis) in subjects without IBD or other major diseases requiring hospitalization and intensive clinical care, we did not compare the VTE proportion between IBD and non-IBD subjects. Furthermore, due to the difficulty in obtaining detailed clinical variables related to the clinical characteristics of IBD and treatment, we were unable to include key clinical variables to assess the independent and added value of PGS in existing clinical risk assessment models. Another major limitation of our study is a lack of ancestral diversity in study subjects (96% of IBD patients in our study are of European ancestry), therefore it is critical to validate our findings in other diverse ancestry groups in future studies. Lastly, we did not include other known major genes for VTE (*SERPINC1*, *PROC*, and *PROS1*) in this study. Mutations in these genes are rare and can only be detected by whole exome sequencing (WES) which is currently available in only 40%

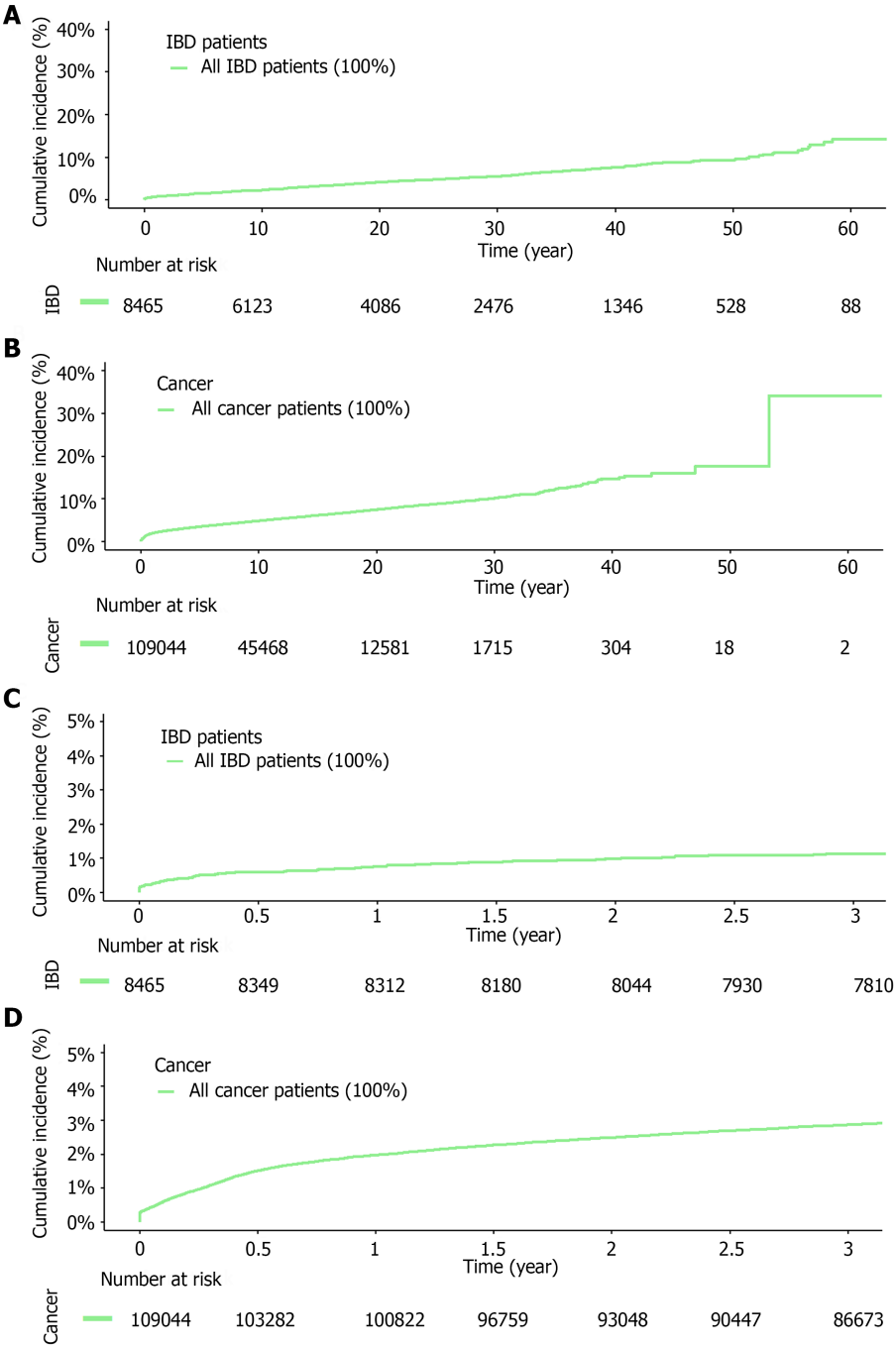

DOI: 10.3748/wjg.v29.i39.5494

Figure 1 Kaplan-Meier analysis. A and B: Kaplan-Meier analysis for time to incident venous thromboembolism in the UK Biobank during the entire follow-up period for inflammatory bowel disease (IBD) patients (A) and cancer patients (B); C and D: Within the 3 years after IBD diagnosis for IBD patients (C) and cancer patients (D). IBD: Inflammatory bowel disease.

of subjects in the UKB[7]. Among 3227 IBD patients with WES data, only 6 (0.19%), 2 (0.06%), and 2 (0.06%) carriers of loss of function mutations were identified, 2 (20%) of whom developed VTE. Larger studies with WES data are required to test these genetic risk factors.

CONCLUSION

In conclusion, we demonstrated that VTE complications are common in IBD patients with the proportion similar to diseases known at increased VTE risk. Furthermore, we showed SNP-based PGS is more informative and superior to *F5*/*F2* mutations in identifying IBD patients at high risk for VTE. These results may have potential implications for developing personalized anticoagulant treatment.

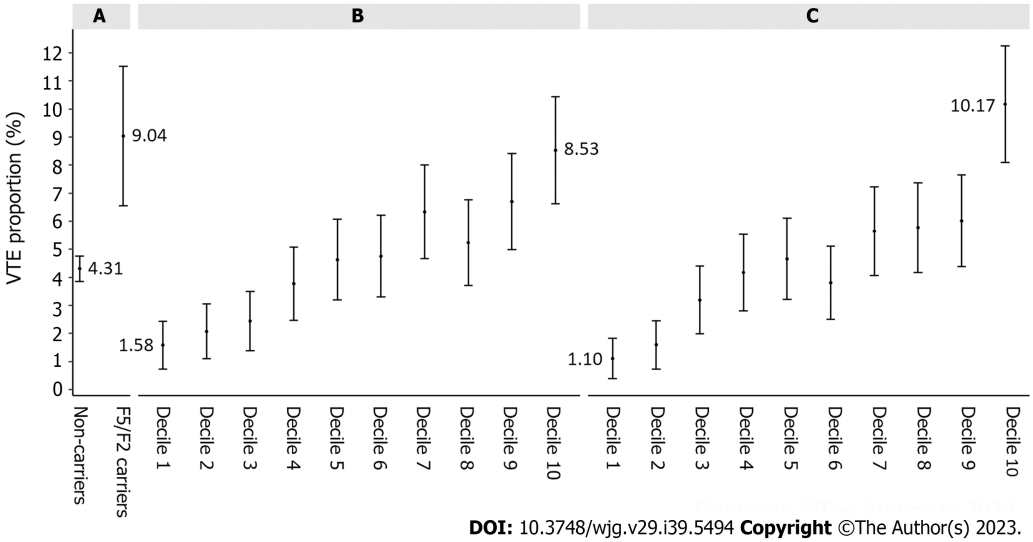

DOI: 10.3748/wjg.v29.i39.5494

Figure 2 Proportion of incident venous thromboembolism in the UK Biobank by carrier status of *F5* factor V leiden and/or *F2* prothrombin gene mutation, decile of polygenic score$_{nonF5/F2}$, and decile of original polygenic score. Dot and vertical line indicate mean and 95% confidence interval, respectively. A: Carrier status of *F5* factor V leiden and/or *F2* prothrombin gene mutation; B: Decile of polygenic score (PGS)$_{nonF5/F2}$; C: Decile of original PGS. Dot and vertical line indicate mean and 95% confidence interval, respectively. VTE: Venous thromboembolism.

ARTICLE HIGHLIGHTS

Research background

Venous thromboembolism (VTE) is a major complication in patients with inflammatory bowel disease (IBD). However, it is often underappreciated among physicians and patients. Furthermore, limited VTE risk stratification tools are available for personalized thromboprophylaxis.

Research motivation

A large IBD patient cohort is available from the UK Biobank (UKB). Its long-term clinical follow-up data and genome-wide genetic data provide a rare and efficient opportunity to address these two major challenges.

Research objectives

To estimate the prevalence of VTE complications among IBD patients and assess the performance of known and novel genetic predictors of VTE risk stratification in these patients.

Research methods

We retrospectively followed the incident VTE complication among 8465 IBD patients in the UKB. The associations of VTE with factor V leiden (FVL) mutation in the *F5* gene, G20210A prothrombin gene mutation (PGM) in the *F2* gene, and polygenic score (PGS) were tested using Cox hazards regression analysis, adjusting for age at IBD diagnosis, gender, and genetic background (top 10 principal components). The performance of genetic risk factors for discriminating VTE complications was estimated using the area under the receiver operating characteristic curve (AUC).

Research results

The overall prevalence of VTE complication after an IBD diagnosis was 4.70%. This prevalence was comparable to that of cancer patients (4.66%) who are well-known at increased risk for VTE. A novel genetic predictor (PGS) was significantly associated with VTE risk and was independent of known genetic predictors (FVL/PGM). The AUC of differentiating VTE complication was significantly higher for PGS [0.68, 95% confidence interval (CI): 0.66-0.71] than that of FVL/PGM (0.64, 95%CI: 0.61-0.67) and was highest by combining these two genetic predictors (0.69, 95%CI: 0.66-0.71).

Research conclusions

VTE complication is common in IBD patients and is similar to that of cancer patients. Newly developed PGS provides a more informative VTE risk stratification tool than known mutations (FVL/PGM).

Research perspectives

Findings from this large study of IBD patients have potential clinical utilities. It not only highlights the significance of VTE complications in IBD patients, but also provides an informative VTE risk assessment tool for developing personalized thromboprophylaxis strategies.

ACKNOWLEDGEMENTS

We are grateful to the Ellrodt-Schweighauser family for establishing Endowed Chair of Cancer Genomic Research (Xu), and Chez and Melman families for establishing Endowed Chairs of Personalized Prostate Cancer Care (Helfand).

FOOTNOTES

Author contributions: Xu J contributed to the concept and design; Shi Z, and Wei J performed the data analysis; Rifkin AS, and Xu J drafted the manuscript; Rifkin AS, Shi Z, Wei J, Zheng SL, Helfand BT, Cordova JS, Biank VF, Tafur AJ, Khan O, and Xu J contributed to the critical revision of the manuscript for important intellectual content; Xu J performed the supervision.

Institutional review board statement: The UK Biobank was approved by North West-Haydock Research Ethics Committee (REC reference: 16/NW/0274; IRAS project ID: 200778).

Informed consent statement: Data from the UK Biobank was accessed through a Material Transfer Agreement under Application Reference Number: 50295. This study was performed in accordance with the Declaration of Helsinki.

Conflict-of-interest statement: NorthShore University HealthSystem has an agreement with GoPath Laboratories and GenomicMD for genetic tests of polygenic risk score.

Data sharing statement: The data used in this study is available in the UK Biobank, a publicly available repository. Data was accessed through a Material Transfer Agreement under Application Reference Number: 50295. For additional information, please feel free to contact the corresponding author, Jianfeng Xu, DrPH.

STROBE statement: The authors have read the STROBE Statement—checklist of items, and the manuscript was prepared and revised according to the STROBE Statement—checklist of items.

Country/Territory of origin: United States

ORCID number: Jianfeng Xu 0000-0002-1343-8752.

S-Editor: Fan JR
L-Editor: A
P-Editor: Cai YX

REFERENCES

1 **Dahlhamer JM**, Zammitti EP, Ward BW, Wheaton AG, Croft JB. Prevalence of Inflammatory Bowel Disease Among Adults Aged ≥18 Years - United States, 2015. *MMWR Morb Mortal Wkly Rep* 2016; **65**: 1166-1169 [PMID: 27787492 DOI: 10.15585/mmwr.mm6542a3]

2 **Ng SC**, Shi HY, Hamidi N, Underwood FE, Tang W, Benchimol EI, Panaccione R, Ghosh S, Wu JCY, Chan FKL, Sung JJY, Kaplan GG. Worldwide incidence and prevalence of inflammatory bowel disease in the 21st century: a systematic review of population-based studies. *Lancet* 2017; **390**: 2769-2778 [PMID: 29050646 DOI: 10.1016/S0140-6736(17)32448-0]

3 **Grainge MJ**, West J, Card TR. Venous thromboembolism during active disease and remission in inflammatory bowel disease: a cohort study. *Lancet* 2010; **375**: 657-663 [PMID: 20149425 DOI: 10.1016/S0140-6736(09)61963-2]

4 **Olivera PA**, Zuily S, Kotze PG, Regnault V, Al Awadhi S, Bossuyt P, Gearry RB, Ghosh S, Kobayashi T, Lacolley P, Louis E, Magro F, Ng SC, Papa A, Raine T, Teixeira FV, Rubin DT, Danese S, Peyrin-Biroulet L. International consensus on the prevention of venous and arterial thrombotic events in patients with inflammatory bowel disease. *Nat Rev Gastroenterol Hepatol* 2021; **18**: 857-873 [PMID: 34453143 DOI: 10.1038/s41575-021-00492-8]

5 **Rosendaal FR**, Reitsma PH. Genetics of venous thrombosis. *J Thromb Haemost* 2009; **7** Suppl 1: 301-304 [PMID: 19630821 DOI: 10.1111/j.1538-7836.2009.03394.x]

6 **Ghouse J**, Tragante V, Ahlberg G, Rand SA, Jespersen JB, Leinøe EB, Vissing CR, Trudsø L, Jonsdottir I, Banasik K, Brunak S, Ostrowski SR, Pedersen OB, Sørensen E, Erikstrup C, Bruun MT, Nielsen KR, Køber L, Christensen AH, Iversen K, Jones D, Knowlton KU, Nadauld L, Halldorsson GH, Ferkingstad E, Olafsson I, Gretarsdottir S, Onundarson PT, Sulem P, Thorsteinsdottir U, Thorgeirsson G, Gudbjartsson DF, Stefansson K, Holm H, Olesen MS, Bundgaard H. Genome-wide meta-analysis identifies 93 risk loci and enables risk prediction equivalent to monogenic forms of venous thromboembolism. *Nat Genet* 2023; **55**: 399-409 [PMID: 36658437 DOI: 10.1038/s41588-022-01286-7]

7 **Bycroft C**, Freeman C, Petkova D, Band G, Elliott LT, Sharp K, Motyer A, Vukcevic D, Delaneau O, O'Connell J, Cortes A, Welsh S, Young A, Effingham M, McVean G, Leslie S, Allen N, Donnelly P, Marchini J. The UK Biobank resource with deep phenotyping and genomic data. *Nature* 2018; **562**: 203-209 [PMID: 30305743 DOI: 10.1038/s41586-018-0579-z]

8 **Klarin D**, Emdin CA, Natarajan P, Conrad MF; INVENT Consortium, Kathiresan S. Genetic Analysis of Venous Thromboembolism in UK

Biobank Identifies the ZFPM2 Locus and Implicates Obesity as a Causal Risk Factor. *Circ Cardiovasc Genet* 2017; **10** [PMID: 28373160 DOI: 10.1161/CIRCGENETICS.116.001643]

9 **Shi Z**, Wei J, Rifkin AS, Wang CH, Billings LK, Woo JSH, Talamonti MS, Vogel TJ, Moore E, Brockstein BE, Khandekar JD, Dunnenberger HM, Hulick PJ, Duggan D, Zheng SL, Lee CJ, Helfand BT, Tafur AJ, Xu J. Cancer-associated thrombosis by cancer sites and inherited factors in a prospective population-based cohort. *Thromb Res* 2023; **229**: 69-72 [PMID: 37419004 DOI: 10.1016/j.thromres.2023.06.023]

10 **Lambert SA**, Gil L, Jupp S, Ritchie SC, Xu Y, Buniello A, McMahon A, Abraham G, Chapman M, Parkinson H, Danesh J, MacArthur JAL, Inouye M. The Polygenic Score Catalog as an open database for reproducibility and systematic evaluation. *Nat Genet* 2021; **53**: 420-425 [PMID: 33692568 DOI: 10.1038/s41588-021-00783-5]

11 **Khera AV**, Chaffin M, Zekavat SM, Collins RL, Roselli C, Natarajan P, Lichtman JH, D'Onofrio G, Mattera J, Dreyer R, Spertus JA, Taylor KD, Psaty BM, Rich SS, Post W, Gupta N, Gabriel S, Lander E, Ida Chen YD, Talkowski ME, Rotter JI, Krumholz HM, Kathiresan S. Whole-Genome Sequencing to Characterize Monogenic and Polygenic Contributions in Patients Hospitalized With Early-Onset Myocardial Infarction. *Circulation* 2019; **139**: 1593-1602 [PMID: 30586733 DOI: 10.1161/CIRCULATIONAHA.118.035658]

12 **Papay P**, Miehsler W, Tilg H, Petritsch W, Reinisch W, Mayer A, Haas T, Kaser A, Feichtenschlager T, Fuchssteiner H, Knoflach P, Vogelsang H, Platzer R, Tillinger W, Jaritz B, Schmid A, Blaha B, Dejaco C, Sobala A, Weltermann A, Eichinger S, Novacek G. Clinical presentation of venous thromboembolism in inflammatory bowel disease. *J Crohns Colitis* 2013; **7**: 723-729 [PMID: 23127785 DOI: 10.1016/j.crohns.2012.10.008]

13 **McCurdy JD**, Israel A, Hasan M, Weng R, Mallick R, Ramsay T, Carrier M. A clinical predictive model for post-hospitalisation venous thromboembolism in patients with inflammatory bowel disease. *Aliment Pharmacol Ther* 2019; **49**: 1493-1501 [PMID: 31066471 DOI: 10.1111/apt.15286]

14 **Faye AS**, Hung KW, Cheng K, Blackett JW, Mckenney AS, Pont AR, Li J, Lawlor G, Lebwohl B, Freedberg DE. Minor Hematochezia Decreases Use of Venous Thromboembolism Prophylaxis in Patients with Inflammatory Bowel Disease. *Inflamm Bowel Dis* 2020; **26**: 1394-1400 [PMID: 31689354 DOI: 10.1093/ibd/izz269]

15 **Miehsler W**, Reinisch W, Valic E, Osterode W, Tillinger W, Feichtenschlager T, Grisar J, Machold K, Scholz S, Vogelsang H, Novacek G. Is inflammatory bowel disease an independent and disease specific risk factor for thromboembolism? *Gut* 2004; **53**: 542-548 [PMID: 15016749 DOI: 10.1136/gut.2003.025411]

16 **Tinsley A**, Naymagon S, Enomoto LM, Hollenbeak CS, Sands BE, Ullman TA. Rates of pharmacologic venous thromboembolism prophylaxis in hospitalized patients with active ulcerative colitis: results from a tertiary care center. *J Crohns Colitis* 2013; **7**: e635-e640 [PMID: 23706933 DOI: 10.1016/j.crohns.2013.05.002]

17 **Zhong M**, Dong XW, Zheng Q, Tong JL, Ran ZH. Factor V Leiden and thrombosis in patients with inflammatory bowel disease (IBD): a meta-analysis. *Thromb Res* 2011; **128**: 403-409 [PMID: 21831411 DOI: 10.1016/j.thromres.2011.07.014]

18 **Liang J**, Wu S, Feng B, Lei S, Luo G, Wang J, Li K, Li X, Xie H, Zhang D, Wang X, Wu K, Miao D, Fan D. Factor V Leiden and inflammatory bowel disease: a systematic review and meta-analysis. *J Gastroenterol* 2011; **46**: 1158-1166 [PMID: 21805067 DOI: 10.1007/s00535-011-0441-7]

19 **Bernstein CN**, Sargent M, Vos HL, Rosendaal FR. Mutations in clotting factors and inflammatory bowel disease. *Am J Gastroenterol* 2007; **102**: 338-343 [PMID: 17156138 DOI: 10.1111/j.1572-0241.2006.00974.x]

20 **Guédon C**, Le Cam-Duchez V, Lalaude O, Ménard JF, Lerebours E, Borg JY. Prothrombotic inherited abnormalities other than factor V Leiden mutation do not play a role in venous thrombosis in inflammatory bowel disease. *Am J Gastroenterol* 2001; **96**: 1448-1454 [PMID: 11374681 DOI: 10.1111/j.1572-0241.2001.03797.x]

21 **Koutroubakis IE**, Sfiridaki A, Tsiolakidou G, Theodoropoulou A, Livadiotaki A, Paspatis G, Kouroumalis EA. Genetic risk factors in patients with inflammatory bowel disease and vascular complications: case-control study. *Inflamm Bowel Dis* 2007; **13**: 410-415 [PMID: 17206678 DOI: 10.1002/ibd.20076]

22 **Heit JA**, Phelps MA, Ward SA, Slusser JP, Petterson TM, De Andrade M. Familial segregation of venous thromboembolism. *J Thromb Haemost* 2004; **2**: 731-736 [PMID: 15099278 DOI: 10.1111/j.1538-7933.2004.00660.x]

23 **Naito T**, Botwin GJ, Haritunians T, Li D, Yang S, Khrom M, Braun J; NIDDK IBD Genetics Consortium, Abbou L, Mengesha E, Stevens C, Masamune A, Daly M, McGovern DPB. Prevalence and Effect of Genetic Risk of Thromboembolic Disease in Inflammatory Bowel Disease. *Gastroenterology* 2021; **160**: 771-780.e4 [PMID: 33098885 DOI: 10.1053/j.gastro.2020.10.019]

24 **Klarin D**, Busenkell E, Judy R, Lynch J, Levin M, Haessler J, Aragam K, Chaffin M, Haas M, Lindström S, Assimes TL, Huang J, Min Lee K, Shao Q, Huffman JE, Kabrhel C, Huang Y, Sun YV, Vujkovic M, Saleheen D, Miller DR, Reaven P, DuVall S, Boden WE, Pyarajan S, Reiner AP, Trégouët DA, Henke P, Kooperberg C, Gaziano JM, Concato J, Rader DJ, Cho K, Chang KM, Wilson PWF, Smith NL, O'Donnell CJ, Tsao PS, Kathiresan S, Obi A, Damrauer SM, Natarajan P; INVENT Consortium; Veterans Affairs' Million Veteran Program. Genome-wide association analysis of venous thromboembolism identifies new risk loci and genetic overlap with arterial vascular disease. *Nat Genet* 2019; **51**: 1574-1579 [PMID: 31676865 DOI: 10.1038/s41588-019-0519-3]

World Journal of Gastroenterology

Submit a Manuscript: https://www.f6publishing.com

World J Gastroenterol 2023 October 21; 29(39): 5503-5525

DOI: 10.3748/wjg.v29.i39.5503

ISSN 1007-9327 (print) ISSN 2219-2840 (online)

SYSTEMATIC REVIEWS

Diagnostic role of transient elastography in patients with autoimmune liver diseases: A systematic review and meta-analysis

Hong Chen, Yue Shen, Sheng-Di Wu, Qin Zhu, Cheng-Zhao Weng, Jun Zhang, Mei-Xia Wang, Wei Jiang

Specialty type: Gastroenterology and hepatology

Provenance and peer review: Invited article; Externally peer reviewed.

Peer-review model: Single blind

Peer-review report's scientific quality classification
Grade A (Excellent): 0
Grade B (Very good): B, B
Grade C (Good): C, C, C
Grade D (Fair): 0
Grade E (Poor): 0

P-Reviewer: Granito A, Italy; Tai DI, Taiwan; Yoshioka K, Japan; Jian-Gao Fan, China

Received: July 2, 2023
Peer-review started: July 2, 2023
First decision: August 30, 2023
Revised: September 9, 2023
Accepted: October 11, 2023
Article in press: October 11, 2023
Published online: October 21, 2023

Hong Chen, Sheng-Di Wu, Cheng-Zhao Weng, Jun Zhang, Mei-Xia Wang, Wei Jiang, Department of Gastroenterology and Hepatology, Zhongshan Hospital (Xiamen), Fudan University, Xiamen 361015, Fujian Province, China

Hong Chen, Yue Shen, Sheng-Di Wu, Qin Zhu, Wei Jiang, Department of Gastroenterology and Hepatology, Zhongshan Hospital of Fudan University, Shanghai 200032, China

Hong Chen, Yue Shen, Sheng-Di Wu, Qin Zhu, Wei Jiang, Shanghai Institute of Liver Diseases, Fudan University Shanghai Medical College, Shanghai 200032, China

Corresponding author: Wei Jiang, MD, PhD, Academic Research, Chief Doctor, Professor, Department of Gastroenterology and Hepatology, Zhongshan Hospital (Xiamen), Fudan University, No. 666 Jinhu Road, Huli District, Xiamen 361015, Fujian Province, China.
jiang.wei@zs-hospital.sh.cn

Abstract

BACKGROUND

Noninvasive methods have been developed to detect fibrosis in many liver diseases due to the limits of liver biopsy. However, previous studies have focused primarily on chronic viral hepatitis and nonalcoholic fatty liver disease. The diagnostic value of transient elastography for autoimmune liver diseases (AILDs) is worth studying.

AIM

To compare the diagnostic accuracy of imaging techniques with serum biomarkers of fibrosis in AILD.

METHODS

The PubMed, Cochrane Library and EMBASE databases were searched. Studies evaluating the efficacy of noninvasive methods in the diagnosis of AILDs [autoimmune hepatitis (AIH), primary biliary cholangitis (PBC) and primary sclerosing cholangitis (PSC)] were included. The summary area under the receiver operating characteristic curve (AUROC), diagnostic odds ratio, sensitivity and specificity were used to assess the accuracy of these noninvasive methods for staging fibrosis.

RESULTS

A total of 60 articles were included in this study, and the number of patients with AIH, PBC and PSC was 1594, 3126 and 501, respectively. The summary AUROC

of transient elastography in the diagnosis of significant fibrosis, advanced fibrosis and cirrhosis in patients with AIH were 0.84, 0.88 and 0.90, respectively, while those in patients with PBC were 0.93, 0.93 and 0.91, respectively. The AUROC of cirrhosis for patients with PSC was 0.95. However, other noninvasive indices (aspartate aminotransferase to platelet ratio index, aspartate aminotransferase/alanine aminotransferase ratio, fibrosis-4 index) had corresponding AUROCs less than 0.80.

CONCLUSION

Transient elastography exerts better diagnostic accuracy in AILD patients, especially in PBC patients. The appropriate cutoff values for staging advanced fibrosis and cirrhosis ranged from 9.6 to 10.7 and 14.4 to 16.9 KPa for PBC patients.

Key Words: Liver stiffness; Serum parameter; Liver fibrosis; Noninvasive diagnosis; Transient elastography; Autoimmune liver disease

Core Tip: Onset of autoimmune liver diseases is frequently insidious, and immune cell infiltration and continuous inflammation drive hepatic fibrosis, which gradually progresses to cirrhosis, causing poorer long-term outcomes. Liver biopsy as the reference standard is an invasive procedure. Thus, repeated biopsies are difficult to implement. Consequently, appropriate noninvasive methods are essential to dynamically monitor the degree of liver fibrosis. Our meta-analysis compared the diagnostic accuracy of imaging techniques with serum biomarkers of fibrosis in autoimmune liver diseases.

Citation: Chen H, Shen Y, Wu SD, Zhu Q, Weng CZ, Zhang J, Wang MX, Jiang W. Diagnostic role of transient elastography in patients with autoimmune liver diseases: A systematic review and meta-analysis. *World J Gastroenterol* 2023; 29(39): 5503-5525
URL: https://www.wjgnet.com/1007-9327/full/v29/i39/5503.htm
DOI: https://dx.doi.org/10.3748/wjg.v29.i39.5503

INTRODUCTION

The incidence of autoimmune liver diseases (AILDs), including autoimmune hepatitis (AIH), primary biliary cholangitis (PBC), primary sclerosing cholangitis (PSC), and multiple overlap syndromes, a group of autoimmune diseases associated with the liver and bile duct is increasing[1,2]. Onset is frequently insidious, with nonspecific symptoms. Immune cell infiltration and continuous inflammation drive hepatic fibrosis, which gradually progresses to cirrhosis, causing poorer long-term outcomes in patients[3-5]. Accordingly, accurate identification of high-risk patients for such conditions is essential in clinical care to guide timely treatment and delay disease progression.

For years, liver biopsy has been recognized as the reference standard for the assessment of liver fibrosis. However, biopsy area restrictions, sampling errors, and interobserver variability may affect the diagnostic accuracy[6,7]. Moreover, because biopsy is an invasive procedure with potentially hazardous complications ranging from pain to more severe events and even death, many patients are reluctant to undergo repeat biopsies[8,9]. Consequently, an increasing number of studies have focused on noninvasive methods to identify the ideal approach for dynamically monitoring the degree of liver fibrosis[10].

In recent years, some noninvasive methods, including biochemical tests and imaging techniques, have been widely developed, including the aspartate aminotransferase to platelet ratio index (APRI), aspartate aminotransferase/alanine aminotransferase (ALT) ratio (AAR), fibrosis-4 index (FIB-4), red cell distribution width to platelet ratio (RPR), Mac-2 binding protein (M2BP), platelet count to spleen diameter (PC/SD) ratio, transient elastography (TE), shear wave elastography (SWE), acoustic radiation force impulse (ARFI), magnetic resonance spectroscopy (MRS) and magnetic resonance elastography (MRE). Previous studies have validated that elastography is a reliable method with a diagnostic accuracy higher than that of blood tests for staging liver fibrosis in chronic viral hepatitis[11-13], nonalcoholic fatty liver disease[14] and AIH[15]; however, no studies have explored the diagnostic accuracy of noninvasive methods for the other two types of AILDs (PBC and PSC).

Therefore, the present meta-analysis aimed to compare the diagnostic accuracy of biochemical tests and imaging techniques for detecting liver fibrosis in patients with AILD, determine whether the same noninvasive methods show different diagnostic values in the three types of AILDs and recommend appropriate cutoff values for different fibrosis stages.

MATERIALS AND METHODS

Literature search strategy

Studies on the diagnosis of AILD published between January 2006 and December 2022 were searched in PubMed, Cochrane Library and EMBASE databases using the following keywords: AIH, PSC, PBC, liver fibrosis, TE, SWE, MRE, APRI, FIB-4 and AAR. The detailed search strategy is presented in Supplementary Table 1.

Study selection criteria

Original studies that fulfilled the following criteria were enrolled: (1) Studies with patient populations with AIH, PBC or PSC with discrete data that could be separately extracted from the mixed liver disease study cohort; (2) Studies in which liver biopsy was used as the gold standard to assess fibrosis based on the Metavir score or another score that could be converted to the Metavir score; (3) Studies assessing the performance and utility of APRI, AAR, FIB-4, RPR, M2BP, ARFI, PC/SD ratio, TE, SWE, MRE or MRS for staging liver fibrosis; and (4) Studies directly reporting the true-positive, false-positive, false-negative and true-negative values or provided data by which they could be calculated to allow the construction of a 2 × 2 table for each test.

The following studies were excluded: (1) Studies exploring the prognostic value of liver stiffness measurement (LSM) for patients with AILD; (2) Animal experiments, reviews, protocols, guidelines, case reports or meta-analyses; (3) Studies on liver fibrosis due to other etiologies, including nonalcoholic fatty liver disease, chronic hepatitis B, or chronic hepatitis C; and (4) Studies without sufficient data for further analysis or with the same or overlapping group of participants.

Data extraction and quality assessment

Two investigators (Chen H and Shen Y) independently evaluated the eligibility and quality of the included studies and extracted the data. Any disagreements were resolved by a senior researcher (Wu SD). We collated the following parameters in Microsoft Excel 2010: authors; year of publication; country; study period and design; pathological type; diagnostic methods; sample size; patient characteristics [age, sex, body mass index (BMI), ALT level, treatment condition]; quality of liver biopsy; and performance of the index test, including cutoff values, sensitivity, specificity, positive predictive value, negative predictive value, and area under the receiver operating characteristic curve (AUROC). Two reviewers (Chen H and Shen Y) independently assessed the risk of bias using the Quality Assessment of Diagnostic Accuracy Studies-2 tool[16].

Data synthesis and statistical analysis

According to the Metavir, Batts-Ludwig and Scheuer scores, liver fibrosis was classified into five stages (F0, F1, F2, F3 and F4), whereas there were seven stages according to the Ishak score. Given that Shiha *et al*[17] proposed that an Ishak score of 3 corresponds to METAVIR score of F2, significant fibrosis (SF), advanced fibrosis (AF) and cirrhosis were defined as stages F2-F4, F3-F4, and F4, respectively. For the data analysis, we constructed 2 × 2 contingency tables with true-positive, false-positive, false-negative and true-negative values based on data directly extracted from the original studies or calculated from indirect variables (sensitivity, specificity and sample size). A bivariate random effects model was subsequently applied to calculate the diagnostic test accuracy variables, including summary sensitivity, summary specificity, positive likelihood ratio, negative likelihood ratio and diagnostic odds ratio (DOR) with their associated 95% confidence intervals (95%CIs). We also performed meta-analyses using hierarchical models to produce summary ROC curves, from which we obtained summary AUROC values to evaluate the diagnostic accuracy of the different noninvasive methods. The method was considered to have excellent accuracy if the summary AUROC value was above 0.90, moderate accuracy if it was greater than 0.80, and poor accuracy if it was less than 0.80[18].

The heterogeneity was assessed using multiple methods. Spearman's correlation coefficient was calculated to evaluate the threshold heterogeneity of the included studies, whereas Cochran's Q and I^2 values were used to assess nonthreshold heterogeneity. If an I^2 value > 50% or P < 0.05 indicated distinct statistical heterogeneity, a random effects model was used to combine the data. A fixed effect model was chosen when the I^2 value ≤ 50% or P ≤ 0.05. However, the number of original studies was sufficient to perform a meta-regression to explore the potential heterogeneity of certain index tests. In addition, we conducted a subgroup analysis according to the sample size, treatment conditions and cutoff value. Deeks' funnel plots were used to evaluate the possible publication bias. The meta-analysis was performed using Stata 12.0, Reviewer Manager Version 5.3 and Meta-Disc Version 1.4.

RESULTS

Characteristics of the included studies and patients

The study selection process is illustrated in Figure 1. A total of 1386 studies were retrieved through our search strategy, of which 427 were excluded as duplicates and 602 were removed following the screening of titles, abstracts and reviews. The remaining 355 potentially eligible studies were selected for further evaluation. Of these, 60 articles were included in the evaluation and analysis. Among them, 22, 29 and 6 studies were regarding AIH, PBC and PSC, respectively (2 studies focused on both AIH and PBC[19,20], while 1 study focused on both PBC and PSC[21]). In total, they included 11 noninvasive index tests. The basic characteristics of the included studies are presented in Table 1. We selected articles published between 2006 and 2022, of which 46 (76.7%) were published between 2016 and 2022. There were 31 (51.7%) retrospective studies, 17 (28.3%) prospective studies, 10 (16.7%) unknown studies and 2 studies with both designs. Most

Table 1 Characteristics of studies included in this study

No.	Ref.	Country	Disease	Study time	Study design	Diagnostic model[1]	Sample size	Mean age in yr	Sex, F/M	Mean BMI in kg/m^2	Mean, ALT in IU/mL	Treatment condition	Scoring system	Interval
1	Youssef *et al*[40], 2013	Egypt	AIH	NA	Retrospective	5	16	NA	NA	NA	NA	NA	Metavir	NA
2	Kim *et al*[41], 2014	Korea	AIH	2008-2014	Retrospective	5	47	NA	41/6	NA	NA	NA	Metavir	NA
3	Abdollahi *et al* [42], 2015	Iran	AIH	2011-2013	NA	1, 2, 3	80	34.75	51/29	NA	106.49	NA	Ishak	NA
4	Harrison *et al*[43], 2016	United Kingdom	AIH	2013-2015	Prospective	5	27	56	25/2	NA	21	Post	Ishak	The same day
5	Hartl *et al*[44], 2016	Germany	AIH	2007-2010	Prospective	5	34	53	28/6	NA	48.5	Post	Scheuer	Within 3 mo
	Hartl *et al*[44], 2016	Germany	AIH	2008-2015	Retrospective	5	60	52	50/10	NA	35	Post	Scheuer	Within 4 mo
6	Nishikawa *et al*[45], 2016	Japan	AIH	2005-2015	Prospective	1, 2, 3, 11	84	64	69/15	NA	57.5	Pre	Scheuer	NA
7	E Anastasiou *et al* [46], 2016	Germany	AIH	2008-2013	Retrospective	1, 2, 3, 5	53	47.3	31/22	NA	606.42	Pre 35 + post 18	Metavir	Within 3 wk
8	Piwczyńska *et al* [47], 2016	Poland	AIH	NA	Prospective	4	46	14.5	33/13	NA	NA	NA	Batts-Ludwig	NA
9	Sheptulina *et al* [48], 2016	Russian	AIH	2008-2014	Prospective	1, 2, 3, 9	76	40	65/11	25	54.4	Pre 22 + post 54	Metavir	Within 7 d
10	Guo *et al*[29], 2017	China	AIH	2012-2017	Retrospective	1, 3, 5	108	46.54	88/20	23.52	146.51	NA	Metavir	Within 3 d
11	Paranagua-Vezozzo *et al*[49], 2016	Brazil	AIH	2012-2015	Prospective	4, 5	33	NA	28/5	28.6	NA	Post	Metavir	The same day
12	Puustinen *et al* [50], 2017	Finland	AIH	NA	Prospective	8	12	42.8	10/2	NA	28.5	NA	Metavir	Within 1 mo
13	Wang *et al*[22], 2017	China	AIH	2007-2015	Retrospective	1, 2, 3, 7	36	51.6	NA	27.7	217.4	Pre 17 + post 19	Metavir	Within 3 mo
14	Xu *et al*[51], 2017	China	AIH	2014-2016	Prospective	1, 3, 5	100	45	81/19	NA	131.5	Pre	Metavir	The same day
15	Zeng *et al*[52], 2017	China	AIH	2011-2016	Prospective	6	62	45.6	NA	21.6	78.5	Pre	Metavir	3 d
16	Liu *et al*[53], 2019	China	AIH	2008-2018	Retrospective	2, 3	45	54.29	37/8	NA	NA	NA	Metavir	The same day

17	Park *et al*[19], 2019	South Korea	AIH	2014-2017	NA	4	49	56	42/7	23.7	163	NA	Metavir	The same day
			PBC				41	55.3	35/6	25.5	45	NA		
18	Li *et al*[54], 2020	China	AIH	2010-2019	Retrospective	1, 2, 3, 10	72	54	64/8	NA	137.55	Post	Metavir	NA
19	Wang *et al*[55], 2020	China	AIH	2016-2019	Retrospective	1, 3, 10	119	52.5	99/20	NA	81.6	Pre	Scheuer	Within 7 d
20	Xing *et al*[30], 2020	China	AIH	2016-2019	Retrospective	1, 3, 6	103	54	81/22	22.5	163	NA	Scheuer	Within 7 d
21	Janik *et al*[31], 2021	Poland	AIH	2015-2020	Prospective	6	63	37	15/48	23.9	130	Post	Batts-Ludwig	Within 3 mo
22	Zachou *et al*[20], 2021	Greece	AIH	2009-2016	Retrospective	5	78	57	54/24	NA	68	Pre 47 + post 31	Metavir	The same day
			PBC				56	52	48/8	NA	47	Pre 37 + post 19		
23	Ferronato *et al*[56], 2022	Italy	AIH	NA	Retrospective	1, 2, 3	122	59	90/32	NA	481.8	Pre	Ishak	Within 23 d
24	Soh *et al*[57], 2022	Korea	AIH	2014-2021	Retrospective	6	69	59.7	60/9	NA	187.1	Pre 44 + post 25	Metavir	The same day
25	Nyblom *et al*[58], 2006	Sweden	PBC	1976-2000	Retrospective	2	121	54	NA	NA	189.9	NA	Metavir	NA
26	Gómez-Dominguez *et al*[59], 2008	Spain	PBC	NA	Prospective	5	80	54	64/16	NA	NA	Post	Metavir	Within 9 mo
27	Alempijevic *et al*[60], 2009	Serbia	PBC	2006	NA	1, 2	112	53.88	104/8	NA	NA	Post	Scheuer	Within 1 wk
28	Ferrara *et al*[61], 2009	Italy	PBC	NA	NA	1, 3	248	52	233/15	NA	NA	NA	Scheuer	The same day
29	Su *et al*[62], 2009	China	PBC	1985-2006	Retrospective	2	46	53.3	34/12	NA	140.6	NA	Scheuer	Within 1 mo
30	Floreani *et al*[63], 2011	Italy	PBC	2009	NA	5	114	58	96/24	24	44	NA	Metavir	Within 6 mo
31	Corpechot *et al*[64], 2012	France	PBC	2004-2010	Prospective	5	103	56	87/16	23.9	76	Post	Metavir	Within 9 mo
32	Zhang *et al*[34], 2014	China	PBC	2011-2013	NA	4	56	45	46/10	NA	NA	NA	Batts-Ludwig	Within 3 d
33	Sheptulina *et al*[21], 2015	Russian	PBC	2008-2014	Retrospective	9	82	54.5	78/4	NA	NA	NA	Metavir	NA
			PSC			3	22	38	6/16	NA	NA	NA		NA
34	Umemura *et al*[65], 2015	Japan	PBC	1981-2014	Retrospective	11	137	57	111/26	NA	41	Post	Metavir	The same day

35	Nishikawa *et al* [66], 2016	Japan	PBC	2005-2014	Prospective	1, 3, 11	57	59	49/8	NA	35	Pre	Scheuer	NA
36	Olmez *et al*[67], 2016	Turkey	PBC	1995-2013	Retrospective	1, 3	40	49.6	40/0	NA	54.5	NA	Scheuer	Within 1 wk
37	Wang *et al*[68], 2016	China	PBC	2010-2015	Retrospective	1, 3, 10	73	52.4	62/11	NA	89.3	Pre	Ludwing and Scheuer	The day before
38	Koizumi *et al*[23], 2017	Japan	PBC	2012-2015	Prospective	1, 2, 3, 5	44	60.5	41/3	NA	65.9	Post	Metavir	Within 1 wk
39	Wang *et al*[69], 2017	China	PBC	2009-2016	Retrospective	1, 3	261	52	230/31	NA	NA	NA	Metavir	NA
40	Jiang *et al*[70], 2018	China	PBC	2009-2015	Retrospective	3, 10	77	62.4	64/13	NA	81.2	Pre	Scheuer	NA
41	Kamal *et al*[71], 2018	Netherlands	PBC	1979-2010	Retrospective	1, 2, 3	85	50	75/10	NA	NA	NA	Ishak	NA
42	Meng *et al*[72], 2018	China	PBC	2013-2017	Retrospective	1, 3, 10	94	51.02	NA	NA	116.58	Pre	Ludwing and Scheuer	Within 1 wk
43	Milovanović *et al* [73], 2018	Serbia	PBC	2009-2011	Prospective	1, 2, 5	122	57.4	NA	NA	50.8	Post	Metavir	Within 1 mo
44	Wang *et al*[74], 2018	China	PBC	2010-2016	Retrospective	1, 3, 10	58	53.3	51/7	NA	90.4	Pre	Ludwing and Scheuer	Within 1 wk
45	Jiang *et al*[75], 2020	China	PBC	2008-2018	Prospective	1, 2, 3, 10	78	52	71/7	NA	NA	Pre 39 + post 39	Scheuer	Within 2 wk
	Jiang *et al*[75], 2020	China b	PBC	2008-2018	Retrospective	1, 3, 10	40	51	35/5	NA	NA	Pre 20 + post 20	Scheuer	Within 2 wk
46	Joshita *et al*[76], 2020	Japan	PBC	2015-2019	NA	5, 11	74	64	62/12	NA	48	Pre	Scheuer	The same day
47	Rossi *et al*[77], 2020	Italy	PBC	NA	NA	5	92	NA	NA	NA	NA	NA	Scheuer	Within 1 mo
48	Yan *et al*[32], 2020	China	PBC	2016-2019	Retrospective	1, 2, 3, 6	157	53	136/21	22.2	72	NA	Scheuer	NA
49	Cristoferi *et al*[78], 2021	Italy	PBC	2006-2019	Prospective	1, 5	126	52	114/12	22.3	52.8	Pre	Batts-Ludwig	Within 12 wk
50	Fujinaga *et al*[79], 2021	Japan	PBC	2000-2019	Retrospective	1, 3, 11	102	61	89/13	NA	68.4	Pre	Scheuer	NA
51	Manesis *et al*[80], 2021	Greece	PBC	2010-2018	Retrospective	6	53	62.6	46/7	25.7	30	Pre 30 + post 23	Scheuer	Within 3 mo
52	Osman *et al*[33], 2021	United States	PBC	2007-2019	Retrospective	5	63	60.95	NA	NA	31.2	NA	Batts-Ludwig	Within 1 yr

						7	98	60.21	NA	NA	36.4	NA		
53	Avcioğlu *et al*[81], 2022	Turkey	PBC	2008-2020	Retrospective	1, 3	35	49.6	33/2	NA	50.6	Pre	Scheuer	Within 1 wk
54	Garrido *et al*[82], 2022	Portugal	PBC	2010-2021	NA	5	79	52	NA	NA	NA	Pre 40 + post 39	Batts-Ludwig	Within 2 mo
55	Corpechot *et al* [83], 2014	France	PSC	2005-20210	Prospective	5	59	40.7	24/35	NA	145.7	Post	Metavir	Within 6 mo
56	Bowlus *et al*[84], 2016,	France	PSC	NA	NA	5	56	43	22/34	NA	255	NA	Ishak	NA
57	Eaton *et al*[85], 2016	United States	PSC	2007-2013	Retrospective	1, 7	266	46.12	81/185	26	48	Pre	Batts-Ludwig	Within 1 yr
58	Ehlken *et al*[86], 2016	Germany	PSC	2006-2014	Retrospective	5	62	38	63/77	NA	38	NA	Scheuer	NA
59	Krawczyk *et al* [87], 2017	Poland	PSC	2014-2016	Prospective	5	30	33	12/18	NA	50	NA	Metavir	NA
60	Umetsu *et al*[88], 2018	Japan	PSC	2007-2016	Retrospective	1, 2, 3, 11	28	14	8/20	NA	56.5	NA	Batts-Ludwig	The same day

[1]Diagnostic models are represented by the following numbers: 1 = Aspartate aminotransferase to platelet ratio index; 2 = caspartate aminotransferase to alanine aminotransferase ratio; 3 = Fibrosis-4 index; 4 = Acoustic radiation force impulse; 5 = Transient elastography; 6 = Shear wave elastography; 7 = Magnetic resonance elastography; 8 = Magnetic resonance spectroscopy; 9 = Platelet count to spleen diameter ratio; 10 = Red cell distribution width to platelet ratio ; 11 = Mac-2-binding protein. AIH: Autoimmune hepatitis; ALT: Alanine aminotransferase; BMI: Body mass index; F: Female; M: Male; NA: Not available; PBC: Primary biliary cholangitis; PSC: Primary sclerosing cholangitis.

included studies were conducted in Asia (28 studies) or Europe (24 studies). A total of 27 studies utilized the Metavir score, 8 studies used the Batts-Ludwig score, 17 studies used the Scheuer score, 5 studies used the Ishak score, and 3 studies used the Ludwig-Scheuer score.

A total of 1594, 3126 and 501 patients with AIH, PBC, and PSC, respectively, were included to analyze the diagnostic performance of noninvasive methods in staging liver fibrosis. Most patients with AIH and PBC were female (72.4% and 87.6%, respectively). In contrast, patients with PSC were predominantly male (73.7%). The average ages of patients with AIH, PBC and PSC were 47.0, 55.2 and 41.5 years, respectively. Patients with AIH (160.29 IU/mL) had higher ALT levels than patients with PBC (69.81 IU/mL).

Quality assessment of the included studies

The results of the quality assessment based on the Quality Assessment of Diagnostic Accuracy Studies-2 scale for all 60 eligible studies are shown in Figure 2 and Supplementary Figure 1. Regarding patient selection, eight studies had an unclear risk of bias owing to the lack of information on whether patients were enrolled randomly or consecutively. Regarding the index test, four studies were determined to have an unclear risk of bias because the results of the index test were interpreted without blinded information on the results of the reference standard. Likewise, 22 studies were regarded as having an unclear risk of bias because the results of the reference standard were interpreted without blinded information regarding the results of the index test. In terms of flow and timing, two studies were considered high-risk because not every subject received a reference standard, while 19 studies were considered unclear risk because of an

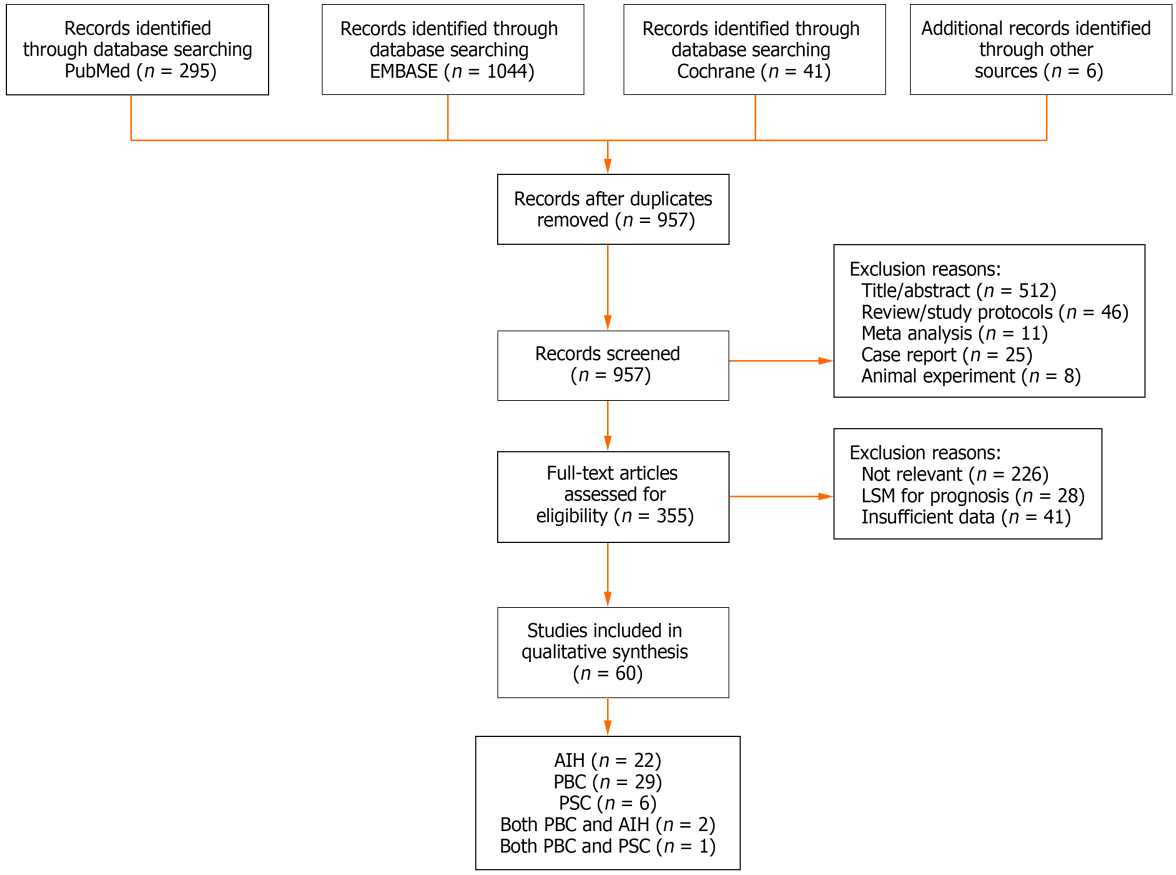

DOI: 10.3748/wjg.v29.i39.5503 **Copyright** ©The Author(s) 2023.

Figure 1 Flowchart of study identification and selection process. AIH: Autoimmune hepatitis; LSM: Liver stiffness measurement; PBC: Primary biliary cholangitis; PSC: Primary sclerosing cholangitis.

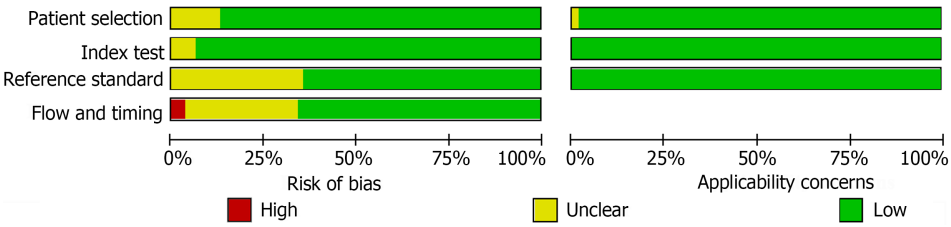

DOI: 10.3748/wjg.v29.i39.5503 **Copyright** ©The Author(s) 2023.

Figure 2 Quality assessment of included studies by Quality Assessment of Diagnostic Accuracy Studies-2. Risk of bias and applicability concerns graph.

unknown time interval between the index and reference tests.

Performance of noninvasive methods in diagnosing SF (F ≥ 2)

Diagnosis of SF for AIH: Fifteen studies (n = 1001) evaluated eight noninvasive methods for detecting SF in patients with AIH. Of these, five (n = 459), two (n = 129), five (n = 459), nine (n = 523) and three (n = 234) studies focused on APRI, AAR, FIB-4, TE and SWE separately, whereas only one study each utilized the ARFI, PC/SD ratio and RPR.

The APRI had moderate summary sensitivity (exceeding 70%) with poor summary specificity (less than 50%), whereas the FIB-4 had the opposite result (Table 2). Interestingly, TE had a relatively greater diagnostic performance than the other laboratory tests, with summary sensitivity and specificity values of 0.82 and 0.73, respectively, and cutoff values ranging from 5.8–7.0 KPa. The summary sensitivity of SWE (0.89; 95%CI: 0.83–0.93) was significantly higher than that of the other six noninvasive methods and slightly greater than that of TE (0.83; 95%CI: 0.78–0.87).

Diagnosis of SF for PBC: Thirteen studies (n = 1389) evaluated nine noninvasive methods for diagnosing SF in patients with PBC. Among them, four (n = 584), three (n = 323), three (n = 462), two (n = 87), five (n = 446) and two (n = 210) studies focused on APRI, AAR, FIB-4, ARFI, TE and SWE, respectively; however, only one study each utilized the PC/SD ratio, MRE and M2BP.

Table 2 Summary sensitivities, specificities, positive likelihood ratio and negative likelihood ratio of noninvasive methods at various diagnostic thresholds for prediction of significant fibrosis, advanced fibrosis and cirrhosis in autoimmune liver diseases patients

Disease	Diagnostic model/Stage	Cutoff values	No. of patients (*n*)	Summary sensitivity	Summary specificity	Summary PLR	Summary NLR
AIH	APRI						
	SF	0.27-0.70	2 (195)	0.80 (0.72-0.86)	0.35 (0.23-0.48)	1.46 (0.55-3.89)	0.36 (0.061-2.09)
		0.88-1.55	3 (264)	0.74 (0.68-0.80)	0.51 (0.38-0.63)	1.52 (1.18-1.96)	0.50 (0.36-0.69)
	AF	0.38-0.90	4 (379)	0.86 (0.81-0.90)	0.48 (0.41-0.56)	1.60 (1.18-2.15)	0.33 (0.24-0.47)
		1.12-3.40	6 (538)	0.80 (0.72-0.86)	0.35 (0.23-0.48)	0.57 (0.51-0.64)	0.68 (0.62-0.73)
	Cirrhosis	0.55-1.81	3 (330)	0.65 (0.56-0.74)	0.47 (0.40-0.54)	1.49 (0.93-2.39)	0.62 (0.46-0.83)
		1.85-2.00	3 (213)	0.70 (0.57-0.81)	0.73 (0.65-0.79)	2.48 (1.75-3.52)	0.42 (0.28-0.62)
	AAR						
	SF	0.72-0.93	2 (129)	0.67 (0.57-0.77)	0.68 (0.49-0.83)	2.22 (1.32-3.72)	0.46 (0.23-0.90)
	AF	0.76-1.18	7 (532)	0.61 (0.54-0.68)	0.72 (0.66-0.77)	2.01 (1.59-2.53)	0.58 (0.46-0.73)
	Cirrhosis	0.94-1.40	3 (213)	0.61 (0.47-0.74)	0.83 (0.76-0.88)	3.31 (1.96-5.59)	0.49 (0.36-0.69)
	FIB-4						
	SF	1.95-2.90	3 (303)	0.64 (0.58-0.71)	0.71 (0.61-0.81)	2.20 (1.48-3.27)	0.50 (0.38-0.65)
		3.20-5.07	2 (156)	0.60 (0.51-0.69)	0.77 (0.60-0.90)	2.66 (1.44-4.92)	0.52 (0.39-0.69)
	AF	1.75-2.37	6 (476)	0.66 (0.59-0.72)	0.63 (0.57-0.69)	2.05 (1.56-2.70)	0.40 (0.20-0.81)
		3.21-5.60	5 (486)	0.47 (0.41-0.54)	0.73 (0.67-0.79)	1.83 (1.24-2.71)	0.68 (0.50-0.92)
	Cirrhosis	2.21-3.40	5 (440)	0.75 (0.67-0.82)	0.56 (0.50-0.62)	2.06 (1.53-2.77)	0.37 (0.19-0.71)
		6.44	1 (103)	0.68	0.64	1.88	0.51
	TE						
	SF	5.80-7.00	7 (423)	0.83 (0.78-0.87)	0.73 (0.65-0.80)	2.89 (2.23-3.76)	0.23 (0.12-0.42)
		9.10-10.05	2 (100)	0.77 (0.67-0.86)	0.94 (0.70-1.00)	7.65 (1.66-35.32)	0.18 (0.02-1.47)
	AF	8.18-9.00	3 (286)	0.80 (0.72-0.87)	0.80 (0.73-0.86)	4.09 (2.64-6.33)	0.24 (0.17-0.35)
		10.40-12.10	4 (174)	0.73 (0.60-0.83)	0.93 (0.86-0.97)	7.67 (2.89-20.31)	0.27 (0.12-0.61)
	Cirrhosis	11.00-12.67	4 (213)	0.89 (0.82-0.94)	0.88 (0.81-0.93)	6.89 (4.38-10.85)	0.14 (0.09-0.23)
		16.00-19.00	3 (147)	0.88 (0.74-0.96)	0.97 (0.92-0.99)	22.08 (5.35-91.22)	0.16 (0.08-0.33)
	2D-SWE						
	SF	8.20-10.00	3 (234)	0.89 (0.83-0.93)	0.72 (0.59-0.83)	3.25 (1.67-6.32)	0.17 (0.11-0.28)
	AF	12.20-15.80	3 (234)	0.82 (0.73-0.89)	0.79 (0.72-0.86)	3.92 (2.79-5.52)	0.24 (0.13-0.44)
	Cirrhosis	14.30-19.30	4 (297)	0.83 (0.74-0.90)	0.86 (0.81-0.91)	5.85 (4.09-8.37)	0.21 (0.13-0.34)
PBC	APRI						
	SF	0.26-1.20	4 (584)	0.84 (0.80-0.87)	0.63 (0.56-0.70)	1.98 (1.54-2.55)	0.34 (0.23-0.51)
	AF	0.3.0-0.75	8 (858)	0.62 (0.57-0.68)	0.54 (0.50-0.58)	1.39 (1.09-1.79)	0.68 (0.48-0.98)
		0.93-2.00	7 (731)	0.73 (0.68-0.78)	0.68 (0.64-0.72)	2.68 (1.80-3.97)	0.46 (0.36-0.58)
	Cirrhosis	0.65-1.39	6 (852)	0.75 (0.67-0.83)	0.51 (0.48-0.55)	2.19 (1.38-3.50)	0.31 (0.10-0.99)
	AAR						
	SF	0.92-1.00	3 (323)	0.69 (0.61-0.76)	0.56 (0.48-0.63)	1.61 (1.33-1.95)	0.52 (0.31-0.87)
	AF	0.81-1.01	5 (559)	0.54 (0.47-0.62)	0.73 (0.68-0.77)	2.15 (1.52-3.03)	0.63 (0.44-0.91)
	Cirrhosis	1.00-1.10	4 (407)	0.81 (0.70-0.90)	0.77 (0.72-0.82)	4.55 (1.98-10.49)	0.28 (0.10-0.79)
	FIB-4						

	SF	1.39-3.90	3 (462)	0.85 (0.81-0.89)	0.77 (0.69-0.83)	2.89 (2.10-3.98)	0.26 (0.10-0.66)
	AF	2.05-2.63	7 (865)	0.77 (0.72-0.81)	0.57 (0.53-0.61)	1.95 (1.51-2.52)	0.31 (0.16-0.61)
		2.81-4.60	6 (431)	0.63 (0.55-0.71)	0.80 (0.75-0.85)	3.25 (1.78-5.94)	0.49 (0.30-0.81)
	Cirrhosis	2.05-4.60	6 (852)	0.87 (0.80-0.93)	0.61 (0.58-0.65)	2.79 (1.92-4.07)	0.16 (0.05-0.52)
	TE						
	SF	5.90-8.80	4 (402)	0.81 (0.76-0.85)	0.95 (0.89-0.98)	10.51 (2.03-54.36)	0.23 (0.12-0.44)
		16.00	1 (44)	0.94	0.81	4.90	0.07
	AF	6.75-7.60	4 (377)	0.80 (0.73-0.86)	0.81 (0.76-0.86)	4.19 (2.35-7.46)	0.19 (0.05-0.79)
		9.60-10.70	3 (317)	0.91 (0.84-0.95)	0.82 (0.77-0.87)	5.68 (2.55-12.69)	0.12 (0.07-0.21)
		11.90-17.90	3 (180)	0.75 (0.60-0.86)	0.94 (0.88-0.97)	11.76 (2.29-60.48)	0.22 (0.06-0.80)
	Cirrhosis	11.40-14.40	3 (256)	0.84 (0.69-0.93)	0.94 (0.90-0.97)	13.46 (7.66-23.65)	0.19 (0.10-0.38)
		15.60-25.10	3 (227)	0.90 (0.74-0.98)	0.93 (0.89-0.96)	22.8 (0.81-639.69)	0.12 (0.04-0.34)
	RPR						
	AF	0.10-0.14	4 (362)	0.49 (0.40-0.58)	0.89 (0.84-0.92)	4.27 (2.22-8.22)	0.59 (0.47-0.74)
	M2BP						
	AF	1.00-1.40	4 (370)	0.68 (0.59-0.77)	0.80 (0.75-0.85)	4.26 (1.82-9.96)	0.32 (0.14-0.75)
PSC	TE						
	SF	8.80	2 (121)	0.76 (0.62-0.87)	0.88 (0.79-0.95)	6.34 (3.25-12.37)	0.29 (0.18-0.46)
	AF	9.60	3 (177)	0.82 (0.70-0.91)	0.83 (0.75-0.89)	4.75 (2.21-10.19)	0.15 (0.02-1.04)
	Cirrhosis	13.70-14.40	4 (207)	0.82 (0.68-0.91)	0.89 (0.83-0.94)	7.46 (3.74-14.88)	0.25 (0.15-0.43)

2D-SWE: Two-dimensional shear wave elastography; AAR: Aspartate aminotransferase to alanine aminotransferase ratio; AF: Advanced fibrosis; AIH: Autoimmune hepatitis; APRI: Aspartate aminotransferase to platelet ratio index; FIB-4: Fibrosis-4 index; M2BP: Mac-2-binding protein; NLR: Negative likelihood ratio; PLR: Positive likelihood ratio; PBC: Primary biliary cholangitis; PSC: Primary sclerosing cholangitis; RPR: Red cell distribution width to platelet ratio; SF: Significant fibrosis; TE: Transient elastography.

As shown in Table 2, the APRI and FIB-4 index had relatively good summary sensitivities of 0.84 and 0.85, respectively, with mild summary specificities of 0.63 and 0.77, respectively. The corresponding values for sensitivity and specificity of the AAR were poor (0.69, 0.56). In contrast, both the summary sensitivity (0.81; 95%CI: 0.76–0.85) and specificity (0.95; 95%CI: 0.89–0.98) of TE were significantly higher than those of the other five noninvasive methods for predicting SF with cutoff values ranging from 5.9–8.8 KPa.

Furthermore, Table 3 shows that the summary DORs of APRI, FIB-4 and TE were 3.9 (95%CI: 2.1–7.3), 5.1 (95%CI: 3.1–8.5) and 16.8 (95%CI: 8.8–32.2), respectively, in patients with AIH, while the summary DORs of APRI and TE were 6.3 (95%CI: 3.5–11.2) and 74.5 (95%CI: 12.2–455.5), respectively, in patients with PBC. Additionally, the summary AUROC value of TE in patients with PBC (0.93, 95%CI: 0.91–0.95) was relatively higher than that of TE in patients with AIH (0.84, 95%CI: 0.80–0.87) but significantly higher than that of FIB-4 (0.74) and APRI (0.67) in patients with AIH and APRI (0.77) in patients with PBC (Table 3 and Figure 3).

Performance of noninvasive methods in diagnosing AF (F ≥ 3)

Diagnosis of AF for AIH: Twenty studies (n = 1435) evaluated 11 noninvasive methods for detecting AF in patients with AIH. Among them, 10 (n = 917), 7 (n = 532), 11 (n = 962), 7 (n = 460), 3 (n = 234) and 2 (n = 191) studies focused on APRI, AAR, FIB-4, TE, SWE and RPR, respectively; however, only one study each utilized the ARFI, MRS, PC/SD ratio, MRE and M2BP methods.

As shown in Table 2, with a cutoff value of 8.2–9.0 KPa, both the summary sensitivity and specificity exceeded 80% when TE was used for predicting AF, whereas with a cutoff value of 10.4–12.1 KPa, there was a better summary specificity (0.93; 95%CI: 0.86–0.97) with a mild summary sensitivity (0.73; 95%CI: 0.60–0.83). Regarding SWE, MRE and the PC/SD ratio, the summary sensitivity and specificity also exceeded 80%. The specificity of MRE was 1.00, but only one study assessed it[22]. For AAR and FIB-4 index, there was a relatively modest summary specificity (< 0.80) and poor summary sensitivity (< 0.60).

Diagnosis of AF for PBC: Twenty-eight studies (n = 2737) evaluated 11 noninvasive methods for detecting AF in patients with PBC. Of these, 15 (n = 1589), 6 (n = 559), 13 (n = 1296), 2 (n = 97), 10 (n = 874), 5 (n = 362), 4 (n = 370) and 2 (n = 210) studies were focused on APRI, AAR, FIB-4, ARFI, TE, RPR, M2BP and SWE, respectively. Only one study each utilized the methods of MRE and RLR.

Table 3 Summary area under the receiver operator curve and diagnostic odds ratio of noninvasive methods for prediction of significant fibrosis, advanced fibrosis and cirrhosis in autoimmune liver diseases patients

Disease	Diagnostic model/Stage	No. of studies (patients)	AUROC (95%CI)	DOR (95%CI)
AIH	APRI			
	SF	4 (383)	0.67 (0.63-0.71)	3.87 (2.1-7.3)
	AF	10 (917)	0.71 (0.67-0.75)	3.85 (2.8-5.3)
	Cirrhosis	6 (543)	0.71 (0.67-0.75)	3.77 (2.2-6.4)
	FIB-4			
	SF	5 (459)	0.74 (0.70-0.78)	5.11 (3.1-8.5)
	AF	11 (962)	0.73 (0.69-0.76)	4.04 (2.4-6.8)
	Cirrhosis	6 (543)	0.72 (0.68-0.76)	5.48 (2.4-12.6)
	TE			
	SF	9 (523)	0.84 (0.80-0.87)	16.83 (8.8-32.2)
	AF	7 (460)	0.88 (0.85-0.90)	25.14 (9.7-65.3)
	Cirrhosis	7 (415)	0.90 (0.87-0.92)	91.77 (40.1-201.2)
	AAR			
	AF	6 (410)	0.73 (0.69-0.77)	4.94 (3.2-7.8)
	2D-SWE			
	Cirrhosis	4 (297)	0.91 (0.89-0.94)	30.68 (15.7-59.9)
PBC	APRI			
	SF	4 (584)	0.77 (0.73-0.80)	6.27 (3.5-11.2)
	AF	15 (1589)	0.70 (0.66-0.74)	3.67 (2.3-5.9)
	Cirrhosis	6 (852)	0.83 (0.79-0.86)	14.55 (1.9-113.8)
	FIB-4			
	AF	13 (1296)	0.79 (0.75-0.82)	7.13 (4.0-12.8)
	Cirrhosis	6 (852)	0.88 (0.85-0.91)	29.79 (5.9-150.3)
	TE			
	SF	5 (446)	0.93 (0.91-0.95)	74.45 (12.2-455.5)
	AF	10 (880)	0.93 (0.90-0.95)	41.84 (19.3-91.0)
	Cirrhosis	6 (483)	0.91 (0.88-0.93)	134.83 (33.0-551.8)
	AAR			
	AF	6 (559)	0.74 (0.70-0.78)	4.13 (2.0-8.6)
	Cirrhosis	4 (407)	0.88 (0.84-0.90)	25.29 (9.0-70.9)
	RPR			
	AF	4 (362)	0.53 (0.49-0.58)	7.98 (4.0-15.8)
	M2BP			
	AF	4 (370)	0.86 (0.82-0.88)	13.17 (4.1-42.4)
PSC	TE			
	Cirrhosis	4 (207)	0.95 (0.93-0.97)	70.59 (15.4-322.7)

2D-SWE: Two-dimensional shear wave elastography; 95%CI: 95% confidence interval; AAR: Aspartate aminotransferase to alanine aminotransferase ratio; AF: Advanced fibrosis; AIH: Autoimmune hepatitis; APRI: Aspartate aminotransferase to platelet ratio index; AUROC: Area under the receiver operator curve; DOR: Diagnostic odds ratio; FIB-4: Fibrosis-4 index; PBC: Primary biliary cholangitis; PSC: Primary sclerosing cholangitis; RPR: Red cell distribution width to platelet ratio; SF: Significant fibrosis; TE: Transient elastography.

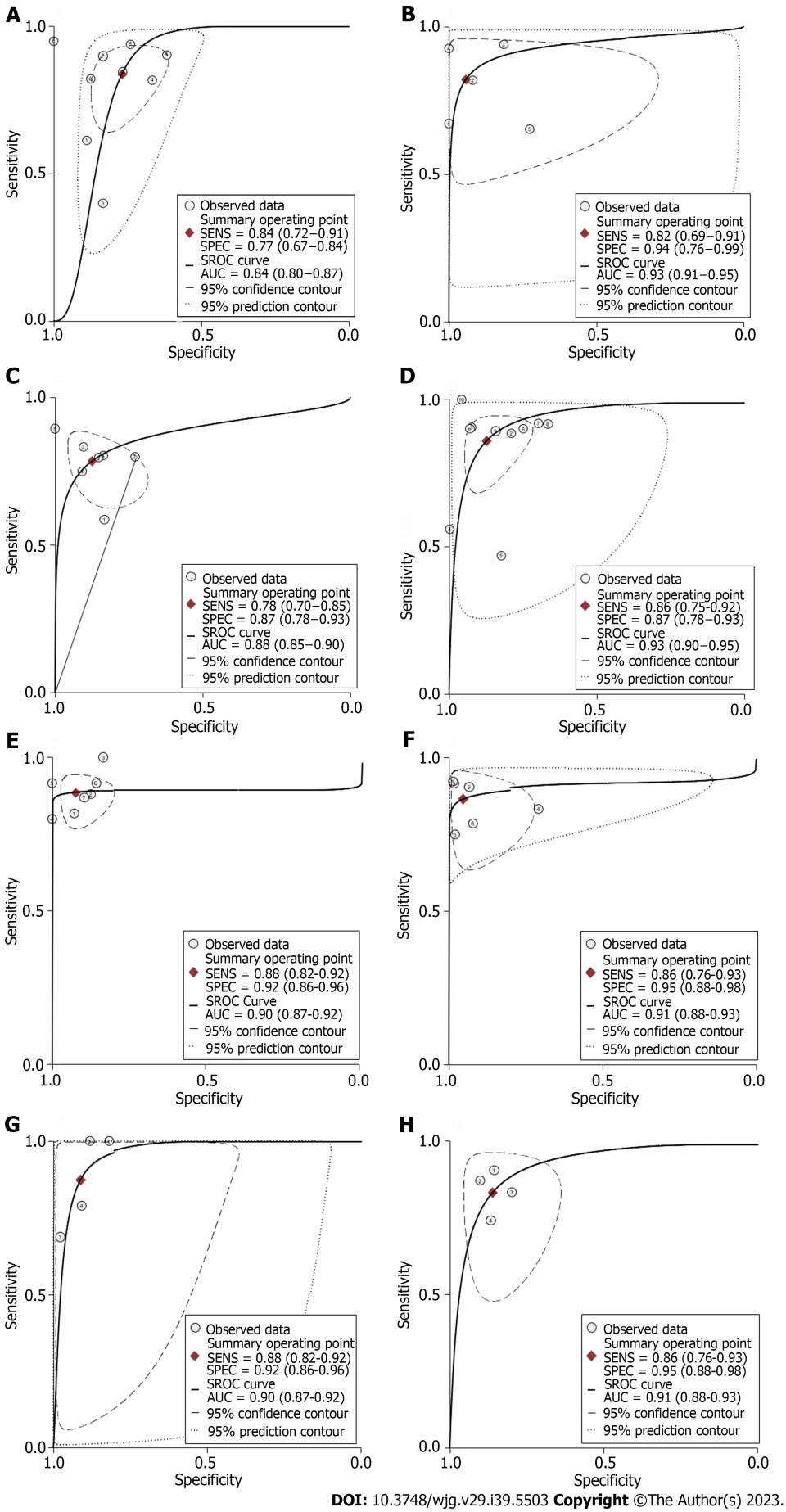

DOI: 10.3748/wjg.v29.i39.5503

Figure 3 The summary receiver operating characteristic curve plots of transient elastography in autoimmune liver disease patients. A and

B: Transient elastography (TE) for detecting significant fibrosis in autoimmune hepatitis (AIH, A) and primary biliary cholangitis (PBC, B) patients; C and D: TE for detecting advanced fibrosis in AIH (C) and PBC (D) patients; E-G: TE for detecting cirrhosis in AIH (E), PBC (F) and primary sclerosing cholangitis (G) patients; H: Shear wave elastography for detecting cirrhosis in AIH patients. AUC: Area under the curve; SENS: Sensitivity; SPEC: Specificity; SROC: Summary receiver operating characteristic.

As shown in Table 2, TE had a good summary sensitivity and specificity (0.91, 0.82) with a cutoff value of 9.6–10.7 KPa, while RPR and M2BP had good summary specificity (0.89 and 0.80, respectively) with poor summary sensitivity (0.49 and 0.68, respectively). Regardless of the cutoff values, the summary sensitivities and specificities of the AAR, APRI and FIB-4 were less than 0.80.

Furthermore, Table 3 shows that the summary DORs of AAR, APRI, FIB-4 and TE were 4.9 (95%CI: 3.2–7.8), 3.9 (95%CI: 2.8–5.3), 4.0 (95%CI: 2.4–6.8) and 25.1 (95%CI: 9.7–65.3), respectively, in patients with AIH and 4.1 (95%CI: 2.0–8.6), 3.7 (95%CI: 2.3–6.0), 7.1 (95%CI: 4.0–12.8) and 41.8 (95%CI: 19.3–91.0), respectively, in patients with PBC. Moreover, the summary DORs of RPR and M2BP in patients with PBC were 8.0 (95%CI: 4.0–15.8) and 13.2 (95%CI: 4.1–42.4), respectively. As shown in Table 3 and Figure 3, the summary AUROC value of TE for detecting AF was 0.88 (95%CI: 0.85–0.90) and 0.93 (95%CI: 0.90–0.95) in patients with AIH and PBC, respectively. The value of M2BP was 0.86 (95%CI: 0.82–0.88) in patients with PBC, whereas the summary AUROC values for AAR, APRI and FIB-4 were less than 0.80 in both patients with AIH and PBC, and the value for RPR in patients with PBC was less than 0.60.

Performance of noninvasive methods in diagnosing cirrhosis (F = 4)

Diagnosis of cirrhosis for AIH: Sixteen studies (n = 1076) evaluated ten noninvasive methods for detecting cirrhosis in patients with AIH. Of these, six (n = 543), three (n = 213), six (n = 543), two (n = 82), seven (n = 415) and four (n = 297) studies focused on APRI, AAR, FIB-4, ARFI, TE and SWE, respectively. Only one study each utilized the PC/SD ratio, MRE, RPR and M2BP.

As shown in Table 2, the summary sensitivities and specificities of APRI and FIB-4 were less than 75%, and those of AAR were 0.61 and 0.83, respectively. Moreover, the summary sensitivity and specificity of TE (cutoff value ranging from 11.0–12.7 KPa) were significantly higher for predicting cirrhosis, with 0.89 (95%CI: 0.82–0.94) and 0.88 (95%CI: 0.81–0.93), respectively, while the summary sensitivity and specificity of SWE (0.83, 0.86) were close to those of TE. Surprisingly, the summary specificity dramatically rose to 0.97 (95%CI 0.92–0.99) with a cutoff value ranging from 16.0–19.0 KPa.

Diagnosis of cirrhosis for PBC: Sixteen studies (n = 1568) evaluated nine noninvasive methods for detecting cirrhosis in patients with PBC. Among them, six (n = 852), four (n = 407), six (n = 852), six (n = 483), two (n = 210) and two (n = 194) studies focused on APRI, AAR, FIB-4, TE, SWE and M2BP, respectively. However, only one study utilized the ARFI and MRE methods.

As listed in Table 2, the summary sensitivities of APRI, AAR and FIB-4 for predicting cirrhosis were 0.75, 0.81 and 0.87, respectively, and their corresponding summary specificities were 0.51, 0.77 and 0.61, respectively. In contrast, TE had higher summary sensitivity (0.90; 95%CI: 0.74–0.98) and specificity (0.93; 95%CI: 0.89–0.96) with a cutoff value ranging from 15.6–25.1 KPa.

Diagnosis of cirrhosis for PSC: Four studies (n = 207) evaluated TE as a predictor of cirrhosis in patients with PSC. Because the diagnosis of PSC does not rely on liver biopsy, few related studies have been conducted. As listed in Table 2, the summary sensitivity and specificity of TE were 0.82 (95%CI: 0.68–0.91) and 0.89 (95%CI: 0.83–0.94), respectively.

Furthermore, Table 3 shows that the summary DORs of APRI and FIB-4 were 3.8 (95%CI: 2.2–6.4) and 5.5 (95%CI: 2.4–12.6) in patients with AIH and 14.6 (95%CI: 1.9–113.8) and 29.8 (95%CI: 5.9–150.3) in patients with PBC. In addition, the summary DOR of TE was highest in patients with PBC, with values of 91.8 (95%CI: 40.1–201.2), 134.8 (95%CI: 33.0–551.8) and 70.6 (95%CI: 15.4–322.7) in patients with AIH, PBC and PSC, respectively. The summary AUROC values of TE for detecting cirrhosis in patients with AIH, PBC and PSC were 0.90 (95%CI: 0.87–0.92), 0.91 (95%CI: 0.88–0.93) and 0.95 (95%CI: 0.93–0.97), respectively, while the summary AUROC values for APRI and FIB-4 were less than 0.80 in patients with AIH and 0.90 in patients with PBC (Table 3 and Figure 3).

Methodological heterogeneity, subgroup analysis and publication bias

As shown in Table 4, threshold heterogeneity was observed only in APRI F2 in both patients with AIH and PBC, whereas nonthreshold heterogeneity was observed in most groups (Figure 4, Supplementary Figures 2 and 3). Because meta-regression to explore the source of heterogeneity requires the number of original studies to exceed 10, we only conducted a meta-regression for AF in patients with AIH and PBC. The heterogeneity of APRI, FIB-4 and TE accuracy was mainly affected by the cutoff value with regard to specificity, whereas FIB-4 and TE were affected by sample size with regard to sensitivity, according to the meta-regression analysis (Supplementary Figure 4).

Subgroup analyses of TE according to sample size, cutoff value and treatment status are shown in Table 5. Because of the limited data, we only conducted an analysis for posttreatment combined with original data for pretreatment (Supplementary Table 2).

Deeks' funnel plot of these noninvasive methods was generated to assess publication bias. There was a publication bias for APRI in detecting SF (P = 0.06) and cirrhosis (P = 0.08) in patients with PBC but not in other methods for detecting SF, AF and cirrhosis (Figure 5, Supplementary Figure 5). Moreover, no publication bias was observed for any noninvasive method in patients with AIH (Figure 5, Supplementary Figure 6).

Table 4 Heterogeneity of all the included studies

		Fibrosis stage	Threshold heterogeneity		Non-threshold heterogeneity	
			r	*P* value	I^2 (%)	*P* value
AIH	TE	SF	0.176	0.651	82.9	0
		AF	-0.429	0.337	93.8	0
		Cirrhosis	0.321	0.482	56.59	0.03
	APRI	SF	1.0	0	62.34	0.05
		AF	0.717	0.02	71.94	0
		Cirrhosis	0.714	0.111	90.93	0
	FIB-4	SF	0.70	0.188	46.81	0.11
		AF	0.627	0.039	98.29	0
		Cirrhosis	-0.029	0.957	88.98	0
	AAR	AF	0.857	0.014	36.46	0.16
	SWE	Cirrhosis	0	1.0	61.97	0.05
PBC	TE	SF	-0.10	0.873	99.99	0
		AF	0.195	0.590	100	0
		Cirrhosis	-0.726	0.027	93.77	0
	APRI	SF	1.0	0	99.9	0
		AF	0.209	0.454	100	0
		Cirrhosis	-0.657	0.156	100	0
	FIB-4	AF	0.418	0.156	100	0
		Cirrhosis	0.029	0.957	100	0
	AAR	AF	0.60	0.208	96.05	0
		Cirrhosis	0.40	0.60	95.37	0
	M2BP	AF	0	1.0	99.24	0
	RPR	AF	0	1.0	94.49	0
PSC	TE	Cirrhosis	0.80	0.20	50.07	0.11

AAR: Aspartate aminotransferase to alanine aminotransferase ratio; AF: Advanced fibrosis; AIH: Autoimmune hepatitis; APRI: Aspartate aminotransferase to platelet ratio index; FIB-4: Fibrosis-4 index; M2BP: Mac-2-binding protein; PBC: Primary biliary cholangitis; PSC: Primary sclerosing cholangitis; RPR: Red cell distribution width to platelet ratio; SF: Significant fibrosis; SWE: Shear wave elastography; TE: Transient elastography.

DISCUSSION

In our review, a total of 60 studies (including 1594, 3126 and 501 patients with AIH, PBC and PSC, respectively) were included to evaluate the diagnostic accuracy of noninvasive methods for predicting SF, AF and cirrhosis in patients with AILDs. TE had excellent accuracy with summary AUROC values of 0.93, 0.93 and 0.91 for SF, AF and cirrhosis, respectively, in patients with PBC, while TE had a moderate to excellent accuracy of 0.84, 0.88 and 0.90, respectively, in patients with AIH. Moreover, the summary AUROC was 0.95 for cirrhosis in patients with PSC. In contrast, other noninvasive methods, such as AAR, APRI, FIB-4 and RPR, had poor accuracy, with summary AUROC values of < 0.80. In addition, the pooled sensitivity and specificity of TE were higher than those of the other noninvasive methods. Our results indicated that LSM using TE had a better diagnostic performance for staging hepatic fibrosis in AILDs, especially in patients with PBC. Moreover, our results showed that TE had mostly higher specificity and relatively low sensitivity for the diagnosis of AILDs. Koizumi *et al*[23] found that TE had high sensitivity and relatively low specificity for the diagnosis of PBC. However, the optimal cutoff values were higher and the range was wider than those in other studies, indicating that different optimal cutoff values may have an effect on diagnostic accuracy.

Meta-regression analysis is a reliable method for screening heterogeneity. In our study, the sample size, cutoff values, prevalence of SF and scoring system provided heterogeneity in summarizing the test results, consistent with previous studies[24,25]. We conducted subgroup analyses based on the sample size and cutoff values. Our results revealed that TE had a better predictive effect in a larger sample of patients with PBC. LSM by TE is the best surrogate marker for staging in SF and AF with a cutoff ranging from 6.4–9.1 KPa and 9.0–11.0 KPa, respectively, in patients with AIH and staging in

Table 5 Subgroup analysis of sample size and treatment status in prediction of significant fibrosis, advanced fibrosis and cirrhosis in autoimmune hepatitis and primary biliary cholangitis patients

Disease	Parameter	Stage	Subgroup	Sensitivity (95%CI)	Specificity (95%CI)	AUROC (95%CI)
AIH	Sample size	SF	$n < 50$	0.83 (0.55-0.95)	0.82 (0.65-0.92)	0.85 (0.82-0.88)
			$n > 50$	0.84 (0.73-0.91)	0.77 (0.63-0.87)	0.87 (0.84-0.90)
		AF	$n < 50$	0.78 (0.54-0.91)	0.91 (0.78-0.96)	0.92 (0.89-0.94)
			$n > 50$	0.78 (0.68-0.86)	0.87 (0.73-0.94)	0.88 (0.84-0.90)
		Cirrhosis	$n < 50$	0.90 (0.65-0.98)	0.92 (0.74-0.98)	0.96 (0.94-0.97)
			$n > 50$	0.88 (0.82-0.93)	0.93 (0.86-0.96)	0.92 (0.89-0.94)
	Treatment status	SF	Post	0.78 (0.44-0.94)	0.76 (0.60-0.86)	0.79 (0.75-0.82)
		AF	Post	0.83 (0.66-0.93)	0.96 (0.84-0.99)	0.93 (0.91-0.95)
		Cirrhosis	Post	0.91(0.77-0.97)	0.97 (0.73-1.00)	0.94 (0.91-0.95)
	Cutoff value	SF	5.80-6.27	0.87 (0.81-0.92)	0.69 (0.60-0.77)	0.86 (0.83-0.89)
			6.40-9.10	0.82 (0.75-0.88)	0.89 (0.74-0.96)	0.92 (0.89-0.94)
		AF	9.00-11.00	0.83 (0.69-0.91)	0.92 (0.73-0.98)	0.88 (0.85-0.91)
			8.18-12.10	0.77 (0.71-0.83)	0.85 (0.80-0.89)	0.88 (0.85-0.90)
		Cirrhosis	11.00-12.67	0.89 (0.82-0.94)	0.88 (0.81-0.93)	0.92 (0.94-0.96)
			11.00-19.00	0.88 (0.82-0.93)	0.92 (0.88-0.95)	0.90 (0.87-0.92)
PBC	Sample size	SF	$n < 100$	0.81 (0.48-0.95)	0.78 (0.60-0.89)	0.82 (0.79-0.86)
			$n > 100$	0.83 (0.68-0.92)	0.98 (0.74-1.00)	0.97 (0.95-0.98)
		AF	$n < 100$	0.90 (0.85-0.94)	0.88 (0.78-0.94)	0.91 (0.88-0.93)
			$n > 100$	0.81 (0.64-0.91)	0.88 (0.75-0.94)	0.91 (0.88-0.93)
		Cirrhosis	$n < 100$	0.82 (0.67-0.91)	0.94 (0.80-0.99)	0.86 (0.82-0.89)
			$n > 100$	0.91 (0.76-0.97)	0.97 (0.90-0.99)	0.94 (0.92-0.96)
	Treatment status	SF	Post	0.89 (0.70-0.97)	0.98 (0.41-1.00)	0.97 (0.95-0.98)
		AF	Post	0.85 (0.68-0.94)	0.92 (0.63-0.99)	0.93 (0.91-0.95)
		Cirrhosis	Post	0.90 (0.71-0.97)	0.96 (0.74-1.00)	0.94 (0.92-0.96)
	Cutoff value	AF	6.75-7.60	0.80 (0.73-0.86)	0.81 (0.76-0.86)	0.88 (0.85-0.91)
			9.60-10.70	0.91 (0.84-0.95)	0.82 (0.77-0.87)	0.92 (0.89-0.94)
			11.90-17.90	0.75 (0.60-0.86)	0.94 (0.88-0.97)	0.93 (0.91-0.95)
		Cirrhosis	11.40-14.40	0.84 (0.69-0.93)	0.94 (0.90-0.97)	0.96 (0.94-0.97)
			14.40-16.90	0.88 (0.72-0.97)	0.99 (0.96-1.00)	0.99 (0.98-1.00)

95%CI: 95% confidence interval; AF: Advanced fibrosis; AIH: Autoimmune hepatitis; AUROC: Area under the receiver operator curve; PBC: Primary biliary cholangitis; SF: Significant fibrosis.

AF and cirrhosis with a cutoff ranging from 9.6–10.7 KPa and 14.4–16.9 KPa, respectively, in patients with PBC.

Several previous studies have demonstrated that inflammation in the liver (reflected by elevated ALT levels)[26] and extrahepatic cholestasis (reflected by total bilirubin)[27] may increase the stiffness value, causing a decrease in the diagnostic accuracy of TE, whereas ALT and bilirubin levels decline after treatment. Because a limited number of studies have reported results for the ALT subgroup, we only conducted a subgroup analysis of treatment conditions, which showed that the diagnostic accuracy for staging liver fibrosis was comparable between pretreatment and posttreatment in patients with both PBC and AIH. In other words, this may indicate that ALT levels have no significant effect on diagnostic accuracy. Meanwhile, two scoring systems [International Autoimmune Hepatitis Group (IAIHG) 1999 and IAIHG 2008] proposed by Granito *et al*[28] for the diagnosis of AIH are not interchangeable. According to our subgroup analysis regarding diagnostic criteria, the IAIHG 2008 showed diagnostic accuracy comparable to that of the IAIHG 1999 in distinguishing patients with AIH (Supplementary Tables 3 and 4). However, due to the limited number of studies, further investigation is required to confirm these results.

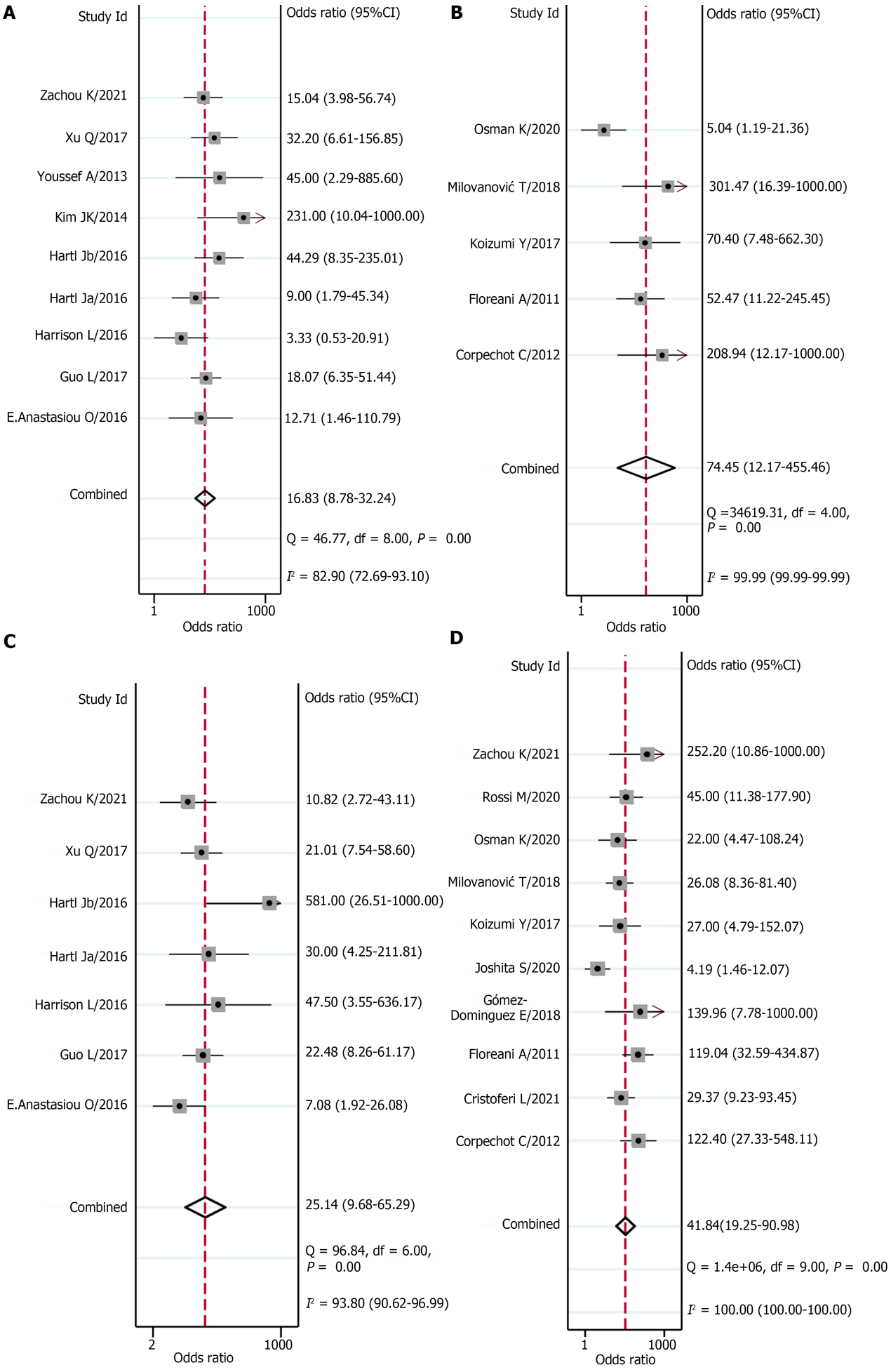
A
Study Id
Odds ratio (95%CI)
Zachou K/2021
15.04 (3.98-56.74)
Xu Q/2017
32.20 (6.61-156.85)
Youssef A/2013
45.00 (2.29-885.60)
Kim JK/2014
231.00 (10.04-1000.00)
Hartl Jb/2016
44.29 (8.35-235.01)
Hartl Ja/2016
9.00 (1.79-45.34)
Harrison L/2016
3.33 (0.53-20.91)
Guo L/2017
18.07 (6.35-51.44)
E.Anastasiou O/2016
12.71 (1.46-110.79)
Combined
16.83 (8.78-32.24)
Q = 46.77, df = 8.00, P = 0.00
I² = 82.90 (72.69-93.10)
1
1000
Odds ratio
B
Study Id
Odds ratio (95%CI)
Osman K/2020
5.04 (1.19-21.36)
Milovanović T/2018
301.47 (16.39-1000.00)
Koizumi Y/2017
70.40 (7.48-662.30)
Floreani A/2011
52.47 (11.22-245.45)
Corpechot C/2012
208.94 (12.17-1000.00)
Combined
74.45 (12.17-455.46)
Q =34619.31, df = 4.00, P = 0.00
I² = 99.99 (99.99-99.99)
1
1000
Odds ratio
C
Study Id
Odds ratio (95%CI)
Zachou K/2021
10.82 (2.72-43.11)
Xu Q/2017
21.01 (7.54-58.60)
Hartl Jb/2016
581.00 (26.51-1000.00)
Hartl Ja/2016
30.00 (4.25-211.81)
Harrison L/2016
47.50 (3.55-636.17)
Guo L/2017
22.48 (8.26-61.17)
E.Anastasiou O/2016
7.08 (1.92-26.08)
Combined
25.14 (9.68-65.29)
Q = 96.84, df = 6.00, P = 0.00
I² = 93.80 (90.62-96.99)
2
1000
Odds ratio
D
Study Id
Odds ratio (95%CI)
Zachou K/2021
252.20 (10.86-1000.00)
Rossi M/2020
45.00 (11.38-177.90)
Osman K/2020
22.00 (4.47-108.24)
Milovanović T/2018
26.08 (8.36-81.40)
Koizumi Y/2017
27.00 (4.79-152.07)
Joshita S/2020
4.19 (1.46-12.07)
Gómez-Dominguez E/2018
139.96 (7.78-1000.00)
Floreani A/2011
119.04 (32.59-434.87)
Cristoferi L/2021
29.37 (9.23-93.45)
Corpechot C/2012
122.40 (27.33-548.11)
Combined
41.84(19.25-90.98)
Q = 1.4e+06, df = 9.00, P = 0.00
I² = 100.00 (100.00-100.00)
1
1000
Odds ratio

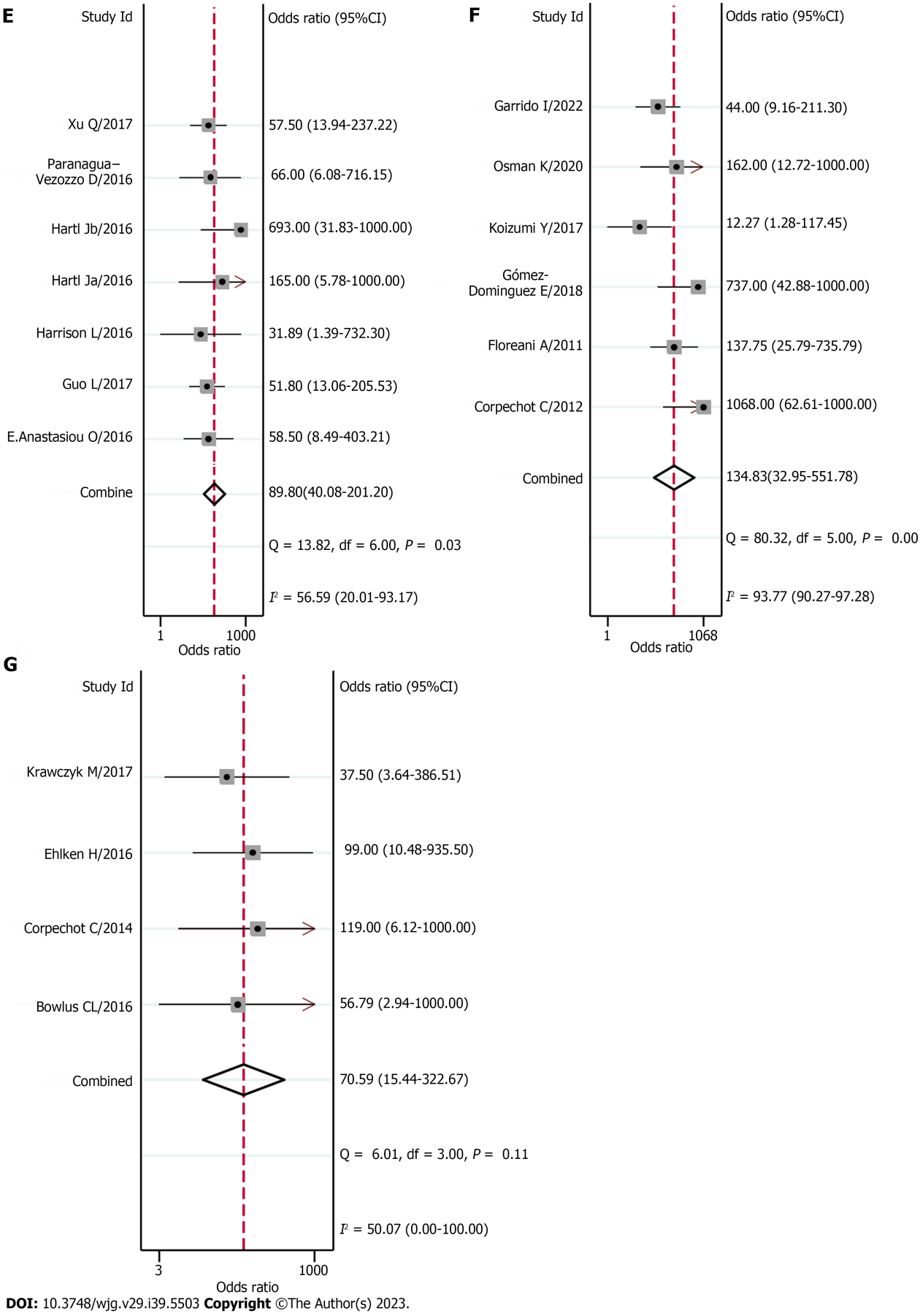

DOI: 10.3748/wjg.v29.i39.5503

Figure 4 Forest plots of diagnostic odds ratio of transient elastography in autoimmune liver disease patients. A and B: Transient elastography (TE) for detecting significant fibrosis in autoimmune hepatitis (AIH, A) and primary biliary cholangitis (PBC, B) patients, respectively; C and D: TE for detecting

advanced fibrosis in AIH (C) and PBC (D) patients; E-G: TE for detecting cirrhosis in AIH (E), PBC (F) and primary sclerosing cholangitis (G) patients. 95%CI: 95% confidence interval.

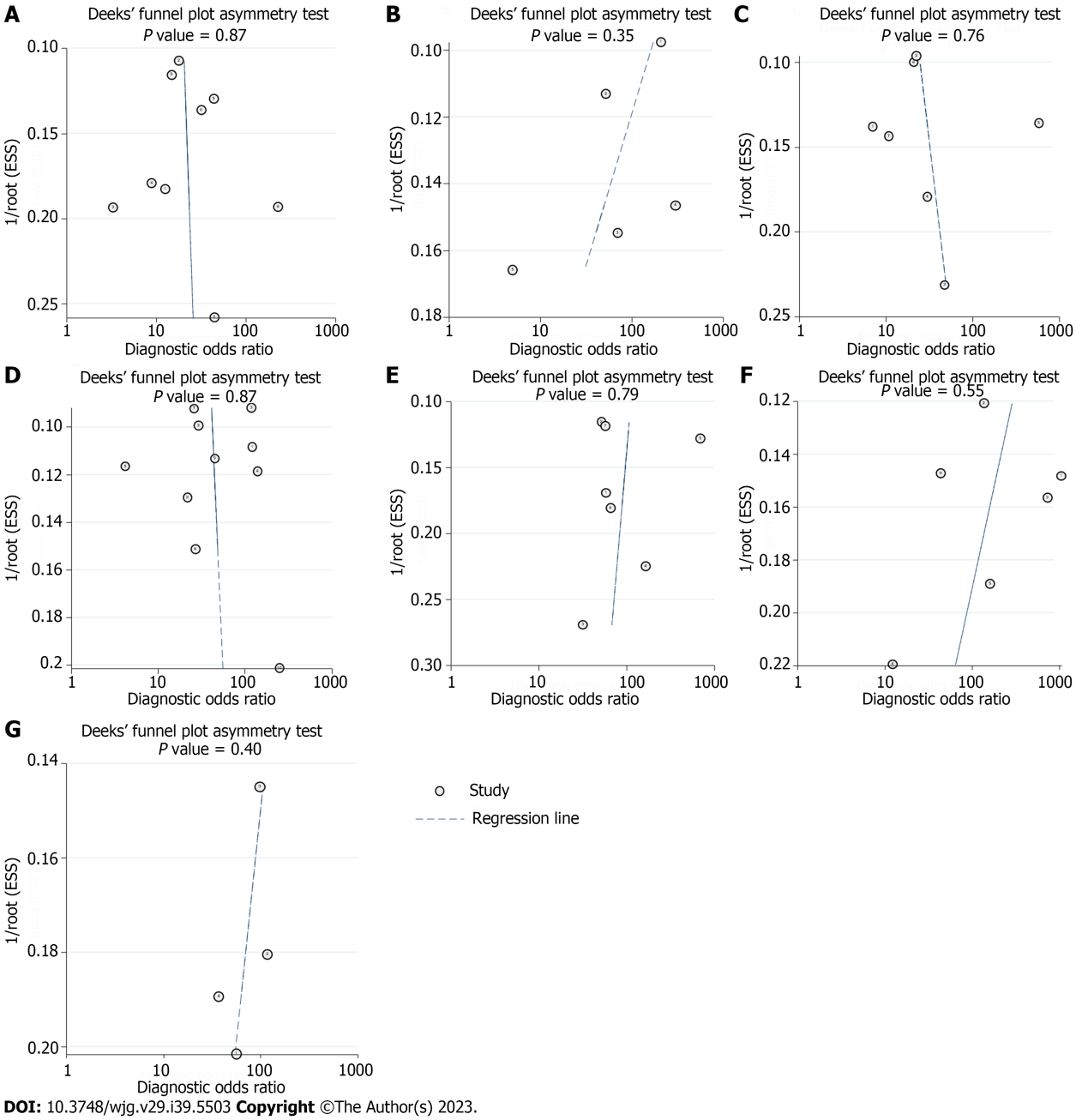

DOI: 10.3748/wjg.v29.i39.5503

Figure 5 Deeks' funnel plot asymmetry test for publication bias of transient elastography in autoimmune liver disease patients. A and B: Transient elastography (TE) for detecting significant fibrosis in autoimmune hepatitis (AIH, A) and primary biliary cholangitis (PBC, B) patients; C and D: TE for detecting advanced fibrosis in AIH (C) and PBC (D) patients; E-G: TE for detecting cirrhosis in AIH (E), PBC (F) and primary sclerosing cholangitis (G) patients.

In addition, some studies have shown that other imaging technologies, including two-dimensional-SWE (2D-SWE)[29-32], MRE[22,33] and ARFI[19,34], also perform well in staging liver fibrosis (Supplementary Table 5). Further, 2D-SWE had excellent accuracy, with a summary AUROC of 0.91 for cirrhosis in patients with AIH (Table 3). In comparison, our findings indicated that 2D-SWE and ARFI had good accuracy with higher sensitivity, specificity and AUROC for AF and cirrhosis in patients with PBC, while the AUROC of MRE was higher in patients with AIH. Interestingly, compared with TE, 2D-SWE produces a two-dimensional grayscale image so that interference from the gallbladder, ascites and large tubular structures in the liver can be effectively avoided. However, the number of studies on 2D-SWE, MRE and ARFI included in our analysis was small. Indeed, the diagnostic accuracies of 2D-SWE and MRE require further studies with larger sample sizes to determine the best method for staging fibrosis in patients with AILDs.

However, the overlap syndrome, one of the AILDs, also deserves attention because it exhibits significantly higher rates of various complications, progresses to cirrhosis more rapidly and has a poor treatment response to ursodeoxycholic acid [35,36]. Hence, the development of noninvasive methods is beneficial for this disease. Wu *et al*[37] reported that the AUROCs of TE for SF, AF and cirrhosis were 0.837, 0.910 and 0.996, respectively. Yan *et al*[38] reported that the AUROCs of SWE were 0.91, 0.97 and 0.96, respectively. These results show that noninvasive imaging techniques have excellent accuracy for overlap syndrome, although more studies are required for further validation.

Our study had some limitations. First, we only included studies published in the English language; therefore, a language bias may have influenced the results. Second, we did not consider the confounding factors such as obesity, whereas a previous study proposed that a high BMI may reduce the efficiency of ultrasound-based elastography techniques in detecting fibrosis[39]. However, only a limited number of studies have provided sufficient data to conduct subgroup analyses to explore the potential impact of BMI on the diagnostic effects. Third, it is unknown whether ALT level is responsible for the difference in the diagnosis of TE between patients with AIH and PBC due to a lack of sufficient data. Moreover, the treatment conditions before inclusion in the study were unknown, and the lack of pretreatment studies made it impossible to compare the effects of treatment on outcomes. Finally, the number of studies on SWE, MRE and ARFI was inadequate to compare the effects of these imaging technologies and TE.

CONCLUSION

In conclusion, LSM using TE had better diagnostic performance for staging hepatic fibrosis in patients with AILDs compared to other serum biomarkers, especially in patients with PBC. The appropriate cutoff value for staging in AF and cirrhosis ranged from 9.6 to 10.7 KPa and 14.4 to 16.9 KPa, respectively, for patients with PBC. Additional recommended optimal cutoff values warrant further investigation to provide a better reference for clinical applications.

ARTICLE HIGHLIGHTS

Research background

Noninvasive criteria are needed for autoimmune liver diseases (AILDs) to assess liver fibrosis stage for prognosis and treatment decisions.

Research motivation

Results of individual diagnostic test accuracy studies assessing the diagnostic accuracy of transient elastography (TE) for the diagnosis of AILD appear promising. However, previous systematic review and meta-analyses have focused primarily on other liver diseases, which is still lacking in AILD.

Research objectives

To compare the diagnostic accuracy of imaging techniques with serum biomarkers of fibrosis in AILD.

Research methods

The PubMed, Cochrane and EMBASE databases were searched for literature. The Quality Assessment of Diagnostic Accuracy Studies-2 tool was used to evaluate the quality. Meta-Disc 1.4 and STATA 12.0 software were used to analyze the combined statistics: sensitivity; specificity; positive likelihood ratio; negative likelihood ratio; diagnostic odds ratio; and area under the curve fitted to the total receiver operating characteristic curve (AUROC).

Research results

A total of 60 studies were included in the meta-analysis. The AUROC curve values were 0.93, 0.93 and 0.91 for significant fibrosis, advanced fibrosis and cirrhosis, respectively, in primary biliary cholangitis patients, while the AUROC curve values were 0.84, 0.88 and 0.90, respectively, in autoimmune hepatitis patients.

Research conclusions

TE is a reliable method for diagnosis in AILD patients, especially in primary biliary cholangitis patients. The appropriate cutoff value for staging advanced fibrosis and cirrhosis ranged from 9.6 to 10.7 KPa and 14.4 to 16.9 KPa, respectively.

Research perspectives

We propose a suitable diagnostic threshold for TE in PBC patients. However, future prospective multicenter studies with TE and histopathology protocol are required to validate our results.

FOOTNOTES

Author contributions: Jiang W conceived and designed the study; Chen H and Shen Y contributed to acquiring the data; Wang MX and

Weng CZ contributed statistical analysis support; Chen H, Shen Y, Wu SD and Zhu Q contributed to analysis and interpretation of the data; Chen H wrote the manuscript; Wu SD and Zhang J contributed to manuscript revision; All authors read and approved the submitted version and are accountable for all aspects of the work.

Supported by Natural Science and Technology Major Project of Fujian Province, No. 2021D033; Natural Science Foundation of Shanghai, No. 20ZR1410900; Medical Innovation Project of Fujian Province, No. 2022CXB020; National Science and Technology Major Project, No. 2017ZX 10203202-003-002.

Conflict-of-interest statement: The authors declare that the research was conducted in the absence of any commercial or financial relationships that could be construed as a potential conflict of interest.

PRISMA 2009 Checklist statement: The authors have read the PRISMA 2009 Checklist, and the manuscript was prepared and revised according to the PRISMA 2009 Checklist.

Country/Territory of origin: China

ORCID number: Hong Chen 0000-0002-3966-5355; Yue Shen 0000-0002-4771-9114; Sheng-Di Wu 0000-0002-3829-2999; Qin Zhu 0000-0002-6661-8343; Cheng-Zhao Weng 0009-0005-5168-8751; Jun Zhang 0009-0008-9410-2011; Mei-Xia Wang 0000-0002-3139-1847; Wei Jiang 0000-0002-9354-6699.

S-Editor: Lin C
L-Editor: Filipodia
P-Editor: Cai YX

REFERENCES

1 **Boonstra K**, Beuers U, Ponsioen CY. Epidemiology of primary sclerosing cholangitis and primary biliary cirrhosis: a systematic review. *J Hepatol* 2012; **56**: 1181-1188 [PMID: 22245904 DOI: 10.1016/j.jhep.2011.10.025]
2 **Tanaka A**, Ma X, Yokosuka O, Weltman M, You H, Amarapurkar DN, Kim YJ, Abbas Z, Payawal DA, Chang ML, Efe C, Ozaslan E, Abe M, Mitchell-Thain R, Zeniya M, Han KH, Vierling JM, Takikawa H. Autoimmune liver diseases in the Asia-Pacific region: Proceedings of APASL symposium on AIH and PBC 2016. *Hepatol Int* 2016; **10**: 909-915 [PMID: 27649967 DOI: 10.1007/s12072-016-9767-9]
3 **Manns MP**, Czaja AJ, Gorham JD, Krawitt EL, Mieli-Vergani G, Vergani D, Vierling JM; American Association for the Study of Liver Diseases. Diagnosis and management of autoimmune hepatitis. *Hepatology* 2010; **51**: 2193-2213 [PMID: 20513004 DOI: 10.1002/hep.23584]
4 **Beringer A**, Miossec P. IL-17 and IL-17-producing cells and liver diseases, with focus on autoimmune liver diseases. *Autoimmun Rev* 2018; **17**: 1176-1185 [PMID: 30321671 DOI: 10.1016/j.autrev.2018.06.008]
5 **Carbone M**, Neuberger JM. Autoimmune liver disease, autoimmunity and liver transplantation. *J Hepatol* 2014; **60**: 210-223 [PMID: 24084655 DOI: 10.1016/j.jhep.2013.09.020]
6 **Poynard T**, Halfon P, Castera L, Charlotte F, Le Bail B, Munteanu M, Messous D, Ratziu V, Benhamou Y, Bourlière M, De Ledinghen V; FibroPaca Group. Variability of the area under the receiver operating characteristic curves in the diagnostic evaluation of liver fibrosis markers: impact of biopsy length and fragmentation. *Aliment Pharmacol Ther* 2007; **25**: 733-739 [PMID: 17311607 DOI: 10.1111/j.1365-2036.2007.03252.x]
7 **Castera L**, Forns X, Alberti A. Non-invasive evaluation of liver fibrosis using transient elastography. *J Hepatol* 2008; **48**: 835-847 [PMID: 18334275 DOI: 10.1016/j.jhep.2008.02.008]
8 **Piccinino F**, Sagnelli E, Pasquale G, Giusti G. Complications following percutaneous liver biopsy. A multicentre retrospective study on 68,276 biopsies. *J Hepatol* 1986; **2**: 165-173 [PMID: 3958472 DOI: 10.1016/s0168-8278(86)80075-7]
9 **Zein CO**, Angulo P, Lindor KD. When is liver biopsy needed in the diagnosis of primary biliary cirrhosis? *Clin Gastroenterol Hepatol* 2003; **1**: 89-95 [PMID: 15017500 DOI: 10.1053/cgh.2003.50014]
10 **Czaja AJ**. Review article: The prevention and reversal of hepatic fibrosis in autoimmune hepatitis. *Aliment Pharmacol Ther* 2014; **39**: 385-406 [PMID: 24387318 DOI: 10.1111/apt.12592]
11 **Friedrich-Rust M**, Ong MF, Herrmann E, Dries V, Samaras P, Zeuzem S, Sarrazin C. Real-time elastography for noninvasive assessment of liver fibrosis in chronic viral hepatitis. *AJR Am J Roentgenol* 2007; **188**: 758-764 [PMID: 17312065 DOI: 10.2214/AJR.06.0322]
12 **Li Y**, Huang YS, Wang ZZ, Yang ZR, Sun F, Zhan SY, Liu XE, Zhuang H. Systematic review with meta-analysis: the diagnostic accuracy of transient elastography for the staging of liver fibrosis in patients with chronic hepatitis B. *Aliment Pharmacol Ther* 2016; **43**: 458-469 [PMID: 26669632 DOI: 10.1111/apt.13488]
13 **Johannessen A**, Stockdale AJ, Henrion MYR, Okeke E, Seydi M, Wandeler G, Sonderup M, Spearman CW, Vinikoor M, Sinkala E, Desalegn H, Fall F, Riches N, Davwar P, Duguru M, Maponga T, Taljaard J, Matthews PC, Andersson M, Mboup S, Sombie R, Shimakawa Y, Lemoine M. Systematic review and individual-patient-data meta-analysis of non-invasive fibrosis markers for chronic hepatitis B in Africa. *Nat Commun* 2023; **14**: 45 [PMID: 36596805 DOI: 10.1038/s41467-022-35729-w]
14 **Xiao G**, Zhu S, Xiao X, Yan L, Yang J, Wu G. Comparison of laboratory tests, ultrasound, or magnetic resonance elastography to detect fibrosis in patients with nonalcoholic fatty liver disease: A meta-analysis. *Hepatology* 2017; **66**: 1486-1501 [PMID: 28586172 DOI: 10.1002/hep.29302]

15 **Wu S**, Yang Z, Zhou J, Zeng N, He Z, Zhan S, Jia J, You H. Systematic review: diagnostic accuracy of non-invasive tests for staging liver fibrosis in autoimmune hepatitis. *Hepatol Int* 2019; **13**: 91-101 [PMID: 30443702 DOI: 10.1007/s12072-018-9907-5]

16 **Whiting PF**, Rutjes AW, Westwood ME, Mallett S, Deeks JJ, Reitsma JB, Leeflang MM, Sterne JA, Bossuyt PM; QUADAS-2 Group. QUADAS-2: a revised tool for the quality assessment of diagnostic accuracy studies. *Ann Intern Med* 2011; **155**: 529-536 [PMID: 22007046 DOI: 10.7326/0003-4819-155-8-201110180-00009]

17 **Shiha G**, Zalata K. Ishak versus METAVIR: Terminology, Convertibility and Correlation with Laboratory Changes in Chronic Hepatitis C. *Liver Biopsy* 2011; **10**: 155-170 [DOI: 10.5772/20110]

18 **Swets JA**. Measuring the accuracy of diagnostic systems. *Science* 1988; **240**: 1285-1293 [PMID: 3287615 DOI: 10.1126/science.3287615]

19 **Park DW**, Lee YJ, Chang W, Park JH, Lee KH, Kim YH, Kang NK, Chung JW, Jang HY, Ahn S, Kim H, Jeong SH, Kim JW, Jang ES. Diagnostic performance of a point shear wave elastography (pSWE) for hepatic fibrosis in patients with autoimmune liver disease. *PLoS One* 2019; **14**: e0212771 [PMID: 30856201 DOI: 10.1371/journal.pone.0212771]

20 **Zachou K**, Lygoura V, Arvaniti P, Giannoulis G, Gatselis NK, Koukoulis GK, Dalekos GN. FibroMeter scores for the assessment of liver fibrosis in patients with autoimmune liver diseases. *Ann Hepatol* 2021; **22**: 100285 [PMID: 33157268 DOI: 10.1016/j.aohep.2020.10.013]

21 **Sheptulina A**, Shirokova E, Ivashkin V. The diagnostic performance of non-invasive serum markers to identify significant liver fibrosis in patients with primary biliary cirrhosis and primary sclerosing cholangitis. In: UEG Week 2015 Poster Presentations. *United European Gastroenterol J* 2015; **3**: 146-687 [DOI: 10.1177/2050640615601623]

22 **Wang J**, Malik N, Yin M, Smyrk TC, Czaja AJ, Ehman RL, Venkatesh SK. Magnetic resonance elastography is accurate in detecting advanced fibrosis in autoimmune hepatitis. *World J Gastroenterol* 2017; **23**: 859-868 [PMID: 28223730 DOI: 10.3748/wjg.v23.i5.859]

23 **Koizumi Y**, Hirooka M, Abe M, Tokumoto Y, Yoshida O, Watanabe T, Nakamura Y, Imai Y, Yukimoto A, Kumagi T, Takeshita E, Ikeda Y, Hiasa Y. Comparison between real-time tissue elastography and vibration-controlled transient elastography for the assessment of liver fibrosis and disease progression in patients with primary biliary cholangitis. *Hepatol Res* 2017; **47**: 1252-1259 [PMID: 28044427 DOI: 10.1111/hepr.12861]

24 **Coco B**, Oliveri F, Maina AM, Ciccorossi P, Sacco R, Colombatto P, Bonino F, Brunetto MR. Transient elastography: a new surrogate marker of liver fibrosis influenced by major changes of transaminases. *J Viral Hepat* 2007; **14**: 360-369 [PMID: 17439526 DOI: 10.1111/j.1365-2893.2006.00811.x]

25 **Xu X**, Su Y, Song R, Sheng Y, Ai W, Wu X, Liu H. Performance of transient elastography assessing fibrosis of single hepatitis B virus infection: a systematic review and meta-analysis of a diagnostic test. *Hepatol Int* 2015; **9**: 558-566 [PMID: 26187292 DOI: 10.1007/s12072-015-9643-z]

26 **Xu XY**, Kong H, Song RX, Zhai YH, Wu XF, Ai WS, Liu HB. The effectiveness of noninvasive biomarkers to predict hepatitis B-related significant fibrosis and cirrhosis: a systematic review and meta-analysis of diagnostic test accuracy. *PLoS One* 2014; **9**: e100182 [PMID: 24964038 DOI: 10.1371/journal.pone.0100182]

27 **Millonig G**, Reimann FM, Friedrich S, Fonouni H, Mehrabi A, Büchler MW, Seitz HK, Mueller S. Extrahepatic cholestasis increases liver stiffness (FibroScan) irrespective of fibrosis. *Hepatology* 2008; **48**: 1718-1723 [PMID: 18836992 DOI: 10.1002/hep.22577]

28 **Granito A**, Muratori P, Ferri S, Pappas G, Quarneti C, Lenzi M, Bianchi FB, Muratori L. Diagnosis and therapy of autoimmune hepatitis. *Mini Rev Med Chem* 2009; **9**: 847-860 [PMID: 19519509 DOI: 10.2174/138955709788452676]

29 **Guo L**, Zheng L, Hu L, Zhou H, Yu L, Liang W. Transient Elastography (FibroScan) Performs Better Than Non-Invasive Markers in Assessing Liver Fibrosis and Cirrhosis in Autoimmune Hepatitis Patients. *Med Sci Monit* 2017; **23**: 5106-5112 [PMID: 29073121 DOI: 10.12659/msm.907300]

30 **Xing X**, Yan Y, Shen Y, Xue M, Wang X, Luo X, Yang L. Liver fibrosis with two-dimensional shear-wave elastography in patients with autoimmune hepatitis. *Expert Rev Gastroenterol Hepatol* 2020; **14**: 631-638 [PMID: 32510248 DOI: 10.1080/17474124.2020.1779589]

31 **Janik MK**, Kruk B, Szczepankiewicz B, Kostrzewa K, Raszeja-Wyszomirska J, Górnicka B, Lammert F, Milkiewicz P, Krawczyk M. Measurement of liver and spleen stiffness as complementary methods for assessment of liver fibrosis in autoimmune hepatitis. *Liver Int* 2021; **41**: 348-356 [PMID: 33159831 DOI: 10.1111/liv.14726]

32 **Yan Y**, Xing X, Lu Q, Wang X, Luo X, Yang L. Assessment of biopsy proven liver fibrosis by two-dimensional shear wave elastography in patients with primary biliary cholangitis. *Dig Liver Dis* 2020; **52**: 555-560 [PMID: 32111390 DOI: 10.1016/j.dld.2020.02.002]

33 **Osman KT**, Maselli DB, Idilman IS, Rowan DJ, Viehman JK, Harmsen WS, Harnois DM, Carey EJ, Gossard AA, LaRusso NF, Lindor KD, Venkatesh SK, Eaton JE. Liver Stiffness Measured by Either Magnetic Resonance or Transient Elastography Is Associated With Liver Fibrosis and Is an Independent Predictor of Outcomes Among Patients With Primary Biliary Cholangitis. *J Clin Gastroenterol* 2021; **55**: 449-457 [PMID: 32976197 DOI: 10.1097/MCG.0000000000001433]

34 **Zhang DK**, Chen M, Liu Y, Wang RF, Liu LP, Li M. Acoustic radiation force impulse elastography for non-invasive assessment of disease stage in patients with primary biliary cirrhosis: A preliminary study. *Clin Radiol* 2014; **69**: 836-840 [PMID: 24837697 DOI: 10.1016/j.crad.2014.03.019]

35 **Park Y**, Cho Y, Cho EJ, Kim YJ. Retrospective analysis of autoimmune hepatitis-primary biliary cirrhosis overlap syndrome in Korea: characteristics, treatments, and outcomes. *Clin Mol Hepatol* 2015; **21**: 150-157 [PMID: 26157752 DOI: 10.3350/cmh.2015.21.2.150]

36 **To U**, Silveira M. Overlap Syndrome of Autoimmune Hepatitis and Primary Biliary Cholangitis. *Clin Liver Dis* 2018; **22**: 603-611 [PMID: 30259856 DOI: 10.1016/j.cld.2018.03.010]

37 **Wu HM**, Sheng L, Wang Q, Bao H, Miao Q, Xiao X, Guo CJ, Li H, Ma X, Qiu DK, Hua J. Performance of transient elastography in assessing liver fibrosis in patients with autoimmune hepatitis-primary biliary cholangitis overlap syndrome. *World J Gastroenterol* 2018; **24**: 737-743 [PMID: 29456412 DOI: 10.3748/wjg.v24.i6.737]

38 **Yan YL**, Xing X, Wang Y, Wang XZ, Wang Z, Yang L. Clinical utility of two-dimensional shear-wave elastography in monitoring disease course in autoimmune hepatitis-primary biliary cholangitis overlap syndrome. *World J Gastroenterol* 2022; **28**: 2021-2033 [PMID: 35664960 DOI: 10.3748/wjg.v28.i18.2021]

39 **Petitclerc L**, Sebastiani G, Gilbert G, Cloutier G, Tang A. Liver fibrosis: Review of current imaging and MRI quantification techniques. *J Magn Reson Imaging* 2017; **45**: 1276-1295 [PMID: 27981751 DOI: 10.1002/jmri.25550]

40 **Youssef A**, Abdel Ghaffar TY, Esmat G, Wanis AAA. Non invasive assessment of hepatic fibrosis in children: Performance of liver stiffness measurement and aspartate transaminase to platelet ratio. *Hepatology* 2013; **58**: 815A [DOI: 10.1002/hep.26862]

41 **Kim JK**, Kim HW, Lee JI, Lee KS. Analysis of liver stiffness measured by transient elastography in autoimmune hepatitis. *Hepatology* 2014; **60**: 364A-365A [DOI: 10.1002/hep.27496]

42 **Abdollahi M**, Pouri A, Ghojazadeh M, Estakhri R, Somi M. Non-invasive serum fibrosis markers: A study in chronic hepatitis. *Bioimpacts* 2015; **5**: 17-23 [PMID: 25901293 DOI: 10.15171/bi.2015.05]

43 **Harrison L**, McFarlane E, Dube A, Gleeson D. Accuracy of transient elastography in predicting histological fibrosis severity in treated autoimmune hepatitis? *Gut* 2016; **65**: A268-A269 [DOI: 10.1136/gutjnl-2016-312388.505]

44 **Hartl J**, Denzer U, Ehlken H, Zenouzi R, Peiseler M, Sebode M, Hübener S, Pannicke N, Weiler-Normann C, Quaas A, Lohse AW, Schramm C. Transient elastography in autoimmune hepatitis: Timing determines the impact of inflammation and fibrosis. *J Hepatol* 2016; **65**: 769-775 [PMID: 27238753 DOI: 10.1016/j.jhep.2016.05.023]

45 **Nishikawa H**, Enomoto H, Iwata Y, Hasegawa K, Nakano C, Takata R, Nishimura T, Yoh K, Aizawa N, Sakai Y, Ikeda N, Takashima T, Iijima H, Nishiguchi S. Clinical significance of serum Wisteria floribunda agglutinin positive Mac-2-binding protein level and high-sensitivity C-reactive protein concentration in autoimmune hepatitis. *Hepatol Res* 2016; **46**: 613-621 [PMID: 26406984 DOI: 10.1111/hepr.12596]

46 **E Anastasiou O**, Büchter M, A Baba H, Korth J, Canbay A, Gerken G, Kahraman A. Performance and Utility of Transient Elastography and Non-Invasive Markers of Liver Fiibrosis in Patients with Autoimmune Hepatitis: A Single Centre Experience. *Hepat Mon* 2016; **16**: e40737 [PMID: 28070199 DOI: 10.5812/hepatmon.40737]

47 **Piwczyńska K**, Marek W, Maciej D, Małgorzata W. APRI as a fibrosis marker in children with autoimmune hepatitis(AIH). In: ESPGHAN 49th ANNUAL MEETING of the European Society for Paediatric Gastroenterology, Hepatology and Nutrition. *Journal of Pediatric Gastroenterology and Nutrition* 2016; **62**: 1-890 [DOI: 10.1097/01.mpg.0000484500.48517.e7]

48 **Sheptulina A**, Shirokova E, Nekrasova T, Blum H, Ivashkin V. Platelet count to spleen diameter ratio non-invasively identifies severe fibrosis and cirrhosis in patients with autoimmune hepatitis. *J Gastroenterol Hepatol* 2016; **31**: 1956-1962 [PMID: 27059170 DOI: 10.1111/jgh.13407]

49 **Paranagua-Vezozzo D**, Terrabuio DR, Moutinho RD, Ono S, Salas V, Carrilho F, Alves VF, Cancado EL. Transient elastography (TE) and acoustic radiation force impulse imaging (ARFI) can predict degree of advanced fibrosis for autoimmune hepatitis in biochemical remission. *Hepatology* 2017; **66**: 187A

50 **Puustinen L**, Hakkarainen A, Kivisaari R, Boyd S, Nieminen U, Färkkilä M, Lundbom N, Arkkila P. (31) Phosphorus magnetic resonance spectroscopy of the liver for evaluating inflammation and fibrosis in autoimmune hepatitis. *Scand J Gastroenterol* 2017; **52**: 886-892 [PMID: 28415898 DOI: 10.1080/00365521.2017.1315738]

51 **Xu Q**, Sheng L, Bao H, Chen X, Guo C, Li H, Ma X, Qiu D, Hua J. Evaluation of transient elastography in assessing liver fibrosis in patients with autoimmune hepatitis. *J Gastroenterol Hepatol* 2017; **32**: 639-644 [PMID: 27505153 DOI: 10.1111/jgh.13508]

52 **Zeng J**, Huang ZP, Zheng J, Wu T, Zheng RQ. Non-invasive assessment of liver fibrosis using two-dimensional shear wave elastography in patients with autoimmune liver diseases. *World J Gastroenterol* 2017; **23**: 4839-4846 [PMID: 28765706 DOI: 10.3748/wjg.v23.i26.4839]

53 **Liu L**, Cao J, Zhong Z, Guo Z, Jiang Y, Bai Y, Xu J. Noninvasive indicators predict advanced liver fibrosis in autoimmune hepatitis patients. *J Clin Lab Anal* 2019; **33**: e22922 [PMID: 31115929 DOI: 10.1002/jcla.22922]

54 **Li X**, Xu H, Gao P. Red Blood Cell Distribution Width-to-Platelet Ratio and Other Laboratory Indices Associated with Severity of Histological Hepatic Fibrosis in Patients with Autoimmune Hepatitis: A Retrospective Study at a Single Center. *Med Sci Monit* 2020; **26**: e927946 [PMID: 33180750 DOI: 10.12659/MSM.927946]

55 **Wang H**, Wang J, Xia J, Yan X, Feng Y, Li L, Chen J, Liu D, Ding W, Yang Y, Huang R, Wu C. Red cell distribution width to platelet ratio predicts liver fibrosis in patients with autoimmune hepatitis. *Medicine (Baltimore)* 2020; **99**: e21408 [PMID: 32846758 DOI: 10.1097/MD.0000000000021408]

56 **Ferronato M**, Lenzi M, Muratori P, Muratori L. Blood-Based Non-Invasive Tests of Hepatic Fibrosis in Autoimmune Hepatitis: Application among Selected Patients Leads to Higher Accuracy. *Gastroenterology Insights* 2022; **13**: 286-295 [DOI: 10.3390/gastroent13030029]

57 **Soh EG**, Lee YH, Kim YR, Yoon KH, Choi KH. Usefulness of 2D shear wave elastography for the evaluation of hepatic fibrosis and treatment response in patients with autoimmune hepatitis. *Ultrasonography* 2022; **41**: 740-749 [PMID: 36195317 DOI: 10.14366/usg.21266]

58 **Nyblom H**, Björnsson E, Simrén M, Aldenborg F, Almer S, Olsson R. The AST/ALT ratio as an indicator of cirrhosis in patients with PBC. *Liver Int* 2006; **26**: 840-845 [PMID: 16911467 DOI: 10.1111/j.1478-3231.2006.01304.x]

59 **Gómez-Dominguez E**, Mendoza J, García-Buey L, Trapero M, Gisbert JP, Jones EA, Moreno-Otero R. Transient elastography to assess hepatic fibrosis in primary biliary cirrhosis. *Aliment Pharmacol Ther* 2008; **27**: 441-447 [PMID: 18081731 DOI: 10.1111/j.1365-2036.2007.03585.x]

60 **Alempijevic T**, Krstic M, Jesic R, Jovanovic I, Sokic Milutinovic A, Kovacevic N, Krstic S, Popovic D. Biochemical markers for non-invasive assessment of disease stage in patients with primary biliary cirrhosis. *World J Gastroenterol* 2009; **15**: 591-594 [PMID: 19195061 DOI: 10.3748/wjg.15.591]

61 **Ferrara F**, Caroli D, Antoniazzi S, Variola A, Cazzagon N, Baldo V, Floreani A. Performance of surrogate markers of hepatic fibrosis in primary biliary cirrhosis. *J Hepatol* 2009; **50**: S243 [DOI: 10.1016/S1590-8658(09)60099-2]

62 **Su CW**, Chan CC, Hung HH, Huo TI, Huang YH, Li CP, Lin HC, Tsay SH, Lee PC, Lee SD, Wu JC. Predictive value of aspartate aminotransferase to alanine aminotransferase ratio for hepatic fibrosis and clinical adverse outcomes in patients with primary biliary cirrhosis. *J Clin Gastroenterol* 2009; **43**: 876-883 [PMID: 19247208 DOI: 10.1097/MCG.0b013e31818980ac]

63 **Floreani A**, Cazzagon N, Martines D, Cavalletto L, Baldo V, Chemello L. Performance and utility of transient elastography and noninvasive markers of liver fibrosis in primary biliary cirrhosis. *Dig Liver Dis* 2011; **43**: 887-892 [PMID: 21783442 DOI: 10.1016/j.dld.2011.06.011]

64 **Corpechot C**, Carrat F, Poujol-Robert A, Gaouar F, Wendum D, Chazouillères O, Poupon R. Noninvasive elastography-based assessment of liver fibrosis progression and prognosis in primary biliary cirrhosis. *Hepatology* 2012; **56**: 198-208 [PMID: 22271046 DOI: 10.1002/hep.25599]

65 **Umemura T**, Joshita S, Sekiguchi T, Usami Y, Shibata S, Kimura T, Komatsu M, Matsumoto A, Ota M, Tanaka E. Serum Wisteria floribunda Agglutinin-Positive Mac-2-Binding Protein Level Predicts Liver Fibrosis and Prognosis in Primary Biliary Cirrhosis. *Am J Gastroenterol* 2015; **110**: 857-864 [PMID: 25916223 DOI: 10.1038/ajg.2015.118]

66 **Nishikawa H**, Enomoto H, Iwata Y, Hasegawa K, Nakano C, Takata R, Nishimura T, Yoh K, Aizawa N, Sakai Y, Ikeda N, Takashima T, Ishii A, Iijima H, Nishiguchi S. Impact of serum Wisteria floribunda agglutinin positive Mac-2-binding protein and serum interferon-γ-inducible protein-10 in primary biliary cirrhosis. *Hepatol Res* 2016; **46**: 575-583 [PMID: 26418076 DOI: 10.1111/hepr.12595]

67 **Olmez S**, Sayar S, Avcioglu U, Tenlik İ, Ozaslan E, Koseoglu HT, Altiparmak E. The relationship between liver histology and noninvasive markers in primary biliary cirrhosis. *Eur J Gastroenterol Hepatol* 2016; **28**: 773-776 [PMID: 27092904 DOI: 10.1097/MEG.0000000000000637]

68 **Wang H**, Xu H, Wang X, Wu R, Gao X, Jin Q, Niu J. Red Blood Cell Distribution Width to Platelet Ratio is Related to Histologic Severity of Primary Biliary Cirrhosis. *Medicine (Baltimore)* 2016; **95**: e3114 [PMID: 26986159 DOI: 10.1097/MD.0000000000003114]

69 **Wang X**, Han Z, Chen Y, Guo C, Han Y. Validity analysis based on non-invasive methods for the assessment of liver fibrosis in primary biliary cholangitis. In: Abstracts of the 26th Annual Conference of APASL. *Hepatol Int* 2017; **11**: S590 [DOI: 10.1007/s12072-016-9783-9]

70 **Jiang X**, Wang Y, Su Z, Yang F, Lv H, Lin L, Sun C. Red blood cell distribution width to platelet ratio levels in assessment of histologic severity in patients with primary biliary cholangitis. *Scand J Clin Lab Invest* 2018; **78**: 258-263 [PMID: 29533114 DOI: 10.1080/00365513.2018.1449011]

71 **Kamal N**, Surana P, Noureddin M, Kleiner D, Hoofnagle J, Heller T, Koh C. Bile Duct Damage and Cirrhosis in Primary Biliary Cholangitis: An Investigation of Non-Invasive Biomarkers. *Gastroenterology* 2018; **154**: S1209 [DOI: 10.1016/s0016-5085(18)33995-7]

72 **Meng J**, Xu H, Liu X, Wu R, Niu J. Increased red cell width distribution to lymphocyte ratio is a predictor of histologic severity in primary biliary cholangitis. *Medicine (Baltimore)* 2018; **97**: e13431 [PMID: 30508955 DOI: 10.1097/MD.0000000000013431]

73 **Milovanović T**, Copertino A, Boričić I, Miličić B, Marković AP, Krstić M, Matović V, Popović D. Transient elastography for noninvasive assessment of liver fibrosis in patients with primary biliary cirrhosis. *Vojnosanitetski Pregled* 2018; **75**: 374-379 [DOI: 10.2298/VSP160409337A]

74 **Wang Z**, Liu X, Xu H, Qu L, Zhang D, Gao P. Platelet count to spleen thickness ratio is related to histologic severity of primary biliary cholangitis. *Medicine (Baltimore)* 2018; **97**: e9843 [PMID: 29443746 DOI: 10.1097/MD.0000000000009843]

75 **Jiang M**, Yan X, Song X, Yan Q, Zhao Y, Wang L, Gao P. Total bile acid to platelet ratio: A noninvasive index for predicting liver fibrosis in primary biliary cholangitis. *Medicine (Baltimore)* 2020; **99**: e20502 [PMID: 32481469 DOI: 10.1097/MD.0000000000020502]

76 **Joshita S**, Yamashita Y, Sugiura A, Uehara T, Usami Y, Yamazaki T, Fujimori N, Matsumoto A, Tanaka E, Umemura T. Clinical utility of FibroScan as a non-invasive diagnostic test for primary biliary cholangitis. *J Gastroenterol Hepatol* 2020; **35**: 1208-1214 [PMID: 31724755 DOI: 10.1111/jgh.14929]

77 **Rossi M**, Alessi N, Cabibi A, Fichera A, Zarcone A, Bianco AL, Marco VD, Cammà C, Craxì A. High rate of misclassification of fibrosis stage using Transient Elastography in patients with Primary Biliary Cholangitis. *Digestive and Liver Disease* 2020; **52**: e34 [DOI: 10.1016/j.dld.2019.12.122]

78 **Cristoferi L**, Calvaruso V, Overi D, Viganò M, Rigamonti C, Degasperi E, Cardinale V, Labanca S, Zucchini N, Fichera A, Di Marco V, Leutner M, Venere R, Picciotto A, Lucà M, Mulinacci G, Palermo A, Gerussi A, D'Amato D, Elisabeth O'Donnell S, Cerini F, De Benedittis C, Malinverno F, Ronca V, Mancuso C, Cazzagon N, Ciaccio A, Barisani D, Marzioni M, Floreani A, Alvaro D, Gaudio E, Invernizzi P, Carpino G, Nardi A, Carbone M; Italian PBC Registry. Accuracy of Transient Elastography in Assessing Fibrosis at Diagnosis in Naïve Patients With Primary Biliary Cholangitis: A Dual Cut-Off Approach. *Hepatology* 2021; **74**: 1496-1508 [PMID: 33724515 DOI: 10.1002/hep.31810]

79 **Fujinaga Y**, Namisaki T, Takaya H, Tsuji Y, Suzuki J, Shibamoto A, Kubo T, Iwai S, Tomooka F, Takeda S, Fujimoto Y, Enomoto M, Murata K, Ishida K, Ogawa H, Takagi H, Ozutsumi T, Furukawa M, Nishimura N, Sawada Y, Kitagawa K, Sato S, Kaji K, Kawaratani H, Moriya K, Noguchi R, Akahane T, Mitoro A, Yoshiji H. Enhanced liver fibrosis score as a surrogate of liver-related complications and mortality in primary biliary cholangitis. *Medicine (Baltimore)* 2021; **100**: e27403 [PMID: 34596167 DOI: 10.1097/MD.0000000000027403]

80 **Manesis EK**, Schina M, Vafiadis I, Gatos I, Theotokas J, Zoumpoulis P, Drazinos P, Ketikoglou J, Delladetsima IK, Tiniakos DG. Liver stiffness measurements by 2-dimensional shear wave elastography compared to histological and ultrasound parameters in primary biliary cholangitis. *Scand J Gastroenterol* 2021; **56**: 1187-1193 [PMID: 34375562 DOI: 10.1080/00365521.2021.1928277]

81 **Avcioğlu U**, Eruzun H, Ustaoğlu M. The gamma-glutamyl transferase to platelet ratio for noninvasive evaluation of liver fibrosis in patients with primary biliary cholangitis. *Medicine (Baltimore)* 2022; **101**: e30626 [PMID: 36221370 DOI: 10.1097/MD.0000000000030626]

82 **Garrido I**, Liberal R, Macedo G. Perfomance of vibrationcontrolled transient elastography in primary biliary cholangitis. *Hepatology* 2022; **76**: S1483-S1483 [DOI: 10.1002/hep.32697]

83 **Corpechot C**, Gaouar F, El Naggar A, Kemgang A, Wendum D, Poupon R, Carrat F, Chazouillères O. Baseline values and changes in liver stiffness measured by transient elastography are associated with severity of fibrosis and outcomes of patients with primary sclerosing cholangitis. *Gastroenterology* 2014; **146**: 970-9; quiz e15 [PMID: 24389304 DOI: 10.1053/j.gastro.2013.12.030]

84 **Bowlus CL**, Montano-Loza AJ, Invernizzi P, Chazouillères O, Hirschfield G, Metselaar HJ, Goodman Z, Myers RP, Aguilar R, Subramanian GM, McHutchison JG, Chapman R, Muir AJ, Eksteen B, Levy C. Liver stiffness measurement by transient elastography for the prediction of fibrosis in patients with primary sclerosing cholangitis in a randomized trial of simtuzumab. *J Hepatol* 2016; **64**: S434

85 **Eaton JE**, Dzyubak B, Venkatesh SK, Smyrk TC, Gores GJ, Ehman RL, LaRusso NF, Gossard AA, Lazaridis KN. Performance of magnetic resonance elastography in primary sclerosing cholangitis. *J Gastroenterol Hepatol* 2016; **31**: 1184-1190 [PMID: 26691631 DOI: 10.1111/jgh.13263]

86 **Ehlken H**, Wroblewski R, Corpechot C, Arrivé L, Rieger T, Hartl J, Lezius S, Hübener P, Schulze K, Zenouzi R, Sebode M, Peiseler M, Denzer UW, Quaas A, Weiler-Normann C, Lohse AW, Chazouilleres O, Schramm C. Validation of Transient Elastography and Comparison with Spleen Length Measurement for Staging of Fibrosis and Clinical Prognosis in Primary Sclerosing Cholangitis. *PLoS One* 2016; **11**: e0164224 [PMID: 27723798 DOI: 10.1371/journal.pone.0164224]

87 **Krawczyk M**, Ligocka J, Ligocki M, Raszeja-Wyszomirska J, Milkiewicz M, Szparecki G, Ilczuk T, Górnicka B, Zieniewicz K, Krawczyk M, Lammert F, Milkiewicz P. Does transient elastography correlate with liver fibrosis in patients with PSC? Laennec score-based analysis of explanted livers. *Scand J Gastroenterol* 2017; **52**: 1407-1412 [PMID: 28851259 DOI: 10.1080/00365521.2017.1370009]

88 **Umetsu S**, Inui A, Sogo T, Komatsu H, Fujisawa T. Usefulness of serum Wisteria floribunda agglutinin-positive Mac-2 binding protein in children with primary sclerosing cholangitis. *Hepatol Res* 2018; **48**: 355-363 [PMID: 29168311 DOI: 10.1111/hepr.13004]

Published by **Baishideng Publishing Group Inc**
7041 Koll Center Parkway, Suite 160, Pleasanton, CA 94566, USA
Telephone: +1-925-3991568
E-mail: bpgoffice@wjgnet.com
Help Desk: https://www.f6publishing.com/helpdesk
https://www.wjgnet.com